Enhancement of Power System Dynamic Performance by Coordinated Design of PSS and FACTS Damping Controllers

Ph.D. thesis submitted in partial fulfillment of the requirements for the degree of

Doctor of Philosophy

in

Electrical Engineering

Submitted by

Rajendraprasad Narne

Roll No: **510EE105**

Under the Supervision of

Prof. P. C. Panda

Department of Electrical Engineering

National Institute of Technology, Rourkela

July 2015

Enhancement of Power System Dynamic Performance by Coordinated Design of PSS and FACTS Damping Controllers

Rajendraprasad Narne

Department of Electrical Engineering

National Institute of Technology, Rourkela

Enhancement of Power System Dynamic Performance by Coordinated Design of PSS and FACTS Damping Controllers

Ph.D. thesis submitted in partial fulfillment of the requirements for the degree of

Doctor of Philosophy

in

Electrical Engineering

Submitted by

Rajendraprasad Narne

Roll No: **510EE105**

Under the Supervision of

Prof. P. C. Panda

Department of Electrical Engineering

National Institute of Technology, Rourkela

July 2015

Dedicated

To

All My Family Members

and

Well-Wishers

...Rajendraprasad Narne

DEPARTMENT OF ELECTRICAL ENGINEERING
NATIONAL INSTITUTE OF TECHNOLOGY, ROURKELA
ORISSA, INDIA – 769008

CERTIFICATE

This is to certify that the thesis entitled "**Enhancement of Power System Dynamic Performance by Coordinated Design of PSS and FACTS Damping Controllers,**" submitted to the National Institute of Technology, Rourkela by **Mr. Rajendraprasad Narne**, Roll No. **510EE105** for the award of **Doctor of Philosophy** in Electrical Engineering, is a bonafide record of research work carried out by him under my supervision and guidance.

The candidate has fulfilled all the prescribed requirements.

The Thesis which is based on candidate's own work, has not submitted elsewhere for a degree/diploma to the best of my knowledge and belief.

In my opinion, the thesis is of standard required for the award of a **Doctor of Philosophy** degree in **Electrical Engineering.**

Prof. P. C. Panda
Professor,
Department of Electrical Engineering,
National Institute of Technology,
Rourkela, India - 769008.
Email: pcpanda@nitrkl.ac.in

Place: Rourkela
Date: 11th July 2015

Acknowledgement

The research reported here has been carried out in the **Dept. of Electrical Engineering, National Institute of Technology Rourkela at the Advanced Power System Laboratory.** I am greatly indebted to many persons for helping me complete this dissertation.

First and foremost, I would like to express my sense of gratitude and indebtedness to my supervisor **Prof. Prafulla Chandra Panda,** Professor, Department of Electrical Engineering, for his inspiring guidance, encouragement, and untiring effort throughout the course of this work. His timely help and painstaking efforts made it possible to present the work contained in this thesis. I consider myself fortunate to have worked under his guidance. Also, I am indebted to him for providing all official and laboratory facilities.

I am grateful to Director, **Prof. S.K. Sarangi** and **Prof. Anup Kumar Panda**, Head of Electrical Engineering Department, National Institute of Technology, Rourkela, for their kind support and concern regarding my academic requirements.

I am grateful to my Doctoral Scrutiny Committee members, **Prof. K.B. Mohanty, Prof. K.K. Mahapatra** and **Prof. B. Majhi,** for their valuable suggestions and comments during this research period. I express my thankfulness to the faculty and staff members of the Electrical Engineering Department for their continuous encouragement and suggestions.

I express my heartfelt thanks to the **international journal reviewers** for giving their valuable comments on the published papers in different international journals, which helps to carry the research work in a right direction. I also thank to the **international conference organizers** for intensely reviewing the published papers.

I am especially indebted to my colleagues in the power system group. First, I would like to thank **Dr. Jose P Therattil**, who helped me in my research work. We shared each other a lot of knowledge in the field of power systems. I would also like to thank other members of APS Lab, **Ms. Rakhee Panigrahi**, **Mr. Sudarshan Swain** and **Mr. Nilamani Rout** for extending their technical and personal support. It has been a great pleasure to work with such a helpful, hardworking, and creative group. I would also thank my seniors **Dr. S. Naresh Kumar**, **Dr. Kala Praveen** and **Dr. Y. Suresh** for their kind assistance and moral support. I would also thank my friends **Dr. M. Suresh, Mr. T. Remesh, Mr. G. Kiran Kumar, Mr. S. Shiva**

Kumar and **Mr. Vinaya Sagaram** for their valuable thoughts in my research and personal career.

I express my deep sense of gratitude and reverence to my beloved father **Sri. Sreenivasa Rao**, Mother **Smt. Padmavathi** and my brother **Mr. Krishna Vardhan Kumar** who supported and encouraged me all the time, no matter what difficulties I encountered. I would like to express my greatest admiration to **all my family members** and **relatives** for their positive encouragement that they showered on me throughout this research work. Without my family's sacrifice and support, this research work would not have been possible. It is a great pleasure for me to acknowledge and express my appreciation to all **my well wishers** for their understanding, relentless supports, and encouragement during my research work. Last but not the least, I wish to express my sincere thanks to all those who helped me directly or indirectly at various stages of this work.

Above all, I would like to thank **The Almighty God** for the wisdom and perseverance that he has been bestowed upon me during this research work, and indeed, throughout my life.

Rajendraprasad Narne

Contents

Abbreviations

AAPSO	Advanced Adaptive Particle Swarm Optimization
AC	Alternative Current
ACVC	STATCOM AC Voltage Controller
API	Application Program Interface
APSO	Advanced Particle Swarm Optimization
ARTEMIS	Advanced Real-Time Electro-Mechanical Transient Simulator
ASVC	Advanced Static Var Compensator
ATC	Available Transfer Capability
AVR	Automatic Voltage Regulator
BFO	Bacterial Foraging Optimization
COTS	Commercial Off The Shelf
CPSO	Conventional Particle Swarm Optimization
DC	Direct Current
DCVC	STATCOM DC voltage controller
DE	Differential Evolution
DSP	Digital Signal Processor
EMT	Electromagnetic Transientcs
EMTP-RV	Electro Magnetic Transients Program - Restructured Version
FACTS	Flexible AC Transmission Systems
FLC	Fuzzy Logic Controller
FPGA	Field-Programmable Gate Array
GA	Genetic Algorithms
GTO	Gate-Turn-Off Thyristor
HDL	Hardware description language
HIL	Hardware-In-the-Loop
HVDC	High-Voltage Direct Current
IEEE	Institute of Electrical and Electronics Engineers
IGBT	Insulated Gate Bipolar Transistor
I/O	Input/output
ITAE	Integral of Time-Multiplied Absolute Value of Error

IWO	Invasive Weed Optimization
JTAG	Joint Test Action Group
MATLAB	Matrix Laboratory
MSO	Mixed Signal Oscilloscope
PC	Personnel Computer
PCI-Express	Peripheral Component Interconnect - Express
PF	Power Factor
PID	Proportional Integral Derivative
POD	Power Oscillations Damping
PSB	Power System Block set
PSCAD	Power Systems Computer Aided Design
PSO	Particle Swarm Optimization
PSS	Power System Stabilizer
PSS/E	Power System Simulator for Engineering
RTOS	Real-Time Operating Systems
RTW	Real-Time Workshop
SA	Simulated Annealing
SMIB	Single Machine Infinite Bus
SSSC	Static Synchronous Series Compensator
STATCOM	Static Synchronous Compensator
SVC	Static Var Compensator
TCP/IP	Transmission Control Protocol / Internet Protocol
TCPST	Thyristor controlled phase shifting transformer
TCR	Thyristor Controlled Reactor
TCSC	Thyristor Controlled Series Capacitor
TNAs	Transient Network Analysers
TSC	Thyristor Switched Capacitor
TVAC	Time-Varying Acceleration Coefficients
UPFC	Unified Power Flow Controller
VAR	Volt Ampere Reactive
VSC	Voltage Source Converter

Notations

A	State matrix
B	Input matrix
B_{SVC}	Susceptance of SVC
B_{SVCref}	Reference Susceptance of SVC
C	Output matrix
c_1	positive cognitive constant
c_2	social component
D	Damping coefficient
$e(t)$	Error signal
E_d	d-axis component of machine voltage
E_{fd}	Equivalent excitation voltage
E_q	q-axis component of machine voltage
$E_q^{'}$	q-axis component voltage behind transient Reactance
f	Frequency
G_i^{best}	The current global best position of the i^{th} particle
I_d	d-axis component of current
I_q	q-axis component of current
$iter_{\max}$	Maximum number of iterations
$iter_{\min}$	Minimum number of iterations
J	Objective function
k	Ratio of AC and DC voltage
K	Gain
K_A	Gain of AVR
K_D	Differential gain
K_I	Integral gain

K_P	Proportional gain
K_S	Gain of SVC
K_T	Gain of TCSC
m	Modulation index of the PWM
M	Inertia constant, $M = 2H$
P	Real power
P_e	Electrical power output
P_i^{best}	The current best position of the i^{th} particle
P_m	Mechanical power input
$P_{\max}$	Maximum number of plants
Q	Reactive power
r_a	Armature resistance of generator
$S_{\max}$	Maximum number of seeds
$S_{\min}$	Minimum number of seeds
T_1, T_2, T_3, T_4	Time constants of Lead-Lag controller
T_A	Time constant of AVR
T_c	Fault clearing time
$T_{d0}^{'}$	d-axis transient open-circuit time constant
T_s	Fault starting time
T_S	Time constant of SVC
T_T	Time constant of TCSC
T_W	Wash out time constant
U_{PSS}	Out-put signal of PSS
$u(t)$	Control signal
V_{DC}	Capacitor DC voltage
V_m	AC voltage of STATCOM

V_i	The current velocity of the i^{th} particle
V_t	Terminal voltage of the generator
$V_{t\,ref}$	Reference value of terminal voltage
w_i	The current inertia weight of the i^{th} particle
X_d	d-axis synchronous reactance
$X_d^{'}$	d-axis transient reactance
X_i	The current position of the i^{th} particle
X_q	q-axis synchronous reactance
X_{TCSC}	Reactance of TCSC
$X_{TCSCref}$	Reference reactance of TCSC
Y	Admittance matrix
Y_R	Reduced admittance matrix
Δu	Input vector
Δx	State vector
Δy	Output vector
δ	Rotor angle of synchronous machine
ω	Rotor speed deviation
ω_0	Initial Rotor speed deviation
Δ	Change / Variation
α	Firing angle
α_S	Phase angle of VSC
σ	Conduction angle
λ_i	i^{th} eigen value
σ_i	Real part of i^{th} eigen value
ω_i	Imaginary part of i^{th} eigen value
ζ_i	damping ratio of i^{th} eigen value
$\sigma_{initial}$	Initial value of standard deviation
σ_{final}	Final value of standard deviation

Abstract

Due to environmental and economical constraints, it is difficult to build new power lines and to reinforce the existing ones. The continued growth in demand for electric power must therefore to a great extent be met by increased loading of available lines. A consequence of this is reduction of power system damping, leading to a risk of poorly damped power oscillations between generators. To suppress these oscillations and maintain power system dynamic performance, one of the conventional, economical and effective solutions is to install a power system stabilizer (PSS). However, in some cases PSS may not provide sufficient damping for the inter-area oscillations in a multi-machine power system. In this context, other possible solutions are needed to be exposed.

With the evolution of power electronics, flexible AC transmission systems (FACTS) controllers turn out to be possible solution to alleviate such critical situations by controlling the power flow over the AC transmission line and improving power oscillations damping. However, coordination of conventional PSS with FACTS controllers in aiding of power system oscillations damping is still an open problem. Therefore, it is essential to study the coordinated design of PSS with FACTS controllers in a multi-machine power system.

This thesis gives an overview of the modelling and operation of power system with conventional PSS. It gives the introduction to emerging FACTS controllers with emphasis on the TCSC, SVC and STATCOM controllers. The basic modelling and operating principles of the controllers are explained in this thesis, along with the power oscillations damping (POD) stabilizers.

The coordination design of PSS and FACTS damping controllers over a wide range of operating conditions is formulated as an optimization problem. The objective function of this optimization problem is framed using system eigen values and it is solved using AAPSO and IWO algorithms. The optimal control parameters of coordinated controllers are obtained at the end of these optimization algorithms. A comprehensive approach to the hybrid coordinated design of PSS with series and shunt FACTS damping controllers is proposed to enhance the overall system dynamic performance. The robustness and effectiveness of proposed hybrid coordinated designs are demonstrated through the eigen value analysis and time-domain simulations.

The proposed hybrid designs provide robust dynamic performance under wide range in load condition and providing significant improvement in damping power system oscillations under severe disturbance. The developed hybrid coordinated designs are tested in different multi-machine power systems using AAPSO and IWO algorithms. The IWO based hybrid designs and AAPSO based hybrid designs are more effective than other control designs. In addition to this, the proposed designs are implemented and validated in real-time using Opal-RT hardware simulator. The real-time simulations of different test power systems with different proposed designs are carried out for a severe fault disturbance. Finally, the proposed controller simulation results are validated with real-time results.

List of Figures

List of Tables

Chapter 1

INTRODUCTION

Chapter 1

Introduction

1.1 An Overview of Power System

Electric power is only form of energy used in several sectors such as, domestic, industrial, commercial and transportation. It is a converted form of energy, since it can be generated in bulk, transmitted over very long distances easily at high efficiency and at a reasonable cost. Electric power systems, including generation, transmission and distribution are considered to be the largest and most expensive man-made system in the present world. In developed societies, the demand of electric power is increasing enormously and it is doubled every ten years. So there is a great need to improve electric power generation. This has motivated construction of new power plants where power generation resources such as, coal mines, water falls or natural gases are located normally at distant locations for economic, environmental and safety reasons. Additionally, modern power systems are highly complex and interconnected. Sharing of generation reserves, exploiting load diversity and economy gained from the use of large efficient units without sacrificing reliability are the advantages of interconnection. Thus building of new transmission systems is necessary to transmit power over long distances to meet the ever growing power demand. Building new transmission systems however faces many challenges due to

- Environment constraints
- Regulatory and financial uncertainties
- Difficulty in acquiring right-of-way
- Competitions due to deregulation of the electric utilities

These issues provide the momentum for exploring new ways of maximizing power transfer capability of the existing transmission facilities. In order to maximize the efficiency of electric power transmission, the transmission utilities are very often pushed to their physical limits, where outage of lines or other equipment could result in the rapid failure of the entire system. Hence, power transfer should ensure that limits due to thermal, voltage and transient stabilities are not violated.

1.2 Power System Stability: Definition and Classification

Power system stability is the ability of an electrical power system, for a given initial operating condition, to regain a state of operating equilibrium after being subjected to a physical disturbance, with most system variables bounded so that practically the entire system remains intact [1]. To understand different aspects and characteristics of power system stability, the following issues need to be considered [1, 2]

1. Power system is a highly nonlinear system which operates in constantly changing condition. However, the stability of the system depends on the initial operating condition as well as nature of the disturbance when it is subjected to a disturbance.
2. Power systems are always subjected over a wide range of disturbances. When the disturbance is small, the system can adjust the operating conditions and operates satisfactorily. Whereas, the large disturbances may lead to structural changes due to the isolation of the faulted elements.
3. The design of power system to be stable for every possible disturbance is impractical and uneconomical. The robust system is designed with respect to large disturbances.

In order to understand and analyze specific type in high dimensional and complex stability problems, it is necessity to classify them in detail based on the following considerations [2].

1. The nature of the resulting instability mode indicated by the observation of certain system variables.
2. The method of calculation and prediction of stability is influenced by the size of disturbance considered.
3. In order to assess stability the time span, devices and processes need to be considered.

Accordingly, the power system stability can be classified as follows:

1.2.1 Rotor Angle Stability

Rotor angle stability is defined as “the ability of synchronous machines of an interconnected power system to remain in synchronism after being subjected to a disturbance.” It depends on the ability of the system to maintain equilibrium between synchronizing torque and the damping torque. Lack of sufficient synchronizing torque leads to aperiodic or non-

oscillatory instability, whereas lack of damping torque leads to oscillatory instability. Rotor angle stability can be classified as follows [1, 2]:

A. Small-Disturbance Rotor Angle Stability

It is the ability of power system to maintain synchronism under small disturbances. At present, small-disturbance rotor angle stability problem is usually associated with insufficient damping of oscillations. However, aperiodic instability problem has been eliminated by generator voltage regulators. These rotor angle oscillations are either local plant oscillations or inter-area mode oscillations. The time frame of these stability studies is in the order of 10 to 20 seconds following the disturbance.

B. Large-Disturbance Rotor Angle Stability (Transient Stability)

It is the ability of the power system to maintain synchronism when subjected to a severe disturbance, as in the case of a short circuit on a transmission line. This stability depends on both the initial operating condition and the severity of disturbance. The time frame of these stability studies is in the order of 3 to 5 seconds following the disturbances.

1.2.2 Voltage Stability

It refers to the ability of a power system to maintain steady voltages at all buses in the system after being subjected to a disturbance from a given initial operating condition. It depends on the ability of the system to maintain equilibrium between load demand and load supply.

A. Large-Disturbance Voltage Stability

Large-disturbance voltage stability refers to the system's ability to maintain steady voltages following large disturbances like system faults, loss of generation, circuit contingencies. This ability is determined by the system and load characteristics, and the interactions between different voltage control devices in the system. The typical time frame is in the order of a few seconds to ten minutes.

B. Small-Disturbance Voltage Stability

Small-disturbance voltage stability refers to the system's ability to maintain steady voltages when subjected to small perturbations like incremental changes in the system load. This can

be influenced by the load characteristics, continuous controls, and discrete controls. This problem is usually studied using power flow based tools.

It is noted that the time frame of interest for voltage stability problems may vary from a few seconds to ten minutes. Hence, voltage stability may be either a short-term or a long-term phenomenon.

1.2.3 Frequency Stability

Frequency stability is defined as the ability of a power system to maintain steady frequency following a severe system upset resulting in a significant imbalance between generation and load. It depends on the ability of system to maintain equilibrium between system generation and load [1]. Due to the difference in the process time frame for different system devices, the frequency stability phenomenon is classified as short-term and long-term frequency stability. The short-term influenced by load shedding, generator controls, and protection devices, covers first several seconds following the disturbance. The long-term frequency stability is influenced by other factors such as the prime mover energy supply, covering several minutes following the disturbance.

The overall picture of power system stability problem with categories and subcategories is shown in Figure 1.1.

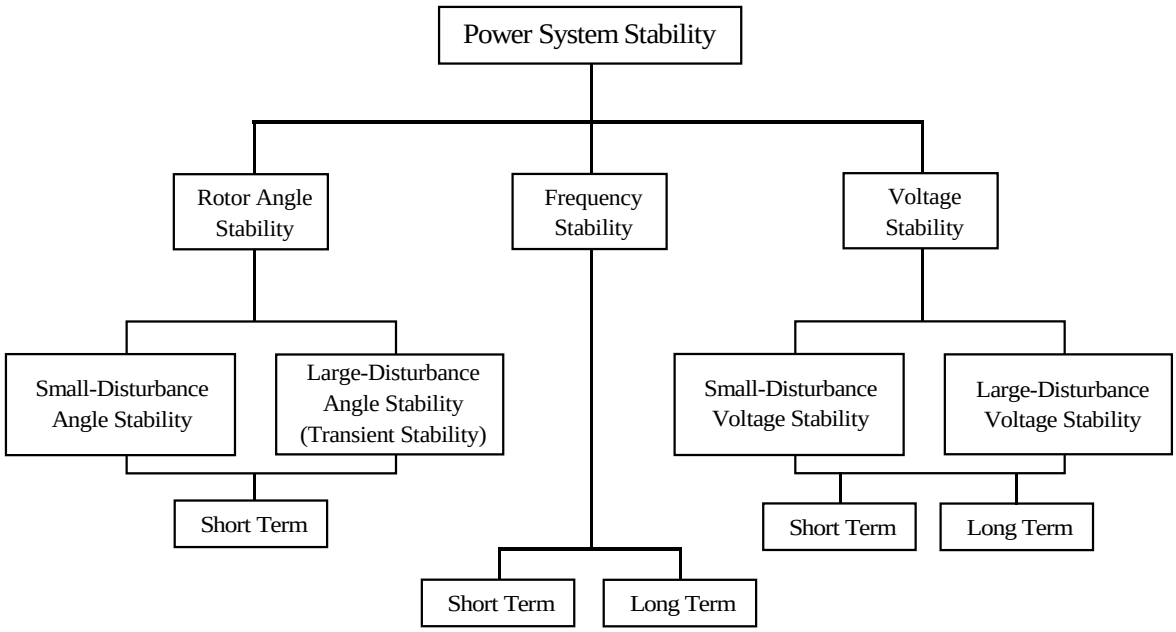

Figure 1.1: **Classification of power system stability [1, 2]**

Power system stability is a complex subject that has challenged power system engineers for many decades. System secured operation is concerned, the power system stability has been recognized as an important problem for power engineers since 1920s [3]. In past, transient instability has been the dominant of stability problem on most systems, and has played much attention of the industries concerning system stability. Now voltage stability, frequency stability and inter-area oscillations have caused much concern. Moreover, power system instability in a large power system can lead to entire system blackout [4].

This overall situation demands the review of traditional transmission methods and practices and the creation of new concepts which would allow the use of existing generation and transmission lines up to their full capabilities without reduction in system stability and security. Another reason that compels the review of traditional transmission methods is the tendency of modern power systems to follow the changes in today's global economy that are leading to deregulation of electrical power markets in order to motivate competition among utilities.

1.3 Flexible AC Transmission Systems (FACTS)

The power flow in the transmission line between two areas is a function of line impedance, the voltage magnitudes of sending and receiving end voltages and the phase angle between the voltages. To illustrate the basic equations of power flow control consider a transmission line connecting two areas is shown in Figure 1.2.

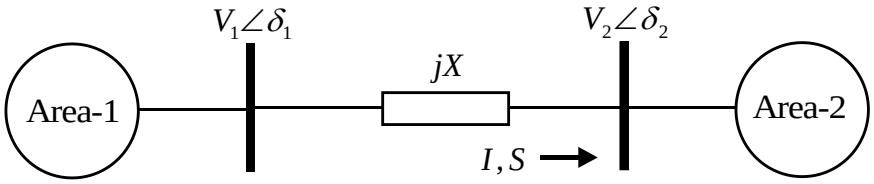

Figure 1.2: **Transmission of power between two areas**

Complex, active and reactive power flows in this transmission system are given as follows respectively:

$$S_1 = P_1 + jQ_1 = V_1 I_1^* \tag{1.1}$$

$$P_1 = \frac{V_1 V_2}{X} \sin\,(\delta_1 - \delta_2) \tag{1.2}$$

$$Q_1 = \frac{V_1 V_2 \cos(\delta_1 - \delta_2) - V_1^2}{X} \tag{1.3}$$

where V_1 and V_2 are the voltage magnitudes of area-1 and area-2 respectively, while δ_1 and δ_2 are phase angles of area-1 and area-2 respectively. X represents the equivalent reactance of the transmission line between two areas.

Hence, the active and reactive powers of the transmission line can be controlled by controlling one or a combination of the power flow parameters. By the introduction of fast acting dynamic control over active and reactive power can increase the stability margins of power transmission and it allows to transmit more power using existing power transmission network.

The invention of fast acting power electronic controllers made the AC transmission network more 'flexible' to adopt the changing conditions caused by load variations and contingencies. This concept and advances in the power electronics led to invent new approach by Electric Power Research Institute (EPRI) in the year 1980, called Flexible AC Transmission Systems or simply FACTS. It makes use of already existing resources in present power systems more efficient and maintains stability in power system.

FATCS is defined as "Alternating current transmission systems incorporating power electronic based and other static controllers to enhance controllability and increase power transfer capability"[5].

FACTS controller is defined as "A power electronic based system and other static equipment that provide control of one or more AC transmission system parameters" [5].

The FACTS controllers can be classified depending on the power electronic devices used in the control as follows:

- Thyristor based controllers
- Voltage source converter (VSC) based controllers

1.3.1 Thyristor Based Controllers

The thyristor based or thyristor controlled FACTS controllers include:

A. Static var compensator (SVC)

B. Thyristor controlled series capacitor (TCSC)

C. Thyristor controlled phase shifting transformer (TCPST)

Each of the above controllers can act on one of the three parameters determining power transmission, voltage (SVC), transmission impedance (TCSC) and transmission angle (TCPST).

A. Static Var Compensator (SVC)

Thyristor control static var compensators are the basic photo type of present FACTS controllers. These controllers were developed in the early 1970's for load compensation of fast changing loads such as steel mills and arc furnaces, they were later adapted for transmission applications. The SVC can produce a compensating reactive current by varying its shunt reactance. It comprises thyristor switched capacitors (TSCs) and thyristor controlled reactors (TCRs) as shown in Figure 1.3. The basic applications of SVC include:

- Increases power transfer in long transmission lines [6]
- Improve voltage stability [5, 7]
- Improve transient and dynamic stability of the transmission system [5]

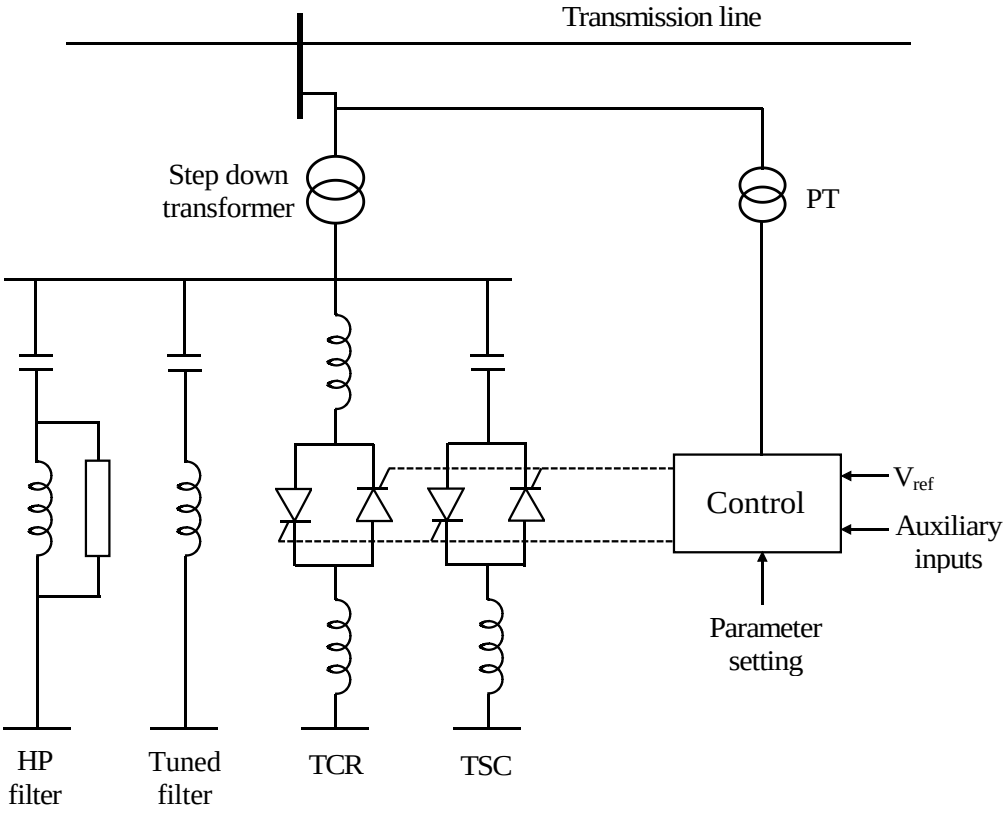

Figure 1.3: **A typical SVC employing TSC and TCR**

B. Thyristor Controlled Series Capacitor (TCSC)

The TCSC is connected in series with the transmission line and hence the voltage compensation is inherently a function of line current. By controlling its effective reactance TCSC can control the voltage across series impedance of a given transmission line.

There are two configurations of TCSC as shown in Figure 1.4.

a) Thyristor switched capacitors

b) Fixed capacitor in parallel with a TCR

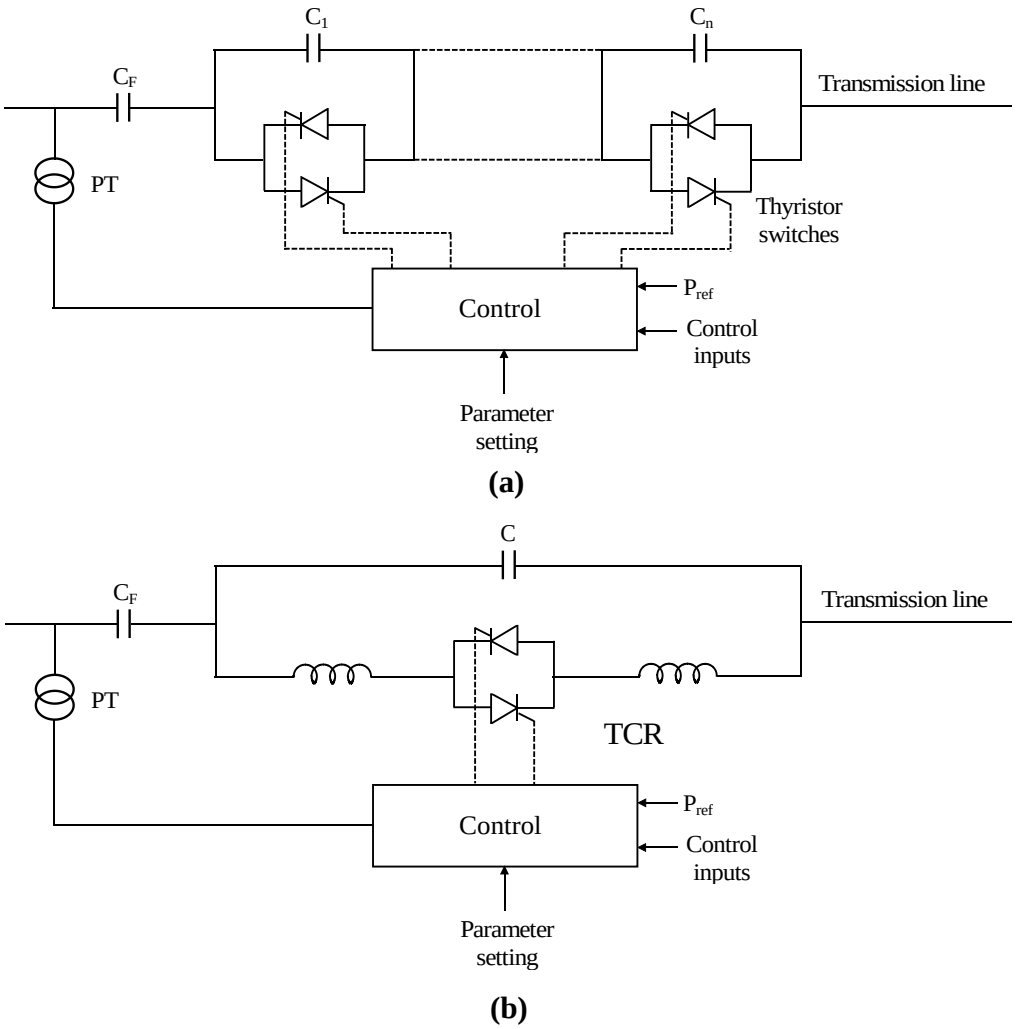

Figure 1.4: **TCSC configuration (a) Thyristor switched capacitors and (b) Fixed capacitor in parallel with a TCR**

In the first configuration, the degree of series compensation depends upon number of series capacitor banks. By controlling the firing angle of the corresponding thyristor pair, the capacitor bank is switched in service or bypassed.

In the second configuration, the variable compensation is obtained by controlling the thyristor conduction period in the TCR. Depending upon conduction of thyristor valves the TCSC can operate in three operating modes such as bypassed, thyristor blocked and vernier control modes.

The basic applications of TCSC include [8]:

- Increase power transfer capacity in tie lines
- Provide power oscillations damping
- Maximize available transfer capability (ATC) of transmission lines
- Improve steady-state and transient stability.

C. Thyristor Controlled Phase Shifting Transformer (TCPST)

The TCPST consists of a shunt connected excitation transformer with appropriate taps, a series boost transformer and a thyristor switch arrangement as shown in Figure 1.5. The TCPST is used to control the system transmission angle by injecting a quadrature voltage in series with the transmission line. Its main motive is to control loop flows and ensure the power flow in the contracted path. These are unable to generate or absorb either real or reactive power and hence any exchange of real and reactive power with the AC system should come from the system itself. Therefore, TCPSTs are not intended to be used in long transmission lines.

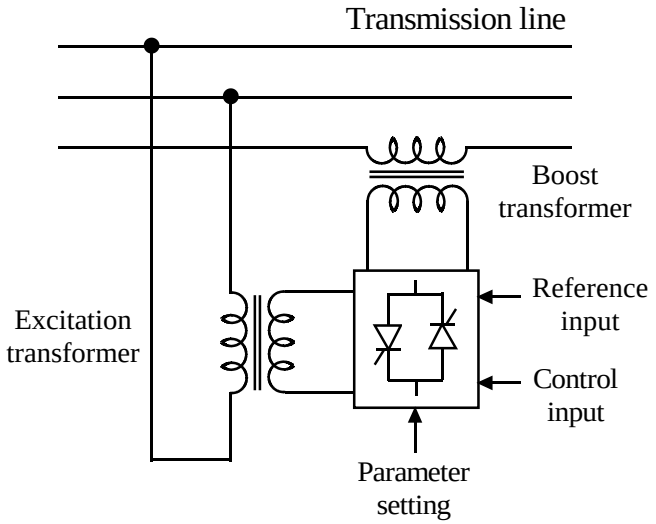

Figure 1.5: **Schematic diagram of TCPST**

The basic applications of TCPST include [8]:

- Controls the voltage magnitude
- Provide low frequency power oscillations damping
- Enhance the transfer capability of AC tie lines

1.3.2 VSC Based Controllers

The VSC based FACTS controllers include:

A. Static synchronous compensator (STATCOM)

B. Static synchronous series compensator (SSSC)

C. Unified power flow controller (UPFC)

This type of FACTS controller generally provides superior performance characteristics over thyristor-based controllers for transmission voltage, effective line impedance, and angle control.

A. Static Synchronous Compensator (STATCOM)

The STATCOM is also known as advanced static var compensator (ASVC). A STATCOM can supply variable reactive power and regulate the voltage of the bus where it is connected. The basic schematic diagram of STATCOM is shown in Figure 1.6. If the converter output voltage increases greater than the system voltage, then the current flows to the system and leads the voltage by 90^0. Whereas the converter voltage falls below the system voltage, then the reactive current flow from the system to the converter and lags the voltage by 90^0. In this way the converter absorbs or delivers the reactive power from the system. However, if the voltages of the converter and the system are equal, then there is no exchange of reactive power.

The basic applications of STATCOM include:

- Regulation of voltage at a load or an intermediate bus.
- Increases power transfer capability
- To damp low frequency oscillations
- Eliminates harmonics and improves power quality in distribution system.

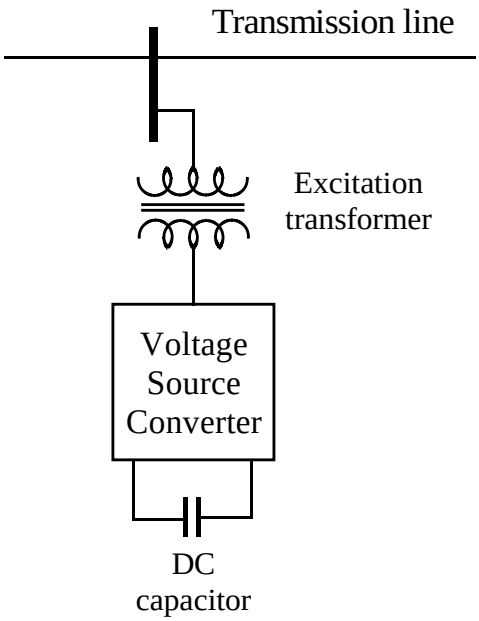

Figure 1.6: **Schematic diagram of STATCOM**

B. Static Synchronous Series Compensator (SSSC)

The SSSC is a VSC based series connected FACTS controller, which can be treated as an advanced type of controlled series compensation. The structure of SSSC was proposed by Gyugyi in 1989 and it is connected in series with the transmission line through a booster transformer, as shown in Figure 1.7. The SSSC generates a controllable compensating capacitive or inductive voltage which helps to control the amount of transmittable power. The SSSC can exchange both real and reactive power with the AC system, simply by controlling the phase angle of the injected voltage with respect to the line current. The exchange of real power requires an energy source that is connected to the DC terminals of the SSSC.

The main applications of SSSC include [5]:

- Damping of system oscillations
- Transient and dynamic stability improvement
- Maintain voltage profile and limits fault currents.

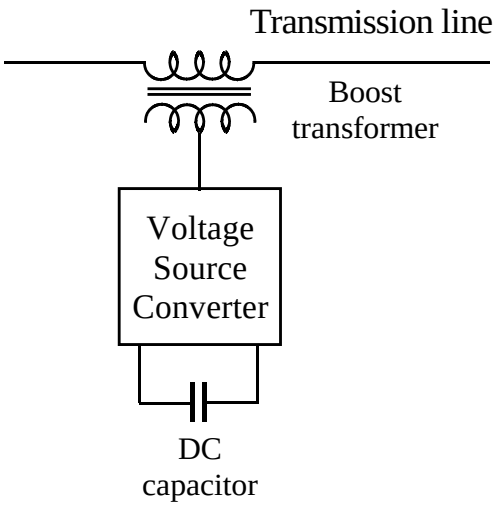

Figure 1.7: **Schematic diagram of SSSC**

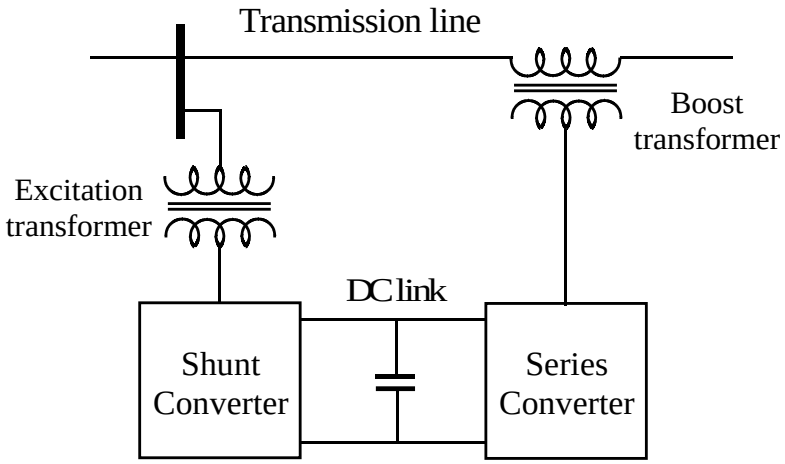

Figure 1.8: **Schematic diagram of UPFC**

C. Unified Power Flow Controller (UPFC)

UPFC is a combination of STATCOM and SSSC that are coupled via a common DC link, to allow bidirectional flow of real power between the series output terminals of SSSC and shunt output terminals of STATCOM. The concept of UPFC was proposed by Gyugyi in 1992 [9], the schematic is shown in Figure 1.8. Since UPFC combines the features of STATCOM and SSSC, it offers major potential advantages for the static and dynamic operation of transmission lines. Hence, the UPFC is able to control concurrently or selectively, all the parameters (such as voltage, impedance and phase angle) affecting power flow in the transmission line. Additionally, it can provide simultaneous real and reactive series line compensation without an external electric energy source. This is a hybrid controller that can control voltage, active and reactive power of the line. The basic function

of shunt converter is to supply or absorb the real power demanded by series converter at the common DC link to support the real power exchange resulting from the series voltage injection.

The main applications of UPFC include:

- Active and reactive power control
- Damping of oscillations
- Transient and dynamic stability improvement
- Maintain voltage profile
- VAR compensation

1.4 Review of Literature

In this section a literature survey related to power system oscillations and control measures to damp these oscillations is highlighted. The power system may be thought as a large interconnected and complex system with many lightly damped electromechanical mode of oscillations. The mechanical inertia and power angle characteristics led to oscillations of 1-3Hz observed in hydro generators at light load, when they operated in parallel. During such oscillations, mechanical kinetic energy is exchanged in the form of electric power between synchronous generators and the network. The speed governors are able to preserve the frequency stability but they cannot guarantee the damping of oscillations among paralleled generators [10].

1.4.1 Convectional Control Methods

DeMello and Concordia [11] used single machine infinite bus (SMIB) system to analyze the nature of the low frequency electromechanical oscillations in power systems. They were the first to explain the phenomena of oscillations by the concepts of synchronous and damping torques, and stated that inadequate damping torque is the reason for oscillations or instability of power system. The excitation controller design has drawn sizable consideration [12] to control synchronous generator and stabilize power system oscillations. Here, the operation of excitation control continues to maintain generator voltage and reactive power output. A high response exciter is helpful in adding synchronizing torque. However, on account of performing, it introduces negative damping. One of the conventional efficient methods to

meet the conflicting exciter behavior with respect to system stability is to install a power system stabilizer (PSS). The basic function of a PSS is to produce an auxiliary stabilizing signal to make electrical torque component in phase with speed variations.

In past two decades, enormous research being conducted on designing of PSS for power system stability enhancement. Different methods like linear design methods [13-17], nonlinear designing methods [18-21] and intelligent optimization methods [27-35] have been proposed. An efficient pole placement method is developed to design a power system stabilizer in an unstable nine machine power system presented in [13]. A robust PSS designed by shifting the real parts of poles to any desired positions while preserving the imaginary parts is discussed in [14]. Using differential geometric linearization approach PSS is designed in a multi-machine system presented in [15]. To enhance power system damping under multi-operating conditions probabilistic eigenvalue sensitivity based PSS is investigated in [16]. H2 optimal control algorithm which applied for adaptive PSS design in SMIB system is presented in [17]. The authors of [18] discussed the design of PSS using frequency response methods based on the concept of damping torque. A self-tuned PSS is developed based on simple fuzzy logic controller (FLC) in a SMIB power system is published in [19]. The authors of [20] had introduced an indirect adaptive FLC based PSS controller using Lyapunov's synthesis method. In [21], dynamic output feedback model-based fuzzy PSS is designed for robust performance of power system. Many modern heuristic optimization techniques (such as genetic algorithms (GA) [22], simulated annealing (SA) [23], particle swarm optimization (PSO) [24], bacterial foraging optimization (BFO) [25], differential evolution (DE) [26] etc.,) were introduced and have been successfully applied for design of PSSs to improve the power system dynamic stability. Optimal PSSs design using GA in a multi-machine power system is presented in [27, 28] and using SA is discussed in [29, 30]. Novel PSSs parameter searching in a multi-machine power system using PSO is proposed in [31-33]. Based on bacteria foraging technique an attempt to optimize simultaneously the control parameters of PSS in a multi-machine system is presented in [34]. The damping of electromechanical modes in a multi-machine power system over large operating conditions using DE tuned optimal PSSs is introduced in [35].

However, with increasing the transmission line loading over very long distance in a multi-machine system, these PSSs cannot guarantee the damping of inter-area oscillations if the operating conditions vary abruptly. Additionally, PSS can cause great variations in the

voltage profile under severe disturbances and they may even result in leading power factor (PF) operation, which causes losing system stability [36]. In such scenarios, it would be feasible to install Flexible AC Transmission Systems (FACTS) controllers that were proposed by Hingorani and Gyugyi [5].

1.4.2 FACTS Controllers

In the last few years, FACTS controllers have gained great research interest due to their versatile capability in mitigating power system stability issues. FACTS controllers have been extensively studied and analyzed for various power system problems such as power flow control, power transfer capability enhancement, voltage regulation, enhancing power system stability and damping the power system oscillations. Here, a brief literature review is given for the FACTS controllers like TCSC, SVC and STATCOM applied for power system stability and damping of power oscillations problems.

A. Static Var Compensator (SVC)

In past, many researchers have applied SVC controller in power systems to enhance system dynamic performance and damping the low frequency oscillations [37-49]. The SVC controller has been installed successfully to improve the transient stability of a synchronous machine [37]. A fundamental analysis of SVC for enhancing the power system stability is presented in [38]. In the articles [39-42], SVC has been analyzed for damping of low frequency oscillations. Here, it has been shown that SVC enhances the system damping of local along with inter-area oscillations. Self-tuning and model reference adaptive stabilizers for SVC controller have been proposed and also designed in [43-45]. A static method is proposed to design a full-scale fuzzy PID based SVC controller for power system stability control [46]. An adaptive backstepping sliding mode H_∞ controller for SVC controller is designed using modified adaptive backstepping sliding mode method is given in [47]. Bacteria foraging optimization algorithm based SVC controller is proposed for the suppression of power system oscillations [48]. Also, an online trained wavelet neural network controller based SVC is designed [49] in order to enhance transient stability of power system.

B. Thyristor Controlled Series Capacitor (TCSC)

The effective control over long distance transmission lines, the thyristor controlled series capacitor (TCSC), one of the most popular controllers of FACTS, can be installed in series with the transmission lines. TCSC damping controllers are installed in the network where the controllability and observability of the inter-area oscillations are better. The application of TCSC for damping of inter-area oscillations is discussed in [50], and enhancing transient stability can be found in [51]. A study on TCSC controller design for stability improvement is carried in [52], and a novel hierarchical controller is developed to enhance both steady state and dynamic stability enhancement. A linearized discrete time model of TCSC is proposed in [53], which is derived in d-q axis frame and then linearized around an operating point. A fuzzy logic based TCSC controller to suppress the inter-area oscillations is discussed in [54], in which an oscillation transient energy function is applied to design the TCSC fuzzy logic damping controller. With the integration of both fuzzy logic and PI controllers a self-tuning fuzzy PI based TCSC controller is proposed in [55] to enhance power system damping. To reduce complexity of fuzzy systems, a reduced rule-base fuzzy PI controller for TCSC is developed based on singular value decomposition technique in [56].

Furthermore, the control tuning problem of TCSC damping controller is evaluated using optimization algorithms [57-61] can be found in literature. A novel output feedback TCSC controller design for damping critical oscillations using SA is presented in [57]. A PSO based TCSC power system oscillations damping controller design in a multi-machine power system is proposed in [58]. Moreover, a comparison between GA and PSO in designing a TCSC damping controller to enhance power system stability is presented in [59]. In this, it is concluded that the performance of PSO is better than that of GA from an evolutionary point. Whereas the computational time is low for GA compared to PSO algorithm. TCSC controller modeling, simulation and optimal tuning using DE algorithm to enhance power system stability is discussed in [60]. In this, a comparison between PI and lead-lag controller is presented and it is concluded that the lead-lag based TCSC controller had better damping characteristics than PI based controller. Recently, the bacteria foraging algorithm is used to design the TCSC damping controller for a multi-machine system [61].

C. Static Synchronous Compensator (STATCOM)

The emergence of FACTS devices and in particular GTO thyristor-based STATCOM has enabled such technology to be proposed as serious competitive alternatives to conventional SVC [62]. From the viewpoint of power system dynamic stability, the STATCOM provides better damping characteristics than the SVC as it is able to transiently exchange active power with the system. The effectiveness of the STATCOM to control the power system voltage is presented in [63]. Abido [64] presented a singular value decomposition (SVD) based approach to assess and measure the controllability of the poorly damped electromechanical modes by STATCOM. It was observed that the electromechanical modes are more controllable via phase modulation channel. It was also concluded that the STATCOM-based damping stabilizers extend the critical clearing time and enhance greatly the power system transient stability. Haque [65] demonstrated that by the use of energy function, a STATCOM can provide additional damping torque to the low frequency oscillations in a power system. The design and location of STATCOM using PSO algorithm is presented in [66]. A STATCOM based variable structure for power system oscillations damping is proposed in [67]. The two internal controllers of STATCOM namely AC and DC voltage controllers are discussed in [68]. Moreover, it is reported that the joint operation of these internal controllers could produce negative interactions.

The literature survey carried out in [69] shows that the number of publications, applications of FACTS to power system stability in particular, has a tremendous increment. In summary, the Table 1.1 shows the performance analysis of above mentioned FACTS controllers. First column of Table 1.1 shows that series controller like TCSC is good for load flow control. While, shunt connected controllers like SVC and STATCOM have great voltage stability performance. Whereas TCSC controller has very good transient stability performance compare to all other controllers. In case of dynamic stability all controllers performs well. Hence, to enhance the overall stability of the power system and to damp the power system oscillations, combined effect of these series and shunt controllers is much needed.

1.4.3 Coordination of PSS and FACTS Controllers

The internal controllers like PSSs are mounted on the generators, can damp the local mode of oscillations effectively, but they cannot promise sufficient damping to inter-area mode of oscillations. In such cases, the external controllers like FACTS controllers, are installed in the power transmission network help to provide sufficient damping to inter-area mode of

oscillations. Therefore, the coordination of PSS and FACTS controllers is needed to damp all types of power system oscillations effectively.

Table 1.1: **Performance analysis of FACTS controllers [70]**

FACTS Controller	Load flow control	Voltage stability	Transient stability	Dynamic stability
SVC	★	★ ★ ★	★	★ ★
STATCOM	★	★ ★ ★	★ ★	★ ★
TCSC	★ ★	★	★ ★ ★	★ ★

In recent past, numerous publications [71-89] reported the coordination of PSS and FACTS damping controllers for maintaining or enhancing electromechanical oscillations damping in power systems. The coordinated design of PSS with TCSC using phase compensation method is discussed in [71] and decentralized state feedback control method is presented in [72]. The authors in [73] proposed the decentralized model control method for pole placement in multi-machine system by coordinated tuning of PSS and FACTS controllers. The probabilistic theory to the coordinated design of damping controller is presented in [74]. Very recently, coordinated design of PSS and FACTS controller to enhance the dynamic characteristics of power system by zero dynamics method is provided in [75].

Moreover, several new optimizations algorithms have been successfully applied to coordinated design of PSS and FACTS controllers to enhance the overall stability of a power system. The coordination of PSS with SVC using GA is discussed in [76] and the authors of [77] applied bacteria foraging optimization (BFO) algorithm. A nonlinear programming model for simultaneously coordinated parameters design of PSS and STATCOM using SA is presented in [78]. A robust coordination scheme to improve the stability of a power system by optimal design of multiple and multi-type damping controllers using DE is observed in [79]. In addition to this, in the literature, a few proposals have been put forth over the coordinated design of PSS and TCSC controller for multi-machine system via optimization algorithms. A pole placement technique for PSS and TCSC damping stabilizers using simulated annealing is presented in [80]. Power system stability enhancement via robust coordinated design of a PSS and TCSC using GA is discussed in [81, 82]. However, these works are limited to SMIB system and moreover GA has slow convergence rate and it needs very long computational time that may vary from few minutes to hours depending upon the

size of the problem under study. In [83, 84] PSO technique is used to develop a simultaneous coordinated designing of TCSC and PSS. The performance of PSO is better than GA in the evolutionary point of view but the computational time is high. Moreover, in PSO, the fixed values of the parameters cause the unnecessary fluctuations of particles when the algorithm reaches convergence [85]. The bacterial swarm optimization algorithm employed to coordinated design of TCSC and PSS in a multi-machine power system is presented in [86].

The coordinated tuning of SVC and TCSC is discussed by few authors. A nonlinear design technique based on direct feedback linearizing is used to deduce the control scheme for the TCSC and SVC. The coordination between two pieces of equipment is also designed in [87]. In order to adapt the changes of operating modes and active power of generators, a neural network algorithm is applied in [88] to determine the control parameters of SVC and TCSC damping controller. From these, the authors treated SVC as supplement of the TCSC. Finally, [89] the integral of squared error technique is used for global tuning of the stabilizers and here the authors consider multi-machine power system equipped with a TCSC and a SVC as well as three PSSs is applied to demonstrate the efficiency and robustness of the proposed tuning procedure.

From the above research background, we summarized that the use of PSS can provide good damping to local mode of oscillations and FACTS controllers can provide good damping to inter-area mode of oscillations. By the help of series FACTS controllers the transient stability of the system is greatly enhanced, with the help of shunt FACTS controllers one can maintain voltage stability of the system. Hence, to damp local as well as inter-area mode of oscillations and to enhance overall system dynamic performance a hybrid coordinated design of PSS with series and shunt FACTS damping controllers is required. Moreover, from the considered literature the validation of coordination design in real-time not exist till date. To overcome the above challenges and to demonstrate the hybrid design, the following contributions are made in this thesis.

1.5 Research Objectives

Though technological barriers exist, as in most technology areas, it is important to overcome them by developing proper understanding of the process with related attributes. The subsequent chapters explained the various efforts directed for improving the power system

oscillations damping applied to multi-machine power system. Extensive literature review reveals that the coordinated design of PSS with multiple FACTS damping controllers are least explored. Similarly, the present work emphasizes real-time validation of hybrid coordinated designs in multi-machine power system.

Based on these guiding principles, the objectives of the current research are as follows:

- To explore the existing conventional methods and models for power system stability study.
- To develop a coordinated design of PSS and different FACTS damping controllers using recent stochastic optimization algorithms.
- To develop a novel hybrid design of PSS with series and shunt FACTS damping controllers in multi-machine power system using two efficient optimization techniques.
- To validate proposed hybrid designs in real-time using Opal-RT hardware simulator.

1.6 Thesis Outline

The other chapters of this thesis are organized as follows:

Chapter 2 gives an overview of basic operation, modelling and interfacing of power system components. In this, modelling of several power system components like synchronous generators, interconnecting transmission network, static loads and other excitation devices such as AVR & PSS are briefly discussed. The operation of simple SMIB test power system with conventional excitation system is examined under various load conditions with severe disturbance applied on the system. The simulations results are compared with different control techniques like no control, AVR with no PSS and AVR with PSS. The basic knowledge of these concepts is essential for controller development in the subsequent chapters.

In chapter 3, the modelling of various FACTS controllers and their optimal designs applied to power oscillations damping (POD) are considered. The detailed comparison between proportional integral derivative (PID) based FACTS POD controllers and Lead-Lag based FACTS POD controllers is discussed. Here, the FACTS controllers like SVC, TCSC and STATCOM are modelled along with POD stabilizers. To find the optimal parameter values of various FACTS damping stabilizers conventional PSO algorithm is used. An objective

function is formulated based on speed variations and voltage variations and the same is minimized using PSO algorithm for finding optimal values. Finally, the performance analysis of different FACTS POD stabilizers over a wide range of loading conditions is discussed for a six cycle fault.

Chapter 4 deals with the coordinated design of PSS and various FACTS damping controllers. The coordinated problem is formulated as an optimization problem and the objective function of that problem is solved using advanced adaptive PSO (AAPSO) algorithm. For the formation of eigen value based objective function, one has to linearize the power system with its components. Hence, the linearization procedure and participation factor method is explained here. The linearization of power system with PSS and different FACTS controller is evaluated to find the poorly damped electro mechanical eigen values of the system. The test system is analyzed with different coordinated designs like (PSS+SVC), (PSS+TCSC) and (PSS+STATCOM) controllers. The robustness of proposed coordinated controllers is tested by comparing its damping characteristics to that of individual controller designs. The chapter concluded by proving that the coordinated design gives a better damping effect and good settling time of oscillations.

In chapter 5, the hybrid coordinated design of PSS with series and shunt FACTS damping controller is presented. The hybrid designs such as (PSS+TCSC+SVC) and (PSS+TCSC+STATCOM) controllers are proposed. The linearization form of power system with these controllers is derived in order to find the eigen values of the system. Here, invasive weed optimization (IWO) algorithm is used to minimize the damping factors and damping ratios based on objective function. The optimal control parameter values of different controllers in hybrid coordinated design are obtained at the end of optimization algorithm. The small signal analysis as well as time domain simulations are provided to prove the effectiveness and robustness of proposed design. The results are compared for different control designs over a wide range of load conditions.

Chapter 6 presents the hybrid coordinated control design of PSS with series and shunt FACTS controllers in multi-machine power system via AAPSO and IWO algorithms. Here, two test power systems are considered for analysis: (a) three-machine nine-bus test power system and (b) two area four-generator eleven-bus power system. The eigen value analysis along with transient analysis of test power system is done using MATLAB. The performances of proposed designs are compared with other control schemes under different

loading conditions. The damping factors, damping ratios and settling time of oscillations are compared with different controllers under different load conditions.

In chapter 7, the real-time implementations of different control designs are carried out to validate the proposed control designs in real world. Opal-RT hardware simulator is used for real time validations. In this, the procedure to interface MATLAB models with Opal-RT hardware simulator environment is clearly explained. The laboratory setup of Opal-RT hardware simulator is discussed. The real-time simulator results are presented and compared for different control schemes under different load conditions.

Finally, the conclusions and suggestions for future work are discussed in chapter 8. It gives overall summary of work done and concludes the present study. It explains the effectiveness and robustness of hybrid coordinated designs to damp the power oscillations under severe disturbances. It also, explains the necessity of validation for proposed designs in real-time. Further, some suggestions on the extension to potential topics for future research are proposed.

1.7 Summary

This chapter highlights the reasons for inter-connections and the difficulties that occur while constructing a new transmission network. The full utilization of the transmission lines without proper controller could result in the rapid failure of the entire system. The chapter also gives the introduction to the classification of power system stability problems and FACTS controllers. Section 1.4 provides the insight into various past developments in the area of power system stability. For the sake of simplicity, it is divided into three main sections. Section A focuses on the brief history of conventional control methods. Section B describes the FACTS damping controllers. Section C gives the literature review about coordination of PSS and FACTS damping controller. The problem of power system oscillation damping is overcome by the coordinated design of PSS and FACTS controllers. This design has ability to damp local as well as inter-area mode of oscillations and to enhance overall system dynamic performance under severe disturbances. The modelling of several power system components and operation of conventional PSS are explained in next chapter.

Chapter 2

Modeling and Operation of Power System Components

Chapter 2

Modelling and Operation of Power System Components

2.1 Introduction

The main objective of this chapter is to present the brief insight in the modeling of various power system components and their basic operation with conventional controllers under severe disturbance.

2.2 Modelling of Power System Components

Studies of electrical power systems are based on the simulation of actual phenomena using models behaving exactly in the identical way as the elements in the physical system. Component modeling thus becomes very important. In research, it is necessary to have models permitting precise and detailed simulation. The different parameters must be accessible and the models are required to follow the physical process as closely and faithfully as possible. Then it is required to solve mathematical equations governing these phenomena. Modeling of active elements such as, generator is relatively difficult while that of passive elements such as transmission line, inductive VAR compensator, etc., are easier. Passive circuit elements are mostly modeled by their parameters in the equivalent circuits while the active power system components are modeled by their operation in steady, transient and sub-transient state. The overall power system representation includes models for the following individual components

- Synchronous generators
- Interconnecting transmission network
- Static loads
- Other devices such as AVR&PSS

The model used for each component should be appropriate for transient stability analysis, and the system equations must be organized in a form such that they are suitable for applying numerical methods. As we will see in what follows, the complete system model consists of a set of differential equations and algebraic equations.The transient stability analysis is thus a differential algebraic initial-value problem.

2.2.1 Synchronous Machine Modelling

In a report prepared by IEEE task force in 1986 [90], modeling of synchronous machine is varied from one to six depending on the degree of detail used. It is suggested that [91] the model 1.1 (third order model) which contains field circuit with one equivalent damper on q-axis is very accurate for large disturbance stability studies and virtually exact for small disturbances with intermediate complexity. Hence, in this study the synchronous machine is represented as model 1.1. For this, the governing differential equations for i^{th} machine are as follows:

$$\dot{\delta}_i = \omega_i - \omega_0 \tag{2.1}$$

$$\dot{\omega}_i = \frac{D_i}{M_i}\left[\omega_i - \omega_0\right] + \frac{\omega_0}{M_i}\left[P_{mi} - P_{ei}\right] \tag{2.2}$$

$$\dot{E}'_{qi} = \frac{1}{T'_{d0i}}\left[E_{fdi} - (X_{di} - X'_{di})I_{di} - E'_{qi}\right] \tag{2.3}$$

Following a disturbance, currents are induced in the machine rotor circuits. Some of these induced rotor currents decay more rapidly than others. Machine parameters that influence rapidly decaying components are called the sub-transient parameters while those influencing the slowly decaying components are called the transient parameters and those influencing sustained components are the synchronous parameters.

In most of the research articles, the effect of rotor damper windings is neglected. In that case, the differential equations (2.1)-(2.3) describe the mathematical model of a synchronous machine. Throughout this thesis we follow the third order representation. The algebraic equation with this representation is given by

$$E_{di} = -r_{ai}I_{di} + X_{qi}I_{qi} \tag{2.4}$$

$$E_{qi} = -r_{ai}I_{qi} + E'_{qi} - X'_{di}I_{di} \tag{2.5}$$

$$P_{ei} = V_{di}I_{di} + V_{qi}I_{qi} \tag{2.6}$$

2.2.2 Load Modelling

The power system loads, other than motors represented by equivalent circuits, can be treated in several ways during the transient period. The commonly used representations are static impedance or admittance to ground, constant currents at fixed power factor, constant real and

reactive power, or a combination of these representations. The constant power load is either equal to the scheduled real and reactive bus load or is a percentage of the specified values in the case of a combined representation. The parameters associated with the static impedance and constant current representations are obtained from the scheduled bus loads and the bus voltages calculated from a load flow solution for the power system prior to a disturbance. The initial value of current for a constant current representation is obtained from

$$I_{Li0} = \frac{P_{Li} - Q_{Li}}{V_{Ti}^*} \tag{2.7}$$

where P_{Li} and Q_{Li} are the scheduled bus loads, and V_{Ti} is the calculated bus voltage. The current I_{Li0} flows from bus i to ground, that is, to bus 0. The magnitude and power factor angle of I_{Li0} remain constant. The static admittance y_{i0} is used to represent the load at bus i, can be obtained from

$$(V_{Ti} - V_0) y_{i0} = I_{Li0} \tag{2.8}$$

where V_0 is the ground voltage, equal to zero. Therefore,

$$y_{i0} = \frac{I_{Li0}}{V_{Ti}} \tag{2.9}$$

Multiplying both the dividend and divisor of above equation by V_{Ti}^* and separating the real and imaginary components,

$$g_{i0} = \frac{P_{Li}}{(V_{Ti})^2} \text{ and } b_{i0} = \frac{Q_{Li}}{(V_{Ti})^2} \quad \text{where} \quad y_{i0} = g_{i0} - jb_{i0}$$

2.2.3 Transmission Network Representation

In stability studies, it has been found adequate to represent the network as a collection of lumped resistances, inductances, and capacitances and to neglect the short-lived electrical transients in the transmission system [92]. As a consequence of this fact, the terminal constraints imposed by the network appear as a set of algebraic equations which may be conveniently solved by matrix methods. The network admittance matrix may be written in partitioned form as

$$Y = \begin{bmatrix} y_1 & y_{12} \\ y_{21} & y_2 \end{bmatrix} \tag{2.10}$$

In the portioned matrix, the subscript 1 is associated with nodes to which controlled sources are connected and subscript 2 refers to those are not connected to the controlled sources. In this analysis, information about nodes associated with subscript 2 is not necessary, and for this reason they are eliminated by a series of single row and column reductions in accordance with

$$Y_R = y_1 - y_{12} y_2^{-1} y_{21} \tag{2.11}$$

The resultant network equations in terms of the reduced admittance matrix are

$$I = Y_R V \tag{2.12}$$

These may be written in expanded form as

$$\begin{bmatrix} I_N \\ I_M \end{bmatrix} = \begin{bmatrix} Y_{NN} & Y_{NM} \\ Y_{MN} & Y_{MM} \end{bmatrix} \begin{bmatrix} V_N \\ V_M \end{bmatrix} \tag{2.13}$$

where, subscript N denotes nodes connected to synchronous machines represented in detail by Park's equations and M denotes nodes behind transient reactance of machines represented by fixed voltages.

2.2.4 Axis Transformation

Equations (2.1)-(2.3) describe an individual machine with respect to its own reference frame. In general the reference frame of each machine is different from that of any other machine as well as from the common reference frame rotating at synchronous speed. Consequently, it is necessary to perform axis transformation at each connection node in order to relate the components of voltages and currents expressed in the *d*, *q* reference axis of each machine to the synchronously rotating reference axis *D*, *Q* of the network [92]. Phasor relations between the two reference frames are shown in Figure 2.1. On its basis, the transformation of e_d, e_q to e_D, e_Q and of i_D, i_Q to i_d, i_q may be stated as

$$\begin{bmatrix} e_d \\ e_q \end{bmatrix} = \begin{bmatrix} \cos\alpha & \sin\alpha \\ -\sin\alpha & \cos\alpha \end{bmatrix} \begin{bmatrix} e_D \\ e_Q \end{bmatrix} \tag{2.14}$$

$$\begin{bmatrix} i_D \\ i_Q \end{bmatrix} = \begin{bmatrix} \cos\alpha & -\sin\alpha \\ \sin\alpha & \cos\alpha \end{bmatrix} \begin{bmatrix} i_d \\ i_q \end{bmatrix} \tag{2.15}$$

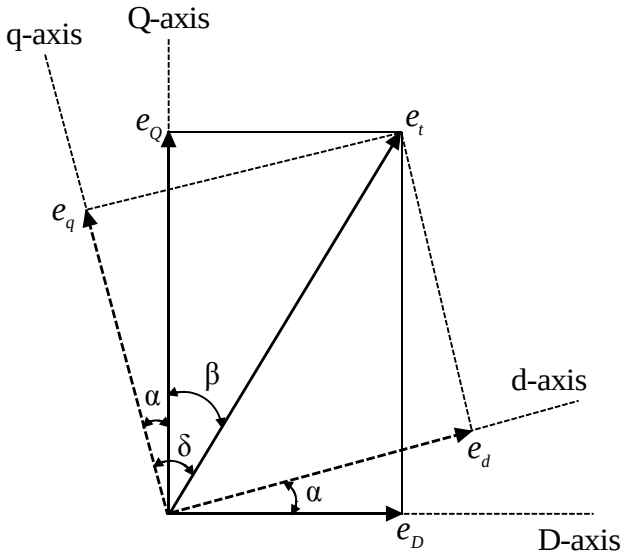

Figure 2.1: **Axis transformation phasor diagram**

2.2.5 Excitation System Modeling

The main objective of the excitation system is to control the field voltage of the synchronous machine and there by field current. The field current is controlled so as to regulate the terminal voltage of the machine. The conventional excitation system consists of automatic voltage regulator (AVR) and power system stabilizer (PSS), which is shown in Figure 2.2. The AVR normally controls the generator stator terminal voltage. But if the fast acting exciters have high gain AVR, it can leads to oscillatory instability in power systems. This type of instability can endanger system security and limits power transfer. A cost efficient, simple and effective solution to this problem of oscillatory instability is to provide damping for generator rotor oscillations.

The basic function of PSS is to add damping to the generator rotor oscillations by controlling its excitation using auxiliary stabilizing signals. To introduce a damping torque component, speed deviation ($\Delta\omega_i$) is used as a logical signal for controlling generator excitation. A widely used conventional PSS structure consists of a gain, washout and phase compensation blocks. The stabilizer gain K_i determines the amount of damping introduced by the PSS. The washout block acts as a high-pass filter with the time constant T_W high enough to allow signals associated with speed oscillations and it is used to restrict the steady state changes in speed. The value of T_W is not critical in view of washout function and its value in the range

1 - 20s. The phase compensation block provides the appropriate phase-lead signals such that the phase lag between the exciter input and the electrical torque is compensated. In this PSS design two stage phase compensation is constructed with two first order blocks. The differential equation that governs the AVR with PSS is given by

$$\dot{E}_{fdi} = \frac{1}{T_A}\left[K_A(V_{ti\,ref} - V_{ti} + U_{PSSi}) - E_{fdi}\right] \tag{2.16}$$

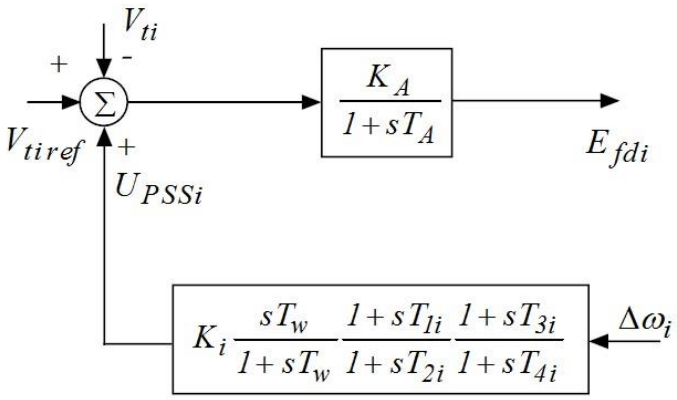

Figure 2.2: **Conventional Excitation System with AVR & PSS**

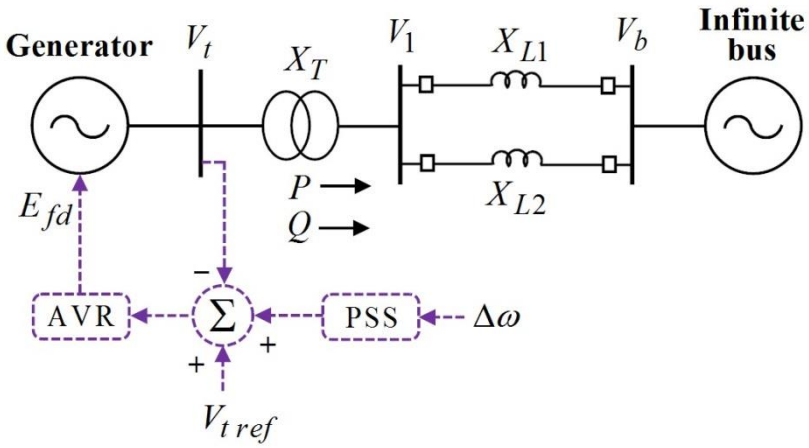

Figure 2.3: **SMIB system equipped with conventional AVR & PSS**

2.3 Operation of SMIB System with Conventional Excitation System

To analyze the basic operation of excitation system, a single machine infinite bus system with conventional AVR & PSS shown in Figure 2.3 is considered. Here, a synchronous generator is connected to infinite bus through a transformer with impedance X_T and two parallel transmission lines with impedances X_{L1} and X_{L2}. The generator terminal voltage

and infinite bus voltages are represented by V_t and V_b respectively. The system data used for this analysis is given in Table 2.1

Table 2.1: **Test system parameters**

Generator	:	$X_d = 1.0pu,\ X_d^{'} = 0.3pu,\ X_q = 0.8pu,$ $T_{d0}^{'} = 5.044s,\ M = 8,\ D = 0,\ f = 60Hz.$
Line & Transformer	:	$X_{L1} = X_{L2} = 0.6pu,\ X_T = 0.1pu.$
AVR & PSS	:	$K_A = 10,\ T_A = 0.01s,\ K_1 = 0.5,$ $T_1 = T_3 = 0.324,\ T_2 = T_4 = 0.033,\ T_w = 5.$

Table 2.2: **Loading conditions considered**

Normal Loading	:	$P = 1.0pu, Q = 0.25pu.$
Heavy Loading	:	$P = 1.2pu, Q = 0.35pu.$
Light Loading	:	$P = 0.8pu, Q = 0.15pu.$
Leading PF condition	:	$P = 0.8pu, Q = -0.15pu.$

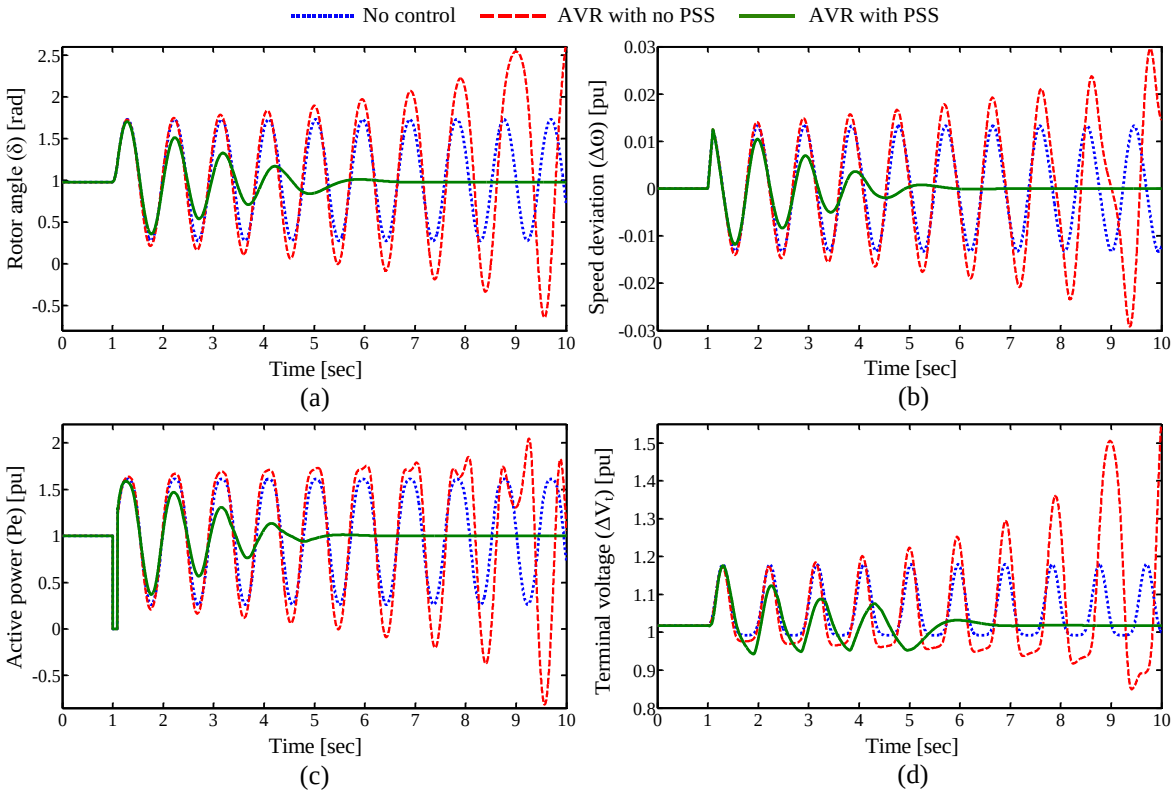

Figure 2.4: **System dynamic response under normal load (a) rotor angle (b) speed variation (c) active power (d) terminal voltage**

The conventional AVR & PSS is tested under a 6-cycle fault disturbance with different loading conditions given in Table 2. The 3-phase fault is applied on one of the transmission lines with starting time 1.0 sec, and it is cleared at 1.1 sec (i.e. fault clearing time $T_c = 100ms$). The dynamic responses of the test system under different loading conditions are shown in Figure 2.4 – Figure 2.7. In these figures, the comparison made over the system responses for different control schemes such as, No control, AVR with no PSS and AVR with PSS. Figures 2.4(a), 2.5(a), 2.6(a) and 2.7(a) show the rotor angle response for different control schemes under normal, heavy, light and leading PF loading respectively. Similarly, in each figure, from 2.4(b) - 2.7(b) represents speed variation of the generator, from 2.4(c) - 2.6(c) represents active power variation and from 2.4(d) - 2.6(d) represents terminal voltage variations of the generator in different loading conditions. In each loading condition, the system which has AVR with PSS gives better damping characteristics. The system consists of AVR with no PSS gives negative damping characteristics and the oscillations keep on increasing.

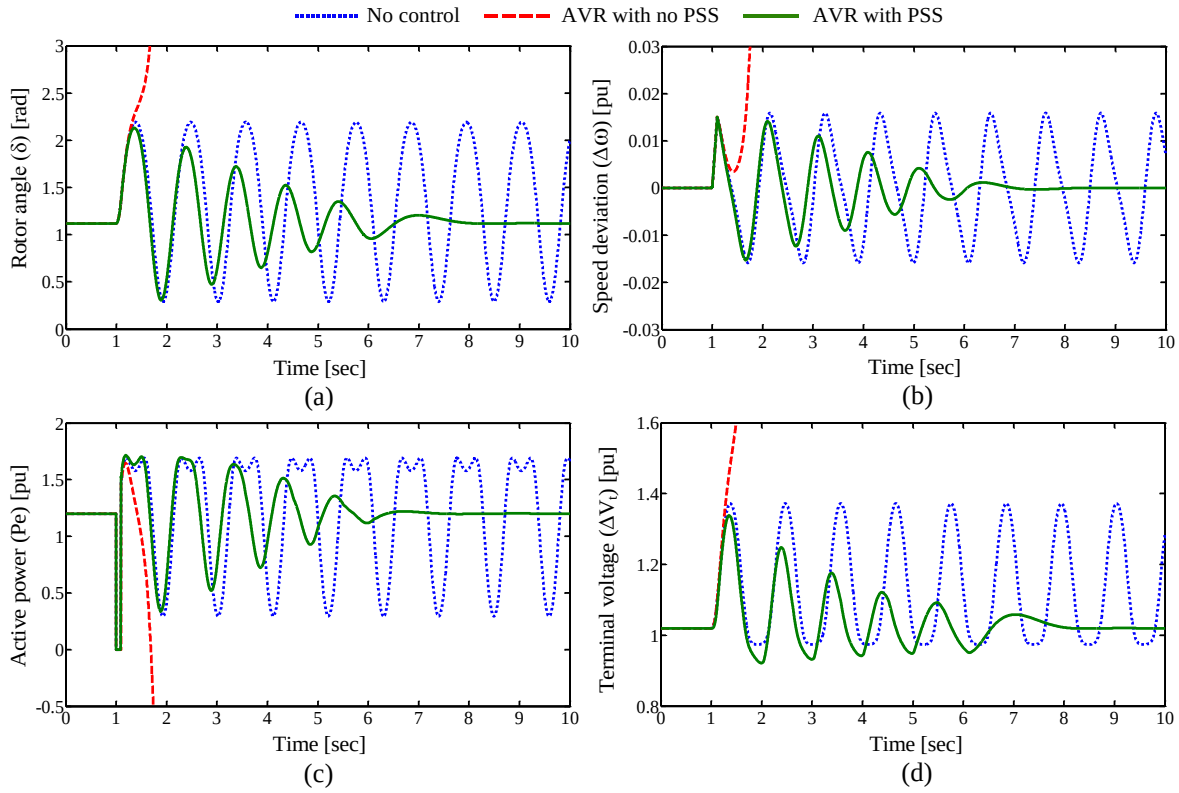

Figure 2.5: **System dynamic response under heavy load (a) rotor angle (b) speed variation (c) active power (d) terminal voltage**

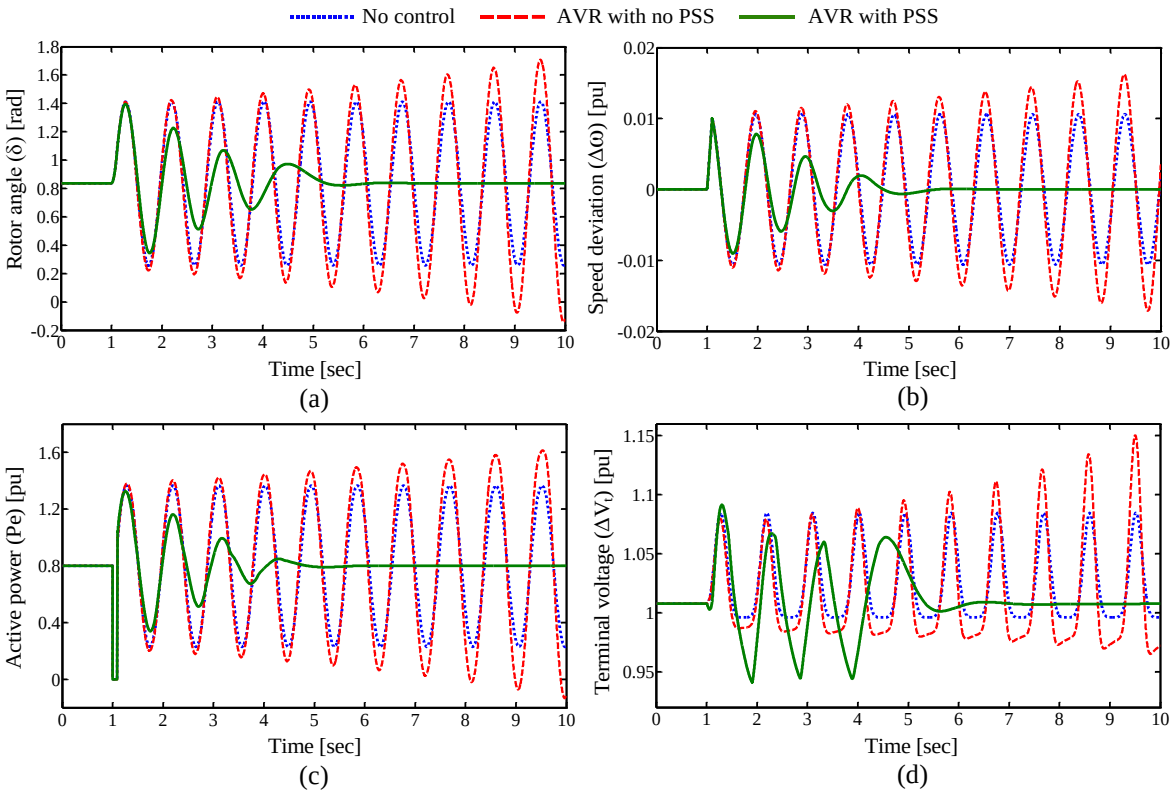

Figure 2.6: S**ystem dynamic response under light load (a) rotor angle (b) speed variation (c) active power (d) terminal voltage**

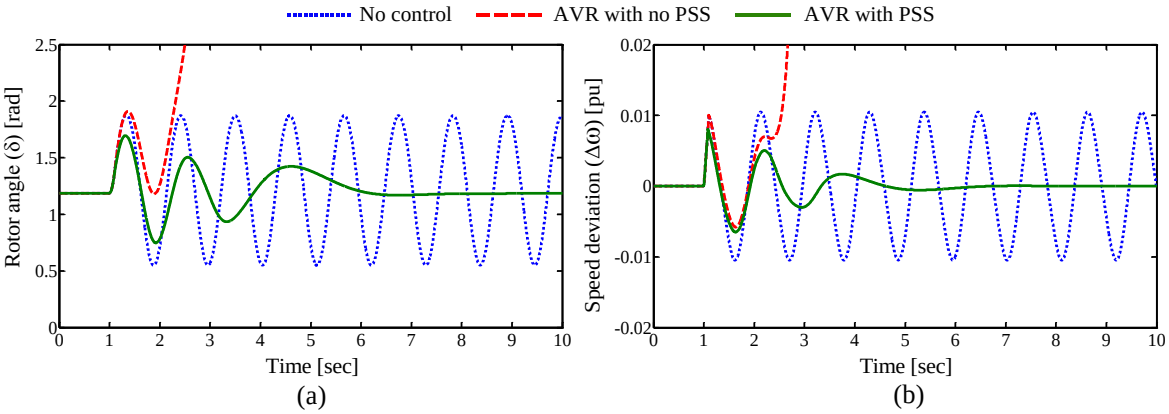

Figure 2.7: S**ystem dynamic response under leading PF condition (a) rotor angle (b) speed variation (c) active power (d) terminal voltage**

In Figure 2.8, response of the system consists of AVR with PSS for different fault clearing times under normal loading is shown. Figure 2.8(a) shows rotor angle response and Figure 2.8(b) shows speed variation of the generator. From this transient response, it is clearly observed that the AVR with PSS provides well damping even for large fault clearing time

140ms. But for the fault duration $T_c = 155ms$, the generator maintains first and second swing stability and loses synchronism during the third swing.

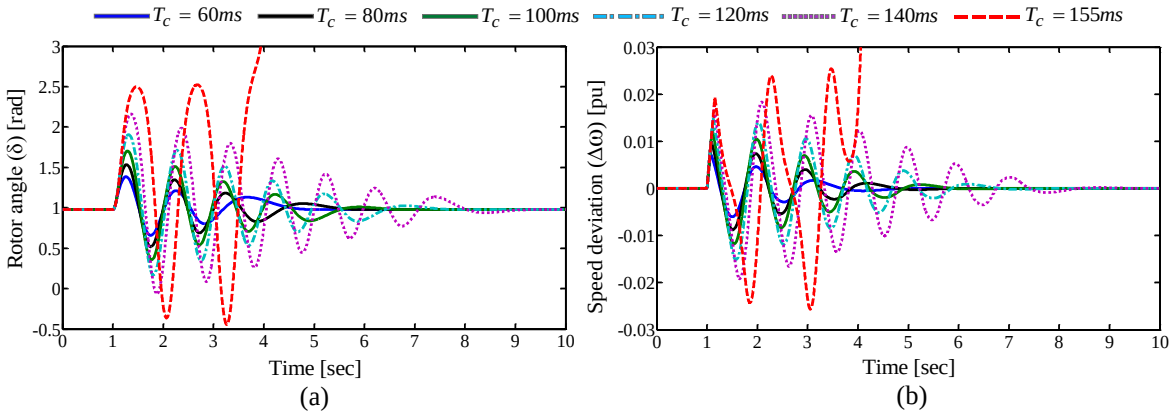

Figure 2.8: **System dynamic response with AVR & PSS for different fault clearing times (T_C) (a) rotor angle (b) speed variation (c) active power (d) terminal voltage**

2.4 Summary

In the first part, modelling of various power system components with excitation system is discussed. The basic operation of conventional AVR with PSS is discussed in the next section. The basic knowledge of these concepts is essential for controller development in the subsequent chapters.

In the modeling part, mathematical representation of different power system components is provided. It contains the model of synchronous generator, transmission system, loads and excitation system. An overview of axis transformation is provided as it helps to transform the machine axis to network and vice versa. The transient characteristics of a conventional lead-lag based PSS in a SMIB system over a wide range of operating conditions is discussed and analyzed with proper simulation results. With this transient analysis, it is observed that the PSS provides enough damping for the compensation of negative damping due to AVR action up to a considerable extent.

In next chapter, modelling of various FACTS controllers is described. Comparison over different structures of FACTS controllers is carried out. The optimal control parameters of these control structures are obtained by minimizing the objective function using an advanced optimization algorithm.

Chapter 3

Modeling and Optimal Control Design of FACTS Damping Controllers in SMIB system

Chapter 3

Modeling and Optimal Control Design of FACTS Damping Controllers in SMIB System

3.1 Introduction

Chapter 2 demonstrated a general introduction to the power system components, including a description of the basic concepts, modeling and interfacing with the power network. In this chapter, the modelling of various FACTS controllers and their optimal designs with power oscillations damping (POD) stabilizers is considered. The detail comparison between proportional integral derivative (PID) based FACTS POD controllers and Lead-Lag based FACTS POD controllers is discussed. Knowledge of the characteristics and modeling of individual system components as discussed in Chapter 2 is helpful in this analysis.

3.2 Modelling of Different FACTS Controllers

The modelling aspects of different FACTS controllers like SVC, TCSC and STATCOM for damping of power oscillations are discussed in brief manner.

3.2.1 Modelling of SVC Controller

In practice, the SVC can be modelled as an adjustable reactance with either firing angle limits or with reactance limits. The most popular configuration of SVC is shown in Figure 3.1 [93]. In this structure, SVC modeled as a parallel combination of fixed capacitor C and thyristor controlled reactor (TCR). The variable TCR equivalent reactance, X_{Leq}, at fundamental frequency is given by

$$X_{Leq} = X_L \frac{\pi}{2(\pi - \alpha) + \sin(2\alpha)} \tag{3.1}$$

where α is the thyristor's firing angle.

The SVC effective reactance X_{eq} is obtained by the parallel combination of X_C and X_{Leq}, which is given by

$$X_{eq} = \frac{X_C X_L}{\frac{X_C}{\pi}(2(\pi - \alpha) + \sin(2\alpha)) - X_L} \tag{3.2}$$

Depending on the ratio X_C/X_L, there is a certain value of firing angle that causes a steady state resonance. The SVC equivalent impedance as function of firing angle is given in equation (3.2).

The SVC equivalent susceptance, B_{SVC}, at fundamental frequency is given in equation (3.3) and the Figure 3.2 depicts the B_{SVC} at fundamental frequency as a function of firing angle.

$$B_{SVC} = -\frac{X_L - \frac{X_C}{\pi}(2(\pi-\alpha)+\sin(2\alpha))}{X_C X_L} \tag{3.3}$$

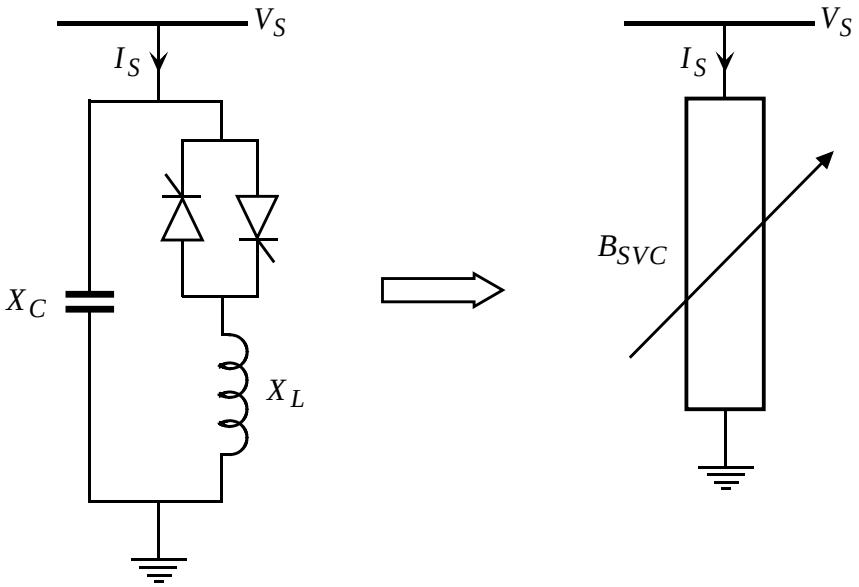

Figure 3.1: **SVC structure**

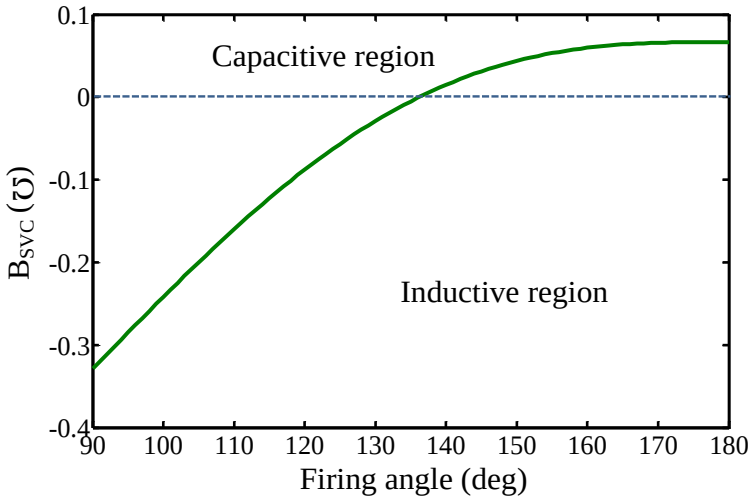

Figure 3.2: **SVC equivalent susceptance as a function of firing angle**

The block diagram of a basic SVC controller incorporating a power oscillations damping stabilizer is shown in Figure 3.3 [94]. Here, V_S is the voltage at bus *S* to which SVC is connected in parallel and U_{SVC} is the output of POD stabilizer. K_S and T_S are the gain and time constants of the SVC controller respectively.

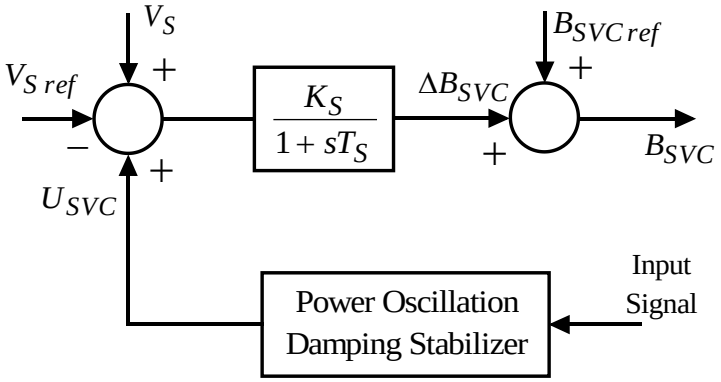

Figure 3.3: **Block diagram of SVC damping controller**

3.2.2 Modelling of TCSC Controller

A typical TCSC for load flow analysis and transient stability studies can be modelled as a variable reactance. The circuit configuration of TCSC is shown in Figure 3.4. This configuration utilizes the concept of variable reactance that can be adjusted with appropriate variation of the firing angle (α) in the range (90^0- 180^0). The relationship between TCSC reactance (X_{TCSC}) and α is given in equation (3.4), where σ is conduction angle. Figure 3.5 depicts the response of X_{TCSC} with respect to the firing angle 'α' [95].

$$X_{TCSC} = X_C - \frac{X_C^2}{(X_C - X_L)}\frac{\sigma + \sin\sigma}{\pi} + \frac{4X_C^2}{(X_C - X_L)}\frac{\cos^2(\sigma/2)}{(k^2-1)}\frac{(k\tan(k\sigma/2) - \tan(\sigma/2))}{\pi} \qquad (3.4)$$

where, $\sigma = 2(\pi - \alpha)$, $k = \sqrt{\frac{X_C}{X_L}}$

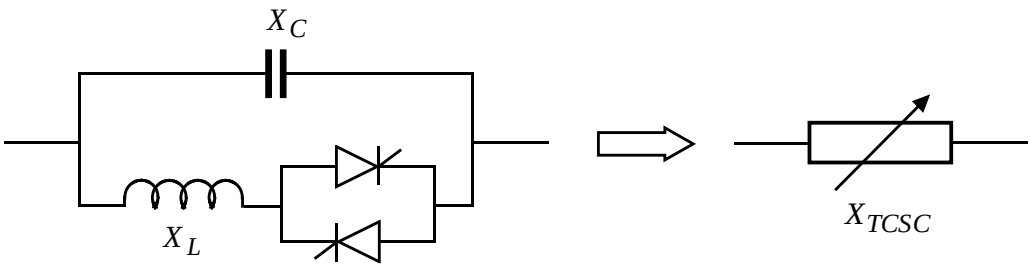

Figure 3.4: **TCSC module structure**

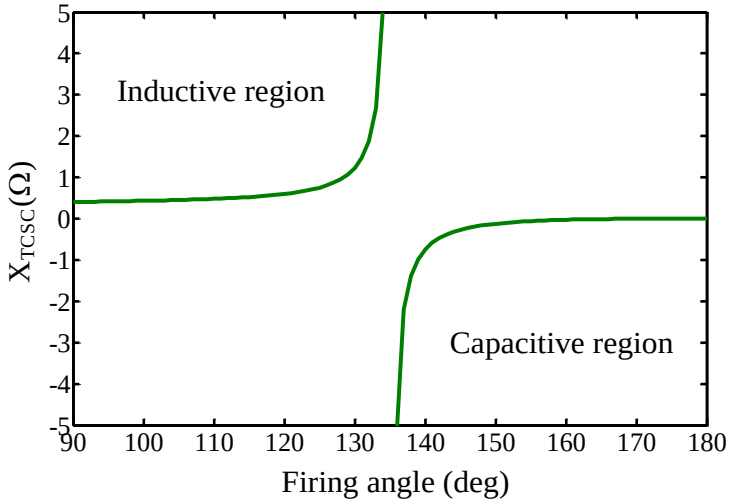

Figure 3.5: **TCSC equivalent reactance as a function of firing angle**

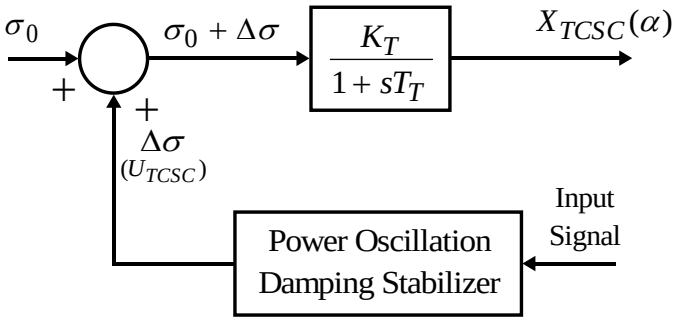

Figure 3.6: **Block diagram of TCSC damping controller**

The block diagram of basic TCSC controller with POD stabilizer is shown in Figure 3.6. Here, σ_0 is the initial (reference) value of conduction angle (σ) and U_{TCSC} is damping signal from POD stabilizer. K_T and T_T are the gain and time constants of the TCSC controller respectively.

3.2.3 Modelling of STATCOM Controllers

Figure 3.7 shows the basic structure of STATCOM. It is connected to a bus *S* with voltage V_S through a transformer of leakage reactance X_S. The STATCOM consists of a 3-phase voltage source converter (VSC) and a DC capacitor with capacitance C_{DC}. The VSC converts DC voltage V_{DC} to a controllable AC voltage V_m at an angle α_s. Due to the difference between these two voltages, there is a power exchange between STATCOM and the power system. Hence, by adjusting the values of voltage magnitude V_m and the phase

angle α_s, we can control the power flow. From Figure 3.7, the control equations of STATCOM are given by [96]

$$V_m = k\,m V_{DC}(\cos\alpha_s + j\sin\alpha_s) = k\,m V_{DC}\angle\alpha_s \tag{3.5}$$

$$\dot{V}_{DC} = \frac{k\,m}{C_{DC}}(I_{Sd}\cos\alpha_s + I_{Sq}\sin\alpha_s) \tag{3.6}$$

where, k is the ratio of AC and DC voltage, m is modulation index of the PWM and α_s is phase angle of VSC.

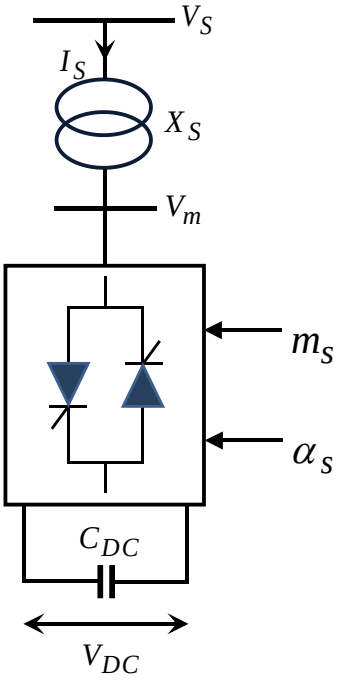

Figure 3.7: **Structure of STATCOM**

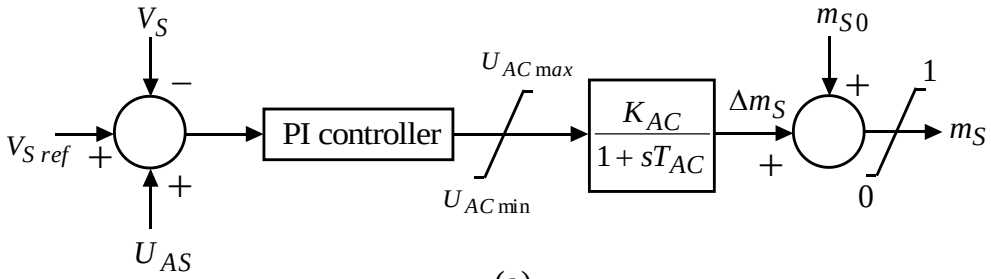

(a)

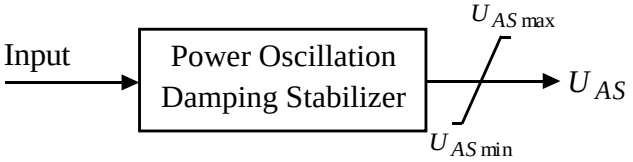

(b)

Figure 3.8: **(a) PI based AC voltage controller and (b) additional POD stabilizer of the STATCOM**

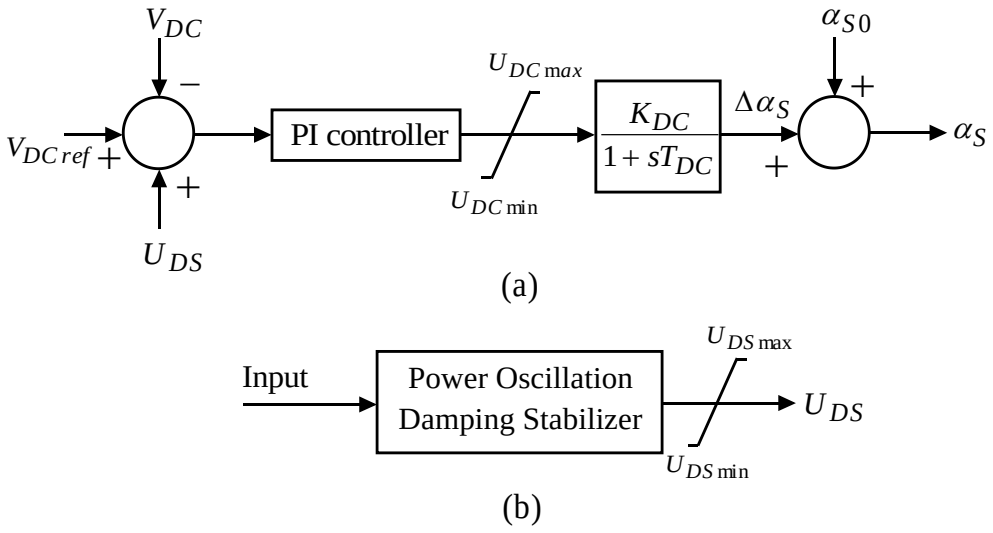

Figure 3.9: **(a) PI based DC voltage controller and (b) additional POD stabilizer of the STATCOM**

The internal controllers [68] of STATCOM are designed with PI based controller, which are shown in Figure 3.8 and 3.9. The Figure 3.8(a) shows the PI based STATCOM AC voltage controller. The difference in AC voltage V_S and its reference value is considered as input of the controller. Here, one more additional input U_{AS} is also taken from POD stabilizer, which is shown in Figure 3.8(b). The PI based AC voltage controller with gains K_{PAC} and K_{IAC} gives modulation index as output. On the other hand, in Figure 3.9(a), the difference of DC voltage of the capacitor V_{DC} and its reference value is given as input to the PI based DC voltage controller and in addition to these two inputs, the output of damping controller is also fed as input as shown in Figure 3.9(b).

3.3 Structure of POD Stabilizers

The power oscillations damping stabilizers give additional damping signal to the FACTS controllers such that they can be able to damp the power system oscillations quickly under disturbance. Recently, several advanced control design approaches based on optimal control, robust control, adaptive control and intelligent control have been developed for power system oscillation damping. In spite of the merits of such advanced controls, many industries and power system utilities still prefer simple PID and Lead-lag based damping controller structures. Here, to analyze the performance of power system under disturbance, the following control structures are discussed.

- PID controller based POD stabilizers
- Lead-Lag controller based POD stabilizers

3.3.1 Structure of PID Controller Based POD Stabilizers

Over past 50 years, the PID controller is most widely used as a feedback controller in many industries. It is a simple, robust, easily realizable and cost effective controller that can provide excellent control performance despite the varied dynamic characteristics of power plant. As the name indicates, PID controller is integration of three basic controllers, those are proportional, integral and derivative controllers. Each controller has their own effect to stabilize the output of the plant. The proportional controller helps to reduce the rise time, but it never eliminates the steady-state error. By this reason, if the proportional gain is too high, then the system becomes unstable where as a small gain results in a small output response to a large input error and less sensitive [97]. The integral controller can eliminate steady-state error, whereas it makes the transient response too worse. High integral gain can cause overshoot and low value will make system response sluggish. The derivative controller will helps to improve the stability of the system, reduce the overshoot and increase the transient response. If the derivative gain is sufficiently high it can cause system unstable and it makes more noise. Conventional fixed gain PID controller is widely used for control process in power industries. In the design of this controller one has to set three main parameters proportional gain (K_P), integral gain (K_I) and derivative gain (K_D). Mostly, the controller gains are tuned by the trial and error method based on the experience over plant behavior. The block diagram of PID controller [98] for a closed loop system is shown in Figure 3.10 and the transfer function is represented by

$$G_{PID} = K_P + \frac{K_I}{s} + sK_D \tag{3.7}$$

The output of PID controller in time domain is given by

$$u(t) = K_P\, e(t) + K_I \int e(t)dt + K_D \frac{de(t)}{dt} \tag{3.8}$$

where $u(t)$ is control signal and $e(t)$ is error signal

In this work, the FACTS POD stabilizers are designed by using PID based controllers. Figure 3.11 represents the structure of PID controller based FACTS POD stabilizers. The input signal given to POD stabilizers is depends on the type of FACTS controller. In general,

for series controllers change in the line active power is given as input signal whereas for shunt connected FACTS controllers change in bus voltage is given as input signal. The output signal of POD stabilizer is also given as one more input to the FACTS controller.

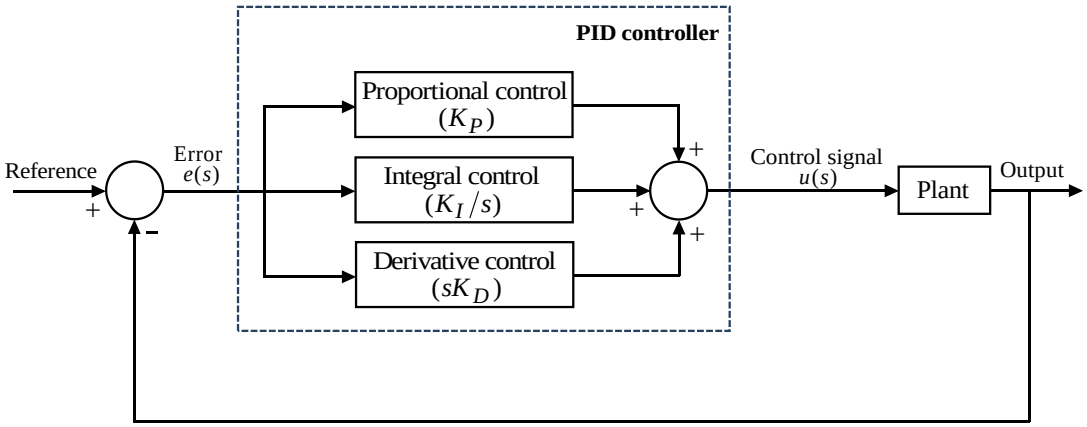

Figure 3.10: **Block diagram representation of PID controller**

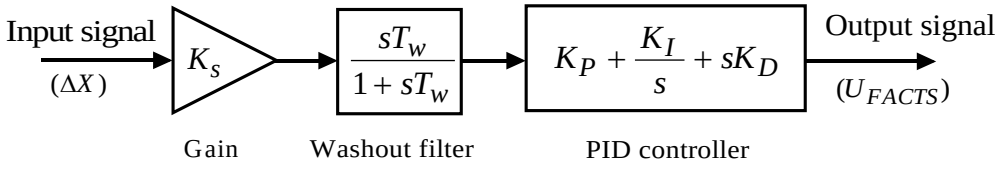

Figure 3.11: **Structure of PID controller based POD stabilizer**

As explain in Chapter 2, the gain K_s determines the amount of damping introduced by the controller and the washout filter acts as high pass filter. For the proper design of FACTS POD controllers, the parameters of PID controller such as K_P, K_I and K_D must be selected by some suitable tuning method to improve the transient response and minimize the steady-state error.

3.3.2 Structure of Lead-Lag Controller Based POD Stabilizers

The Lead-Lag controller is simple yet effective controller, which is commonly used in many industries for error compensation. For the design of a Lead-Lag compensator (or controller), an engineer much consider whether the system needs Lead-compensator, Lag-compensator, or a combination of the two. Lead compensation essentially yields an appropriate improvement in transient response and a little improvement in steady state accuracy. On the other hand, Lag compensation yields an appreciable enhancement in steady state accuracy as the expense of increasing the transient response time. The Lead-Lag compensation combines the characteristics of both lead compensation and lag compensation. Hence, Lead-Lag

controller can improve system parameters such as reducing steady state error, reducing resonant peak, improving system transient response by reducing the rise time. The basic block diagram of two stage Lead-Lag controller is shown in Figure 3.12 and the transfer function is given by

$$G_{LL} = \frac{(1+sT_1)}{(1+sT_2)}\frac{(1+sT_3)}{(1+sT_4)} \tag{3.9}$$

where, T_1, T_2, T_3 and T_4 are time constants of Lead-Lag controller.

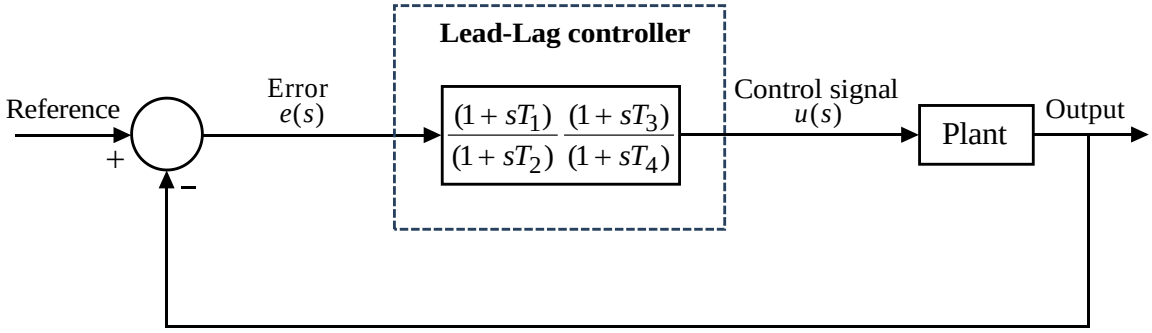

Figure 3.12: **Block diagram representation of Lead-Lag controller**

The Lead-Lag controller provides lead compensation if the numerator time constants are greater than denominator time constants (i.e. $T_1 > T_2,\ T_3 > T_4$). Similarly, it provides lag compensation if time constants of numerator are lesser than time constants of denominator (i.e. $T_1 < T_2,\ T_3 < T_4$). Figure 3.13 represent the structure of Lead-Lag controller based POD stabilizer.

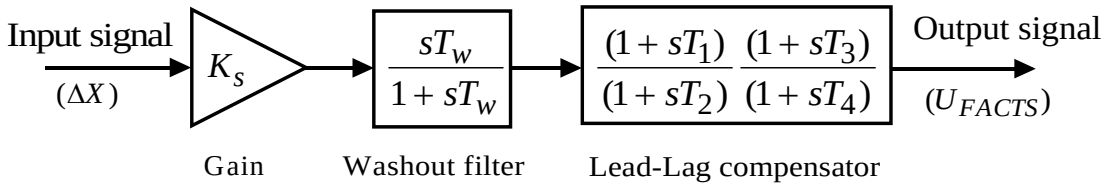

Figure 3.13: **Structure of Lead-Lag controller based POD stabilizer**

To improve the dynamic response and to damp the power system oscillations, proper tuning of control parameters associated with these POD stabilizers is requisite. Several techniques have been proposed for tuning of control parameters in POD stabilizers. In this work, conventional particle swarm optimization (CPSO) is used to find the optimal control parameters of different POD stabilizers.

3.4 Particle Swarm Optimization: An Overview

Particle swarm optimization (PSO) is a population based optimization method first proposed by Kennedy and Ebaerhart [24, 99]. Many popular algorithms are deterministic, like the gradient based algorithms. The PSO, similarly to the algorithms belonging to the evolutionary algorithm family, is a stochastic algorithm that does not need gradient information derived from the error function. This allows PSO to be used on functions where the gradient is either unavailable or computationally expensive to obtain.

The PSO is a heuristic global optimization method, which is developed from swarm intelligence and based on the research of bird and fish flock movement behavior [24]. Birds are searching for food from one place to another, there is always transmitting information so that they flock to the place where food can be found. The PSO algorithm is concerned, solution swarm is compared to the bird swarm, the birds moving from one place to another is equal to the development of the solution swarm, good information is equal to most optimist solution and the food resource is equal to the best optimist solution in entire course. The most optimist solution can be found in PSO by the mutual cooperation of each individual particle. Due to its many advantages including its simplicity and easy implementation, this algorithm can be used widely to solve many complex engineering problems.

3.4.1 The PSO Algorithm

The algorithm maintains a population of *n* particles, where each particle represents a potential solution to an optimization problem. Each particle *i* can be represented as an object with several characteristics. These characteristics and basic elements of PSO can be stated as follows:

- X_i : The *current position* of the i^{th} particle
- V_i : The *current velocity* of the i^{th} particle
- w_i : The *current inertia weight* of the i^{th} particle
- P_i^{best} : The current best position of the i^{th} particle
- G_i^{best} : The current global best position of the i^{th} particle

In PSO algorithm, each particle is *k*-dimensional real valued vector, where *k* is the number of parameters to be optimized. Hence, each optimized parameter represents a dimension of the problem space. The PSO technique [31] can be described in following steps:

Step 1: Generate random *n* number of particles with random initial velocities and set the iteration count $iter = 1$. The velocity *V* is generated by randomly selecting a value with uniform probability over the k^{th} dimension in range of $[-V_k^{\max}, V_k^{\max}]$. Each particle *i* in the initial population fitness is evaluated using the objective function *J*, search for the best value of the objective function J_{best}. Set the particle associated with J_{best} as the global best (G^{best}). Set the initial value of inertia weight w_0.

Step 2: Update the iteration count $iter = iter + 1$.

Step 3: Update the inertia weight $w_{iter} = w_{iter+1}$.

Step 4: Using the global best and individual position best, the i^{th} particle velocity and position is updated according the following equations:

$$V_{i,iter+1} = wV_{i,iter} + c_1 r_1 (P_{i,iter}^{best} - X_{i,iter}) + c_2 r_2 (G_{i,iter}^{best} - X_{i,iter}) \quad (3.10)$$

$$X_{i,iter+1} = X_{i,iter} + V_{i,iter+1} \quad (3.11)$$

where, c_1 and c_2 are constants namely positive cognitive and social components that are responsible for varying the particle velocity towards the P_i^{best} and G_i^{best}. r_1 and r_2 are two random numbers in the range [0-1]. The inertia weight *w* is responsible for dynamically adjusting the velocity of the particles.

Step 5: To enhance the efficiency of PSO, one can adjust the inertia weight *w* to linearly reduce during the iterations. The inertia weight is updated by the following equation:

$$w = (w_{\max} - w_{\min}) \times \left(\frac{iter_{\max} - iter}{iter_{\max}} \right) + w_{\min} \quad (3.12)$$

where, $iter_{\max}$ is the maximum number of iterations and *iter* is the current number of iteration. $w_{\max}$ and $w_{\min}$ are the maximum and minimum values of inertia weight respectively. The typical range of *w* from 0.9 at the beginning of the search to 0.4 at the end of the search [100].

Step 6: Each particle is evaluated according to the updated position. $J_{i,iter+1} < J_{i,iter}$, the updated individual position best (P_i^{best}) and go to next step.

Step 7: Search for the minimum value of the objective function, if $J_{i,iter+1}^{\min} < J_{i,iter}^{\min}$ then set the particle associated with minimum value of objective function as global best.

Step 8: If the stopping criteria is satisfied, then stop, or else go to step 2.

The PSO algorithm that is described in above procedural steps is known as conventional PSO (CPSO). In this work, for the optimal tuning of FACTS POD controllers like SVC, TCSC and STATCOM controllers CPSO is used. The flow chart for CPSO technique is depicted in Figure 3.14.

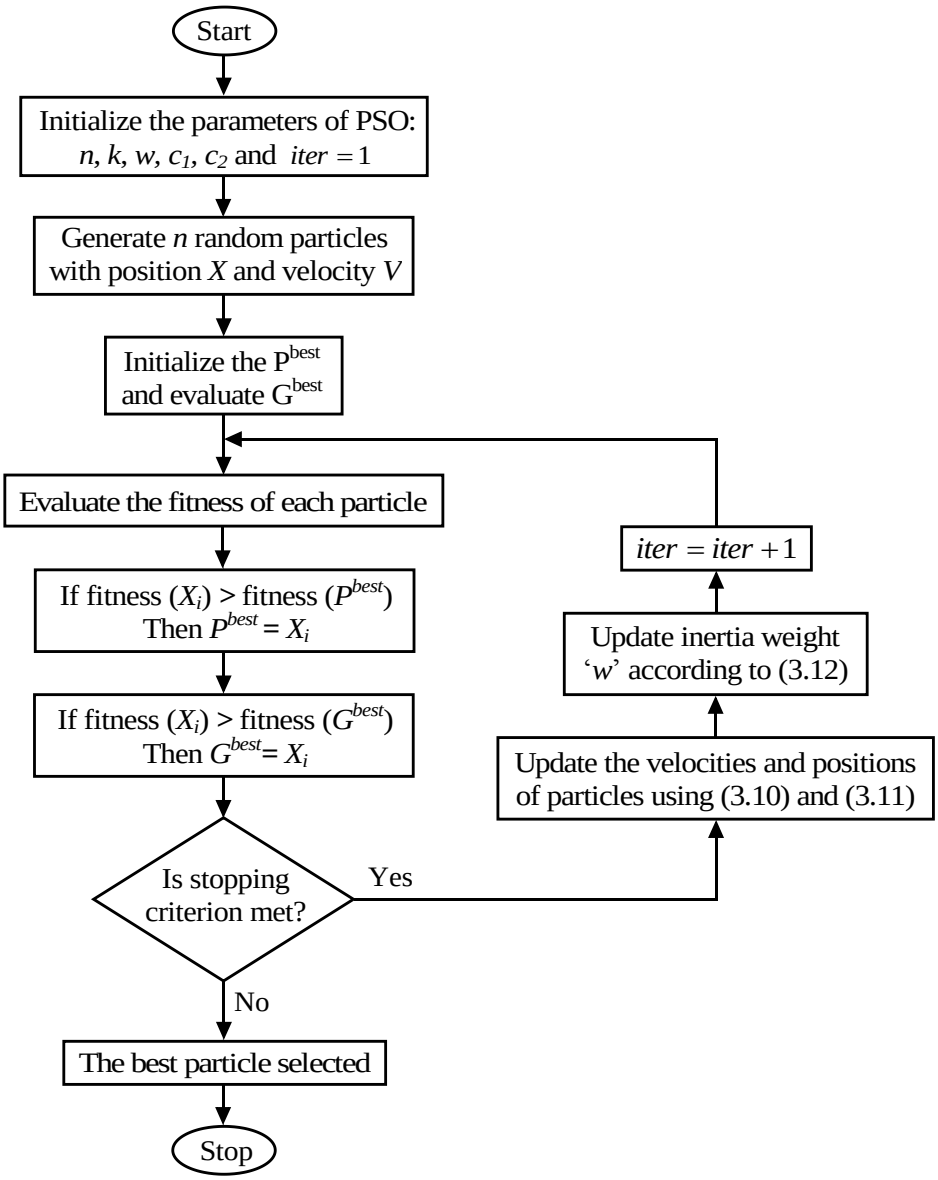

Figure 3.14: **Flowchart depicts the CPSO algorithm**

3.5 Objective Function

In an optimization process to find the optimal parameter values, which results in a maximum or minimum of a function, is called an objective function. The objective function is a mathematical expression describing a relationship of the optimization parameters that uses the optimization parameters as inputs. To find the optimal parameter values of FACTS POD controllers, which is installed in SMIB test power system, integral of time-multiplied absolute value of error (ITAE) is considered as objective function. Since, in power system stability problems time is considered very important factor, it is required that settling time should be less and also oscillations should die out soon. However, the main objective is to damp the power oscillations and to maintain the voltage profile of the test power system effectively. This objective can be achieved by minimizing the value of speed deviation along with terminal voltage variations. So the objective function is formulated with the integration of speed variation and terminal voltage variation of the generator. In this work, for SMIB test power system objective function is considered as:

$$J = \int_0^t t\left[\left|\Delta\omega_i\right| + \left|\Delta V_{Ti}\right|\right]dt \tag{3.13}$$

where, t is total simulation time, $\Delta\omega_i$ is the change in speed in p.u. and ΔV_{Ti} is the change in terminal voltage.

In order to maintain stability and to provide efficient damping, it is aimed to minimize the objective function. To reduce the computational burden in this work, the value of the wash out time constant T_w is fixed at 5s for both PID as well as Lead-Lag based POD stabilizers. In Lead-Lag based POD stabilizer the values of T_2 and T_4 are usually pre-specified, based on engineering experience [101]. In this context, tuning of T_1 and T_3 are chosen to achieve the net phase lead required by the system. Therefore, the optimization problem is formulated as:

Minimize 'J' (3.14)

For PID based POD stabilizers the above equation is subjected to constraints that are given by

$$K_P^{\min} \le K_P \le K_P^{\max}$$

$$K_I^{\min} \le K_I \le K_I^{\max}$$

$$K_D^{\min} \le K_D \le K_D^{\max}$$

For Lead-Lad based POD stabilizers equation (3.14) is subjected to constraints that are given by

$$K_s^{\min} \le K_s \le K_s^{\max}$$

$$T_1^{\min} \le T_1 \le T_1^{\max}$$

$$T_3^{\min} \le T_3 \le T_3^{\max}$$

The value of fixed gain PID based POD stabilizer is kept constant at 5 and the time constants T_2 and T_4 of Lead-Lad based POD stabilizers are chosen as 0.05. The typical ranges of the optimized parameters are [0.01-50] for K_P, [0.01-10] for K_I, [0.01-10] for K_D, [0.01-50] for K_s, and [0.06-1] for T_1, T_3. Hence, CPSO is applied to minimize the objective function with subjected constraints and to search the optimal control parameters values of FACTS POD stabilizers.

3.6 Performance Analysis of Test System with FACTS POD Controllers

The performance of SMIB test system with different FACTS POD controllers is analyzed and compared with the simulation results. Here SVC, TCSC and STATCOM controllers with both PID as well as Lead-Lad based POD stabilizers are considered for the analysis. A three-phase fault is applied on one of the transmission lines of considered power system to test the performance with different controllers.

3.6.1 Performance Analysis of Test System with SVC POD Controller

SVC controller is installed in SMIB system is shown in Figure 3.15. As discussed in chapter 2, the generator is modelled as a third order model and it is connected to infinite bus with two parallel transmission lines having impedances X_{L1} and X_{L2}. Here SVC modelled as a variable reactance model with susceptance B_{SVC}. SVC is connected to the bus with voltage V_S, which is nearer to the generator terminal. SVC controller with PID and Lead-Lag based POD stabilizers are shown in Figure 3.16 and Figure 3.17 respectively. The change in bus voltage (ΔV_S) and SVC susceptance are the input and output of SVC damping controllers respectively.

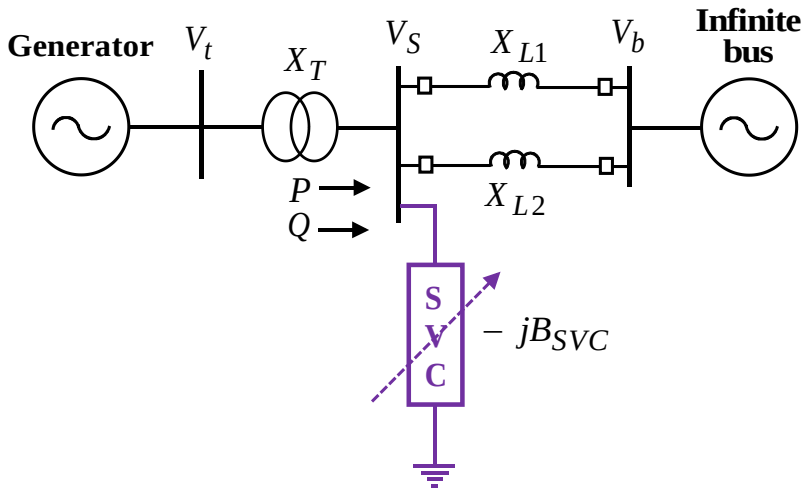

Figure 3.15: **SMIB test system with SVC**

CPSO parameters used in simulations for different FACTS controllers (SVC, TCSC and STATCOM) are chosen as number of particles, number of iterations, c_1 and c_2 are equal to 50, 100, 2 and 2 respectively. In order to extract the optimal parameter values of SVC controller, CPSO algorithm is run for several times. The obtained optimal values based on proposed objective function using CPSO algorithm for PID and Lead-Lag POD stabilizers are given in Table 3.1.

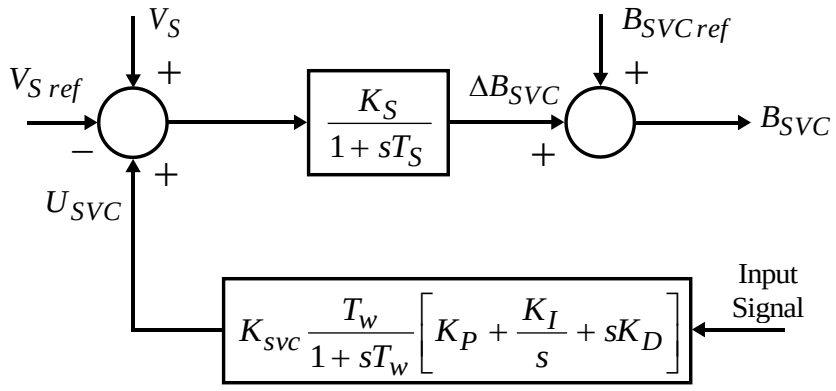

Figure 3.16: **SVC controller with PID based POD stabilizer**

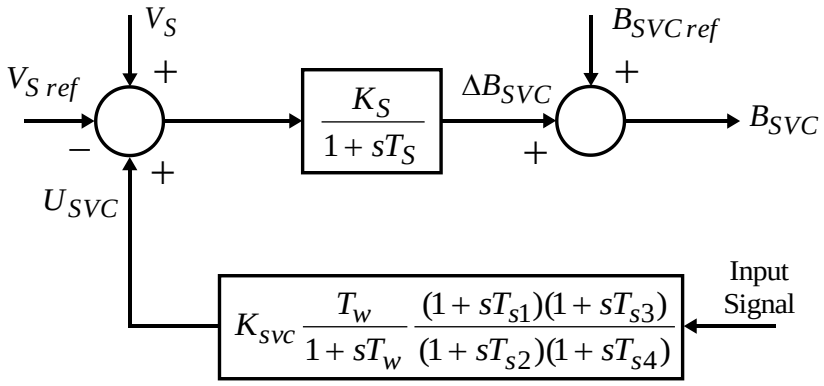

Figure 3.17: **SVC controller with Lead-Lag based POD stabilizer**

Table 3.1: **CPSO tuned optimal parameter values of SVC controllers**

PID based POD	:	$K_P = 26.78,\ K_I = 7.23,\ K_D = 1.42$
Lead-Lag based POD	:	$K_S = 10.64,\ T_1 = 0.6122,\ T_3 = 0.5937$

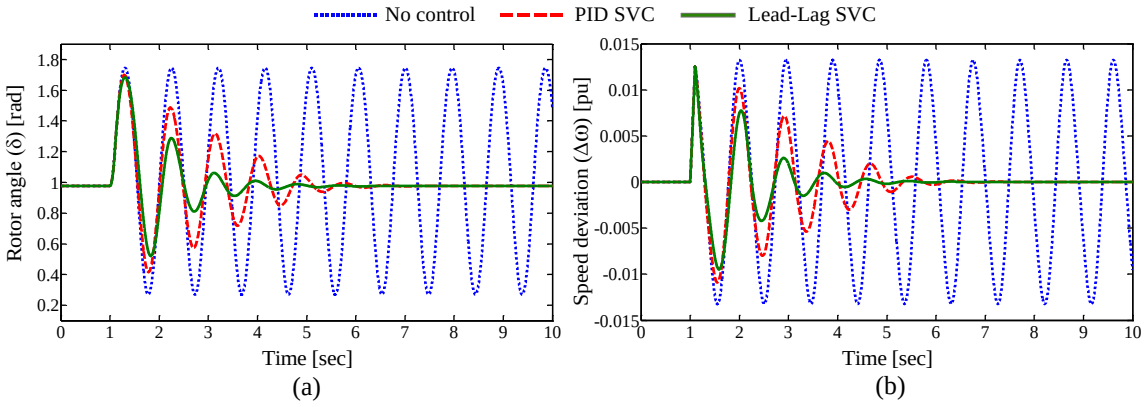

Figure 3.18: **Test system dynamic response for a six cycle 3-phase fault under normal load**

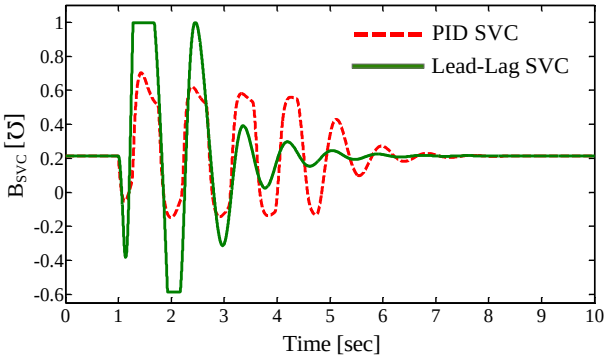

Figure 3.19: **Variation of B_{SVC} for different controllers**

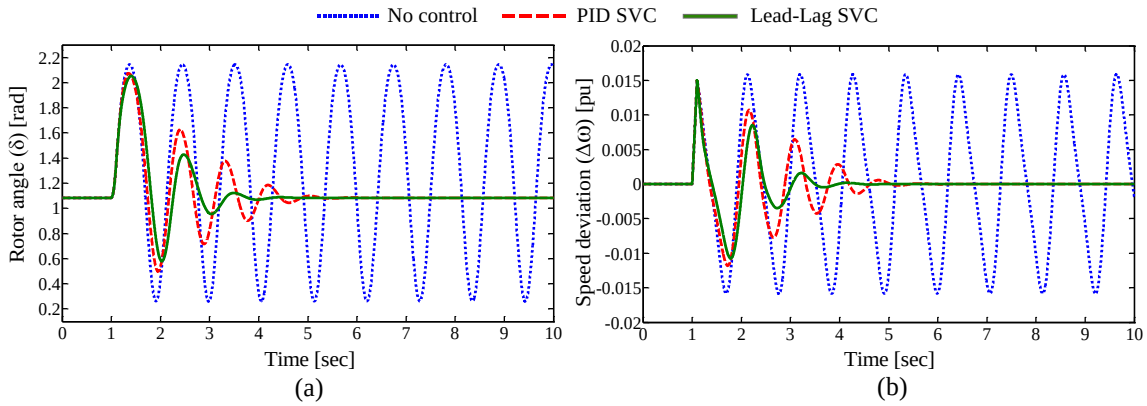

Figure 3.20: **Test system dynamic response for a six cycle 3-phase fault under heavy load**

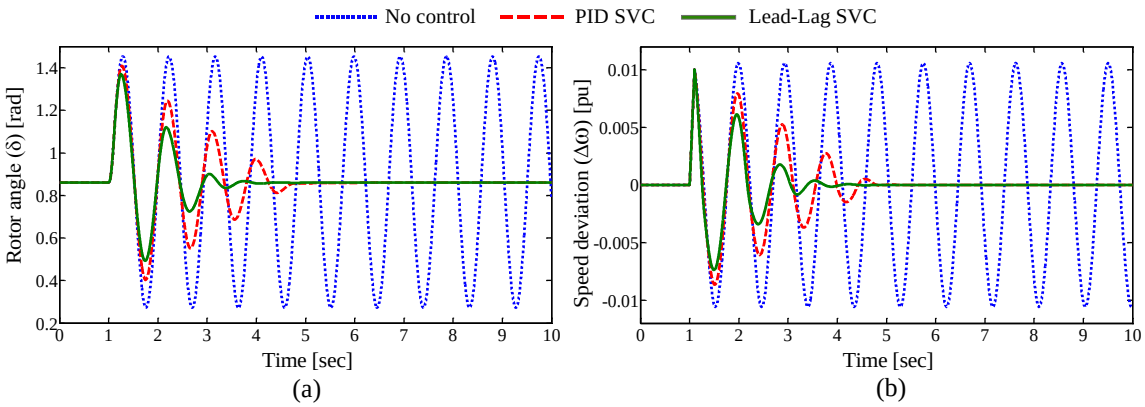

Figure 3.21: **Test system dynamic response for a six cycle 3-phase fault under light load**

To analyze the robustness and the effectiveness of SVC controller, simulations are carried out for 3-phase fault disturbance over a wide range of load conditions. The fault is applied at 1.0sec., and it is cleared after 1.1sec (i.e six cycle fault is applied). SMIB test system dynamic responses under fault disturbance over a wide range of operating conditions are shown in Figures 3.18-3.22. In this work, four load conditions are applied to the SMIB test system, which are discussed in Chapter 2, Table 2.2. The Figure 3.18(a) shows the response of rotor angle oscillations in radians and Figure 3.18(b) shows the speed deviation in per unit for different control schemes under normal load conditions. Similarly, in Figures 3.20-3.22 (a) represent rotor angle oscillations and (b) represent speed deviations under heavy load, light load and leading PF conditions respectively for different control schemes.

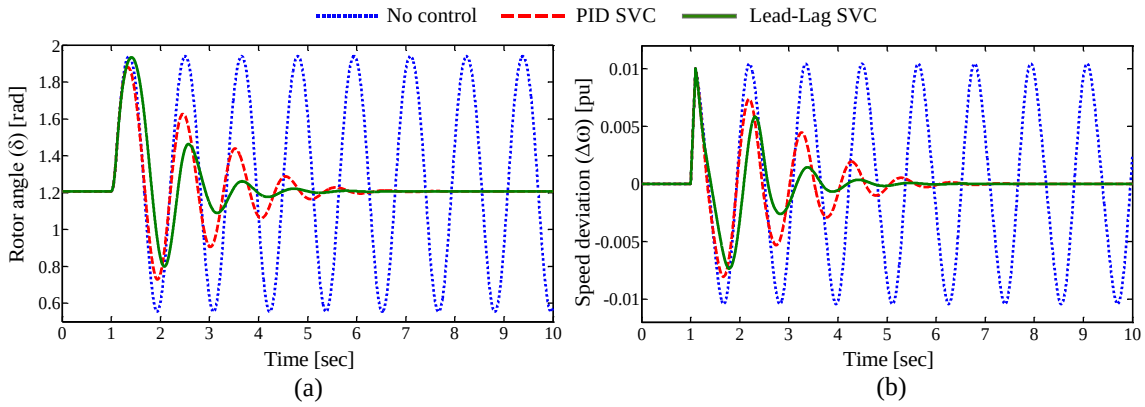

Figure 3.22: **Test system dynamic response for six cycle 3-phase fault under leading PF condition**

The comparison of variations in SVC susceptance (B_{SVC}) for different control schemes in damping oscillations is shown in Figure 3.19. The test system performance is compared for three different control schemes namely, no control, PID based SVC and Lead-Lag based SVC control. From the response curves, it is observed that CPSO tuned SVC controller gives

very good performance in damping the oscillations and settles the oscillations more quickly. The system with out control will not able to damp out the oscillations. Moreover, Lead-Lag based SVC controller gives somewhat better performance as compared to PID based SVC controller in terms of damping effect and settling times of the oscillations.

3.6.2 Performance Analysis of Test System with TCSC POD Controller

TCSC installed in SMIB test system as shown in Figure 3.23. It is installed in series with the transmission line and to near the generator terminals. Here, TCSC is modelled as variable reactance model with a variable X_{TCSC}. TCSC controller with PID and Lead-Lag based POD stabilizers are shown in Figure 3.24 and Figure 3.25 respectively. The generator speed deviation is input to the TCSC damping controllers and the TCSC reactance which varies with firing angle is final output of the controller. The optimal control parameter values of CPSO based TCSC damping controllers are given in Table 3.2.

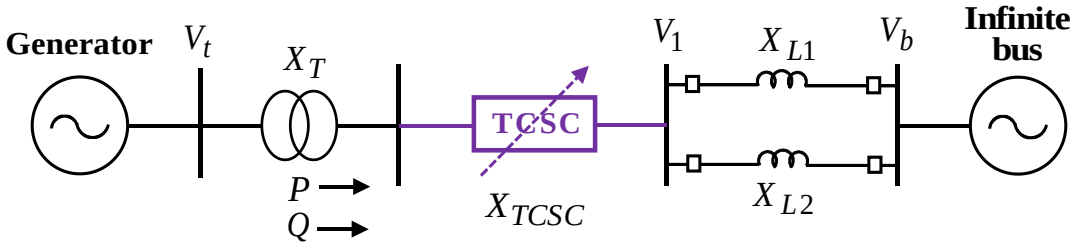

Figure 3.23: **SMIB test system with TCSC**

Table 3.2: **CPSO tuned optimal parameter values of TCSC controllers**

PID based POD	:	$K_P = 6.57,\ K_I = 2.64,\ K_D = 0.91$
Lead-Lag based POD	:	$K_S = 12.57,\ T_1 = 0.4581,\ T_3 = 0.3720$

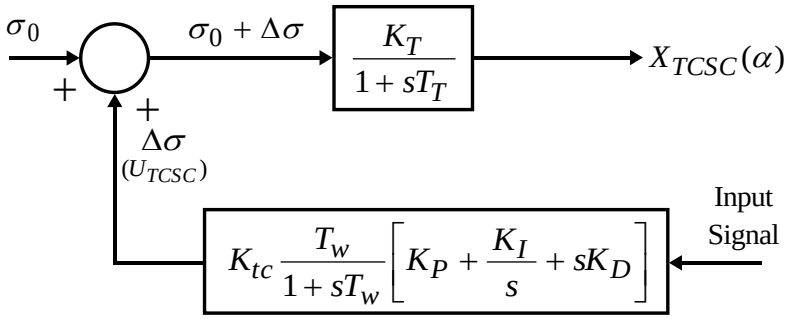

Figure 3.24: **TCSC controller with PID based POD stabilizer**

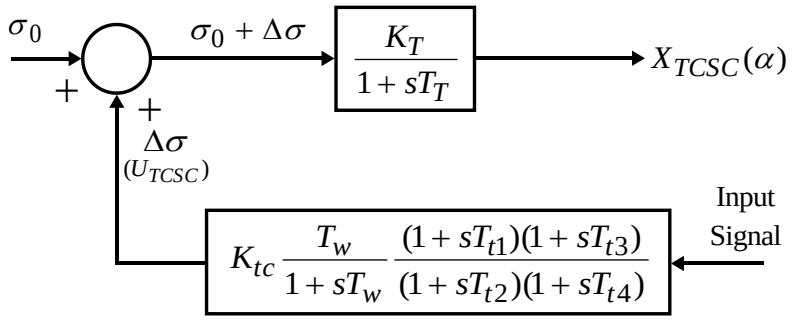

Figure 3.25: **TCSC controller with Lead-Lag based POD stabilizer**

The transient analysis is carried out to evaluate the robustness of proposed TCSC damping controllers. A 3-phase fault disturbance is applied on the test system with starting time $t_s = 1.0\,\text{sec.}$, and the fault is cleared at $t_c = 1.1\text{sec}$. The system is tested for different load conditions (which are mentioned in Chapter 2, Table 2. 2). Figure 3.26 shows the response of rotor angle variation and speed deviation under normal load condition for a six cycle fault disturbance. Figure 3.27 shows the variation of the TCSC reactance for different controllers under normal load condition.

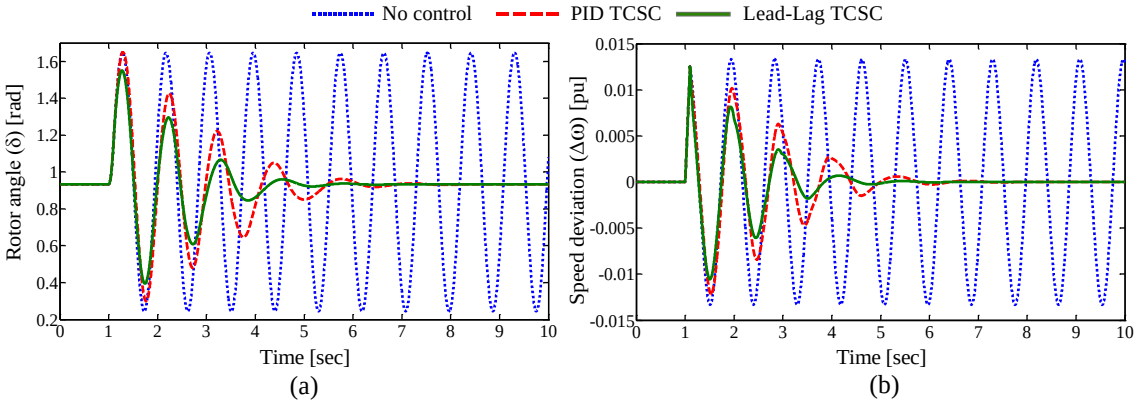

Figure 3.26: **Test system dynamic response for a six cycle 3-phase fault under normal load**

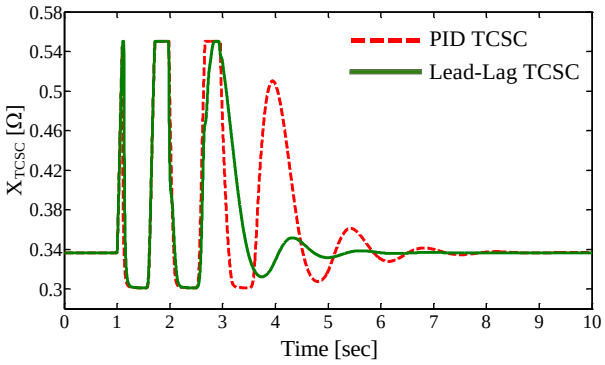

Figure 3.27: **Variation of X_{TCSC} for different controllers**

Similarly, Figures 3.28 – 3.30 show the test system dynamic responses for heavy load, light load and leading PF conditions respectively. It is evident from the response curves that the test system with CPSO tuned TCSC damping controllers settles much faster and damp out the system oscillations quickly. However, TCSC controller with Lead-Lag based POD stabilizer is comparatively effective than TCSC controller with PID based POD stabilizer.

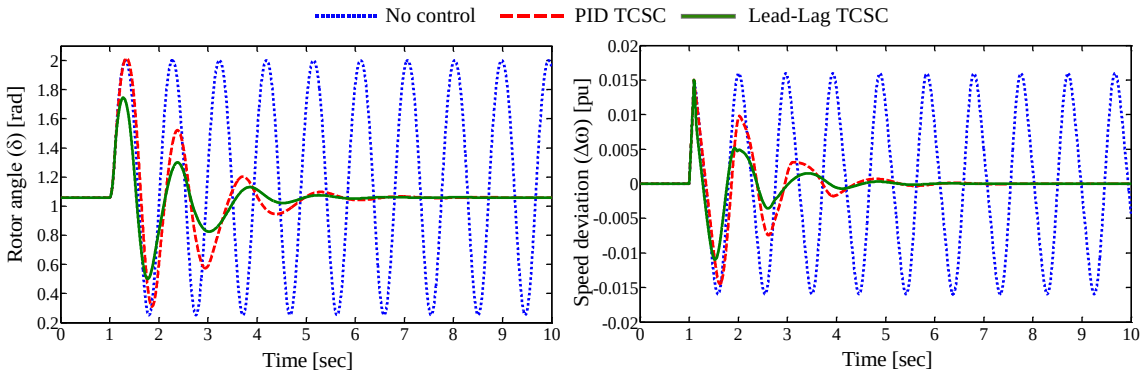

(a) (b)

Figure 3.28: **Test system dynamic response for a six cycle 3-phase fault under heavy load**

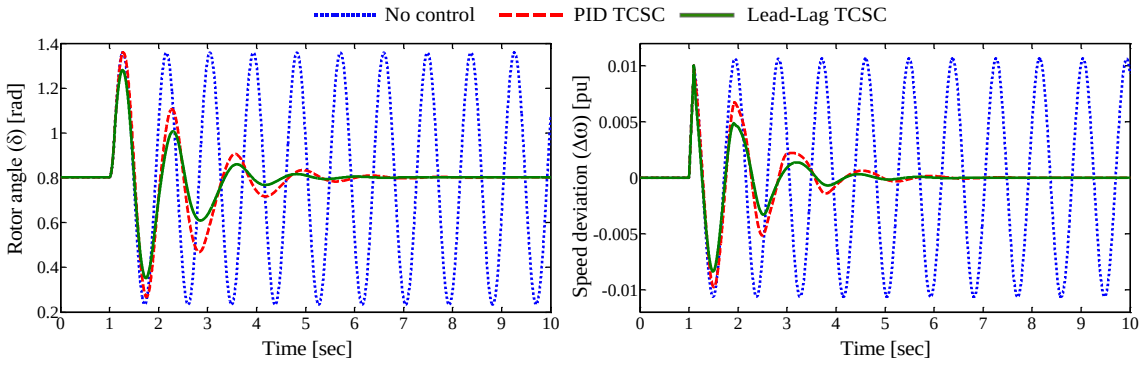

(a) (b)

Figure 3.29: **Test system dynamic response for a six cycle 3-phase fault under light load**

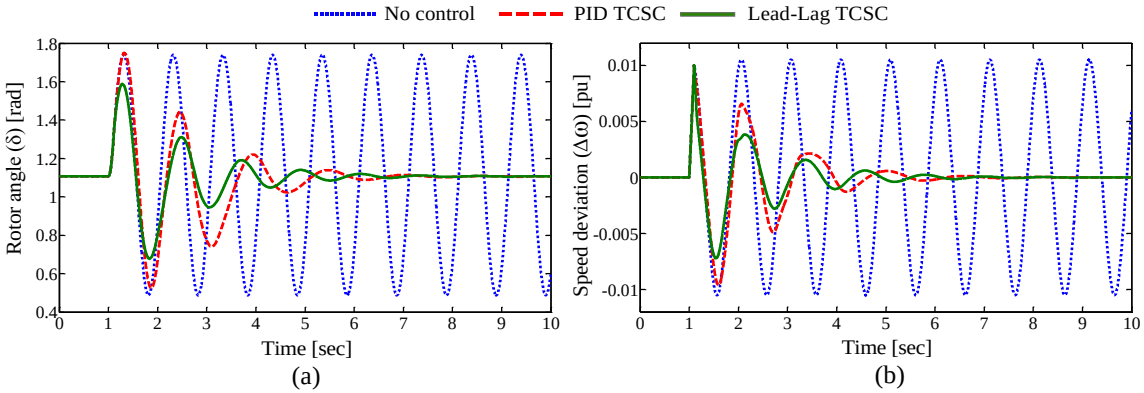

(a) (b)

Figure 3.30: **Test system dynamic response for a six cycle 3-phase fault under leading PF condition**

3.6.3 Performance Analysis of Test System with STATCOM POD Controllers

STATCOM is installed nearer to the generator terminals of SMIB test system as shown in Figure 3.31. Here, STATCOM has two internal controllers namely

1. STATCOM AC voltage controller (ACVC)
2. STATCOM DC voltage controller (DCVC)

The above two controllers have an additional POD stabilizer which can be based on either PID controller or Lead-Lag controller. The PID and Lead-Lag based POD stabilizers of ACVC are shown in Figure 3.32(a) and Figure 3.32(b) respectively. Similarly, both types of POD stabilizers for DCVC are shown in Figure 3.33(a) and Figure 3.33(b). The speed deviation of the generator is considered as input to the STATCOM damping controllers. The ACVC gives modulation index (m_s) as output and DCVC gives phase angle (α_s) as output. The optimal parameter values of CPSO tuned ACVC and DCVC are obtained and tabulated in Table 3.3.

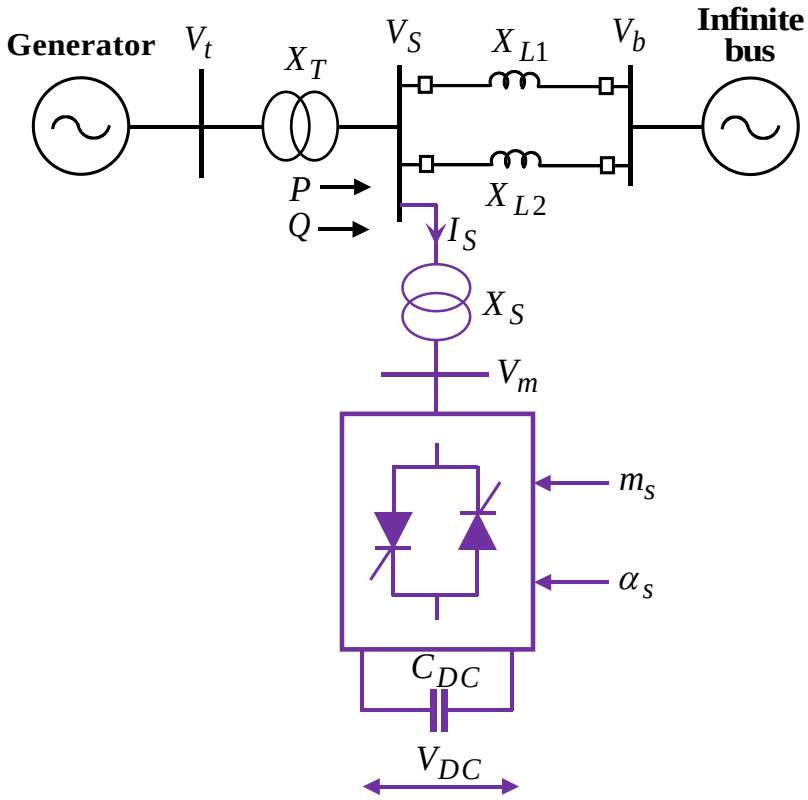

Figure 3.31: **SMIB test system with STATCOM**

The time domain simulations are performed for a six cycle fault to analyze the effectiveness of considered controllers. The system has undergone several operating conditions to test the robustness of different controllers for severe disturbance. The fault is applied at time

$t_s = 1.0\text{sec.}$, and it is cleared at $t_c = 1.1\text{sec.}$ From Figures 3.34-3.47 show the response curves for different types of STATCOM damping controllers in different operating conditions.

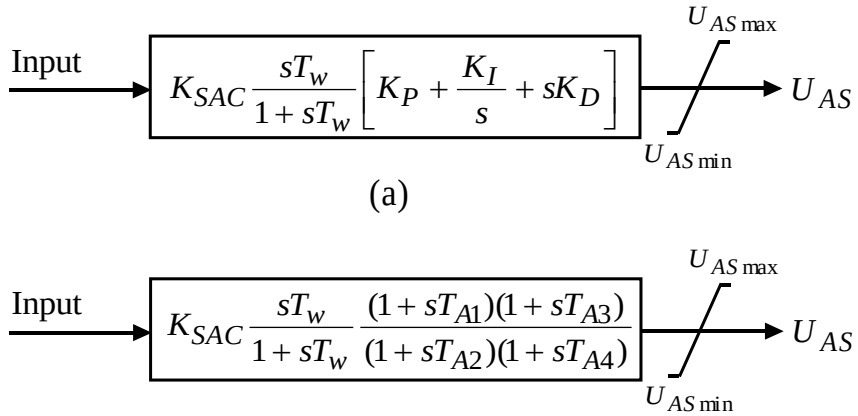

Figure 3.32: **(a) PID based POD stabilizer (b) Lead-Lag based POD stabilizer for ACVC**

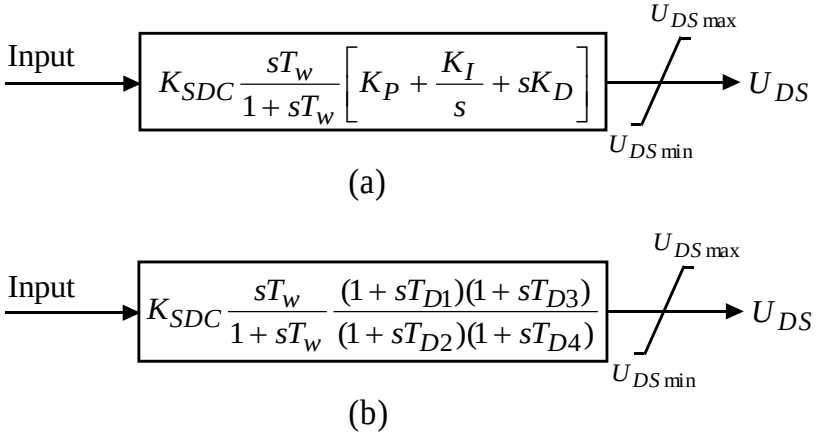

Figure 3.33: **(a) PID based POD stabilizer (b) Lead-Lag based POD stabilizer for DCVC**

Table 3.3: **CPSO tuned optimal parameter values of STATCOM controllers**

PID based ACVC POD :	$K_P = 10.84,\ K_I = 4.26,\ K_D = 2.03$
Lead-Lag based ACVC POD :	$K_S = 9.72,\ T_1 = 0.534,\ T_3 = 0.4712$
PID based DCVC POD :	$K_P = 12.32,\ K_I = 5.47,\ K_D = 1.93$
Lead-Lag based DCVC POD :	$K_S = 13.67,\ T_1 = 0.4221,\ T_3 = 0.4380$

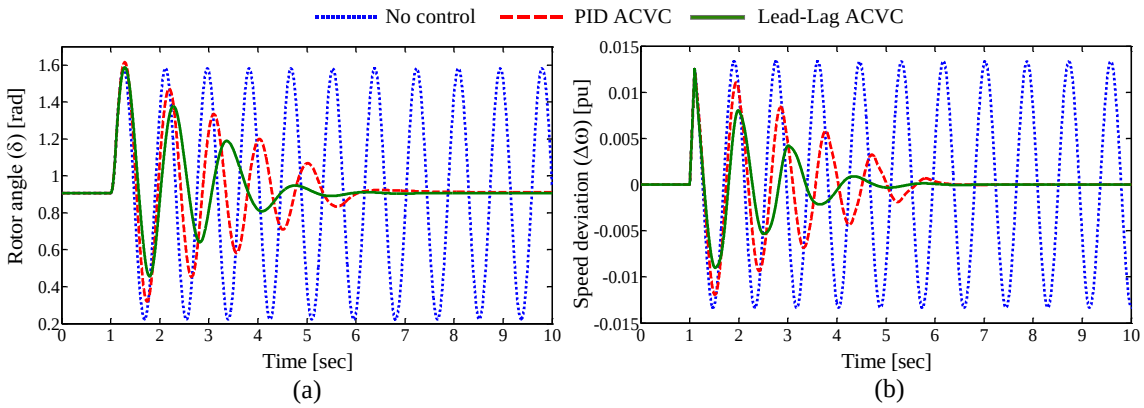

(a) (b)

Figure 3.34: **Test system dynamic response for a six cycle 3-phase fault under normal load**

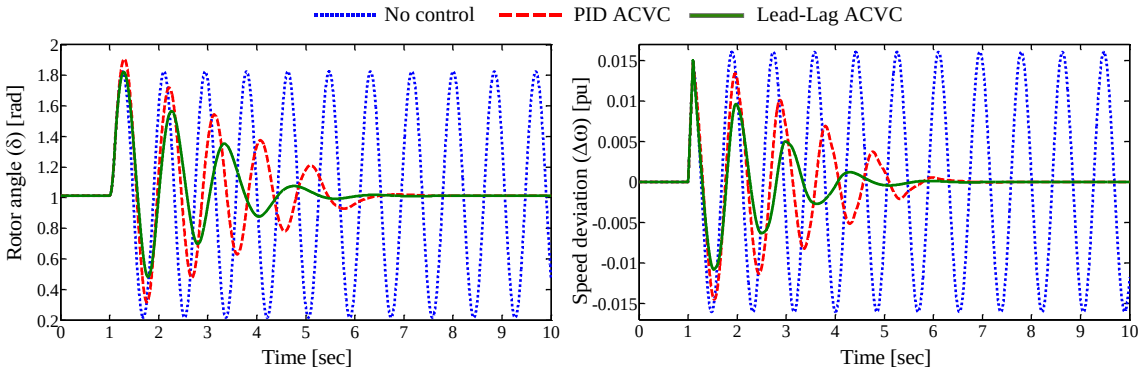

(a) (b)

Figure 3.35: **Test system dynamic response for a six cycle 3-phase fault under heavy load**

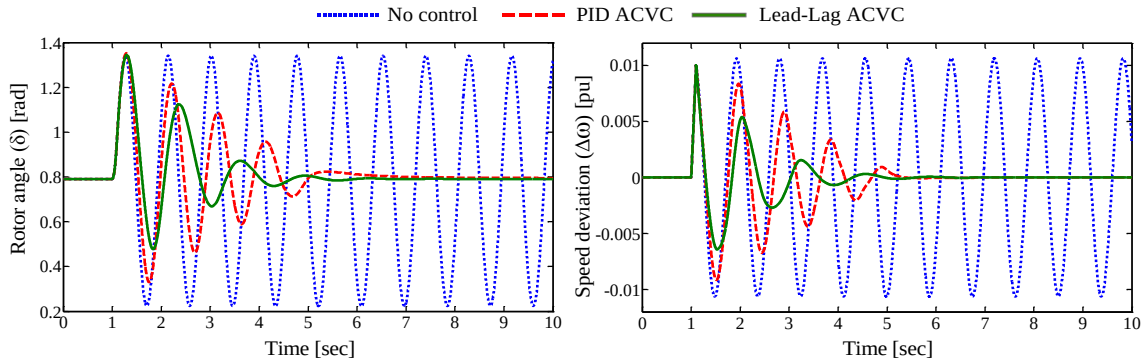

(a) (b)

Figure 3.36: **Test system dynamic response for a six cycle 3-phase fault under light load**

Figures 3.34-3.37 show the response of test system with ACVC under normal load, heavy load, light load and leading PF conditions respectively. In each of these figures (a) represents rotor angle variation and (b) represents speed deviations of the generator. The Figure 3.38 represents variation of modulation index for different types of ACVC. Here, three control schemes are compared. In each figure, solid line indicates the response of test system with

Lead-Lag based ACVC, dashed line indicates the response with PID based ACVC and dotted line indicates the response without controller. From the responses, it is clearly understood that CPSO tuned ACVC gives better performance for fault disturbance under different load conditions. Comparatively the Lead-Lag based ACVC is slightly better than that of PID based ACVC in damping the power oscillations.

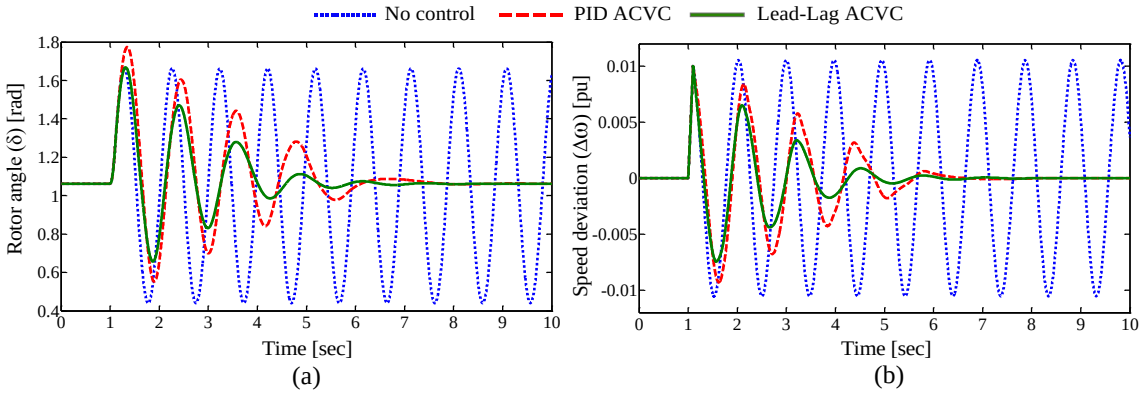

Figure 3.37: **Test system dynamic response for a six cycle 3-phase fault under leading PF condition**

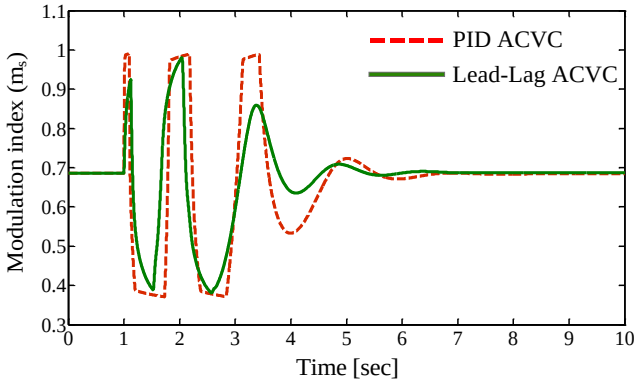

Figure 3.38: **Variation of modulation index (m_s) for different ACVC under normal load**

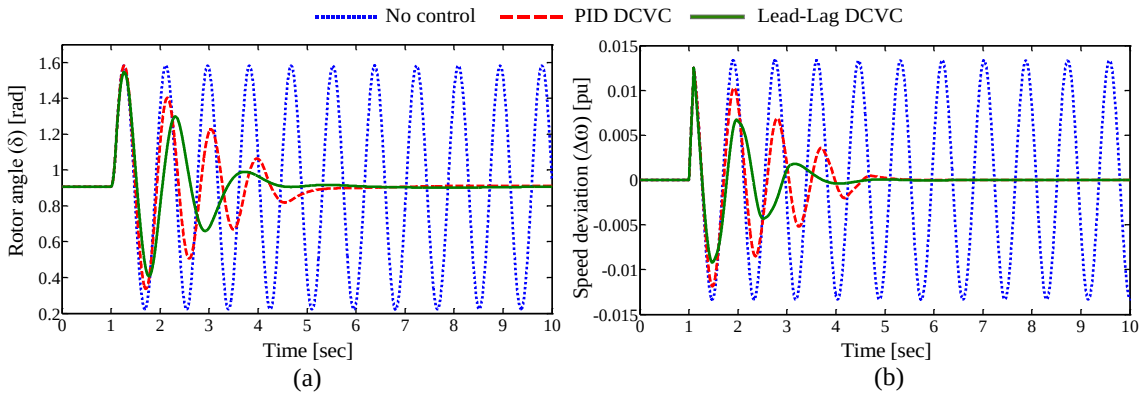

Figure 3.39: **Test system dynamic response for a six cycle 3-phase fault under normal load**

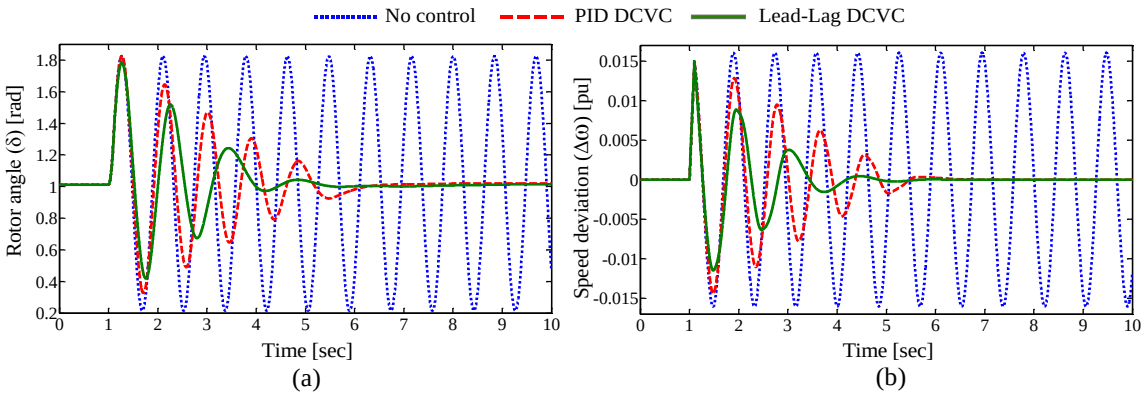

Figure 3.40: **Test system dynamic response for a six cycle 3-phase fault under heavy load**

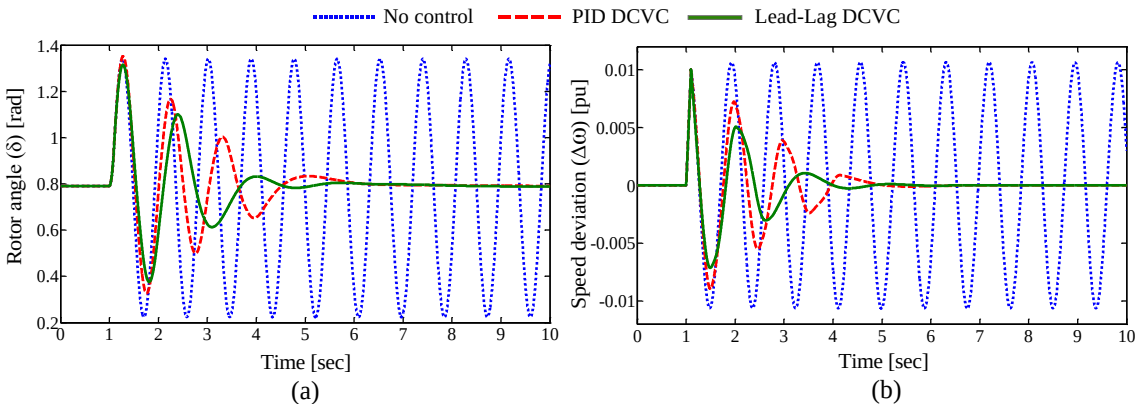

Figure 3.41: **Test system dynamic response for a six cycle 3-phase fault under light load**

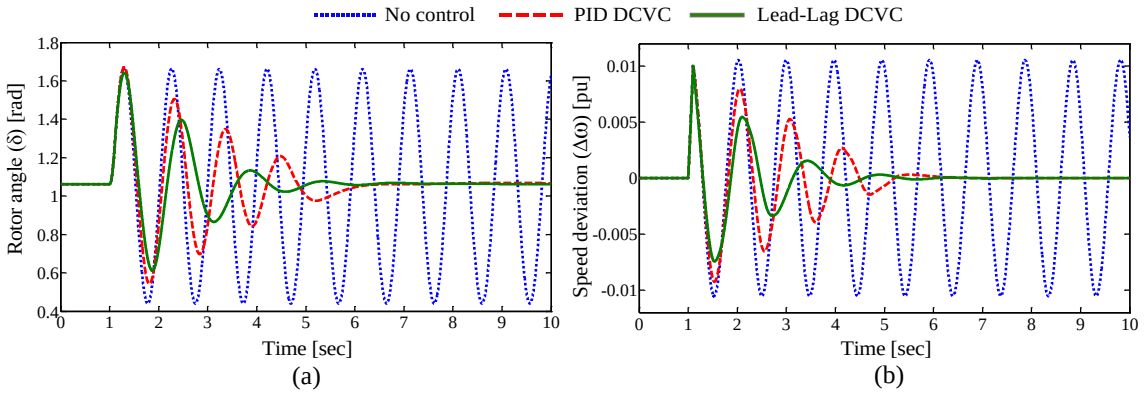

Figure 3.42: **Test system dynamic response for a six cycle 3-phase fault under leading PF condition**

Also, Figures 3.39-3.42 represent the test system dynamic response with DCVC under normal load, heavy load, light load and leading PF conditions respectively. Figure 3.43 depicts the variations of firing angle for different DCVC. Moreover, the comparison is done for Lead-lag based ACVC and DCVC under above mentioned load conditions and these are shown in Figures 3.44-3.47. The optimized controllers give good performance under fault

disturbance and damping out the power oscillations more quickly. The Lead-Lag based DCVC gives more damping effect compared to all other types of STATCOM damping controllers.

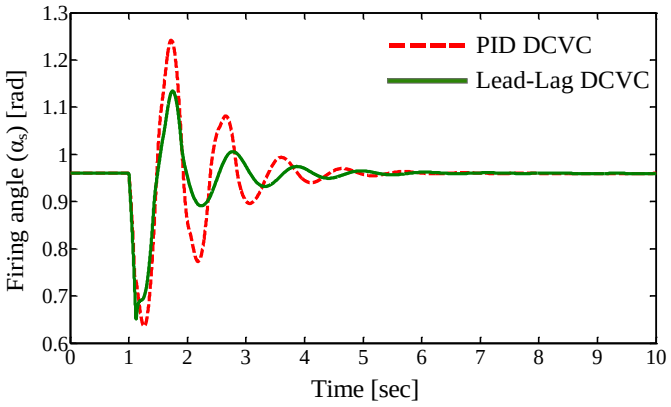

Figure 3.43: **Variation of phase angle (α_s) for different DCVC under normal load**

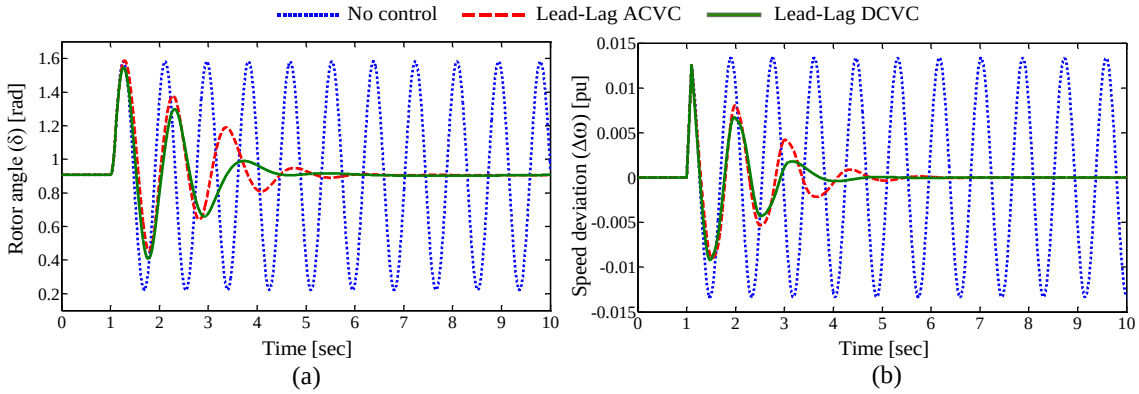

Figure 3.44: **Test system dynamic response for a six cycle 3-phase fault under normal load**

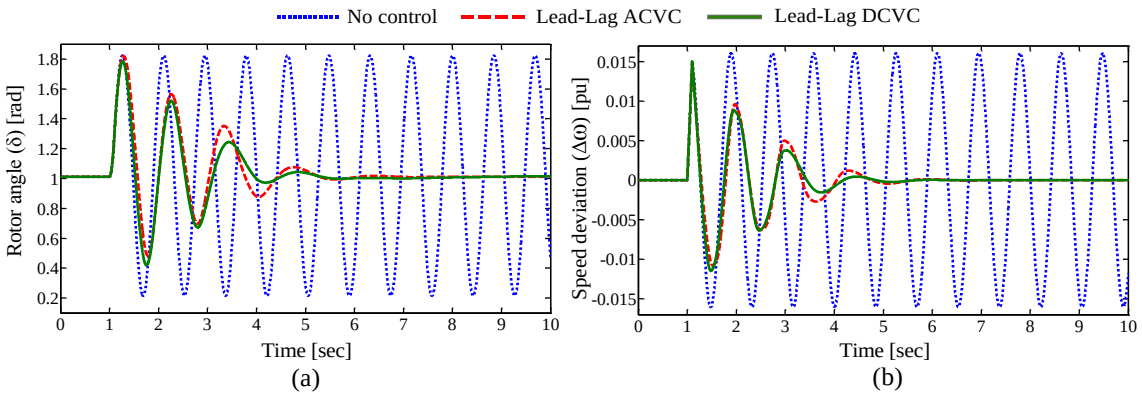

Figure 3.45: **Test system dynamic response for a six cycle 3-phase fault under heavy load**

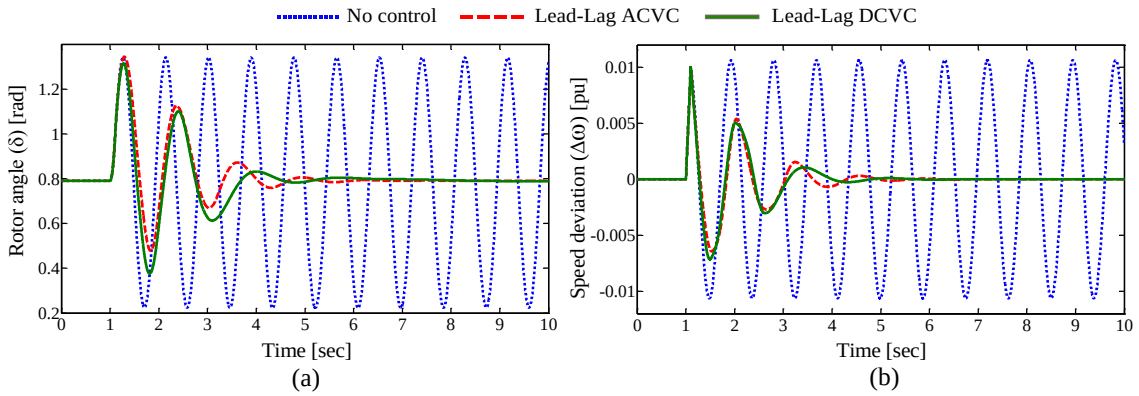

Figure 3.46: **Test system dynamic response for a six cycle 3-phase fault under light load**

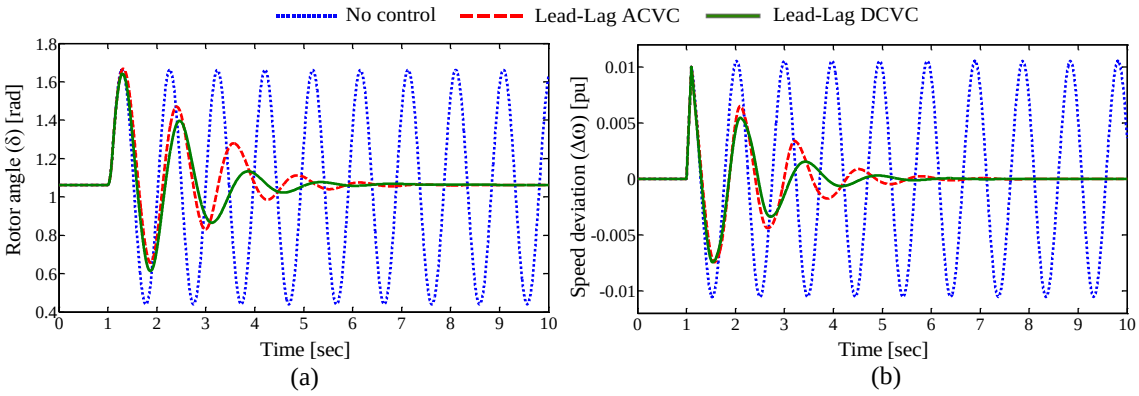

Figure 3.47: **Test system dynamic response for a six cycle 3-phase fault under leading PF condition**

3.7 Summary

This chapter has discussed the modelling with appropriate simulations for different types of FACTS damping controllers to damp the power system oscillations. Two types of FACTS POD stabilizers (PID and Lead-Lag) are considered for all mentioned FACTS controllers. The variations of both speed and voltage deviations are combinedly considered as objective function. The parameters of the developed damping controller are optimized using CPSO algorithm by minimizing the objective function. Finally, the simulation results are compared for three control schemes under specified range of operating conditions. From the simulation analysis, it is clearly observed that the effectiveness of suggested Lead-Lag based FACTS controllers in damping power oscillations is better than PID based FACTS controllers.

Chapter 4

Coordinated Design of PSS and FACTS Damping Controllers using Advanced Adaptive PSO

Chapter 4

Coordinated Design of PSS and FACTS Damping Controllers using Advanced Adaptive PSO

4.1 Introduction

Chapter 3 demonstrated general modelling and optimal design of FACTS controllers, their effectiveness and robustness for a fault disturbance over a wide range of operating conditions applied to the SMIB test system is discussed. In this chapter, the coordinated design of PSS and various FACTS controllers is analyzed in detail. The coordinated designing problem is formulated as an optimization problem and the objective function of this optimization problem is evaluated using advanced adaptive PSO algorithm. Knowledge of the modeling and operation of PSS with power system and basic design of FACTS damping controller are helpful in this coordinated controller design analysis.

4.2 Linearization and Participation Factor

4.2.1 Linearization

The linearized model of the power system including PSS and different FACTS damping controllers can be used for small signal analysis and coordinated controller design. The linearization of dynamic model is derived from the following approach (as described in [102]).

The behavior of a dynamic system, such as a power system, may be described by a set of *n* first order nonlinear ordinary differential equations, represented by the following form:

$$\dot{x}_i = f_i(x_1, x_2, \ldots\ldots\ldots x_n; u_1, u_2, \ldots\ldots\ldots u_r; t) \qquad i = 1,2,\ldots\ldots n \qquad (4.1)$$

where *n* is the order of the system and *r* is the number of inputs. The above equation (4.1) can be written in the following form by using vector-matrix notation as:

$$\dot{x} = f(x, u, t) \qquad (4.2)$$

where $x = [x_1 \;\; x_2 \;\; \ldots\ldots \;\; x_n]^T$, $u = [u_1 \;\; u_2 \;\; \ldots\ldots \;\; u_n]^T$, $f = [f_1 \;\; f_2 \;\; \ldots\ldots \;\; f_n]^T$

Here, the column vector x is referred to as the state vector, and its entries x_i as state variables. The column vector u is the vector of inputs to the system. These are the external signals that influence the performance of the system. Time is denoted by t, and the derivative of a state variable x with respect to time is denoted by $\dot{x}$. If the derivatives of the state variables are not explicit functions of time, then the system is said to be autonomous. In this case, the above equation simplifies to

$$\dot{x} = f(x,u) \tag{4.3}$$

We are often interested in output variables which can be observed on the system. These may be expressed in terms of the state variables and the input variables in the following form:

$$y = g(x,u) \tag{4.4}$$

where $y = [y_1 \quad y_2 \quad ..... \quad y_n]^T$, $g = [g_1 \quad g_2 \quad ..... \quad g_n]^T$

The column vector y is the vector of outputs, and g is a vector of nonlinear functions relating state and input vector corresponding to the equilibrium point about which the small signal performance is to be investigated. Since x_0 and u_0 satisfy equation (4.3), we have

$$\dot{x} = f(x_0, u_0) = 0 \tag{4.5}$$

Let us perturb the system from the above state, by letting

$$x = x_0 + \Delta x,\ u = u_0 + \Delta u$$

where the prefix Δ denotes a small deviation. The new state must satisfy equation (4.5).

Hence, $$\dot{x} = \dot{x}_0 + \Delta\dot{x} = f[(x_0 + \Delta x), (u_0 + \Delta u)] \tag{4.6}$$

As the perturbations are assumed to be small, the linear functions $f(x,u)$ can be expressed in terms of Taylor's series expansion. With terms involving second and higher order powers of Δx and Δu are neglected, we may write like:

$$\begin{aligned} \dot{x}_i = \dot{x}_{i0} + \Delta\dot{x}_i &= f_i[(x_0 + \Delta x), (u_0 + \Delta u)] \\ &= f_i(x_0 + u_0) + \frac{\partial f_i}{\partial x_1}\Delta x_1 + ... \frac{\partial f_i}{\partial x_n}\Delta x_n + \frac{\partial f_i}{\partial u_1}\Delta u_1 + ... \frac{\partial f_i}{\partial u_r}\Delta u_r \end{aligned} \tag{4.7}$$

Since $\dot{x}_{i0} = f_i(x_0, u_0) = 0,$ we obtain

$$\Delta\dot{x}_i = \frac{\partial f_i}{\partial x_1}\Delta x_1 + ... \frac{\partial f_i}{\partial x_n}\Delta x_n + \frac{\partial f_i}{\partial u_1}\Delta u_1 + ... \frac{\partial f_i}{\partial u_r}\Delta u_r \qquad i = 1,2,....n. \tag{4.8}$$

In a similar manner from equation (4.4), we have

$$\Delta y_i = \frac{\partial g_j}{\partial x_1}\Delta x_1 + ... \frac{\partial g_j}{\partial x_n}\Delta x_n + \frac{\partial g_j}{\partial u_1}\Delta u_1 + ... \frac{\partial g_j}{\partial u_r}\Delta u_r \qquad j = 1,2,....m. \tag{4.9}$$

Therefore, the linearized forms of equations (4.3) and (3.4) are

$$\left.\begin{aligned} \Delta \dot{x} &= A\Delta x + B\Delta u \\ \Delta y &= C\Delta x + D\Delta u \end{aligned}\right\} \tag{4.10}$$

where $A = \begin{bmatrix} \frac{\partial f_1}{\partial x_1} & .... & \frac{\partial f_1}{\partial x_n} \\ .... & .... & .... \\ \frac{\partial f_n}{\partial x_1} & .... & \frac{\partial f_n}{\partial x_n} \end{bmatrix}$, $B = \begin{bmatrix} \frac{\partial f_1}{\partial u_1} & .... & \frac{\partial f_1}{\partial u_r} \\ .... & .... & .... \\ \frac{\partial f_n}{\partial u_1} & .... & \frac{\partial f_n}{\partial u_r} \end{bmatrix}$,

$C = \begin{bmatrix} \frac{\partial g_1}{\partial x_1} & .... & \frac{\partial g_1}{\partial x_n} \\ .... & .... & .... \\ \frac{\partial g_m}{\partial x_1} & .... & \frac{\partial g_m}{\partial x_n} \end{bmatrix}$, $D = \begin{bmatrix} \frac{\partial g_1}{\partial u_1} & .... & \frac{\partial g_1}{\partial u_r} \\ .... & .... & .... \\ \frac{\partial g_m}{\partial u_1} & .... & \frac{\partial g_m}{\partial u_r} \end{bmatrix}$

The above partial derivatives are evaluated at the equilibrium point about which the small perturbation is being analyzed.

The terms in equation (4.10),

- Δx is the state vector of dimension *n*
- Δy is the output vector of dimension *m*
- Δu is the input vector of dimension *r*
- A is the $n \times n$ plant matrix
- B is the $n \times r$ input matrix
- C is the $m \times n$ output matrix
- D is the $m \times r$ feed forward matrix

Eigen values of the matrix A, $\lambda_i = \sigma_i \pm j\omega_i$, where $i = 1,2,....n$, are the roots of the characteristic polynomial

$$p(\lambda) = |\lambda I - A| \tag{4.11}$$

where, I is an $n \times n$ identity matrix. Complex eigen values are always appear in pair of complex conjugate numbers.

4.2.2 Participation Factor

The eigen values of the system matrix (A) can be used to analyze the stability of the linear system. In order to study small signal stability of the system, it is essential to identify which state variables significantly participate in the selected modes. Participation factor analysis depicts the involvement of state variables to identify how each state variable affects a given mode. To evaluate the participation matrix (P) the knowledge about right and left eigen vectors is required.

Right eigen vectors:

For any eigen value λ_i, the n-column vector γ_i which satisfies $A\gamma_i = \lambda_i\gamma_i$ is called the right eigen vector of matrix A associated with eigen value λ_i

$$[A]\begin{bmatrix}\gamma_{1i}\\ \gamma_{2i}\\ :\\ \gamma_{ni}\end{bmatrix} = \lambda_i \begin{bmatrix}\gamma_{1i}\\ \gamma_{2i}\\ :\\ \gamma_{ni}\end{bmatrix} \tag{4.12}$$

Left eigen vectors:

For any eigen value λ_i, the n-row vector w_i which satisfies $w_i A = \lambda w_i$ is called the left eigen vector of matrix A associated with eigen value λ_i

$$\begin{bmatrix}w_{i1} & w_{i2} & .. & w_{in}\end{bmatrix}[A] = \lambda_i \begin{bmatrix}w_{i1} & w_{i2} & .. & w_{in}\end{bmatrix} \tag{4.13}$$

Then the participation factor corresponding to eigen value λ_i is given by

$$P_i = \begin{bmatrix}P_{1i}\\ P_{2i}\\ :\\ P_{ni}\end{bmatrix} = \begin{bmatrix}\gamma_{1i}\, w_{i1}\\ \gamma_{2i}\, w_{i2}\\ :\\ \gamma_{ni}\, w_{in}\end{bmatrix} \tag{4.14}$$

The element $P_{ki} = \gamma_{ki}\, w_{ik}$ is termed as participation factor. It is a measure of the relative participation of k^{th} state variable in the i^{th} mode [2].

4.3 Linearized Model for SMIB System with PSS and FACTS Controllers

The linearized model of the power system including excitation system and FACTS controllers is derived in this section. Here, the linearization of SMIB test power system with PSS and different FACTS controllers, as discussed in Chapter 3 (i.e. SVC, TCSC and STATCOM), is considered for analysis. These models can be used for small signal stability analysis and coordinated controller design.

4.3.1 Linearization of Power System with PSS and SVC Controller

The single line diagram of SMIB with SVC controller is shown in Figure 4.1. Here, PSS is installed on the generator and SVC is connected to the bus with voltage V_S. The leakage reactance of transformer is taken as X_T, the transmission line has an equivalent reactance X_L and SVC is represented by an equivalent susceptance B_{SVC}.

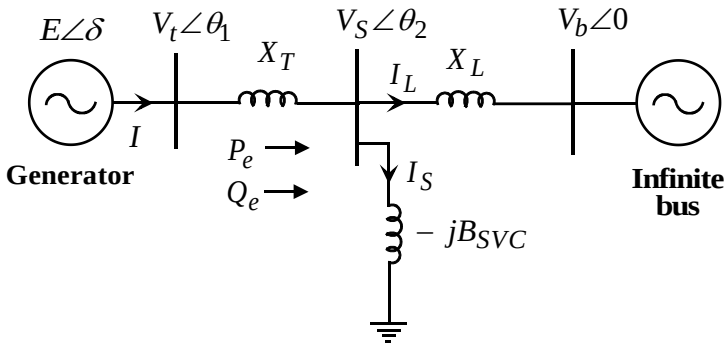

Figure 4.1: **Single line diagram of SMIB with SVC**

A third order model of generator, as explained in section 2.2, is considered for linearization. In deriving the algebraic equations, resistance of transformer, transmission lines and generator, etc. are neglected. In addition the transients present in the transmission lines are also ignored.

In Figure 4.1, V_t and V_b are the generator terminal and infinite bus voltages respectively. The voltage E is the generator voltage behind the synchronous reactance and δ is the rotor angle of the generator. The algebraic equations are

$$P_e = V_{td}\, I_d + V_{tq}\, I_q \tag{4.15}$$

where, $V_{td} = X_q\, I_q$; $\quad V_{tq} = E_q^{'} - X_d^{'}\, I_d$; $\quad E_q^{'} = E_q - (X_d - X_d^{'})\, I_d$

$I_d = I_{Ld} + I_{Sd}$; $\quad I_q = I_{Lq} + I_{Sq}$; $\quad V_t = \sqrt{(V_{td})^2 + (V_{tq})^2}$

where, E_q and $E_q^{'}$ are the voltage back of q-axis synchronous reactance and q-axis component of voltage back of transient reactance of the generator respectively. I_d and I_q represents the *d* and *q* components of the generator terminal current I. I_{Ld}, I_{Sd} and I_{Lq}, I_{Sq} are the d-q components of the transmission line (I_L) and SVC controller (I_S) currents respectively. Form Figure 4.1, we have

$$V_t = jX_T\, I + V_S \tag{4.16}$$

$$V_S = jX_L\, I_L + V_b \tag{4.17}$$

$$I_S = -jB_{SVC}\, V_S \tag{4.18}$$

Subsequent manipulation besides rearrangement of above equations gives

$$I_{Ld} = \frac{1}{X_{DBL}} E_q^{'} - \frac{X_{dTB}}{X_{DT}} V_b \cos\delta \tag{4.19}$$

$$I_{Lq} = \frac{X_{qTB}}{X_{QT}} V_b \sin\delta \tag{4.20}$$

$$I_{Sd} = \frac{X_L}{X_{DT}} E_q^{'} + \frac{X_{dT}}{X_{DT}} V_b \cos\delta \tag{4.21}$$

$$I_{Sq} = -\frac{X_{qT}}{X_{QT}} V_b \sin\delta \tag{4.22}$$

The non-linear equations that represent the generator model and excitation system (as discussed in section 2.2) can be linearized around an operating point are given [11] as,

$$\Delta\dot{\delta} = \Delta\omega \tag{4.23}$$

$$\Delta\dot{\omega} = \frac{\omega_0}{2H}\left[-\Delta P_e - D_1\frac{\Delta\omega}{\omega_0}\right] \tag{4.24}$$

$$\Delta\dot{E}_q^{'} = \frac{1}{T_{d0}^{'}}\left[\Delta E_{fd} - (X_d - X_d^{'})\Delta I_d - \Delta E_q^{'}\right] \tag{4.25}$$

$$\Delta\dot{E}_{fd} = \frac{1}{T_A}\left[K_A(-\Delta V_t + \Delta U_{PSS}) - \Delta E_{fd}\right] \tag{4.26}$$

To derive the state space model of above equations, the linearized network components such as currents, voltages and power, etc. can be written as,

$$\Delta I_{Ld} = a_1 \Delta\delta + a_3 \Delta E_q^{'} + a_5 \Delta B_{SVC}; \qquad \Delta I_{Lq} = b_1 \Delta\delta + b_5 \Delta B_{SVC}$$

$$\Delta I_{Sd} = c_1 \Delta\delta + c_3 \Delta E_q^{'} + c_5 \Delta B_{SVC}; \qquad \Delta I_{Sq} = d_1 \Delta\delta + d_5 \Delta B_{SVC}$$

$$\Delta I_d = e_1 \Delta\delta + e_3 \Delta E_q^{'} + e_5 \Delta B_{SVC}; \qquad \Delta I_q = f_1 \Delta\delta + f_5 \Delta B_{SVC}$$

$$\Delta V_{td} = g_1 \Delta\delta + g_5 \Delta B_{SVC}; \qquad \Delta V_{tq} = h_1 \Delta\delta + h_3 \Delta E_q^{'} + h_5 \Delta B_{SVC}$$

$$\Delta V_t = i_1 \Delta\delta + i_3 \Delta E_q^{'} + i_5 \Delta B_{SVC}; \qquad \Delta P_e = j_1 \Delta\delta + j_3 \Delta E_q^{'} + j_5 \Delta B_{SVC}$$

The linearized power system model can be written in the form of state space model as,

$$\begin{bmatrix} \dot{\Delta\delta} \\ \dot{\Delta\omega} \\ \dot{\Delta E_q^{'}} \\ \dot{\Delta E_{fd}} \end{bmatrix} = \begin{bmatrix} 0 & 1 & 0 & 0 \\ -\frac{\omega_0}{2H} j_1 & -\frac{D_1}{2H} & -\frac{\omega_0}{2H} j_3 & 0 \\ -\frac{(X_d - X_d^{'})}{T_{d0}^{'}} e_1 & 0 & -\frac{(X_d - X_d^{'})}{T_{d0}^{'}} e_3 & \frac{1}{T_{d0}^{'}} \\ -\frac{K_A}{T_A} i_1 & 0 & -\frac{K_A}{T_A} i_3 & -\frac{1}{T_A} \end{bmatrix} \begin{bmatrix} \Delta\delta \\ \Delta\omega \\ \Delta E_q^{'} \\ \Delta E_{fd} \end{bmatrix} + \begin{bmatrix} 0 & 0 \\ 0 & -\frac{\omega_0}{2H} j_5 \\ 0 & -\frac{(X_d - X_d^{'})}{T_{d0}^{'}} e_5 \\ \frac{K_A}{T_A} & -\frac{K_A}{T_A} i_5 \end{bmatrix} \begin{bmatrix} \Delta U_{PSS} \\ \Delta B_{SVC} \end{bmatrix} \tag{4.27}$$

The expressions of unknown reactance and constants in the linearization model are mentioned in Appendix A.

4.3.2 Linearization of Power System with PSS and TCSC Controller

The single line diagram of SMIB system equipped with TCSC controller is shown in Figure 4.2. Here, TCSC is connected in series with the transmission line and it is represented as equivalent reactance X_{TCSC}. The network equation from Figure 4.2 is given by,

$$V_t = j\,(X_T - X_{TCSC} + X_L)\,I + V_b \tag{4.28}$$

After manipulation and dividing the *d* and *q* components of currents we have,

$$I_d = \frac{1}{X_{DT}} E_q^{'} - \frac{1}{X_{DT}} V_b \cos\delta \tag{4.29}$$

$$I_q = \frac{1}{X_{QT}} V_b \sin\delta \tag{4.30}$$

To derive the state space model of equations (4.23) -(4.26), the linearized network components such as currents, voltages and power, etc. can be written as,

$$\Delta I_d = a_1 \Delta\delta + a_3 \Delta E_q^{'} + a_5 \Delta X_{TCSC}\,; \qquad \Delta I_q = b_1 \Delta\delta + b_5 \Delta X_{TCSC}$$

$$\Delta V_{td} = c_1 \Delta\delta + c_5 \Delta X_{TCSC}\,; \qquad \Delta V_{tq} = d_1 \Delta\delta + d_3 \Delta E_q^{'} + d_5 \Delta X_{TCSC}$$

$$\Delta V_t = e_1 \Delta\delta + e_3 \Delta E_q^{'} + e_5 \Delta X_{TCSC}\,; \qquad \Delta P_e = f_1 \Delta\delta + f_3 \Delta E_q^{'} + f_5 \Delta X_{TCSC}$$

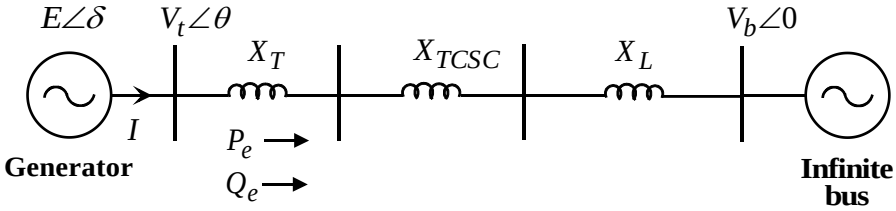

Figure 4.2: **Single line diagram of SMIB with TCSC**

The linearized power system model can be represented in the form of following state space model,

$$\begin{bmatrix} \dot{\Delta\delta} \\ \dot{\Delta\omega} \\ \dot{\Delta E_q^{'}} \\ \dot{\Delta E_{fd}} \end{bmatrix} = \begin{bmatrix} 0 & 1 & 0 & 0 \\ -\frac{\omega_0}{2H} f_1 & -\frac{D_1}{2H} & -\frac{\omega_0}{2H} f_3 & 0 \\ -\frac{(X_d - X_d^{'})}{T_{d0}^{'}} a_1 & 0 & -\frac{(X_d - X_d^{'})}{T_{d0}^{'}} a_3 & \frac{1}{T_{d0}^{'}} \\ -\frac{K_A}{T_A} e_1 & 0 & -\frac{K_A}{T_A} e_3 & -\frac{1}{T_A} \end{bmatrix} \begin{bmatrix} \Delta\delta \\ \Delta\omega \\ \Delta E_q^{'} \\ \Delta E_{fd} \end{bmatrix} + \begin{bmatrix} 0 & 0 \\ 0 & -\frac{\omega_0}{2H} f_5 \\ 0 & -\frac{(X_d - X_d^{'})}{T_{d0}^{'}} a_5 \\ \frac{K_A}{T_A} & -\frac{K_A}{T_A} e_5 \end{bmatrix} \begin{bmatrix} \Delta U_{PSS} \\ \Delta X_{TCSC} \end{bmatrix} \tag{4.31}$$

The expressions of unknown reactance and the constants in linearization model are mentioned in Appendix A.

4.3.3 Linearization of Power System with PSS and STATCOM Controllers

The single line diagram of SMIB with STATCOM controllers is shown in Figure 4.3. Here, STATCOM is connected to a bus with voltage V_S . STATCOM (cited in section 3.2) has two internal controllers with the control variables modulation index (m_S) and phase angle (α_S).

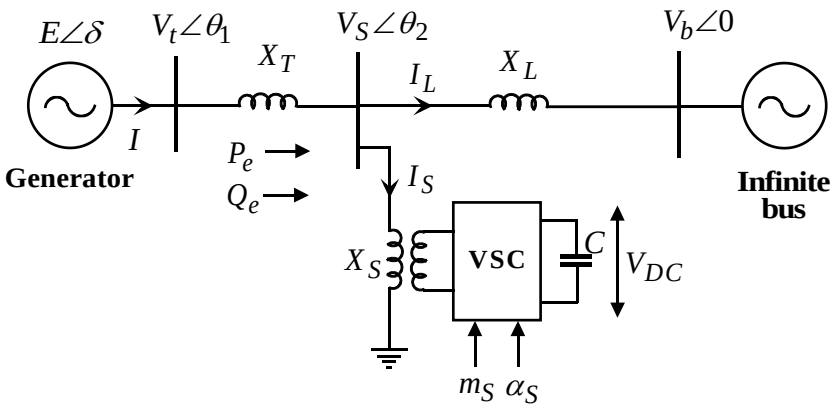

Figure 4.3: **Single line diagram of SMIB with STATCOM**

From the Figure 4.3, the network equations are,

$$V_t = j\,X_T\,I + V_S \tag{4.32}$$

$$V_S = j\,X_L\,I_L + V_b \tag{4.33}$$

$$\begin{bmatrix} V_{Sd} \\ V_{Sq} \end{bmatrix} = \begin{bmatrix} 0 & -X_S \\ X_S & 0 \end{bmatrix} \begin{bmatrix} I_{Sd} \\ I_{Sq} \end{bmatrix} + \begin{bmatrix} \frac{m_S V_{DC}}{2}\cos\alpha_S \\ \frac{m_S V_{DC}}{2}\sin\alpha_S \end{bmatrix} \tag{4.34}$$

$$\left.\begin{aligned} I_d &= I_{Ld} + I_{Sd} \\ I_q &= I_{Lq} + I_{Sq} \end{aligned}\right\} \tag{4.35}$$

where, I, I_L and I_S are the generator armature current, transmission line current and the current flowing through STATCOM respectively. After solving the above network equations and rearranging, we have

$$I_{Ld} = \frac{X_S}{X_{DT}}E_q^{'} + \frac{X_{dT}}{X_{DT}}\frac{m_S V_{DC}}{2}\sin\alpha_S - \frac{X_{dTS}}{X_{DT}}V_b\cos\delta \tag{4.36}$$

$$I_{Lq} = -\frac{X_{qT}}{X_{QT}}\frac{m_S V_{DC}}{2}\cos\alpha_S + \frac{X_{qTS}}{X_{QT}}V_b\sin\delta \tag{4.37}$$

$$I_{Sd} = \frac{X_L}{X_{DT}}E_q^{'} + \frac{X_{dT}}{X_{DT}}V_b\cos\delta - \frac{X_{dTL}}{X_{DT}}\frac{m_S V_{DC}}{2}\sin\alpha_S \tag{4.38}$$

$$I_{Sq} = -\frac{X_{qT}}{X_{QT}}V_b\sin\delta + \frac{X_{qTL}}{X_{QT}}\frac{m_S V_{DC}}{2}\cos\alpha_S \tag{4.39}$$

In the linearization process of power system, the linear equations that correspond to power system model are given in equations (4.23) – (4.26). In addition to these equations one more equation that belongs to STATCOM will appear as,

$$\dot{\Delta V}_{DC} = a_1 \Delta I_{Sd} + a_2 \Delta I_{Sq} + a_3 \Delta m_S + a_4 \Delta \alpha_S \tag{4.40}$$

where,

$$\Delta I_{Ld} = b_1 \Delta\delta + b_3 \Delta E_q^{'} + b_5 \Delta V_{DC} + b_6 \Delta m_S + b_7 \Delta \alpha_S$$

$$\Delta I_{Lq} = c_1 \Delta\delta + c_5 \Delta V_{DC} + c_6 \Delta m_S + c_7 \Delta \alpha_S$$

$$\Delta I_{Sd} = d_1 \Delta\delta + d_3 \Delta E_q^{'} + d_5 \Delta V_{DC} + d_6 \Delta m_S + d_7 \Delta \alpha_S$$

$$\Delta I_{Sq} = e_1 \Delta\delta + e_5 \Delta V_{DC} + e_6 \Delta m_S + e_7 \Delta \alpha_S$$

$$\Delta I_d = f_1 \Delta\delta + f_3 \Delta E_q^{'} + f_5 \Delta V_{DC} + f_6 \Delta m_S + f_7 \Delta \alpha_S$$

$$\Delta I_q = g_1 \Delta\delta + g_5 \Delta V_{DC} + g_6 \Delta m_S + g_7 \Delta \alpha_S$$

$$\Delta V_{td} = h_1 \Delta\delta + h_5 \Delta V_{DC} + h_6 \Delta m_S + h_7 \Delta \alpha_S$$

$$\Delta V_{tq} = i_1 \Delta\delta + i_3 \Delta E_q^{'} + i_5 \Delta V_{DC} + i_6 \Delta m_S + i_7 \Delta \alpha_S$$

$$\Delta V_t = j_1 \Delta\delta + j_3 \Delta E_q^{'} + j_5 \Delta V_{DC} + j_6 \Delta m_S + j_7 \Delta \alpha_S$$

$$\Delta P_e = k_1 \Delta\delta + k_3 \Delta E_q^{'} + k_5 \Delta V_{DC} + k_6 \Delta m_S + k_7 \Delta \alpha_S$$

The sate space model representation of power system with PSS and STATCOM is given by,

$$\begin{bmatrix} \dot{\Delta\delta} \\ \dot{\Delta\omega} \\ \dot{\Delta E_q^{'}} \\ \dot{\Delta E_{fd}} \\ \dot{\Delta V_{DC}} \end{bmatrix} = \begin{bmatrix} 0 & 1 & 0 & 0 & 0 \\ -\frac{\omega_0}{2H} k_1 & -\frac{D_1}{2H} & -\frac{\omega_0}{2H} k_3 & 0 & -\frac{\omega_0}{2H} k_5 \\ -\frac{(X_d - X_d^{'})}{T_{d0}^{'}} f_1 & 0 & -\frac{(X_d - X_d^{'})}{T_{d0}^{'}} f_3 & \frac{1}{T_{d0}^{'}} & -\frac{(X_d - X_d^{'})}{T_{d0}^{'}} f_5 \\ -\frac{K_A}{T_A} j_1 & 0 & -\frac{K_A}{T_A} j_3 & -\frac{K_A}{T_A} & -\frac{K_A}{T_A} j_5 \\ l_1 & 0 & l_3 & 0 & l_5 \end{bmatrix} \begin{bmatrix} \Delta\delta \\ \Delta\omega \\ \Delta E_q^{'} \\ \Delta E_{fd} \\ \Delta V_{DC} \end{bmatrix} + \begin{bmatrix} 0 & 0 & 0 \\ 0 & -\frac{\omega_0}{2H} k_6 & -\frac{\omega_0}{2H} k_7 \\ 0 & -\frac{(X_d - X_d^{'})}{T_{d0}^{'}} f_6 & -\frac{(X_d - X_d^{'})}{T_{d0}^{'}} f_7 \\ \frac{K_A}{T_A} & -\frac{K_A}{T_A} j_6 & -\frac{K_A}{T_A} j_7 \\ 0 & l_6 & l_7 \end{bmatrix} \begin{bmatrix} \Delta U_{PSS} \\ \Delta m_S \\ \Delta \alpha_S \end{bmatrix} \tag{4.41}$$

The expressions of unknown reactance and the constants in linearization model are mentioned in Appendix A.

4.4 Objective Function and Optimization Problem

The coordinated design of PSS and FACTS controller is formulated here as an optimization problem. An objective function (*J*) is considered to formulate the optimization problem. The main aim of this controller design is to provide greater damping and to maintain over all stability of the system. Hence, the eigen value based proposed objective function is formulated as,

$$J = \sum_{j=1}^{nop} \sum_{\sigma_{ij} \geq \sigma_0} (\sigma_0 - \sigma_{ij})^2 + \sum_{j=1}^{nop} \sum_{\zeta_{ij} \leq \zeta_0} (\zeta_0 - \zeta_{ij})^2 \tag{4.42}$$

where *nop* is number of operating points considered in the designing process, σ_i and ζ_i are the real part and damping ratio of the i^{th} electromechanical mode eigen value (λ_i) respectively. σ_0 and ζ_0 are chosen threshold values and these values represent the desirable level of system damping. The conditions $\sigma_{ij} \geq \sigma_0$ and $\zeta_{ij} \leq \zeta_0$ are imposed on the evaluation of objective function to consider only the unstable or poorly damped modes that mainly belong to the electromechanical modes [27], which place the system closed loop eigen values inside the D-shape sector in *s*-plane as shown in Figure 4.4. In this study, the values of σ_0 and ζ_0 are considered as -0.5 and 0.10 respectively.To reduce the computational burden, the value of washout time constant T_w is fixed at 5s, the Lead-Lag controller's time constants T_2 and T_4 are chosen as 0.05. The typical ranges of damping stabilizers gain (K_i) and the time constants T_1, T_3 are chosen as [0.1-50] and [0.06 - 1] respectively. Therefore, based on the objective function, the optimization problem can be defined as:

Minimize J,

Subjected to,

For PSS:

$$\left.\begin{aligned} K_i^{\min} \leq K_i \leq K_i^{\max} \\ T_1^{\min} \leq T_1 \leq T_1^{\max} \\ T_3^{\min} \leq T_3 \leq T_3^{\max} \end{aligned}\right\} \tag{4.43}$$

For different FACTS stabilizers:

$$\left.\begin{aligned} K_F^{\min} \le K_F \le K_F^{\max} \\ T_{F1}^{\min} \le T_{F1} \le T_{F1}^{\max} \\ T_{F3}^{\min} \le T_{F3} \le T_{F3}^{\max} \end{aligned}\right\} \tag{4.44}$$

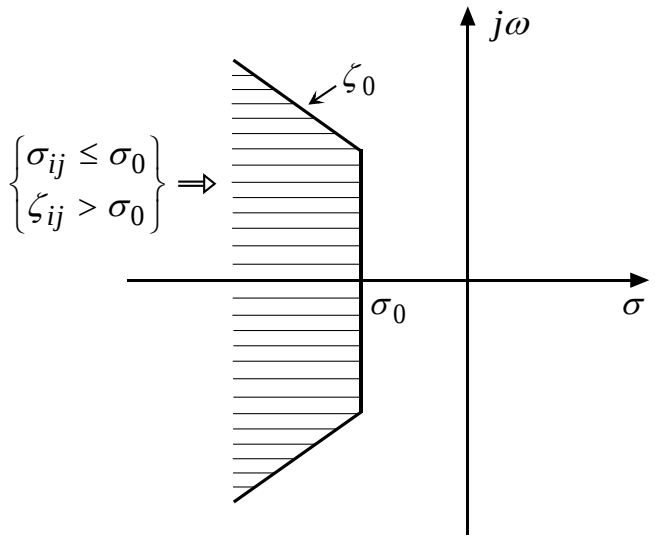

Figure 4.4: **A D-shape sector in *s*-plane, where $\sigma \le \sigma_0$ and $\zeta > \zeta_0$**

where the subscript '*F*' represents different FACTS controllers namely SVC, TCSC and STATCOM AC, DC voltage controllers (i.e $F = s, t, A, D$, where *s* is for SVC, *t* is for TCSC, *A* and *D* are STATCOM AC and DC voltage controllers respectively).

4.5 Advanced Adaptive PSO: An Overview

The conventional particle swarm optimization (CPSO) is discussed in section 3.4 with flow chart. To overcome the few drawbacks and to get faster convergence, an advanced adaptive particle swarm optimization (AAPSO) is proposed in this section.

4.5.1 Advanced Particle Swarm Optimization (APSO)

The CPSO has a drawback of its inadequate convergence towards global optima. To improve the convergence nature of the algorithm and to avoid the explosion of the particle swarm (i.e. the state where the particle velocities and positional coordinates careen toward infinity), an advance PSO technique was introduced by Clerc et al. [103]. The APSO hosting a new parameter called constriction factor '*K*' in the velocity equation. Hence, the particles in the swarm can update their velocities and positions by using the following equations [103]:

$$V_{i,iter+1} = K\,[wV_{i,iter} + c_1 r_1 (P_{i,iter}^{best} - X_{i,iter}) + c_2 r_2 (G_{i,iter}^{best} - X_{i,iter})] \tag{4.45}$$

$$X_{i,iter+1} = X_{i,iter} + V_{i,iter+1} \tag{4.46}$$

where $K = \dfrac{2}{\left| 2 - \varphi - \sqrt{\varphi^2 - 4\varphi} \right|}$, $\varphi = c_1 + c_2, \varphi > 4$

Usually c_1 and c_2 are selected in the range of 0 to 4.

4.5.2 Advanced Adaptive Particle Swarm Optimization (AAPSO)

In population based optimization methods, the policy is to encourage the individuals to roam through the entire search space without clustering around local optima during the initial stages. However, to find the optimum solution efficiently convergence towards the global optima should be encouraged during latter stages. The concept of time-varying acceleration coefficients (TVAC), c_1 and c_2, in addition to time-varying inertia weight factor, is introduced in advanced adaptive PSO technique such that AAPSO can efficiently control the local search and provide adequate convergence towards the global optimum solution. During the initial stages, a large c_1 and a small c_2, allow the particles to move around search space instead of moving the population best prematurely. At latter stages, a small c_1 and a large c_2, allow the particles to converge towards the global optima. Acceleration coefficients are adaptively changed as follows [104]

$$c_1 = c_1^{final}\left(\frac{iter}{iter_{\max}}\right) + c_1^{initial}\left(\frac{iter_{\max} - iter}{iter_{\max}}\right), c_1^{final} < c_1^{initial} \tag{4.47}$$

$$c_2 = c_2^{final}\left(\frac{iter}{iter_{\max}}\right) + c_2^{initial}\left(\frac{iter_{\max} - iter}{iter_{\max}}\right), c_2^{final} > c_2^{initial} \tag{4.48}$$

where $c_1^{initial}, c_2^{initial}$ and c_1^{final}, c_2^{final} are initial and final values of the acceleration coefficients c_1 and c_2 respectively. The coordinated design procedure of PSS and different FACTS controller using AAPSO is depicted in the form of flowchart, as shown in Figure 4.5.

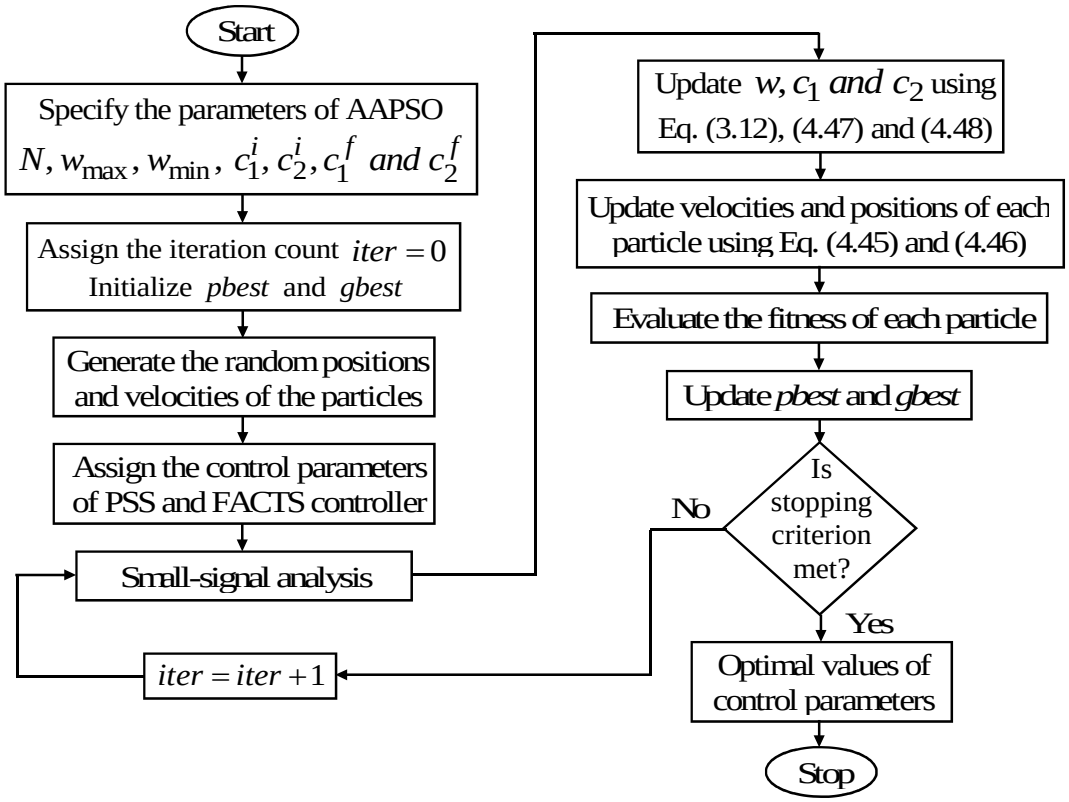

Figure 4.5: **Flowchart depicts the AAPSO algorithm**

4.6 Case study with Different Designs

In this part, the coordinated designs of PSS and different FACTS controllers are analyzed with small signal stability analysis and transient stability studies.

4.6.1 Coordinated Design of PSS and SVC Damping Controller

The eigen value based objective function is optimized using proposed AAPSO algorithm and the obtained optimal control parameter values of different controllers are given in Table 4.1.

Table 4.1: **AAPSO tuned optimal parameter values of PSS and SVC controller**

Control parameter	PSS	SVC
K_i / K_S	8.5721	1.4150
T_1 / T_{S1}	0.6154	0.3129
T_3 / T_{S3}	0.5248	0.4507

Table 4.2: **Electromechanical modes and ζ under different controllers and load conditions**

No control	AAPSO-PSS	AAPSO-SVC	Coordinated design
Normal load			
0.0190±7.0083i,-0.0027	-1.7069±6.9589i,0.2382	-1.2325±4.4737i,0.2656	-2.3668±6.7507i,0.3309
Heavy load			
0.0551±7.0383i,-0.0078	-1.7948±6.9485i,0.2501	-1.3604±4.416i,0.2944	-2.3347±6.6206i,0.3326
Light load			
-0.0101±6.8497i,0.0015	-1.5580±6.8264i,0.2225	-1.0895±4.5835i,0.2313	-2.3233±6.7116i,0.3271
Leading PF condition			
0.0258±5.9776i,-0.0043	-1.7104±5.8164i,0.2821	-0.8933±3.9517i,0.2205	-2.2107±5.5111i,0.3723

In Table 4.2, the test system electromechanical mode eigen values (λ_i) and their damping ratios (ζ_i) with different control schemes and load conditions are shown. It is clear that the system with coordinated controller design provides great damping ratio compare to individual controller designs. The damping ratios of poorly damped electromechanical eigen values are enhanced to 0.331, 0.332, 0.327 and 0.372 for normal, heavy, light and leading PF conditions respectively. Moreover, proposed coordinated controller successfully shift the real part of electromechanical mode eigen values from 0.01, 0.05, -0.01 and 0.02 to -2.36, -2.33, -2.32, -2.21 for normal, heavy, light and leading PF conditions respectively. Therefore, compared to AAPSO-PSS and AAPSO-SVC individual designs, the coordinated design AAPSO-(PSS+SVC) provides enhanced performance towards damping of electromechanical modes of the test system.

Also, the time-domain simulations are conducted for a 6-cycle three phase fault applied on one of the transmission lines of the test system. The rotor angle (δ) variations, speed deviation ($\Delta\omega$), active power (P_e) variations and terminal voltage (V_t) of the test system under normal load condition is shown in Figure 4.6. The system response under heavy, light and leading PF conditions is shown are Figures 4.7 - 4.9 respectively. In all these figures, the coordinated design of PSS and SVC is compared with individual designs. Here, the coordinated design combines the damping effect of two controllers. So response of the system with coordinated design is more prominent than the other two control designs. By analyzing simulation results, it is noticed that the coordinated controller is very quick in damping system oscillations.

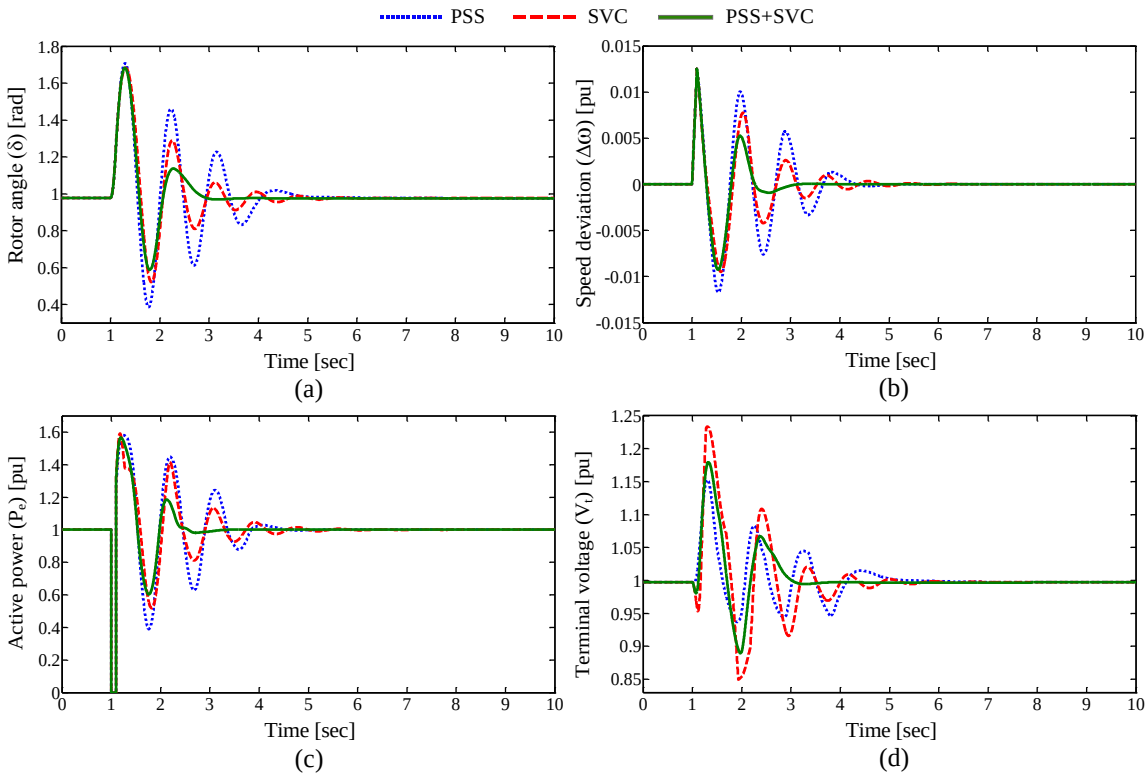

Figure 4.6: **Test system dynamic response for a six cycle 3-phase fault under normal load**

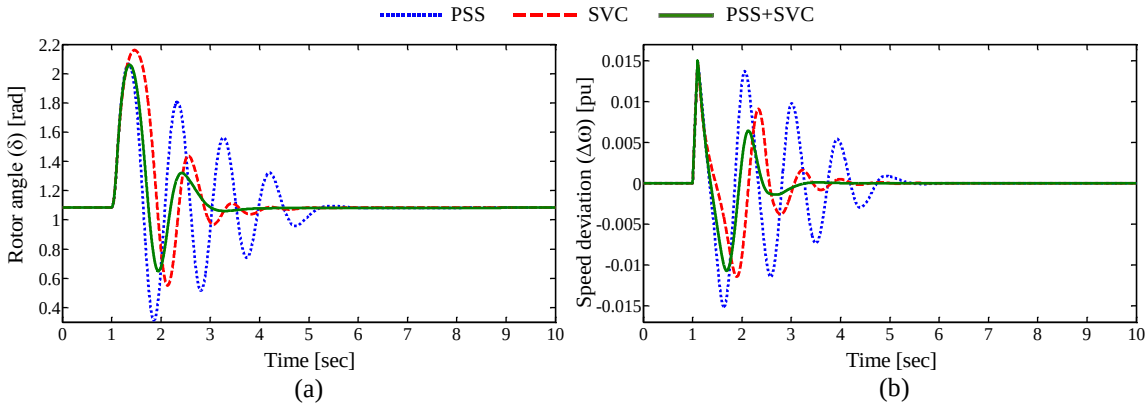

Figure 4.7: **Test system dynamic response for a six cycle 3-phase fault under heavy load**

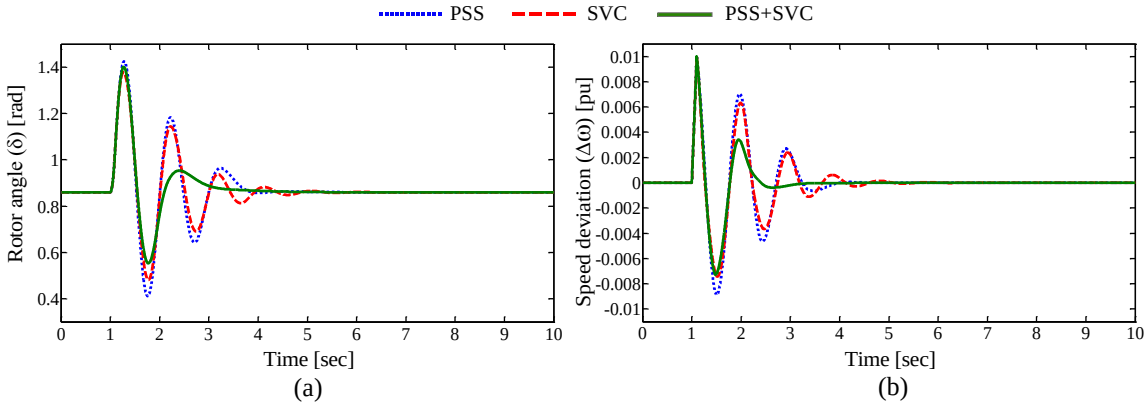

Figure 4.8: **Test system dynamic response for a six cycle 3-phase fault under light load**

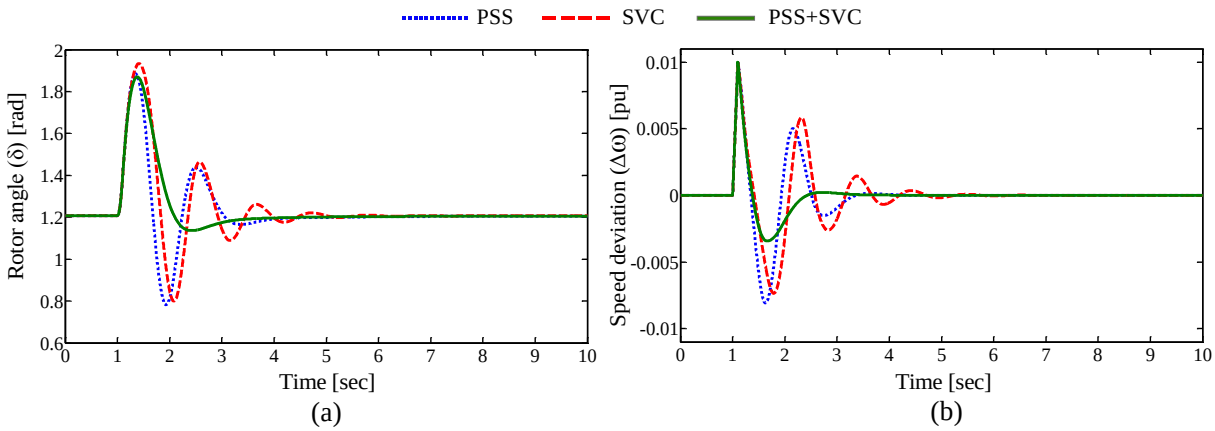

Figure 4.9: **Test system dynamic response for a six cycle 3-phase fault under leading PF condition**

4.6.2 Coordinated Design of PSS and TCSC Damping Controller

Now, the test system is fitted with PSS as well as TCSC damping controller. For the coordinated design of these two controllers, the eigen value based objective function is minimized and the obtained control parameter values are given in Table 4.3. With the help of these control parameter values, the eigen value analysis is carried out using linearized power system derived in section 4.3. The electromechanical modes and the damping ratios of test power system with different controller designs and under different load conditions are given in Table 4.4. The real part of the poorly damped eigen values are shifted in the left part of S-plane from -0.005, 0.027, -0.028 and -0.032 to -2.943, -3.195, -2.607 and -2.726 for normal, heavy, light and leading PF conditions respectively with proposed coordinated design. The damping ratios are also enhanced to 0.48, 0.53, 0.42 and 0.48 for normal, heavy, light and leading PF conditions respectively.

The response curves of the test system with different control designs under different load conditions are represented in Figures 4.10 – 4.13. The rotor angle response, speed deviations, active power variation, and terminal voltage variations of the test system for a 3-phase six cycle fault under normal load condition are shown in Figure 4.10. (a) - (d) respectively. Similarly, the rotor angle response and speed deviation of the test system under heavy, light and leading PF conditions are shown in Figures 4.11 – 4.13 respectively. From all these figures, it is observed that the proposed coordinated design (PSS+TCSC) provides better damping compare to PSS, TCSC individual designs.

Table 4.3: **AAPSO tuned optimal parameter values of PSS and TCSC controller**

Control parameter	PSS	TCSC
K_i / K_t	15.2532	0.8742
T_1 / T_{t1}	0.4154	0.4933
T_3 / T_{t3}	0.5691	0.3515

Table 4.4: **Electromechanical modes and ζ under different controllers and load conditions**

No control	AAPSO-PSS	AAPSO-TCSC	Coordinated design
Normal load			
-0.0056±7.3608i, 0.0007	-1.6700±7.5405i,0.2162	-1.5061±5.2226i,0.2771	-2.9433±5.3399i,0.4827
Heavy load			
0.0277±7.3718i,-0.004	-1.7984±7.5335i,0.2322	-1.6426±4.8609i,0.3201	-3.1952±5.0182i,0.5371
Light load			
-0.0283±7.2078i,0.0039	-1.4826±7.3794i,0.1970	-1.3156±5.5226i,0.2317	-2.6078±5.6064i,0.4218
Leading PF condition			
-0.0329±6.5398i,0.0050	-1.8000±6.6226i,0.2623	-1.3535±4.9450i,0.2640	-2.7267±4.9671i,0.4812

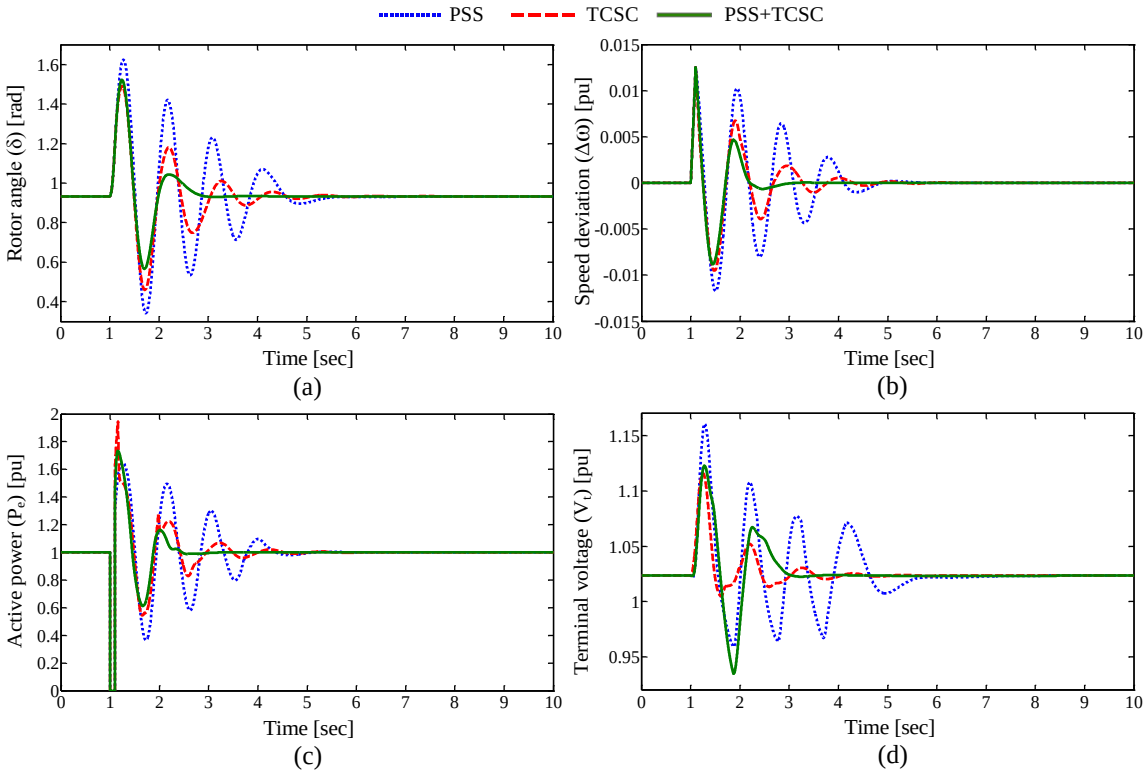

Figure 4.10: **Test system dynamic response for a six cycle 3-phase fault under normal load**

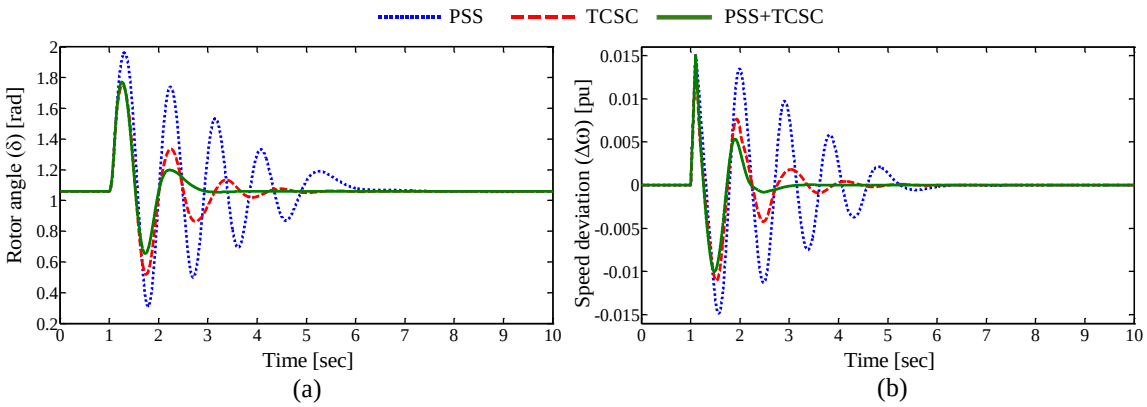

Figure 4.11: **Test system dynamic response for a six cycle 3-phase fault under heavy load**

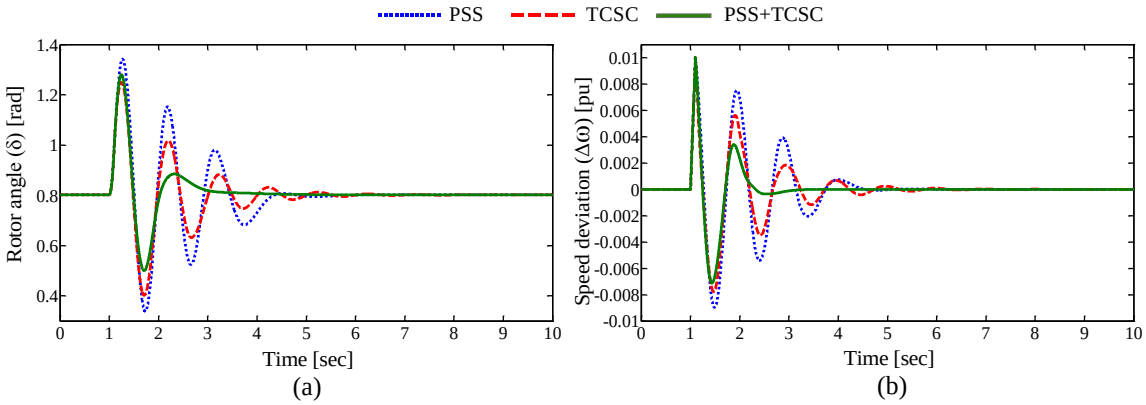

Figure 4.12: **Test system dynamic response for a six cycle 3-phase fault under light load**

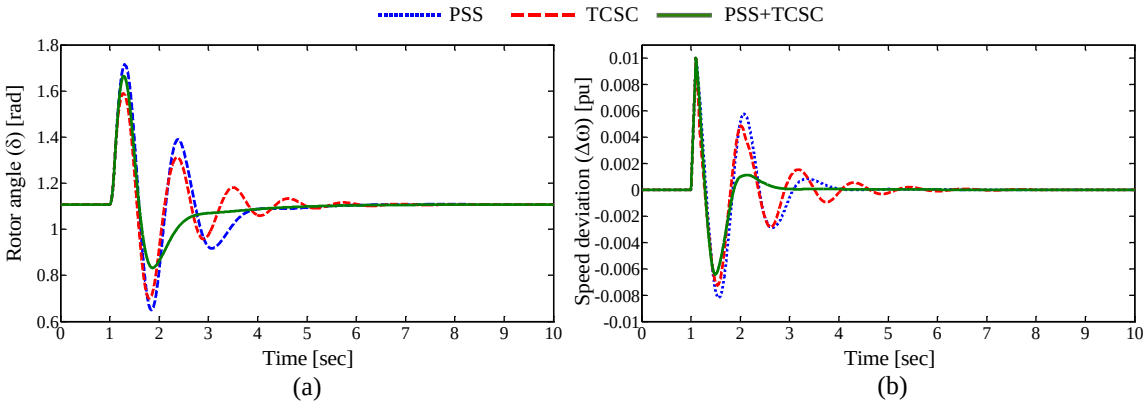

Figure 4.13: **Test system dynamic response for a six cycle 3-phase fault under leading PF condition**

4.6.3 Coordinated Design of PSS and STATCOM Damping Controllers

The coordinated designs of PSS and STATCOM controllers are analyzed in this section with both small signal analysis and time domain simulations. Here, the coordinated design

parameter values of (PSS+ACVC) and (PSS+DCVC) are obtained using AAPSO algorithm by minimizing the objective function defined in section 4.4. The AAPSO tuned control parameter values of PSS with (PSS+ACVC) and (PSS+DCVC) are given in Tables 4.5 and 4.6 respectively.

Table 4.5: **AAPSO tuned optimal parameter values of PSS and ACVC**

Control parameter	PSS	ACVC
K_i / K_t	10.1483	1.0128
T_1 / T_{t1}	0.5123	0.5654
T_3 / T_{t3}	0.4704	0.4871

Table 4.6: **AAPSO tuned optimal parameter values of PSS and DCVC**

Control parameter	PSS	DCVC
K_i / K_t	10.9657	0.9218
T_1 / T_{t1}	0.5972	0.3285
T_3 / T_{t3}	0.5047	0.4526

Table 4.7: **Electromechanical modes and ζ under different controllers and load conditions**

No control	AAPSO-PSS	AAPSO-(PSS+ACVC)	AAPSO- (PSS+DCVC)
Normal load			
0.0435±4.6321i,-0.0094	-1.3886±4.5713i,0.2906	-1.6876±3.5364i,0.4307	-2.1104±4.0948i,0.4581
Heavy load			
-0.0380±4.7394i,0.0080	-1.4707±4.6906i,0.2992	-1.7421±3.5683i,0.4387	-2.408±4.1225i,0.5044
Light load			
0.1387±4.4213i,-0.0313	-1.2701±4.3557i,0.2799	-1.5746±3.451i,0.4151	-1.7413±3.9681i,0.4018
Leading PF condition			
-0.0758±4.1095i,0.0184	-1.3217±4.1446i,0.3038	-1.5226±3.5053i,0.3984	-1.7067±3.9191i,0.3993

Table 4.7 provided the poorly damped eigen values and their damping ratios with proposed coordinated designs. It is clearly observed that the real parts of the mechanical modes are shifted towards left side of S-plane and the damping ratios of corresponding eigen values also enhanced to a great extent with proposed coordinated designs.

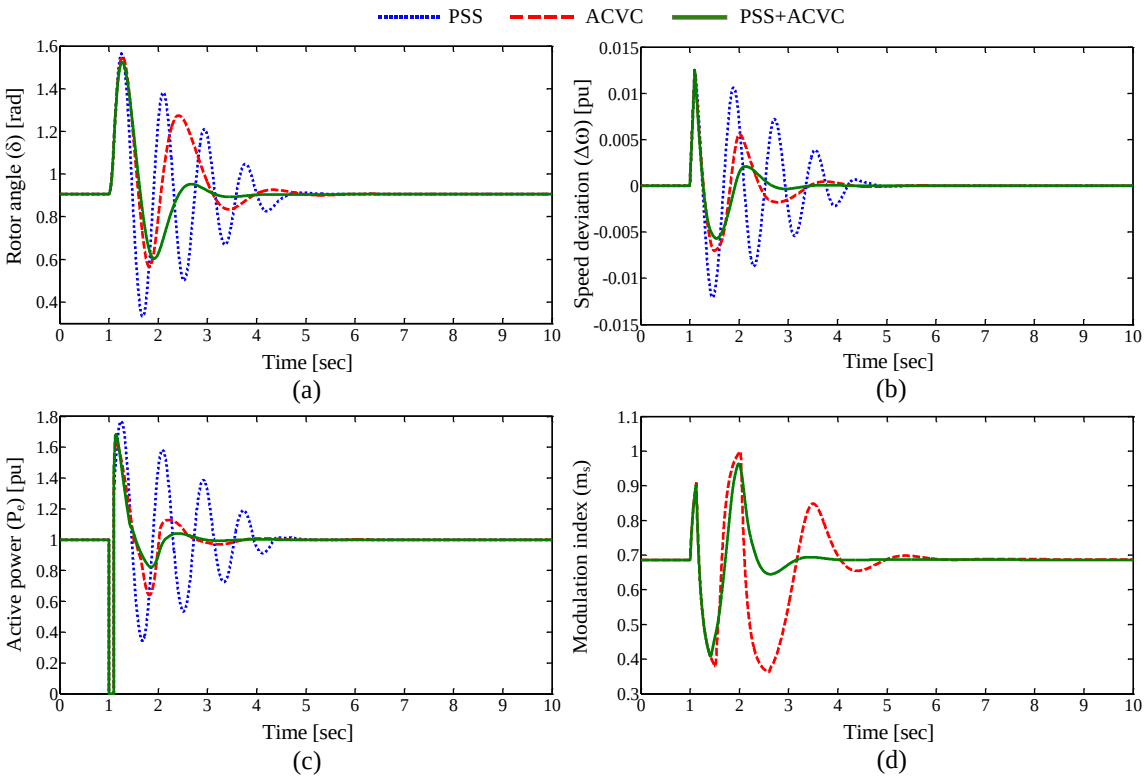

Figure 4.14: **Test system dynamic response for a six cycle 3-phase fault under normal load**

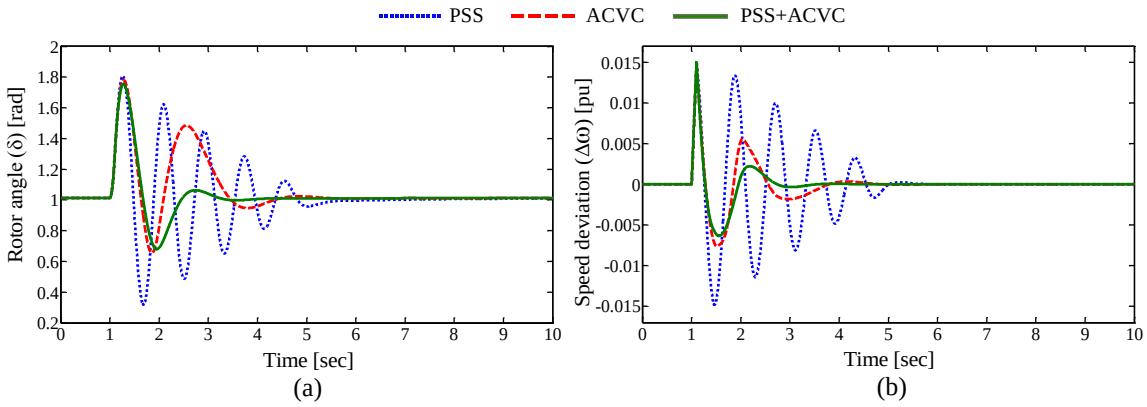

Figure 4.15: **Test system dynamic response for a six cycle 3-phase fault under heavy load**

The test system with PSS and STATCOM damping controller is subjected to a six cycle 3-phase fault under a wide range of load conditions. The rotor angle response, speed variations, active power variations and the modulation index variations are shown in Figure 4.14 under normal load condition for different control designs. The Figures 4.15 – 4.17 show the test system response under heavy, light and leading PF conditions respectively for control designs like only PSS, only ACVC and coordinated design (PSS+ACVC).

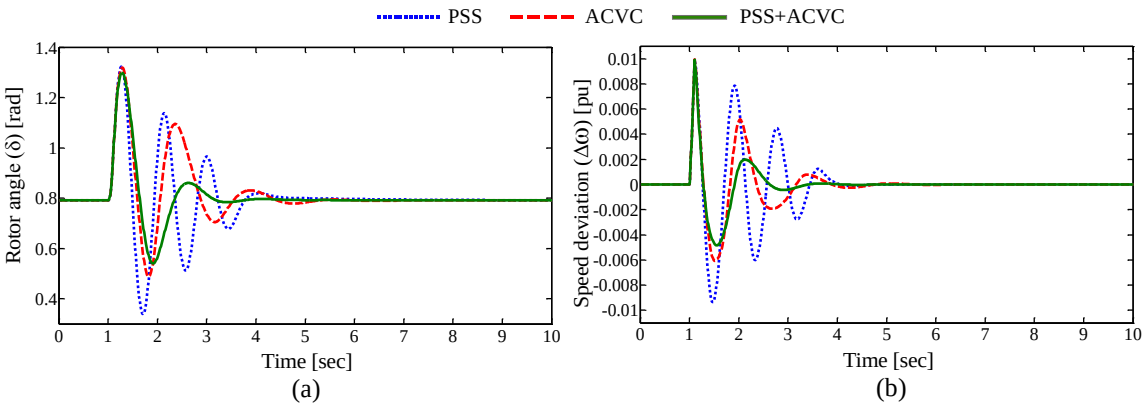

Figure 4.16: **Test system dynamic response for a six cycle 3-phase fault under light load**

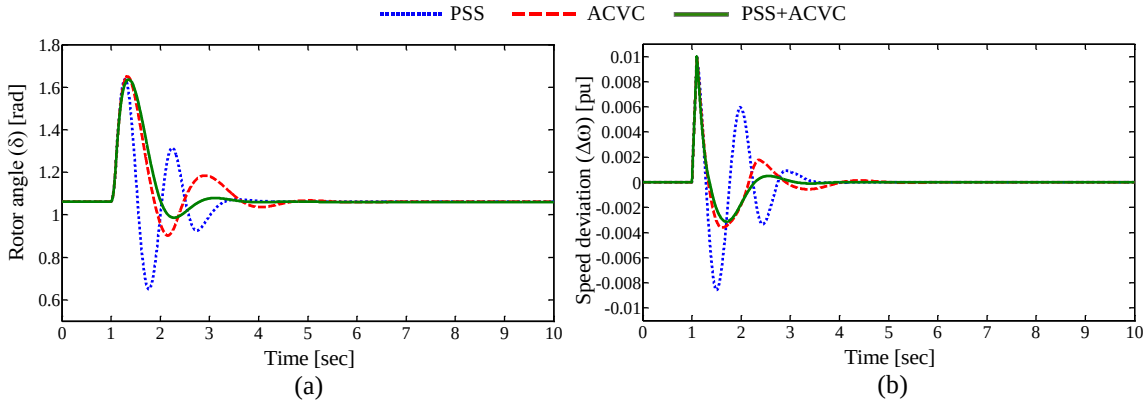

Figure 4.17: **Test system dynamic response for a six cycle 3-phase fault under leading PF condition**

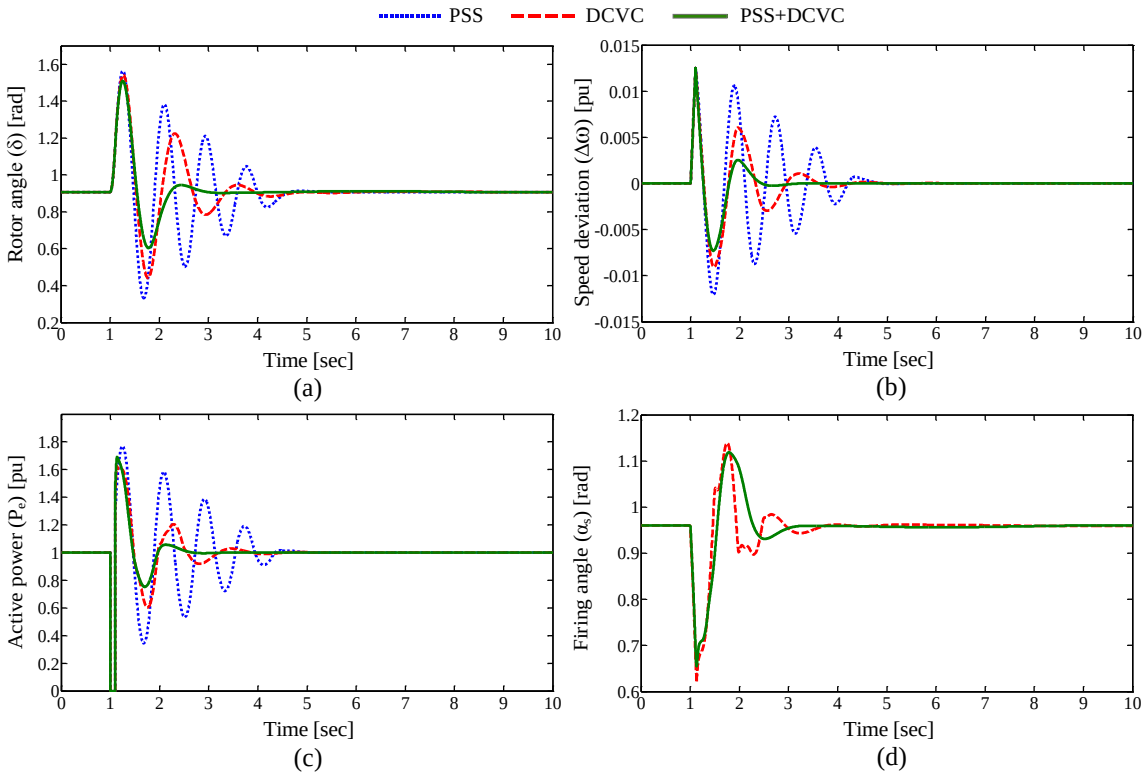

Figure 4.18: **Test system dynamic response for a six cycle 3-phase fault under normal load**

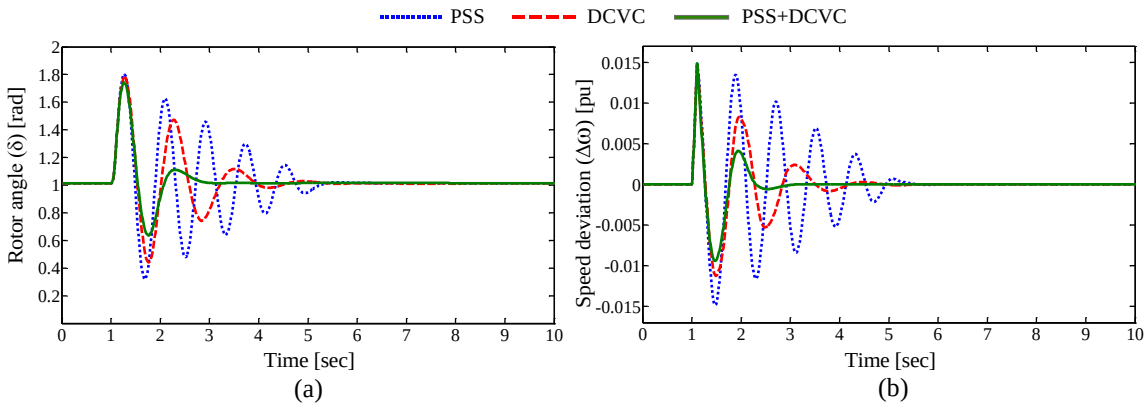

(a) (b)

Figure 4.19: **Test system dynamic response for a six cycle 3-phase fault under heavy load**

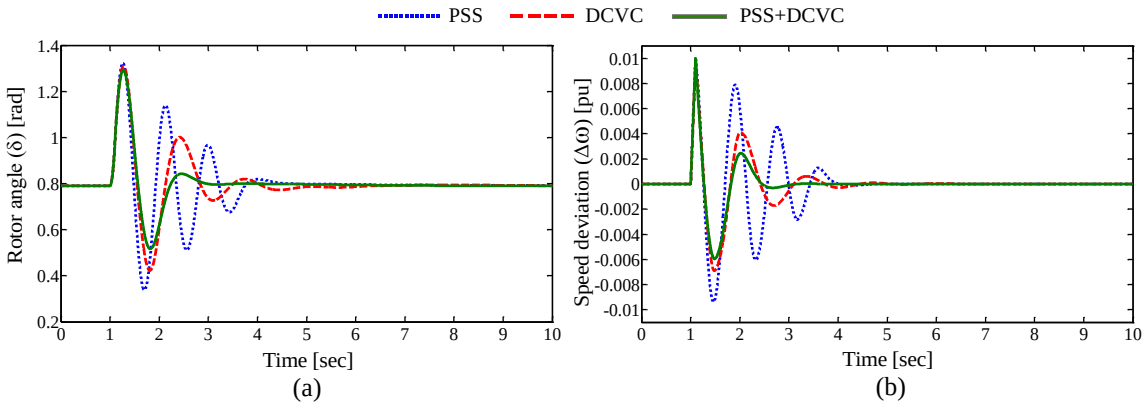

(a) (b)

Figure 4.20: **Test system dynamic response for a six cycle 3-phase fault under light load**

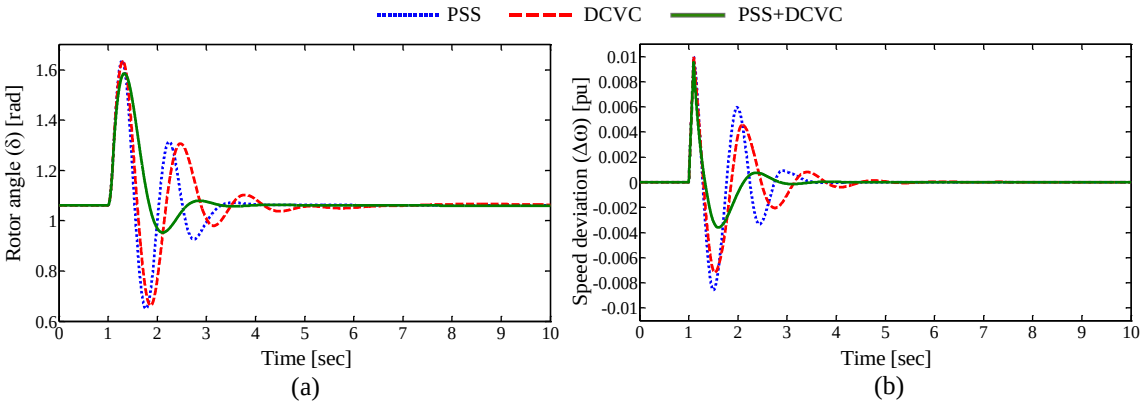

(a) (b)

Figure 4.21: **Test system dynamic response for a six cycle 3-phase fault under leading PF condition**

The test system response of PSS and DCVC controllers with individual designs as well as coordinated designs are compared over a wide range of load conditions and shown in Figures 4.18 – 4.21. The rotor angle, speed, active power and firing angle variations under normal load condition are represented in Figure 4.18. The test system responses under heavy, light and leading PF conditions are shown in Figures 4.19 – 4.21 respectively. The both coordinated designs of PSS with STATCOM controllers (i.e. PSS+ACVC and

PSS+DCVC) provide great settling time of oscillations and be evidence for better damping characteristics compare to individual uncoordinated designs.

4.7 Summary

In this chapter, the modelling of optimal coordinated designs of PSS and different FACTS controllers to damp power system oscillations is proposed. For the proposed designs an extensive simulation study is done. The coordinated design of different controllers is formulated as an optimization problem, which is solved by minimizing the proposed objective function using AAPSO algorithm. The objective function is constructed with poorly damped eigen values of linearized power system under wide range of load conditions. The proposed coordinated designs are compared with the individual designs and the proposed design outshines the individual controller designs in improving damping ratios and in damping of system oscillations under all operating conditions. At the end, the results of small signal analysis and transient analysis are provided for better understanding of robustness of proposed designs.

Chapter 5

Hybrid Coordinated Design of PSS with Series and Shunt FACTS Controllers

Chapter 5

Hybrid Coordinated Design of PSS with Series and Shunt FACTS Controllers

5.1 Introduction

Chapter 4 provided the coordinated design algorithm of PSS and FACTS damping controllers using AAPSO algorithm. An objective function is formulated based on eigen values of the linearized power system with different controllers and the same was minimized using AAPSO algorithm to get optimal control parameter values. The robustness of proposed coordinated designs is compared with the individual designs and the comparison characteristics are analyzed over a wide range of operating conditions. In this chapter, the hybrid coordinated design of PSS with series and shunt FACTS damping controllers is presented in detail. The hybrid coordinated design is formulated as an optimization problem and its objective function is optimized using invasive weed optimization (IWO) algorithm. Knowledge of the linearization process and participation factor method as discussed in Chapter 4 is helpful in this hybrid coordinated controller designing process.

5.2 Linearized Model for a SMIB System with PSS and Multi-type FACTS Controllers

The process of linearizing the power system model including PSS and multi-type FACTS damping controllers is discussed in this section. Here, the linearization of SMIB test power system with PSS, series and shunt (multi-type) FACTS controllers are considered. Two combinations of hybrid coordinated controller are chosen as follows:

- Hybrid coordinated design of PSS with TCSC and SVC damping controllers
- Hybrid coordinated design of PSS with TCSC and STATCOM damping controllers

The design problem is started with linearization of test power system with installed controllers as discussed in the following section.

5.2.1 Linearization of Power System with PSS, TCSC and SVC Damping Controllers

The single line diagram of SMIB with TCSC and SVC controllers is represented in Figure 5.1. Here, the PSS is installed on the generator, TCSC is connected in series to the transmission line and the SVC is connected to the bus with voltage magnitude V_S. The TCSC and SVC are represented by an equivalent reactance X_{TCSC} and susceptance B_{SVC} respectively.

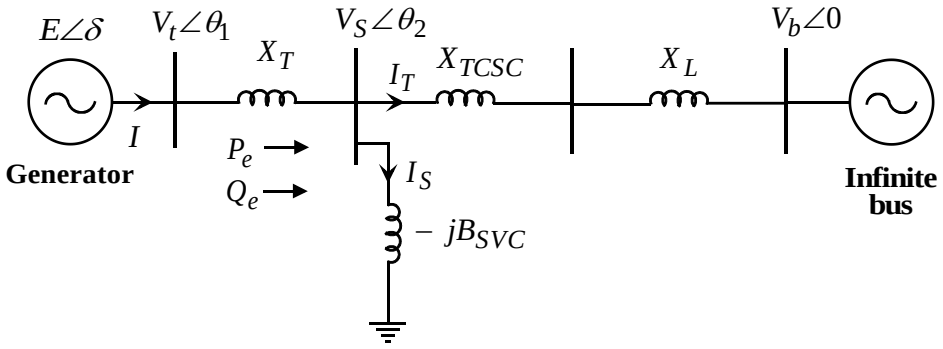

Figure 5.1: **Single line diagram of SMIB with TCSC and SVC**

The algebraic equations are

$$P_e = V_{td}\, I_d + V_{tq}\, I_q \tag{5.1}$$

where, $V_{td} = X_q\, I_q$; $\quad V_{tq} = E_q^{'} - X_d^{'}\, I_d$; $\quad E_q^{'} = E_q - (X_d - X_d^{'})\, I_d$

$I_d = I_{Td} + I_{Sd}$; $\quad I_q = I_{Tq} + I_{Sq}$; $\quad V_t = \sqrt{(V_{td})^2 + (V_{tq})^2}$

where, I_{Td}, I_{Sd} and I_{Tq}, I_{Sq} are the d-q components of the TCSC (I_T) and SVC controller (I_S) currents respectively. From Figure 5.1, we have

$$V_t = jX_T\, I + V_S \tag{5.2}$$

$$V_S = j(X_L - X_{TCSC})\, I_T + V_b \tag{5.3}$$

$$I_S = -jB_{SVC}\, V_S \tag{5.4}$$

Subsequent manipulation besides rearrangement of above equations gives

$$I_{Td} = \frac{1}{X_{DB}} E_q^{'} - \frac{X_{dTB}}{X_{DT}} V_b \cos\delta \tag{5.5}$$

$$I_{Tq} = \frac{X_{qTB}}{X_{QT}} V_b \sin\delta \tag{5.6}$$

$$I_{Sd} = \frac{X_{LTC}}{X_{DT}} E_q^{'} + \frac{X_{dT}}{X_{DT}} V_b \cos\delta \tag{5.7}$$

$$I_{Sq} = -\frac{X_{qT}}{X_{QT}} V_b \sin\delta \tag{5.8}$$

To derive the state space model of above equations the linearized network components such as currents, voltages and power, etc. can be written as,

$$\Delta I_{Td} = a_1 \Delta\delta + a_3 \Delta E_q^{'} + a_5 \Delta X_{TCSC} + a_6 \Delta B_{SVC}$$

$$\Delta I_{Lq} = b_1 \Delta\delta + b_5 \Delta X_{TCSC} + b_6 \Delta B_{SVC}$$

$$\Delta I_{Sd} = c_1 \Delta\delta + c_3 \Delta E_q^{'} + c_5 \Delta X_{TCSC} + c_6 \Delta B_{SVC}$$

$$\Delta I_{Sq} = d_1 \Delta\delta + d_5 \Delta X_{TCSC} + d_6 \Delta B_{SVC}$$

$$\Delta I_d = e_1 \Delta\delta + e_3 \Delta E_q^{'} + e_5 \Delta X_{TCSC} + e_6 \Delta B_{SVC}$$

$$\Delta I_q = f_1 \Delta\delta + f_5 \Delta X_{TCSC} + f_6 \Delta B_{SVC}$$

$$\Delta V_{tq} = h_1 \Delta\delta + h_3 \Delta E_q^{'} + h_5 \Delta X_{TCSC} + h_6 \Delta B_{SVC}$$

$$\Delta V_{td} = g_1 \Delta\delta + g_5 \Delta X_{TCSC} + g_6 \Delta B_{SVC}$$

$$\Delta V_t = i_1 \Delta\delta + i_3 \Delta E_q^{'} + i_5 \Delta X_{TCSC} + i_6 \Delta B_{SVC}$$

$$\Delta P_e = j_1 \Delta\delta + j_3 \Delta E_q^{'} + j_5 \Delta X_{TCSC} + j_6 \Delta B_{SVC}$$

The linearized power system model can be written in the form of state space model as,

$$\begin{bmatrix} \Delta\dot{\delta} \\ \Delta\dot{\omega} \\ \Delta\dot{E}_q^{'} \\ \Delta\dot{E}_{fd} \end{bmatrix} = \begin{bmatrix} 0 & 1 & 0 & 0 \\ -\frac{\omega_0}{2H} j_1 & -\frac{D_1}{2H} & -\frac{\omega_0}{2H} j_3 & 0 \\ -\frac{(X_d - X_d^{'})}{T_{d0}^{'}} e_1 & 0 & -\frac{(X_d - X_d^{'})}{T_{d0}^{'}} e_3 & \frac{1}{T_{d0}^{'}} \\ -\frac{K_A}{T_A} i_1 & 0 & -\frac{K_A}{T_A} i_3 & -\frac{1}{T_A} \end{bmatrix} \begin{bmatrix} \Delta\delta \\ \Delta\omega \\ \Delta E_q^{'} \\ \Delta E_{fd} \end{bmatrix} + \begin{bmatrix} 0 & 0 & 0 \\ 0 & -\frac{\omega_0}{2H} j_5 & -\frac{\omega_0}{2H} j_6 \\ 0 & -\frac{(X_d - X_d^{'})}{T_{d0}^{'}} e_5 & -\frac{(X_d - X_d^{'})}{T_{d0}^{'}} e_6 \\ \frac{K_A}{T_A} & -\frac{K_A}{T_A} i_5 & -\frac{K_A}{T_A} i_6 \end{bmatrix} \begin{bmatrix} \Delta U_{PSS} \\ \Delta X_{TCSC} \\ \Delta B_{SVC} \end{bmatrix} \tag{5.9}$$

The expressions of unknown reactance and the constants in linearization model are given in Appendix B.

5.2.2 Linearization of Power System with PSS, TCSC and STATCOM Damping Controllers

The single line diagram of SMIB system equipped with TCSC and STATCOM damping controllers is shown in Figure 5.2. Here, the TCSC is connected in series with the transmission line and STATCOM is shunted with the bus with voltage magnitude is V_S. The network equations from Figure 5.2 are given by,

$$V_t = j\,X_T\,I + V_S \tag{5.10}$$

$$V_S = j\,(X_L - \mathrm{X_{TCSC}})\,I_T + V_b \tag{5.11}$$

$$\begin{bmatrix} V_{Sd} \\ V_{Sq} \end{bmatrix} = \begin{bmatrix} 0 & -X_S \\ X_S & 0 \end{bmatrix} \begin{bmatrix} I_{Sd} \\ I_{Sq} \end{bmatrix} + \begin{bmatrix} \frac{m_S V_{DC}}{2}\cos\alpha_S \\ \frac{m_S V_{DC}}{2}\sin\alpha_S \end{bmatrix} \tag{5.12}$$

$$\left.\begin{aligned} I_d &= I_{Td} + I_{Sd} \\ I_q &= I_{Tq} + I_{Sq} \end{aligned}\right\} \tag{5.13}$$

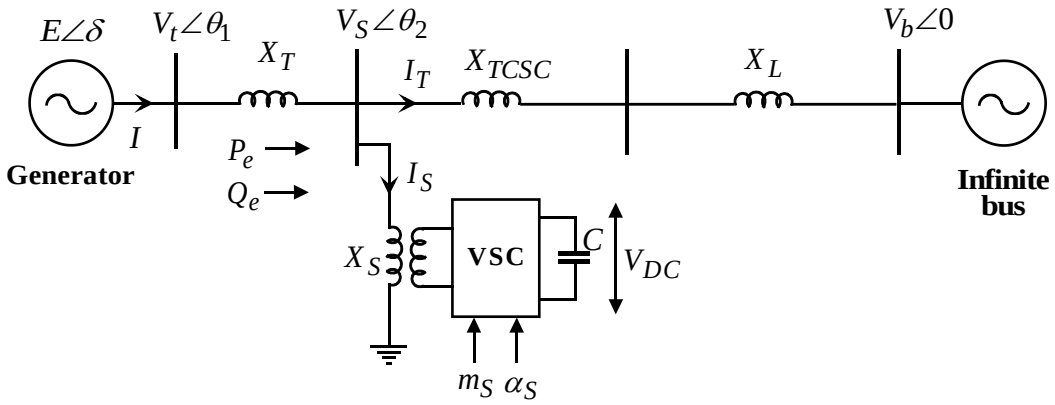

Figure 5.2: **Single line diagram of SMIB with TCSC and STATCOM**

where, I, I_T and I_S are the generator armature current, current flowing through the TCSC and STATCOM respectively. After solving the above network equations and rearranging we have,

$$I_{Td} = \frac{X_S}{X_{DT}}E_q^{'} + \frac{X_{dT}}{X_{DT}}\frac{m_S V_{DC}}{2}\sin\alpha_S - \frac{X_{dTS}}{X_{DT}}V_b\cos\delta \tag{5.14}$$

$$I_{Tq} = -\frac{X_{qT}}{X_{QT}}\frac{m_S V_{DC}}{2}\cos\alpha_S + \frac{X_{qTS}}{X_{QT}}V_b\sin\delta \tag{5.15}$$

$$I_{Sd} = \frac{X_{LTC}}{X_{DT}}E_q^{'} + \frac{X_{dT}}{X_{DT}}V_b\cos\delta - \frac{X_{dTLTC}}{X_{DT}}\frac{m_S V_{DC}}{2}\sin\alpha_S \tag{5.16}$$

$$I_{Sq} = -\frac{X_{qT}}{X_{QT}} V_b \sin\delta + \frac{X_{qTLTC}}{X_{QT}} \frac{m_S V_{DC}}{2} \cos\alpha_S \tag{5.17}$$

In the linearization process of power system, linear network components that correspond to power system model as discussed in section 4.3 are formulated as,

$\Delta I_{Td} = b_1 \Delta\delta + b_3 \Delta E_q^{'} + b_5 \Delta V_{DC} + b_6 \Delta \mathrm{X}_{\mathrm{TCSC}} + b_7 \Delta m_S + b_8 \Delta\alpha_S$;

$\Delta I_{Tq} = c_1 \Delta\delta + c_5 \Delta V_{DC} + c_6 \Delta \mathrm{X}_{\mathrm{TCSC}} + c_7 \Delta m_S + c_8 \Delta\alpha_S$;

$\Delta I_{Sd} = d_1 \Delta\delta + d_3 \Delta E_q^{'} + d_5 \Delta V_{DC} + d_6 \Delta \mathrm{X}_{\mathrm{TCSC}} + d_7 \Delta m_S + d_8 \Delta\alpha_S$;

$\Delta I_{Sq} = e_1 \Delta\delta + e_5 \Delta V_{DC} + e_6 \Delta \mathrm{X}_{\mathrm{TCSC}} + e_7 \Delta m_S + e_8 \Delta\alpha_S$;

$\Delta I_d = f_1 \Delta\delta + f_3 \Delta E_q^{'} + f_5 \Delta V_{DC} + f_6 \Delta \mathrm{X}_{\mathrm{TCSC}} + f_7 \Delta m_S + f_8 \Delta\alpha_S$;

$\Delta I_q = g_1 \Delta\delta + g_5 \Delta V_{DC} + g_6 \Delta \mathrm{X}_{\mathrm{TCSC}} + g_7 \Delta m_S + g_8 \Delta\alpha_S$;

$\Delta V_{td} = h_1 \Delta\delta + h_5 \Delta V_{DC} + h_6 \Delta \mathrm{X}_{\mathrm{TCSC}} + h_7 \Delta m_S + h_8 \Delta\alpha_S$;

$\Delta V_{tq} = i_1 \Delta\delta + i_3 \Delta E_q^{'} + i_5 \Delta V_{DC} + i_6 \Delta \mathrm{X}_{\mathrm{TCSC}} + i_7 \Delta m_S + i_8 \Delta\alpha_S$;

$\Delta V_t = j_1 \Delta\delta + j_3 \Delta E_q^{'} + j_5 \Delta V_{DC} + j_6 \Delta \mathrm{X}_{\mathrm{TCSC}} + j_7 \Delta m_S + j_8 \Delta\alpha_S$;

$\Delta P_e = k_1 \Delta\delta + k_3 \Delta E_q^{'} + k_5 \Delta V_{DC} + k_6 \Delta \mathrm{X}_{\mathrm{TCSC}} + k_7 \Delta m_S + k_8 \Delta\alpha_S$;

The sate space model representation of power system with PSS, TCSC and STATCOM is given by,

$$\begin{bmatrix} \dot{\Delta\delta} \\ \dot{\Delta\omega} \\ \dot{\Delta E_q^{'}} \\ \dot{\Delta E_{fd}} \\ \dot{\Delta V_{DC}} \end{bmatrix} = \begin{bmatrix} 0 & 1 & 0 & 0 & 0 \\ -\frac{\omega_0}{2H} k_1 & -\frac{D_1}{2H} & -\frac{\omega_0}{2H} k_3 & 0 & -\frac{\omega_0}{2H} k_5 \\ -\frac{(X_d - X_d^{'})}{T_{d0}^{'}} f_1 & 0 & -\frac{(X_d - X_d^{'})}{T_{d0}^{'}} f_3 & \frac{1}{T_{d0}^{'}} & -\frac{(X_d - X_d^{'})}{T_{d0}^{'}} f_5 \\ -\frac{K_A}{T_A} j_1 & 0 & -\frac{K_A}{T_A} j_3 & -\frac{K_A}{T_A} & -\frac{K_A}{T_A} j_5 \\ l_1 & 0 & l_3 & 0 & l_5 \end{bmatrix} \begin{bmatrix} \Delta\delta \\ \Delta\omega \\ \Delta E_q^{'} \\ \Delta E_{fd} \\ \Delta V_{DC} \end{bmatrix} + \begin{bmatrix} 0 & 0 & 0 & 0 \\ 0 & -\frac{\omega_0}{2H} k_6 & -\frac{\omega_0}{2H} k_7 & -\frac{\omega_0}{2H} k_8 \\ 0 & -\frac{(X_d - X_d^{'})}{T_{d0}^{'}} f_6 & -\frac{(X_d - X_d^{'})}{T_{d0}^{'}} f_7 & -\frac{(X_d - X_d^{'})}{T_{d0}^{'}} f_8 \\ \frac{K_A}{T_A} & -\frac{K_A}{T_A} j_6 & -\frac{K_A}{T_A} j_7 & -\frac{K_A}{T_A} j_8 \\ 0 & l_6 & l_7 & l_8 \end{bmatrix} \begin{bmatrix} \Delta U_{PSS} \\ \Delta X_{TCSC} \\ \Delta m_S \\ \Delta\alpha_S \end{bmatrix} \tag{5.18}$$

The expressions of unknown reactance and the constants in linearization model are given in Appendix B.

5.3 IWO Algorithm and Its Implementation

In recent times, many numerical optimization techniques are developed with the inspiration from ecological phenomena. One of such optimization techniques that is inspired from colonization of invasive weeds is labeled as invasive weed optimization (IWO). The term weed refers to a robust wild plant that grows in gardens or fields of crops that prevents the growth of actual plant. The robustness, adaptation and randomness of weeds motivated to propose the concept of IWO algorithm by Mehrabian and Lucas [105] in 2006. Since then, the researchers pursued the IWO algorithm to adopt the incredible features in different application domains. The IWO algorithm has become a finest alternative to the other conventional optimization algorithms due to its quick convergence and decent complexity. This algorithm is already applied in several problems like solving nonlinear equations [106], antenna design [107-110], wireless communications [111], and electricity markets [112]. The algorithm is simple yet powerful in converging to optimal solution by employing basic properties like seeding, growth and competition in a weed colony. The basic steps involved in modelling and simulating the colonizing behavior of weeds are initialization, reproduction, spatial distribution and competitive exclusion. The procedure of IWO algorithm adopted here for designing a robust coordinated controller in multi-machine power system is summarized in the following steps and the flowchart for the same is shown in Figure. 5.3.

Step 1: *Initialization:* Define 'N' variables of the coordinated controller and their maximum and minimum values. Then a finite number of weeds are generated randomly and spread over the N-dimensional search space. Here, each weed representing one trail solution of optimization problem which has to be minimized.

Step 2: *Reproduction:* Each individual will be assigned with its corresponding fitness value, which is obtained from the proposed objective function in (4.42). Each member of the population can become a plant and is allowed to produce seeds depending on its own, as well as the colony's lowest and highest fitness such that the number of seeds produced by a weed increases linearly from lowest possible seeds to the maximum number of seeds. Here, a weed with worst fitness produces lowest possible seeds and a weed with better fitness will produce maximum number of seeds. In other words, all plants in the colony are assigned with an individual rank depending upon their fitness value. The plant with minimum fitness value will produce maximum number of seeds (S_{max}) and is assigned with first rank. Similarly,

the plant with highest fitness value will produce minimum number of seeds (S_{min}). Figure 5.4, illustrates the seeds reproduction in a weed colony that varies from S_{max} to S_{min}.

Step 3: *Spatial dispersal:* The produced seeds are being randomly distributed over the N-dimensional search space with a mean equal to zero and varying standard deviation (σ). Hence, the standard deviation value will start from $\sigma_{initial}$ at initial iteration (i.e. $iter = 1$), and it will become σ_{final} as iteration reaches to maximum number of iterations $iter_{\max}$. Thus, for simulations, the standard deviation at each iteration can be calculated using the following equation [105]

$$\sigma_{iter} = \frac{(iter_{\max} - iter)^m}{(iter_{\max})^m}(\sigma_{initial} - \sigma_{final}) + \sigma_{final} \tag{5.19}$$

where, *m* is the nonlinear modulation index.

This step ensures that the probability of dropping a seed in a distant area decreases nonlinearly with iterations, which results in grouping fitter plants and elimination of inappropriate plants.

Step 4: *Competitive exclusion:* In this step, each plant is allowed some kind of competition among other plants in the colony for limiting the maximum number of plants. In the initial stages, the plants in a colony reproduce in a faster way and all produced plants will be included in the colony until the population reaches $P_{\max}$ value. From then onwards, a mechanism works to eliminate the plants with poor fitness and to always keep $P_{\max}$ number of plants in each iteration. The termination criterion will progress by checking whether the number of iterations reached $iter_{\max}$ or not. The above process will continue until the stopping criterion is attained.

Finally, after the IWO process stops, the best individual with minimum fitness value is taken as the optimal value. The N-variables of that individual are selected as optimal coordinated controller parameters.

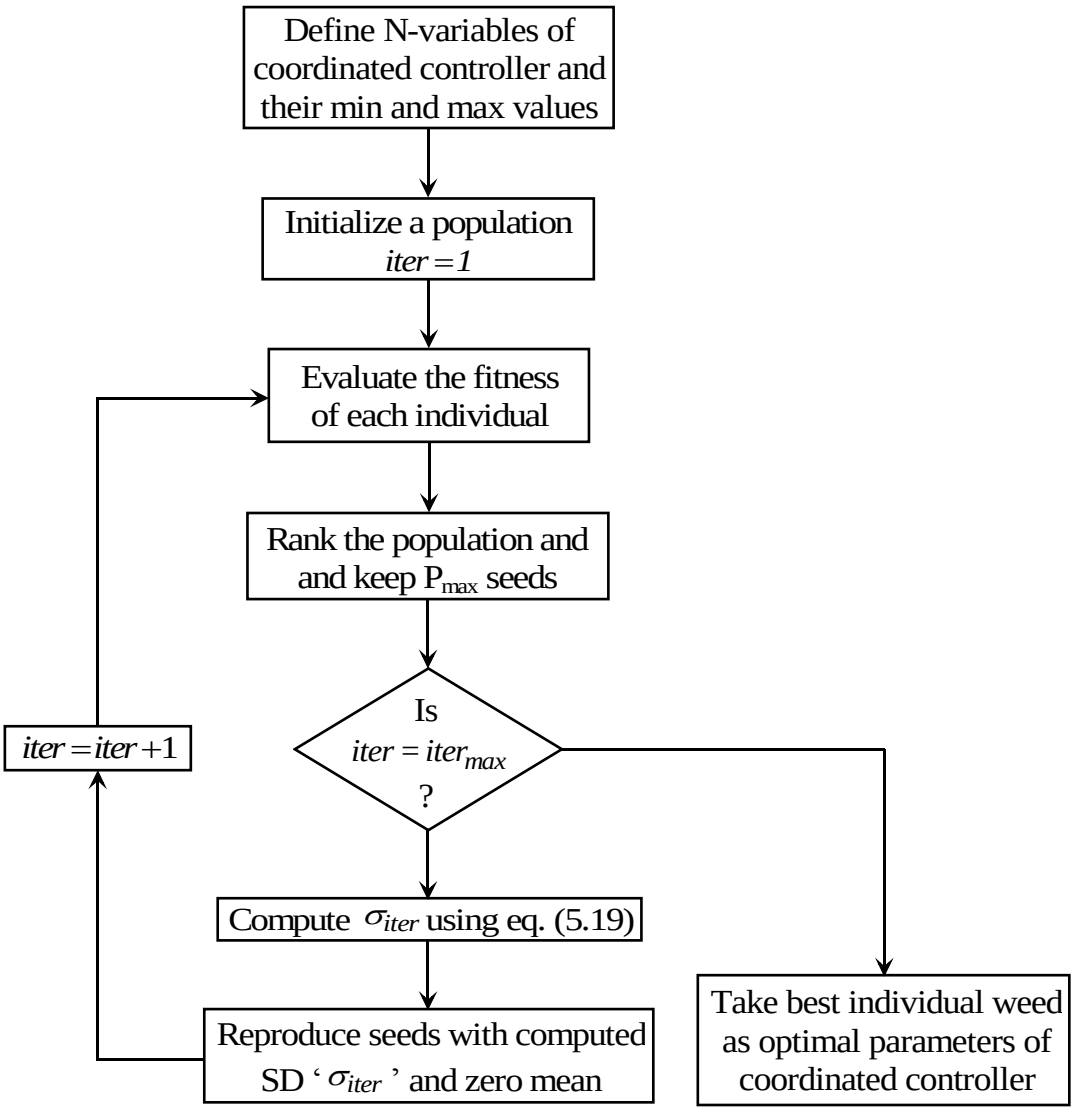

Figure 5.3: **Flowchart of IWO algorithm for proposed controller design**

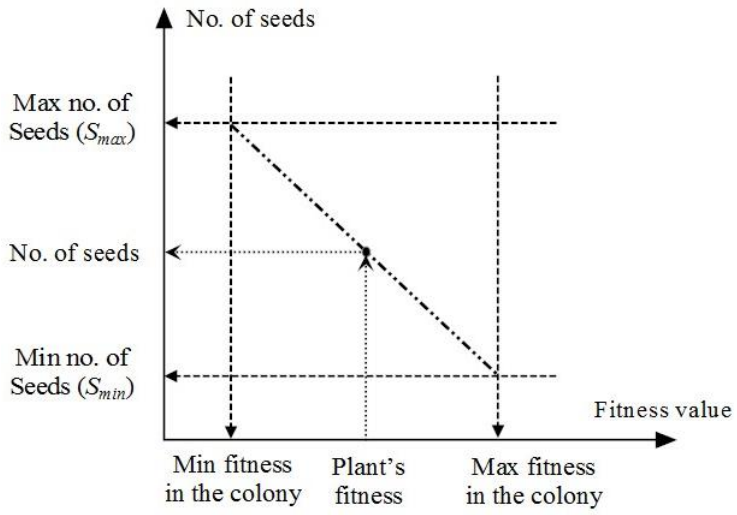

Figure 5.4: **Seed reproduction procedure in a weed colony**

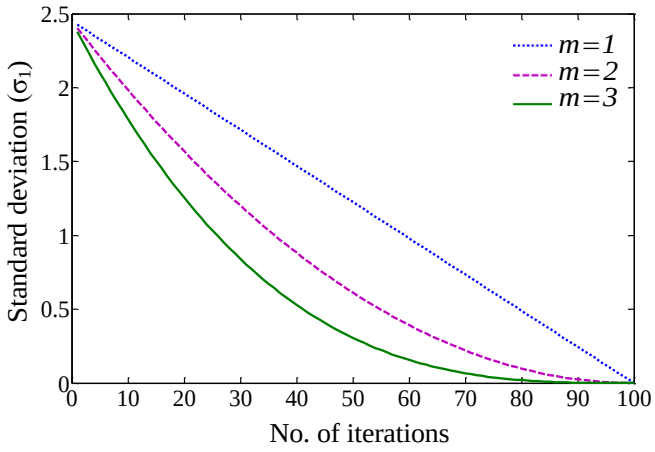

Figure 5.5: **Variation in standard deviation (σ_1) over number of iterations**

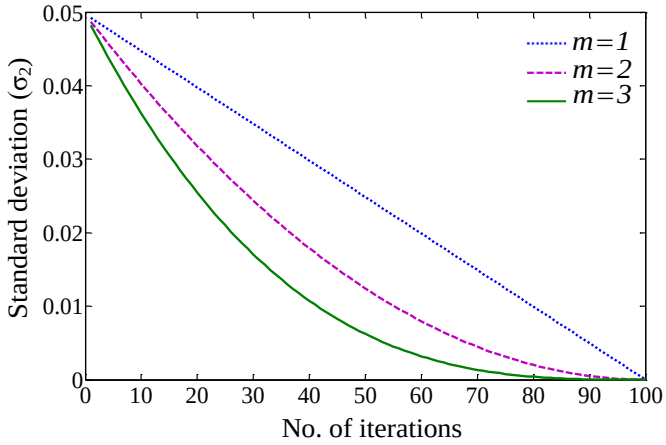

Figure 5.6: **Variation in standard deviation (σ_2) over number of iterations**

5.4 Control Parameters Selection of IWO Algorithm

The selection of control parameters of proposed IWO algorithm is very much important for the performance analysis. The basic parameters that affect the convergence of the IWO algorithm are nonlinear modulation index *m*, initial value of standard deviation $\sigma_{initial}$ and the final value of standard deviation σ_{final}. These three parameters should be tuned carefully in order to achieve the proper σ_{iter} value in each iteration depending on equation (5.19). To allow the weeds to explore the entire search area, a high value of standard deviation should be preferred at the initial stages and the value goes on decreasing till it finally reaches the minimum. The initial value of the standard deviation is generally set around a percent in tolerance 1 to 5 in the search range of each variable. However, the final value should be a very smaller one to allow the optimizer in order to find an optimal solution as accurate as possible. In this work, the values of control parameters are chosen in two

different search ranges as described in section 4.4. Hence, two different ranges of $\sigma_{initial}$ and σ_{final} are considered as $[\sigma_{1i}, \sigma_{1f}] = [2.45, 0.0049]$ and $[\sigma_{2i}, \sigma_{2f}] = [0.0475, 0.000095]$. The value of *m* places a key role on IWO convergence. In [107], it is suggested that the best choice for choosing the value of *m* is equals to 3. The variation of σ_1 and σ_2 with number of iterations for different values of *m*, is shown in Figure 5.5 and 5.6 respectively. From the figures, one can conclude that the best choice to select the value of *m* is equal to 3. The control parameters setup, in IWO algorithm for minimization of the proposed objective function, is specified in Table 5.1.

Table 5.1: **IWO algorithm parameter values for proposed coordinated controller designing problem**

Symbol	Quantity	Value
$P_{\max}$	Population Size	100
$I_{\max}$	Number of Iterations	100
X_{rg}	Variable search range	[1-50] for K_i and K_t [0.05-1] for T_1, T_3, T_{F1} and T_{F3}
$S_{\max}$	Maximum number of seeds	5
$S_{\min}$	Minimum number of seeds	1
m	Nonlinear modulation index	3
$\sigma_{initial}$	Initial value of standard deviation	5% of entire search area ($\sigma_{1i} = 2.45$ and $\sigma_{2i} = 0.0475$)
σ_{final}	final value of standard deviation	0.01% of entire search area ($\sigma_{1f} = 0.0049$ and $\sigma_{2f} = 0.000095$)

5.5 Simulation Study and Performance Analysis of Test System with Different Designs

An extensive simulation study has been undertaken for comparing the performances of the proposed hybrid coordinated designs with other control designs. Both these designs are

analyzed using eigen value analysis as well as time-domain simulations for severe disturbance over a wide range of load conditions.

5.5.1 Coordinated Design of PSS with TCSC and SVC Controllers

With the control parameters that are given in Table 5.1, the IWO algorithm optimal parameter values of hybrid coordinated design controllers are given in Table 5.2. The test system electromechanical mode eigen values (λ_i) and their damping ratios (ζ_i) with different control schemes and load conditions are shown in Table 5.3.

Table 5.2: **IWO tuned optimal parameter values of PSS, TCSC and SVC controllers**

Control parameter	PSS	TCSC	SVC
K_i / K_S	9.5721	0.7802	1.0150
T_1 / T_{S1}	0.5243	0.3809	0.3042
T_3 / T_{S3}	0.4385	0.4551	0.3214

Table 5.3: **Electromechanical modes and ζ under different controllers and load conditions**

No control	IWO-(PSS+TCSC)	IWO-(PSS+SVC)	proposed design
Normal load (λ_i, ζ_i)			
-0.3637± 8.076i, 0.0450	-1.7989±3.7059i, 0.4367	-1.7327±4.3077i, 0.3732	-2.3120±2.8779i, 0.6263
Heavy load (λ_i, ζ_i)			
-0.2562±8.2205i, 0.0312	-1.8129±3.3181i, 0.4795	-1.7647±4.7715i, 0.3469	-2.3817±2.7229i, 0.6584
Light load (λ_i, ζ_i)			
-0.4954±7.7546i, 0.0638	-1.7502±4.1483i, 0.3887	-1.7334±3.8436i, 0.4111	-2.2206±2.9599i, 0.6001
Leading PF condition (λ_i, ζ_i)			
-0.30795±6.9016i, 0.0446	-1.4306±3.434i, 0.3846	-1.6969±5.0338i, 0.3194	-2.3870±2.9806i, 0.6251

From the table, it can be observed that the system with proposed hybrid design IWO-(PSS+TCSC+SVC) provides great damping ratio than other control designs, like No control, IWO-(PSS+TCSC), and IWO-(PSS+SVC). The proposed coordinated design effectively shifts the real parts of electromechanical modes from -0.36, -0.25, -0.49 and -0.30 to -2.31, -2.38, -2.22 and -2.38 for normal, heavy, light and leading PF conditions respectively. Moreover, the damping ratios of the poorly damped electromechanical eigen values are boosted to 0.62, 0.65, 0.60, 0.62 for normal, heavy, light and leading PF conditions respectively. Hence, compared to other control designs, the coordinated design provides enhanced performance towards damping of electromechanical modes of the test system.

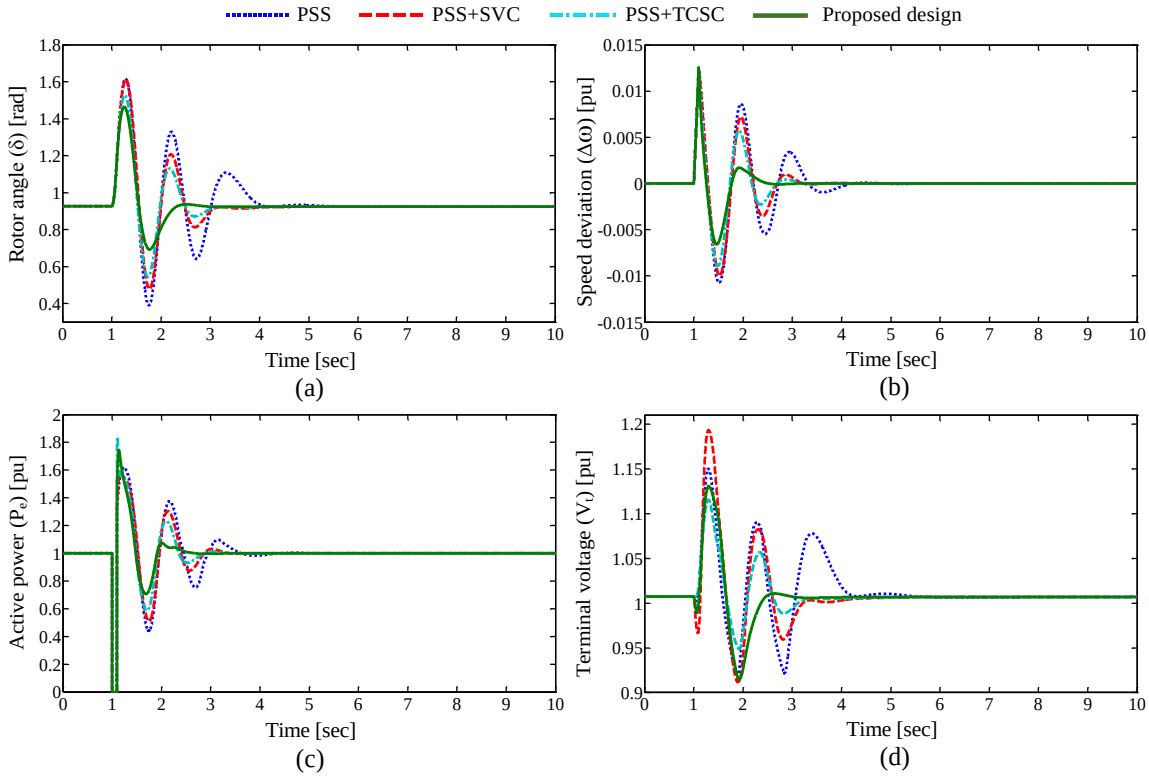

Figure 5.7: **Test system dynamic response for a six cycle 3-phase fault under normal load**

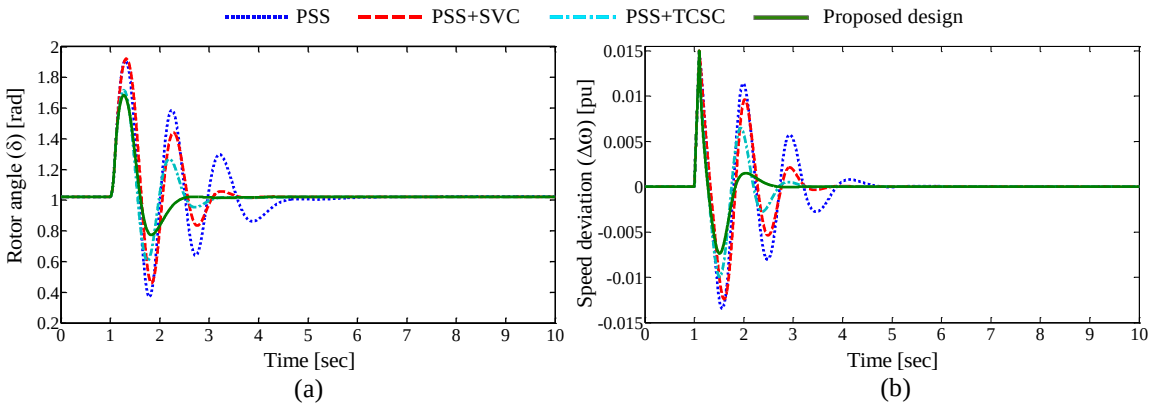

(a) (b)

Figure 5.8: **Test system dynamic response for a six cycle 3-phase fault under heavy load**

The effectiveness of the performance of proposed IWO-(PSS+TCSC+SVC) under severe disturbance is verified by applying a six cycle three phase fault at 1.0s on one of the transmission lines those are connected in between generator terminal and the infinite bus. Figures 5.7 – 5.10 show the response of test power system due to the severe disturbance for normal, heavy, light and leading PF conditions respectively. From these figures, it is observed that the proposed hybrid coordinated design provides robust performance and achieves superior damping in comparison with the other control designs.

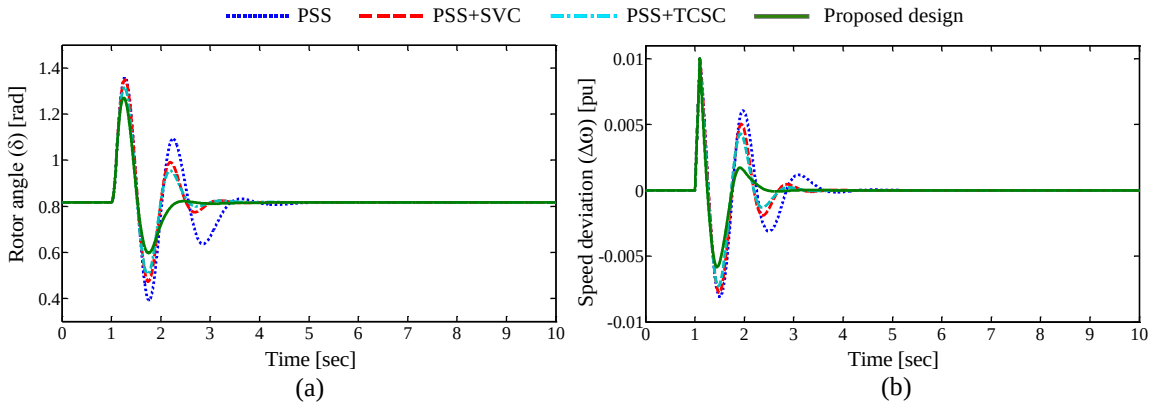

(a) (b)

Figure 5.9: **Test system dynamic response for a six cycle 3-phase fault under light load**

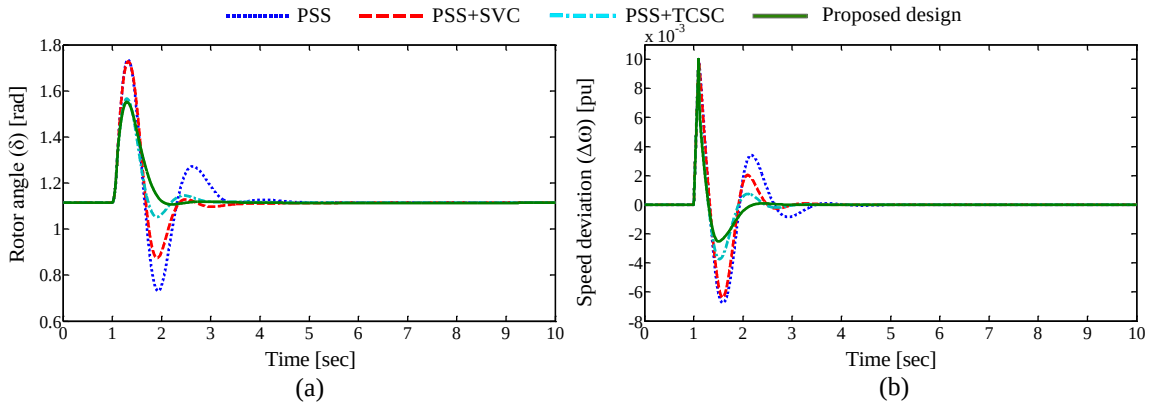

(a) (b)

Figure 5.10: **Test system dynamic response for a six cycle 3-phase fault under leading PF condition**

5.5.2 Coordinated Design of PSS with TCSC and STATCOM Controllers

The coordinated design of PSS, TCSC and STATCOM controllers is done by applying IWO algorithm for the minimization of the eigen value based objective function. Here, we have two hybrid coordinated designs such as 'PSS+TCSC+ACVC' and 'PSS+TCSC+DCVC'. The obtained control parameters of controllers in these designs are given in Table 5.4 and Table 5.5 respectively. The electromechanical modes and the damping ratios of test power system with different controller designs under different load conditions are given in Table 5.64. From these results, one can notice that the real parts of the poorly damped eigen values are shifted to the left side of D-shape curve in the S-plane. For the instance electromechanical modes are shifted from -0.161, 0.174, -0.152 and -0.197 to -3.932, -4.278, -3.447 and -3.130 for normal, heavy, light and leading PF conditions respectively with proposed coordinated design. However, the damping ratios are also enriched to 0.74, 0.77, 0.69 and 0.67 for normal, heavy, light and leading PF conditions respectively.

Table 5.4: **IWO tuned optimal parameter values of proposed (PSS+TCSC+ACVC)**

Control parameter	PSS	TCSC	ACVC
K_i	13.2848	1.0586	1.5640
T_1	0.3714	0.2540	0.2723
T_3	0.3058	0.3879	0.4199

Table 5.5: **IWO tuned optimal parameter values of proposed (PSS+TCSC+DCVC)**

Control parameter	PSS	TCSC	DCVC
K_i	11.7512	0.9554	1.1912
T_1	0.2567	0.2616	0.3643
T_3	0.4835	0.2015	0.4029

To assess the effectiveness and robustness of proposed designed controllers, simulation studies are carried out for six cycle severe fault over a wide range of system load conditions. The response curves of the test system under different load conditions are represented in Figures 5.11 - 5.14, with the proposed coordinated design (PSS+TCSC+ACVC). The performance of the IWO based hybrid coordinated design is quite prominent in comparison

to IWO-PSS, IWO-(PSS+TCSC) and IWO-(PSS+ACVC) controller designs. The overshoots and settling time are significantly improved for the proposed coordinated design.

Table 5.6: **Electromechanical modes and ζ under different controllers and load conditions**

No control	IWO-(PSS+TCSC)	IWO-(PSS+TCSC+ACVC)	IWO-(PSS+TCSC+DCVC)
Normal load			
-0.1615±4.8128i, 0.0335	-1.9441±3.4185i, 0.4944	-3.9249±3.8318i, 0.7155	-3.9322±3.5654i, 0.7408
Heavy load			
-0.1740±4.9589i, 0.0351	-1.9781±3.3800i, 0.5051	-4.2406±3.7515i, 0.7490	-4.2786±3.5095i, 0.7732
Light load			
-0.1521±4.5620i, 0.0333	-1.8873±3.3985i, 0.4855	-3.4832±3.8496i, 0.6709	-3.4470±3.5640i, 0.6952
Leading PF condition			
-0.1975±3.6022i, 0.0547	-1.6246±2.8755i, 0.4919	-3.0910±3.5806i, 0.6535	-3.1303±3.4649i, 0.6704

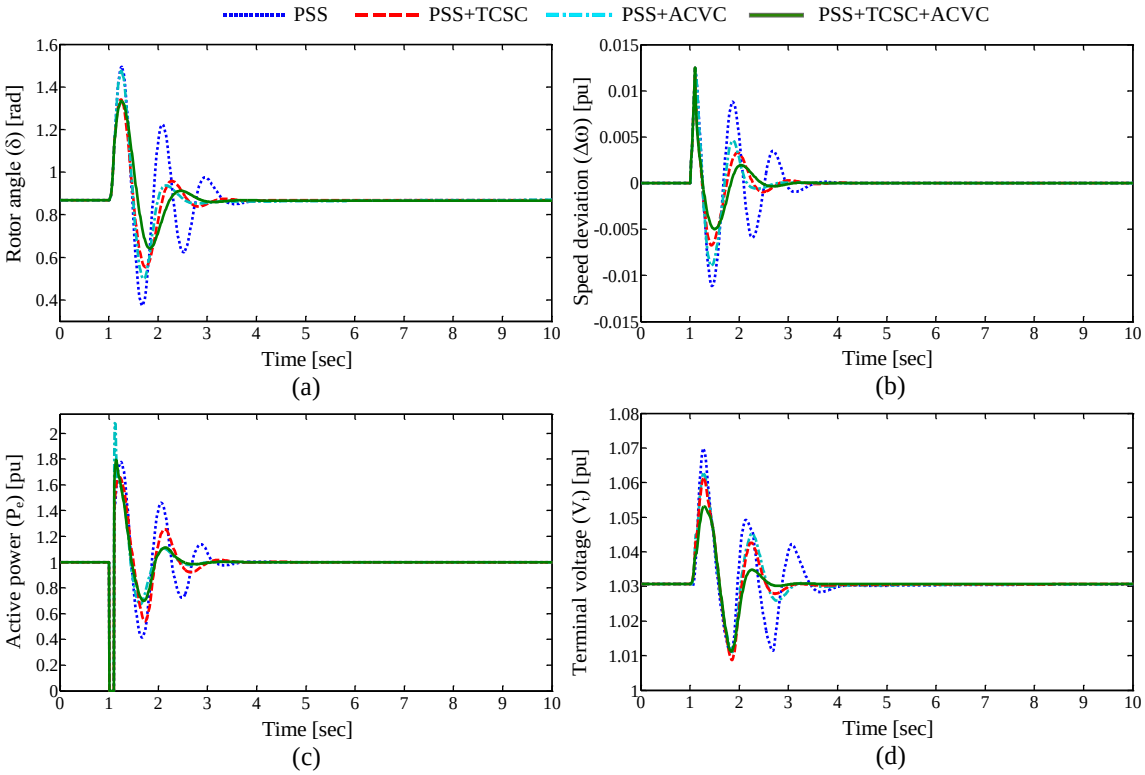

Figure 5.11: **Test system dynamic response for a six cycle 3-phase fault under normal load**

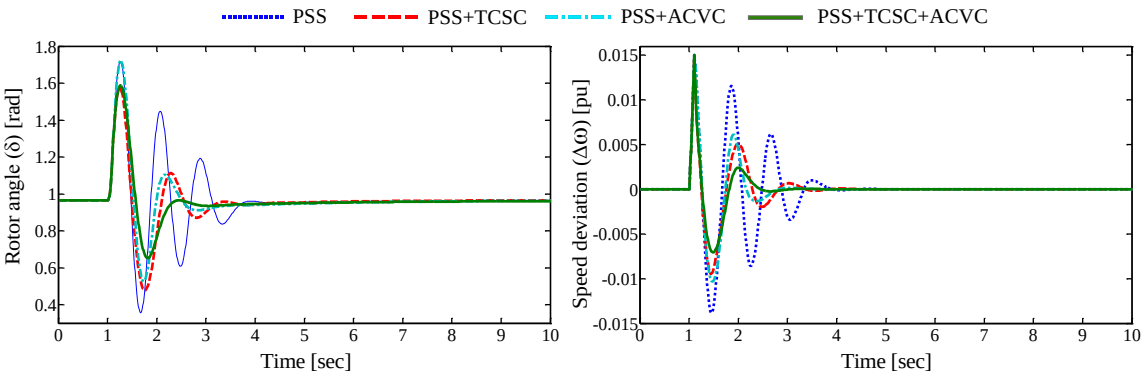

(a) (b)

Figure 5.12: **Test system dynamic response for a six cycle 3-phase fault under heavy load**

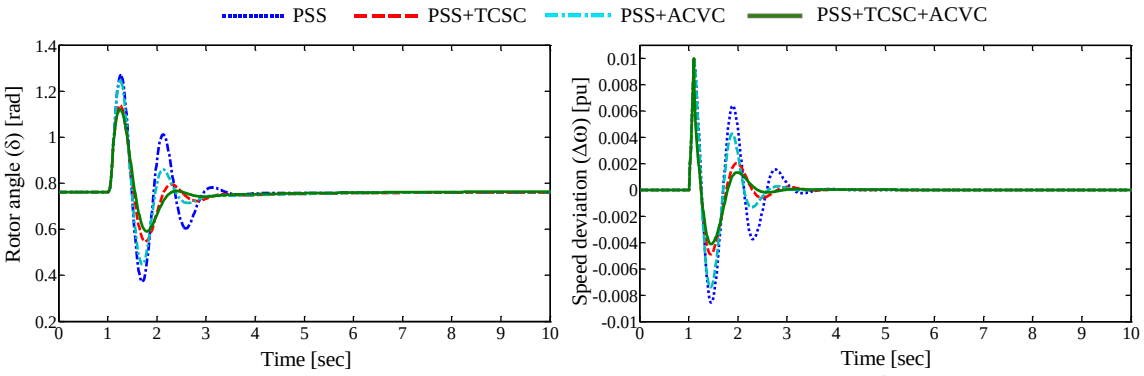

(a) (b)

Figure 5.13: **Test system dynamic response for a six cycle 3-phase fault under light load**

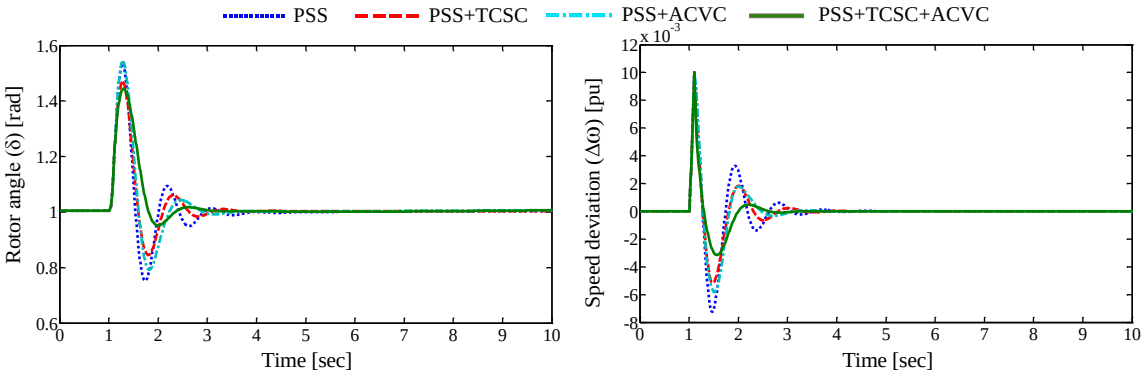

(a) (b)

Figure 5.14: **Test system dynamic response for a six cycle 3-phase fault under leading PF condition**

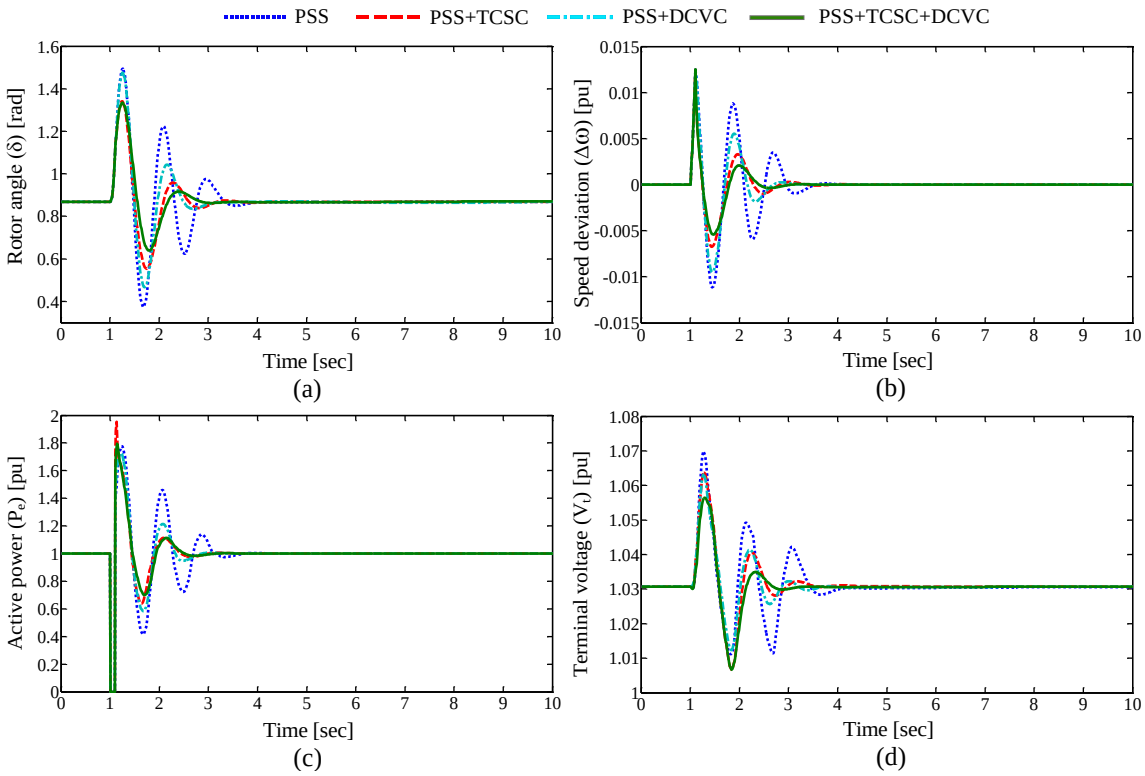

Figure 5.15: **Test system dynamic response for a six cycle 3-phase fault under normal load**

Also, the Figures 5.15 – 5.18 show the system responses under different load conditions with proposed hybrid coordinated design (PSS+TCSC+DCVC) and other control designs. From these response curves, it has seen that the application of proposed IWO based simultaneous design (PSS+TCSC+DCVC) achieves the best response in terms of settling time and damping characteristics.

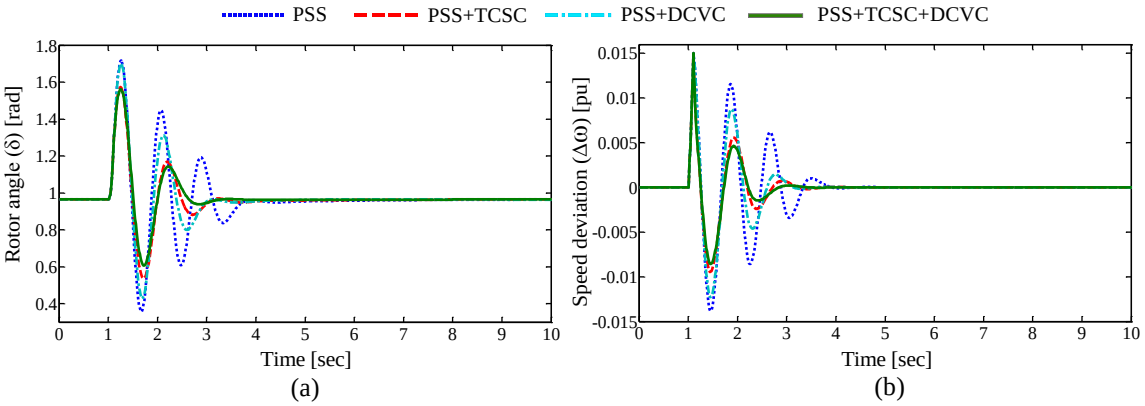

Figure 5.16: **Test system dynamic response for a six cycle 3-phase fault under heavy load**

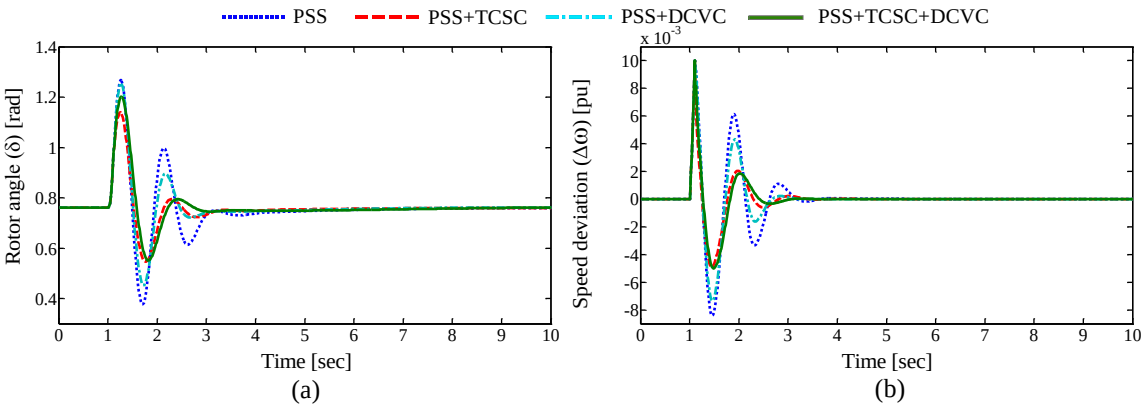

Figure 5.17: **Test system dynamic response for a six cycle 3-phase fault under light load**

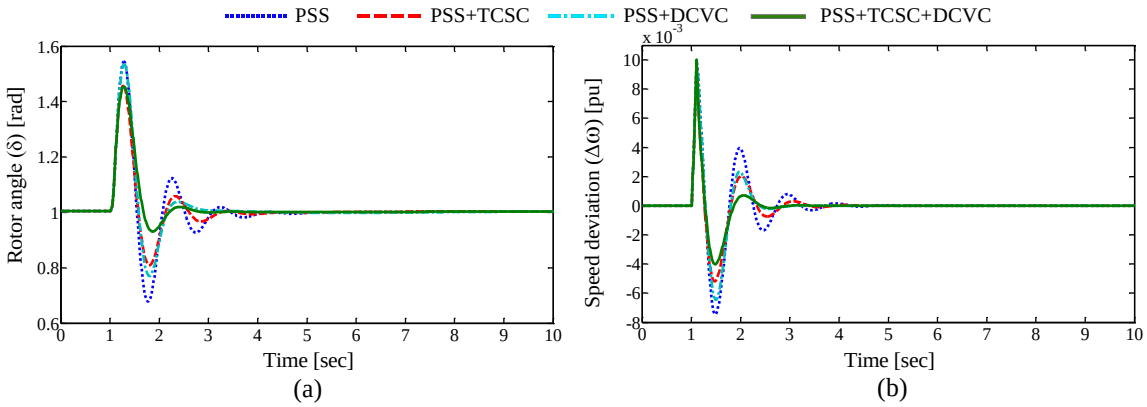

Figure 5.18: **Test system dynamic response for a six cycle 3-phase fault under leading PF condition**

5.6 Summary

This chapter proposed the algorithm for the hybrid coordinated design of PSS with series and shunt damping controllers. Here, TCSC, SVC and STATCOM damping controllers are considered for hybrid coordinated design. Two STATCOM internal controllers are considered for analysis namely ACVC and DCVC. The problem of selecting the damping controller parameter values of different controllers in coordinated design is modeled as optimization problem. Then, the IWO algorithm is successfully applied to find the optimal solution of the design problem. The effectiveness of proposed coordinated tuned controllers has been tested on a simple test power system through the simulation studies under different loading conditions. The eigen value analysis and nonlinear time domain simulation results show the robustness of proposed controllers and their ability to provide good damping of system oscillations under severe disturbance.

Chapter 6

PSS with Series and Shunt FACTS Controllers Coordinated Design using AAPSO and IWO algorithms in Multi-Machine Power System

Chapter 6

PSS with Series and Shunt FACTS Controllers Coordinated Design using AAPSO and IWO algorithms in Multi-Machine Power System

6.1 Introduction

In Chapter 5, the coordinated design procedure of PSS and different FACTS damping controllers using IWO algorithm is discussed. The eigen value based objective function is minimized using IWO algorithm and the control parameter values of different controllers are obtained at the end of IWO algorithm. The proposed hybrid designs are compared with other coordinated designs and compared results are given over a wide range of operating conditions. In Chapters 2-5, a simple SMIB system is used as a test power system to analyze the robustness of proposed controllers. Although, SMIB system qualitatively exhibits important aspects of multi-machine system, to analyze the inter area issues in real world one has to exercise with multi-machine power system. In this chapter, two multi-machine power systems (3-machine 9-bus and 4-machine 11-bus) are considered to analyze the performance of hybrid designs. A wide range of comparisons are made for different hybrid designs via AAPSO and IWO algorithms over different operating conditions.

6.2 3-Machine 9-Bus Power System

In this study, the 3-machine 9-bus power system is considered for the analysis of proposed hybrid coordinated designs. This 9 bus system shown in Figure 6.1 consists of 3 generators and 3 loads. Details of the test system are provided in [91]. Here, the 3 generators G_1, G_2 and G_3 represent in third axis model which is discussed in section 2.2. The loads A, B and C are located nearer to the buses 4, 5 and 6 respectively. Three individual PSSs are mounted on 3 generators in the test system. The eigen value analysis as well as time domain simulations are provided for different hybrid designs with different optimization algorithms.

6.2.1 Test System with PSS, TCSC and SVC Damping Controllers

In this section, three PSS, TCSC and SVC damping controllers are installed in test power system. The test system with these damping controllers is operated over a wide range of

operating conditions as given in Table 6.1. To identify the appropriate location for installing the TCSC, base case power flow is carried out and the results are provided in Table 6.2. Base on the results, it is observed that the power flow in line 4-9 is very high and it is the longest line in the system under study. This demonstrates that the line 4-9 is the best location to install TCSC controller which has been considered in this thesis. However, the bus no 4, which is much closer to large generator G1, is more suitable to install SVC [77].

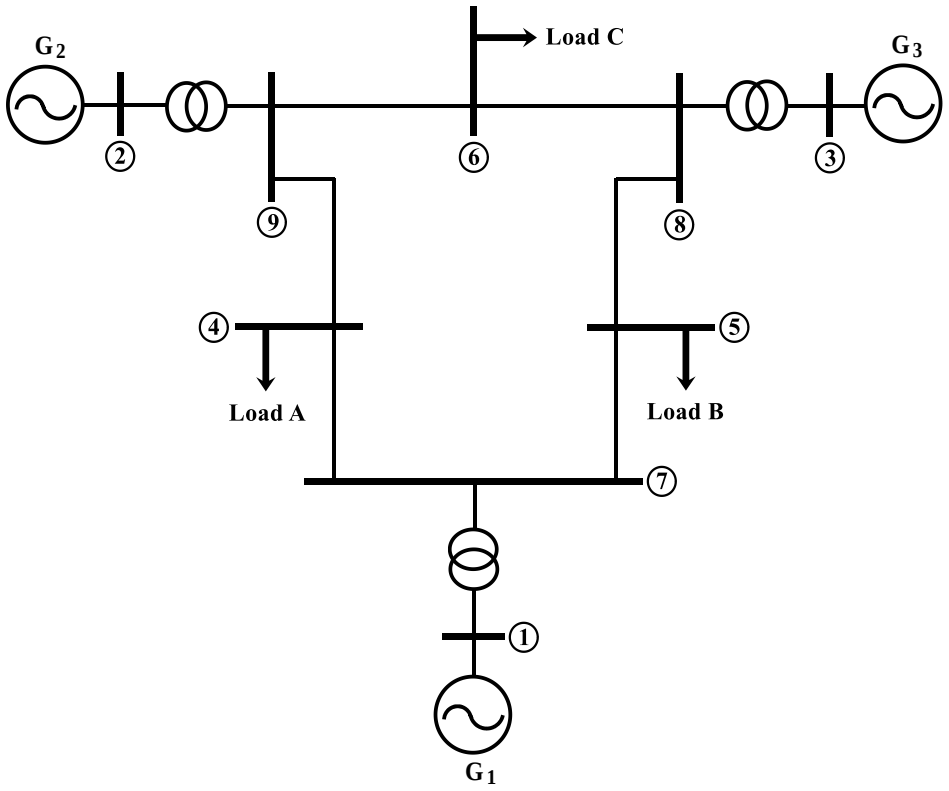

Figure 6.1: **3-machine 9-bus power system**

A. Eigen Value Analysis and Discussions

The designed eigen value based objective function in section 4.4 is minimized using AAPSO and IWO algorithms and the obtained optimum coordinated designed controllers parameter values are provided in Table 6.3 and 6.4 respectively. Convergence analysis for AAPSO and IWO algorithms is shown in Figure 6.2. To operate both these optimization algorithms at equal complexities, we considered 100 iterations/generations and each of it consists of 100 individuals. The objective function declines monotonically over iterations of AAPSO and IWO algorithms. From the results, it was found that the IWO algorithm had the fast convergence rate compare to that of AAPSO algorithm. Here, the IWO reaches its convergence value near about 50 iterations, whereas AAPSO takes more than 65 iterations.

Table 6.1: **Operating conditions of test power system with TCSC and SVC (p.u)**

	Normal		**Heavy**		**Light**	
	P	**Q**	**P**	**Q**	**P**	**Q**
Generator						
G_1	0.6908	0.3241	0.7758	0.6937	0.4609	-0.1039
G_2	1.6300	0.1076	2.4450	0.5063	0.8150	-0.2051
G_3	0.8500	-0.0909	1.2750	0.1662	0.4250	-0.2412
Load						
A	1.25	0.50	1.90	0.75	0.65	0.25
B	0.90	0.30	1.30	0.45	0.45	0.15
C	1.00	0.35	1.50	0.50	0.50	0.17

Table 6.2: **Base case power flow on 100-MVA base**

From bus	**To Bus**	**Real power flow (p.u)**
7	4	0.2438
4	9	**0.9847**
9	6	0.6132
6	8	0.3864
8	5	0.4617
5	7	0.4436

Table 6.3: **Optimal control parameter values obtained using AAPSO algorithm**

Control parameters	**PSS1**	**PSS2**	**PSS3**	**TCSC**	**SVC**
K_S	37.6917	19.2972	7.3608	0.9824	1.0544
T_1	0.4241	0.4712	0.3923	0.2715	0.3801
T_3	0.5155	0.5057	0.4145	0.2924	0.2540

Table 6.5 shows the system eigen values and damping ratios of poorly damped mechanical modes with different loading conditions. It is clear that the system with open loop (No control) has very poor damping ratios for normal, heavy and light load conditions. Moreover, AAPSO-(PSS+TCSC+SVC) and IWO-(PSS+TCSC+SVC) hybrid coordinated designs shifts substantially the electromechanical mode eigenvalues to the left of the *D* shape

in the *S*-plane. The values of damping factors are greatly improved and the damping ratios of electromechanical modes are very much enhanced with the control of proposed hybrid coordinated designs. Hence, compared to open loop system the proposed coordinated designs are significantly improve the damping characteristics of poorly damped electromechanical modes of the test power system.

Table 6.4: **Optimal control parameter values obtained using IWO algorithm**

Control parameters	PSS1	PSS2	PSS3	TCSC	SVC
K_S	33.9698	22.2974	6.8167	1.0582	1.1145
T_1	0.3741	0.5095	0.3896	0.2813	0.4024
T_3	0.4990	0.4841	0.4243	0.2596	0.2495

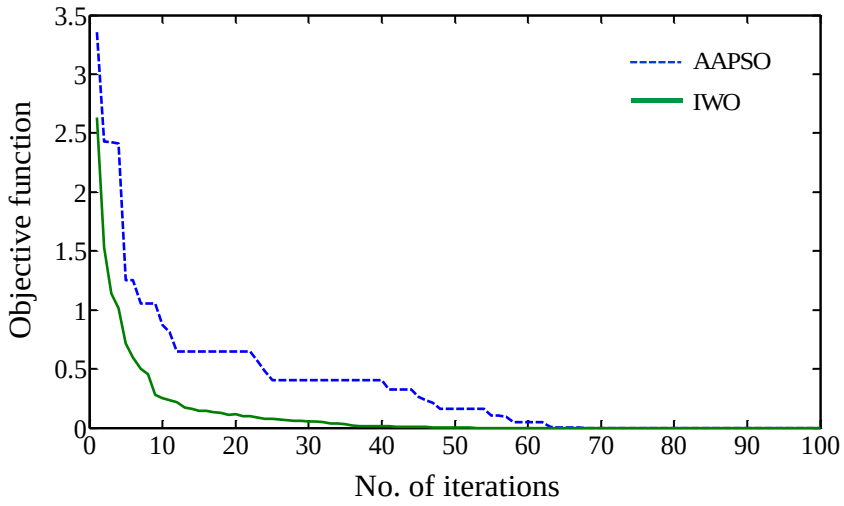

Figure 6.2: **Convergence of objective function**

B. Time Domain Simulation Results and Discussions

The dynamic performance of test system is analysed with different control schemes under three different loading conditions namely normal, heavy and light load conditions as mentioned in Table 6.1. In the test system, a three-phase fault is applied on the line 9-6 with fault starting time at 1s and it continues for duration of 100ms (i.e. a six cycle fault).

Test system response with AAPSO tuned coordinated controllers:

The system response with different control schemes namely no control, coordinated designs (PSS+TCSC), (PSS+SVC), and hybrid coordinated design (PSS+TCSC+SVC), is compared

under normal load conditions which is shown in Figures 6.3 and 6.4. The rotor angle deviations between G_2 and G_1 ($\Delta\delta_{21}$) as well as G_3 and G_1 ($\Delta\delta_{31}$) is represented in Figure 6.3. The inter-area oscillations $\Delta\omega_{12}, \Delta\omega_{23}$ and $\Delta\omega_{31}$ (where, $\Delta\omega_{12} = \Delta\omega_1 - \Delta\omega_2$, $\Delta\omega_{23} = \Delta\omega_2 - \Delta\omega_3$ and $\Delta\omega_{31} = \Delta\omega_3 - \Delta\omega_1$) are shown in Figure 6.4. From these response curves, it is observed that the open loop system unable to damp the system oscillations. However, the other coordinated designs are very good enough in damping the rotor angle and also inter-area oscillations. Particularly, the hybrid coordinated design provides great damping characteristics than the other two designs.

Table 6.5: **Electromechanical modes and ζ under different load conditions**

No control	AAPSO-(PSS+TCSC+SVC)	IWO-(PSS+TCSC+SVC)
Normal load (λ_i, ζ_i)		
-0.1698±12.735i, 0.0133	-5.7425±10.097i, 0.4944	-5.8674±9.6107i, 0.5211
-0.0824±9.5206i, 0.0086	-2.2178±8.9836i, 0.2397	-2.4314±8.847i, 0.2650
Heavy load (λ_i, ζ_i)		
0.0340±13.384i, -0.0025	-6.2585±10.212i, 0.5225	-6.3023±9.6756i, 0.5458
0.0158±9.4125i, -0.0016	-2.2031±8.6467i, 0.2469	-2.3992±8.4817i, 0.2722
Light load (λ_i, ζ_i)		
-0.1969±11.37i, 0.0173	-4.5636±9.4885i, 0.4334	-4.7476±9.2121i, 0.4581
-0.0983±9.2076i, 0.0106	-2.0089±8.8268i, 0.2219	-2.1659±8.7483i, 0.2403

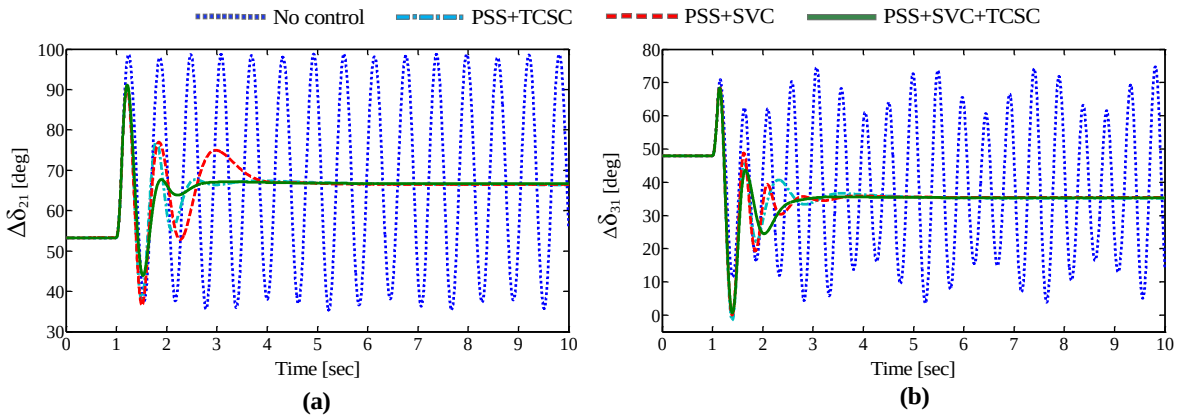

Figure 6.3: R**esponse of test system with AAPSO tuned coordinated designs for a six cycle fault under normal load (a) Δδ21 (b) Δδ31**

Similarly, the Figures 6.5 and 6.6 show the inter-area speed oscillations of the test power system with different control schemes under heavy and light load conditions respectively. In heavy load case, the generator's active powers and the loads are increased 50% more than that of the normal load case. Due to heavy load applied on the test system, the open loop system is no more stable and it loses the synchronism. Whereas the system with coordinated designed controllers provide enhanced damping effect to the inter-area speed oscillations and after some time system becomes stable. Also, in case of light load conditions the generator's active powers and the loads are decreased 50% less than that of normal load conditions. By observing the system operating points of light load condition, we can spot that all the generators are operating in leading PF conditions. In this context, the open loop controller performance is not enough to damp the oscillations while the system with other coordinated designs provides good damping. From all these results, the proposed coordinated design of PSS, TCSC and SVC is most robust design and has best damping behavior for severe disturbances.

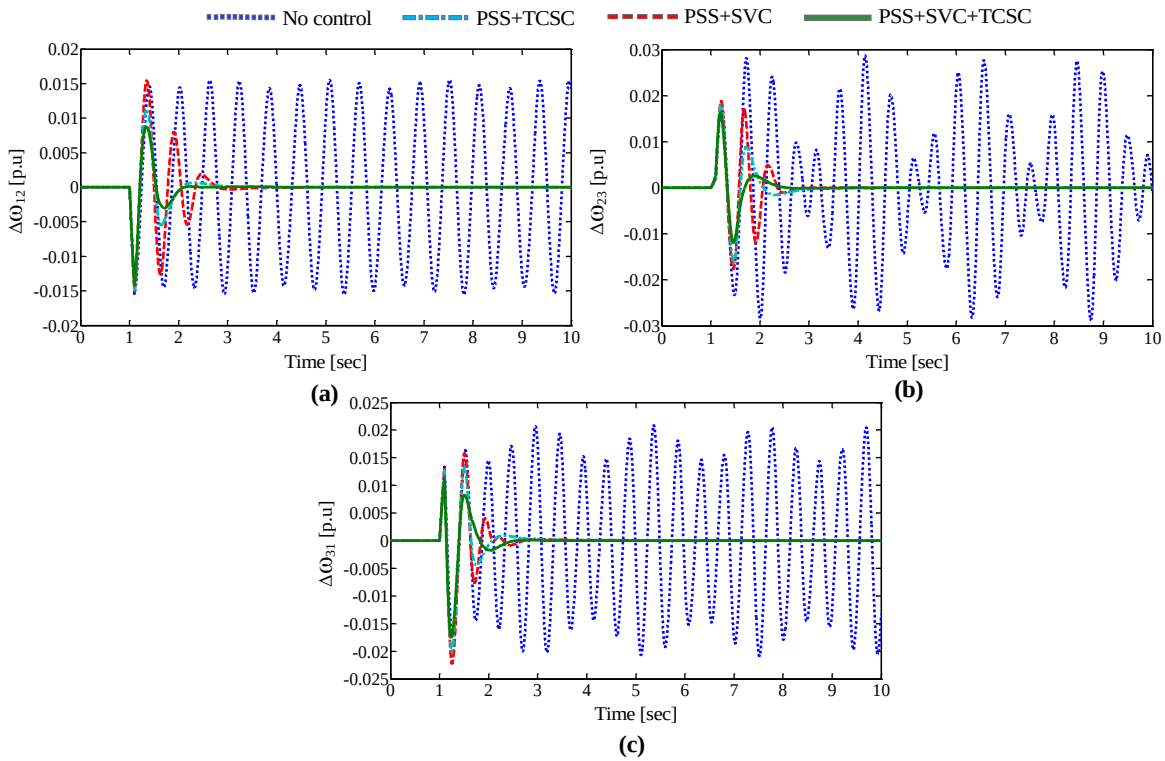

Figure 6.4: **Response of test system with AAPSO tuned coordinated designs for a six cycle fault under normal load (a) $\Delta\omega_{12}$ (b) $\Delta\omega_{23}$ (c) $\Delta\omega_{31}$**

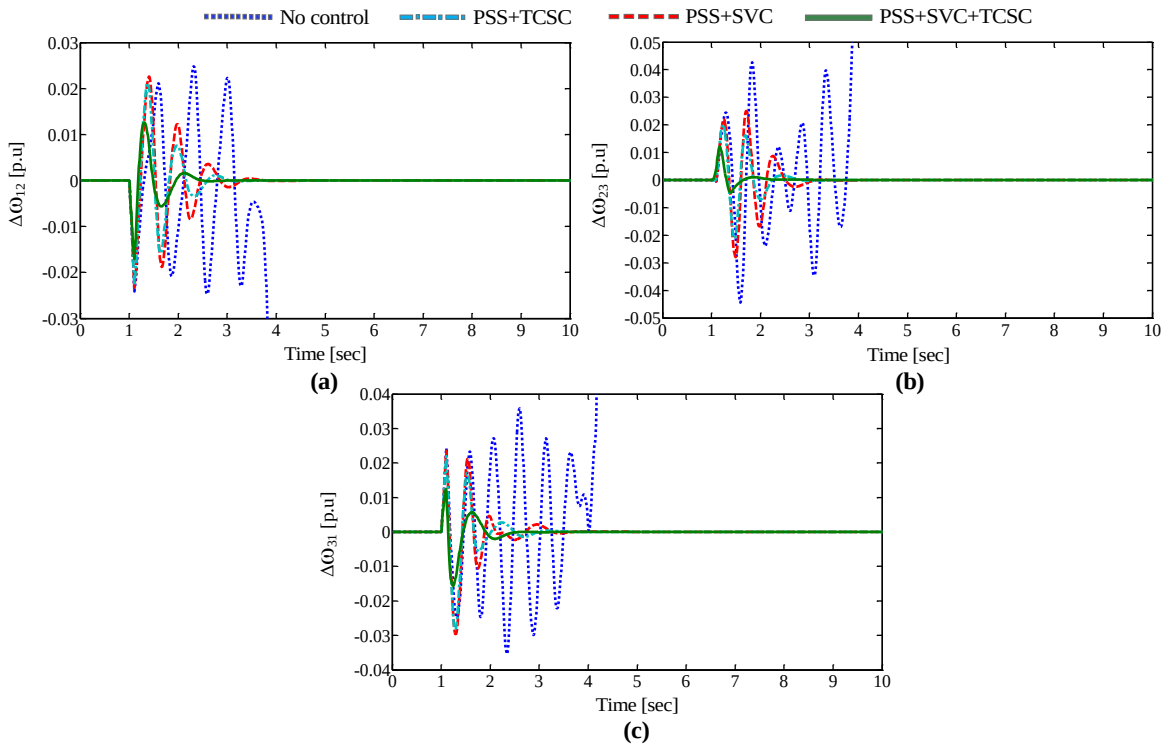

Figure 6.5: **Response of test system with AAPSO tuned coordinated designs for a six cycle fault under heavy load (a) Δω12 (b) Δω23 (c) Δω31**

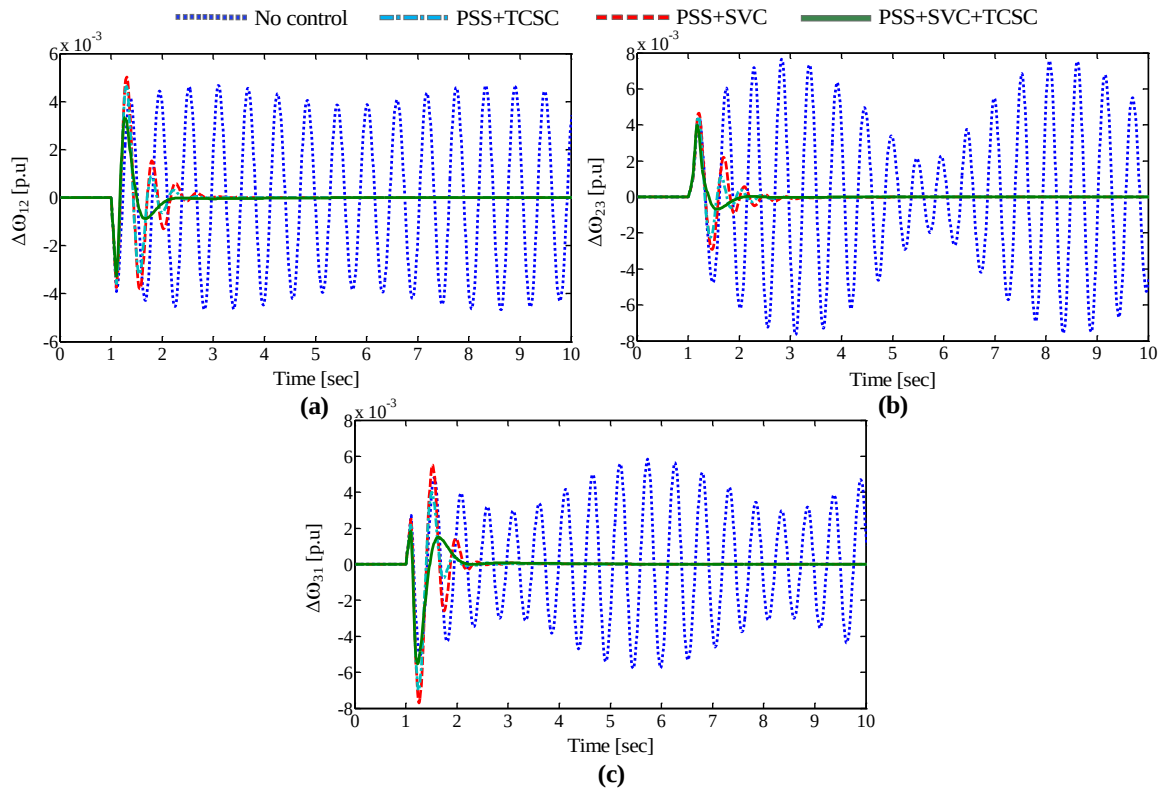

Figure 6.6: **Response of test system with AAPSO tuned coordinated designs for a six cycle fault under light load (a) Δω12 (b) Δω23 (c) Δω31**

Test system response with IWO tuned coordinated controllers:

Figures 6.7 and 6.8 show the system response curves with different IWO tuned coordinated controllers under normal loading condition. Figure 6.7 depicts rotor angle variations and Figure 6.8 depicts inter-area speed variations of the generators. The system responses under heavy and light load conditions are shown in Figures 6.9 and 6.10 respectively. In all these response plots, the open loop system (i.e. system has no control) is not capable to damp system oscillations, and in certain operating conditions like under heavy load it goes out of synchronism. But, the system with IWO based coordinated designs like coordinated designs (PSS+TCSC), (PSS+SVC) and hybrid coordinated design (PSS+TCSC+SVC) gives great stableness to the system under all operating conditions. Moreover, the combined coordinated design of all three controllers gives ample damping effect and great settling times for the rotor angle as well as inter-area speed oscillations.

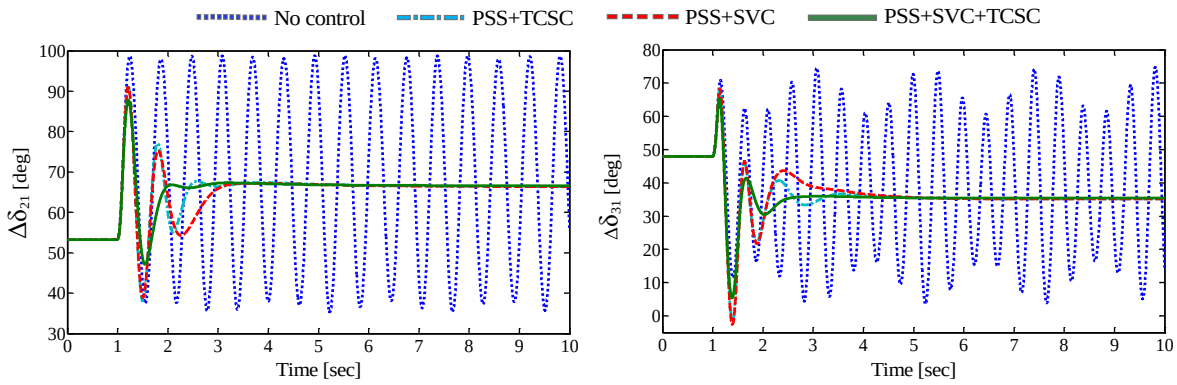

Figure 6.7: R**esponse of test system with IWO tuned coordinated designs for a six cycle fault under normal load (a) $\Delta\delta_{21}$ (b) $\Delta\delta_{31}$**

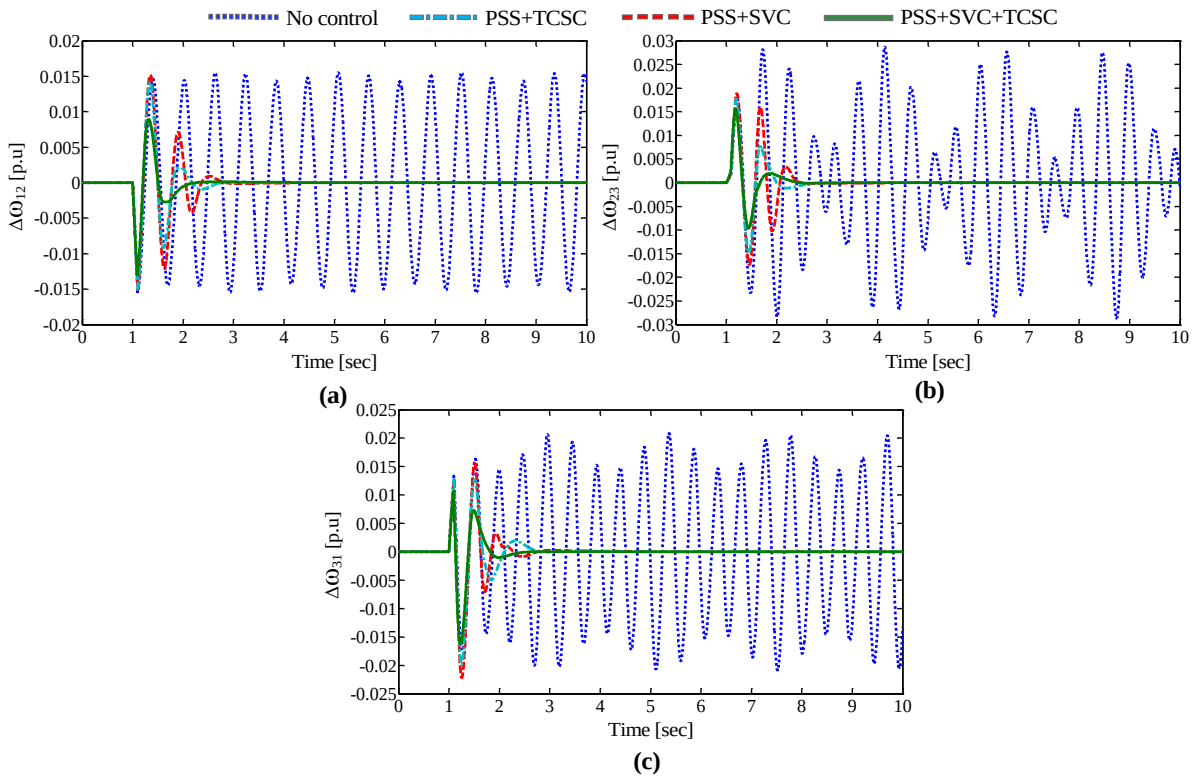

Figure 6.8: **Response of test system with IWO tuned coordinated designs for a six cycle fault under normal load (a) $\Delta\omega_{12}$ (b) $\Delta\omega_{23}$ (c) $\Delta\omega_{31}$**

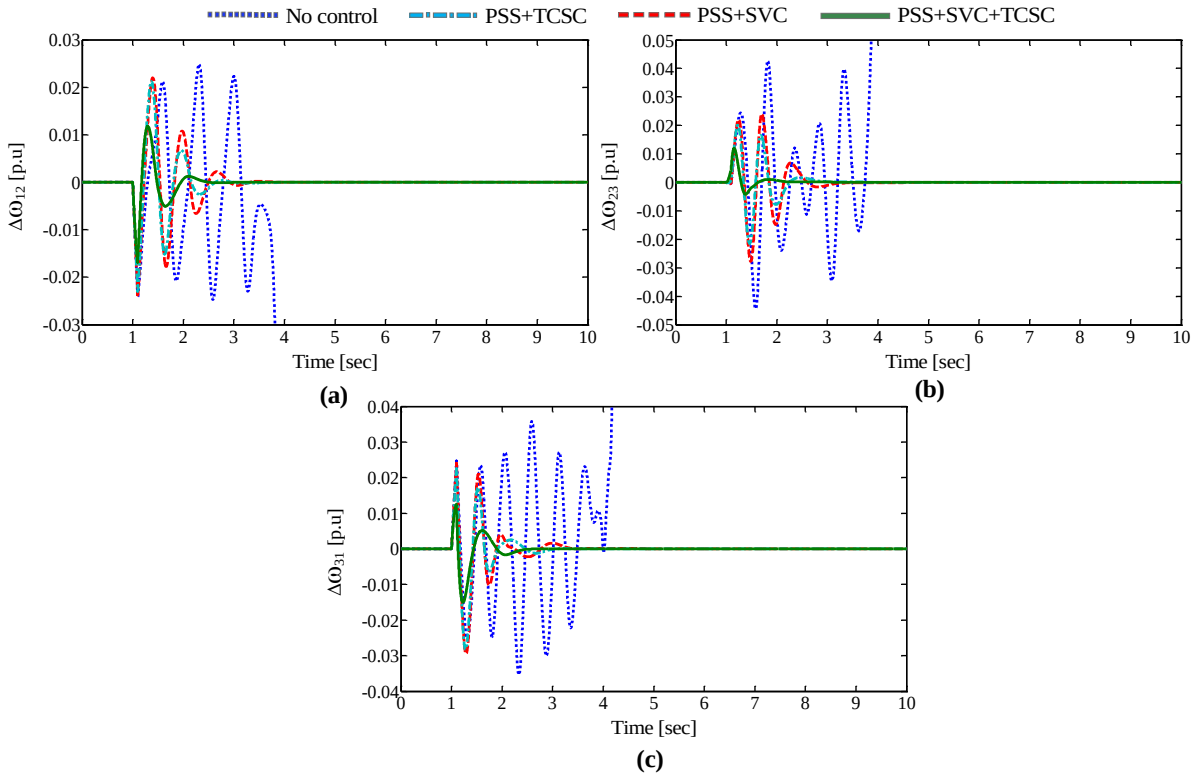

Figure 6.9: **Response of test system with IWO tuned coordinated designs for a six cycle fault under heavy load (a) $\Delta\omega_{12}$ (b) $\Delta\omega_{23}$ (c) $\Delta\omega_{31}$**

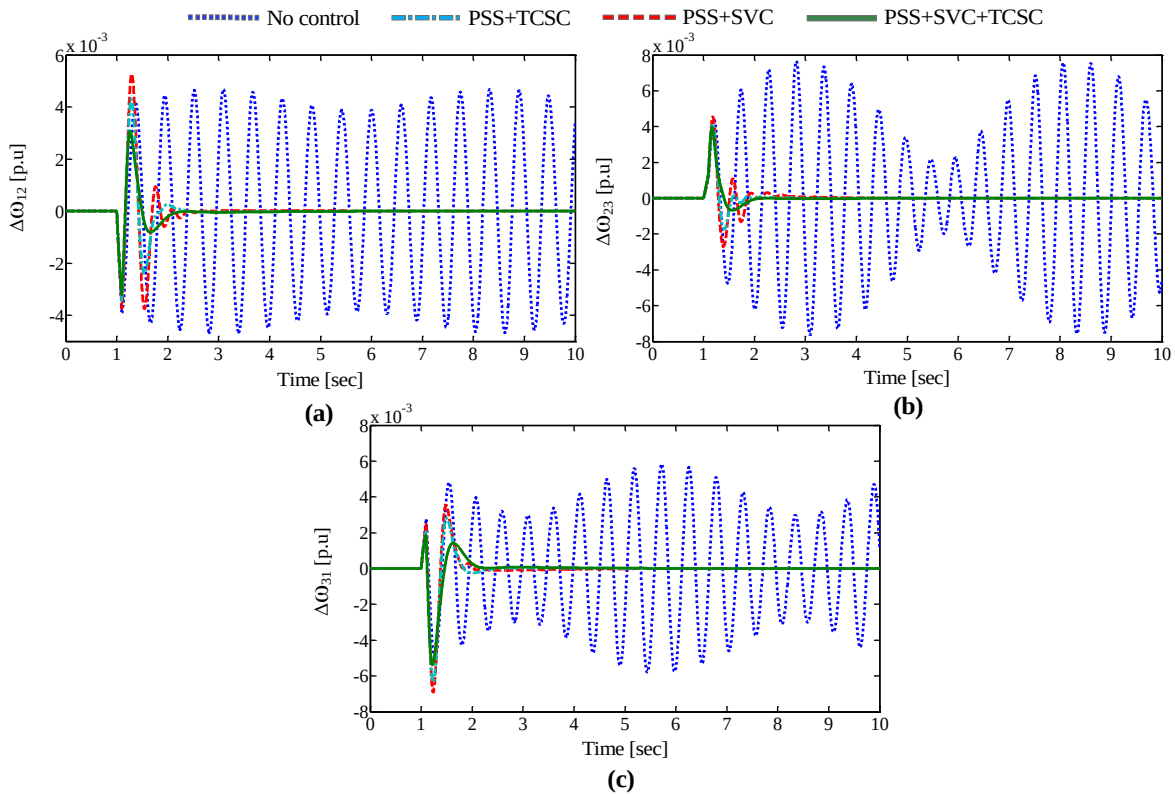

Figure 6.10: **Response of test system with IWO tuned coordinated designs for a six cycle fault under light load (a) Δω12 (b) Δω23 (c) Δω31**

Settling time Comparison of different response curves:

Here, comparison graphs are plotted with the settling time of different responses to show the damping effectiveness of proposed coordinated controller over the other coordinated designs. Figure 6.11 shows the settling times comparison of different inter-area speed oscillations over normal, heavy and light load conditions with AAPSO based different control schemes. Likewise, Figure 6.12 shows the settling time of different responses with IWO based coordinated control designs under different operating conditions. The proposed AAPSO based hybrid coordinated design settles the inter-area oscillations $\Delta\omega_{12}$, $\Delta\omega_{23}$ and $\Delta\omega_{31}$ around $T_s = 2.2, 2.6$ and 2.6s for normal load, $T_s = 2.7, 2.4$ and 2.6s for heavy load and $T_s = 2.1, 2.4$ and 2.4s for light load conditions respectively. Similarly, the proposed IWO based hybrid design provides settling time around $T_s = 2.3, 2.5$ and 2.5s for normal load, $T_s = 2.5, 2.2$ and 2.6s for heavy load and $T_s = 2.2, 2.1$ and 2.1s for light load conditions respectively. Hence, the proposed hybrid coordinated design proved its uniqueness in damping the oscillations earlier than other coordinated designs. The IWO based proposed coordinated designs provide better settling times than the AAPSO based designs.

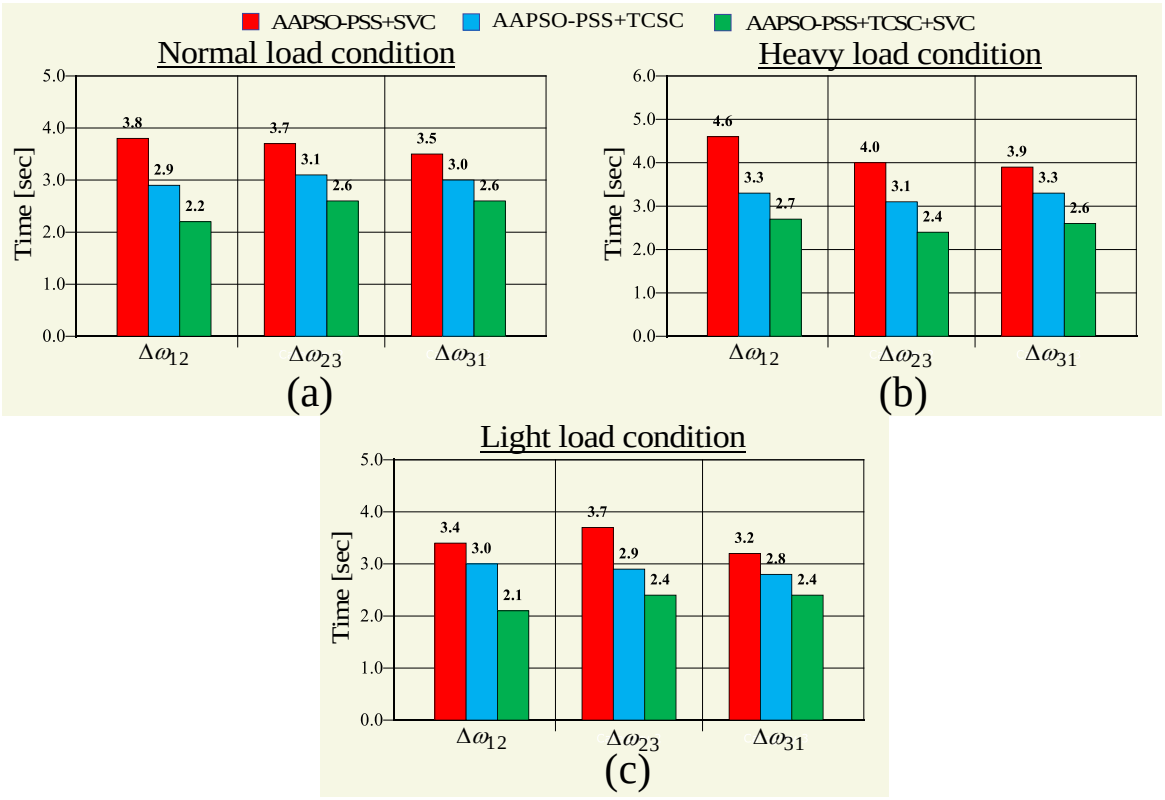

Figure 6.11: **Settling time comparison of speed oscillations with AAPSO based coordinated designs (a) Normal load (b) Heavy load (c) Light load**

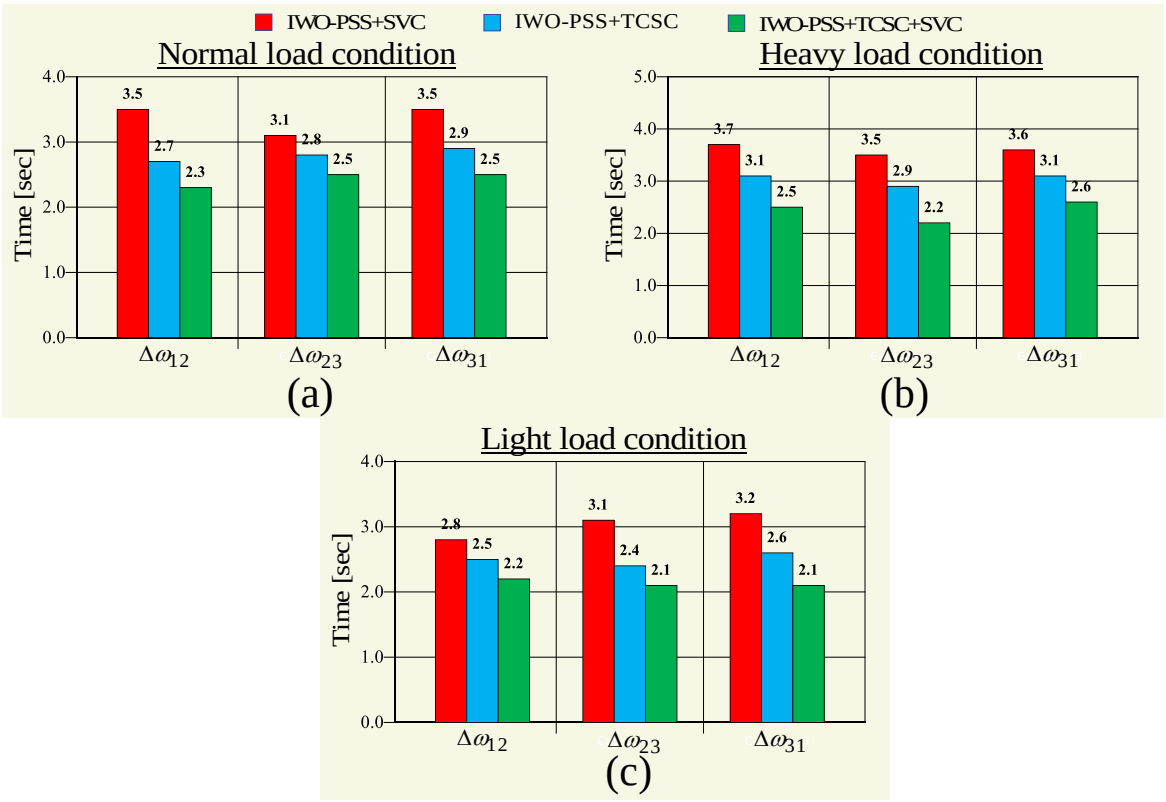

Figure 6.12: **Settling time comparison of speed oscillations with IWO based coordinated designs (a) Normal load (b) Heavy load (c) Light load**

6.2.2 Test System with PSS, TCSC and STATCOM Damping Controllers

The test power system is employed with PSS, TCSC and STATCOM damping controllers. In this section, the test power system is operated under three different operating conditions those are specified in Table 6.6. Here, three PSS are installed at individual generators, a TCSC is installed in series with the line 4-9, and a STATCOM is installed at bus 4 of the test power system.

Table 6.6: **Operating conditions of test system with TCSC and STATCOM (p.u)**

	Nomal		**Heavy**		**Light**	
	P	**Q**	**P**	**Q**	**P**	**Q**
Generator						
G_1	0.7326	0.2436	0.8320	0.6178	0.5278	-0.3088
G_2	1.6300	0.0215	2.4450	0.4248	0.8150	-0.2431
G_3	0.8500	-0.1217	1.2750	0.1373	0.4250	-0.2343
Load						
A	1.25	0.50	1.90	0.75	0.65	0.25
B	0.90	0.30	1.30	0.45	0.45	0.15
C	1.00	0.35	1.50	0.50	0.50	0.17

Table 6.7: **Optimal control parameter values obtained using AAPSO algorithm**

Control parameters	**PSS1**	**PSS2**	**PSS3**	**TCSC**	**DCVC**
K_S	31.0942	23.3672	8.7327	1.2457	1.4723
T_1	0.4357	0.3725	0.5274	0.2886	0.3421
T_3	0.5012	0.4589	0.4055	0.2514	0.2920

Table 6.8: **Optimal control parameter values obtained using IWO algorithm**

Control parameters	**PSS1**	**PSS2**	**PSS3**	**TCSC**	**DCVC**
K_S	30.7324	17.2620	6.7314	1.2604	0.9873
T_1	0.4025	0.3525	0.2967	0.3063	0.3124
T_3	0.4622	0.4562	0.4133	0.2369	0.2559

A. Eigen Value Analysis and Discussions

The AAPSO and IWO tuned hybrid coordinated designed controllers parameter values are given in Tables 6.7 and 6.8 respectively. The system eigen values and damping ratios of poorly damped mechanical modes with different control schemes and different loading conditions are given in Table 6.9. Eigen values and daping ratios witness the system with proposed hybrid coordinated deigns (i.e AAPSO and IWO based coordinated designs of PSS, TCSC and STATCOM) is able to shift the damping factors to the left of *S*-plane and the damping ratios are significantly improved. While, the open loop system has very poor values of damping factors and damping ratios.

Table 6.9: **Electromechanical modes and ζ under different load conditions**

No control	AAPSO-(PSS+TCSC+DCVC)	IWO-(PSS+TCSC+DCVC)
Normal load (λ_i, ζ_i)		
-0.1131±16.5800i, 0.0068	-4.3730±10.7720i, 0.3761	-4.4757±10.545i, 0.3907
-0.0551±12.3620i, 0.0045	-7.4545±8.8548i, 0.6440	-7.4005±8.6827i, 0.6487
Heavy load (λ_i, ζ_i)		
0.1135±17.3470i, -0.0065	-3.8763±10.07i, 0.3592	-3.9546±9.8627i, 0.3722
0.0527±12.1820i, -0.0043	-7.6721±8.8263i, 0.6560	-7.5956±8.6204i, 0.6611
Light load (λ_i, ζ_i)		
-0.1116±13.586i, 0.0082	-3.2362±10.2980i, 0.2998	-3.4032±10.1540i, 0.3178
-0.0572±11.0540i, 0.0052	-6.2520±9.1945i, 0.5623	-6.2616±8.8713i, 0.5766

B. Time Domain Simulations and Discussion

The time domain simulations are carried out for a 6 cycle fault applied on line 9-6 of the test power system. Here, different operating conditions are employed on test system to validate the robustness of proposed designs. The system response with AAPSO and IWO based coordinated control designs are analyzed and the simulation results are given.

Test system response with AAPSO tuned coordinated controllers:

The Figures 6.13 and 6.14 represent the rotor angle and inter-area speed variations of test system with different control schemes under normal load conditions. Here, four control schemes are compared namely no control, coordinated design (PSS+TCSC), hybrid

coordinated designs PSS+TCSC+STATCOM damping controllers (ACVC and DCVC). By analysing the simulation scenario in figures, the proposed coordinated controllers AAPSO-(PSS+TCSC+ACVC) and AAPSO-(PSS+TCSC+DCVC) provided good damping of rotor angle as well as inter-area speed oscillations.

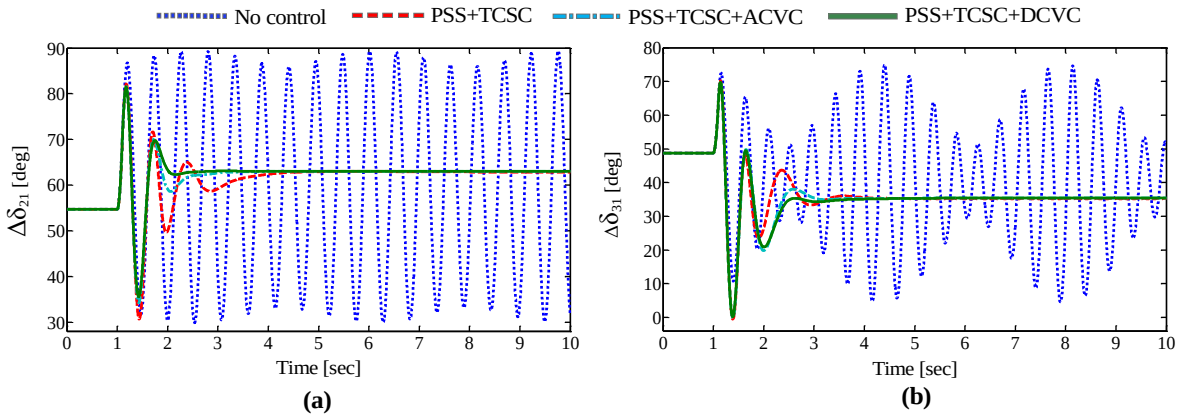

Figure 6.13: R**esponse of test system with AAPSO tuned coordinated designs for a six cycle fault under normal load (a) Δδ21 (b) Δδ31**

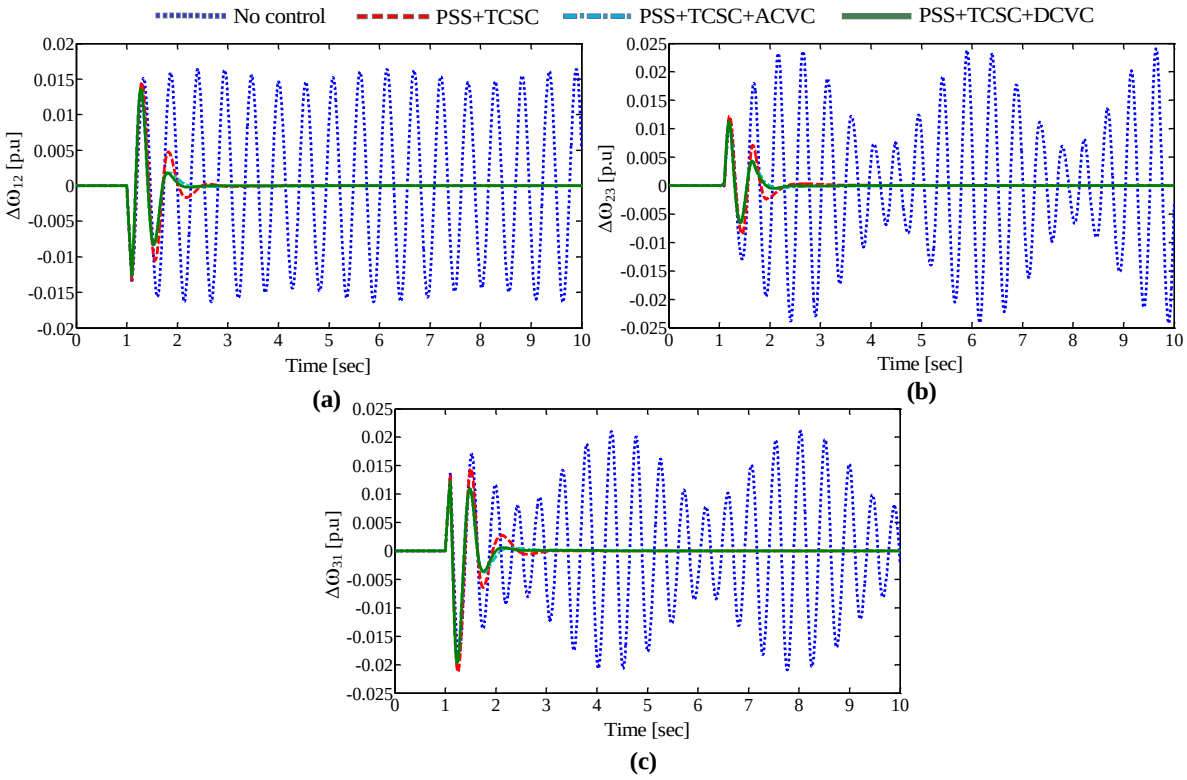

Figure 6.14: **Response of test system with AAPSO tuned coordinated designs for a six cycle fault under normal load (a) Δω12 (b) Δω23 (c) Δω31**

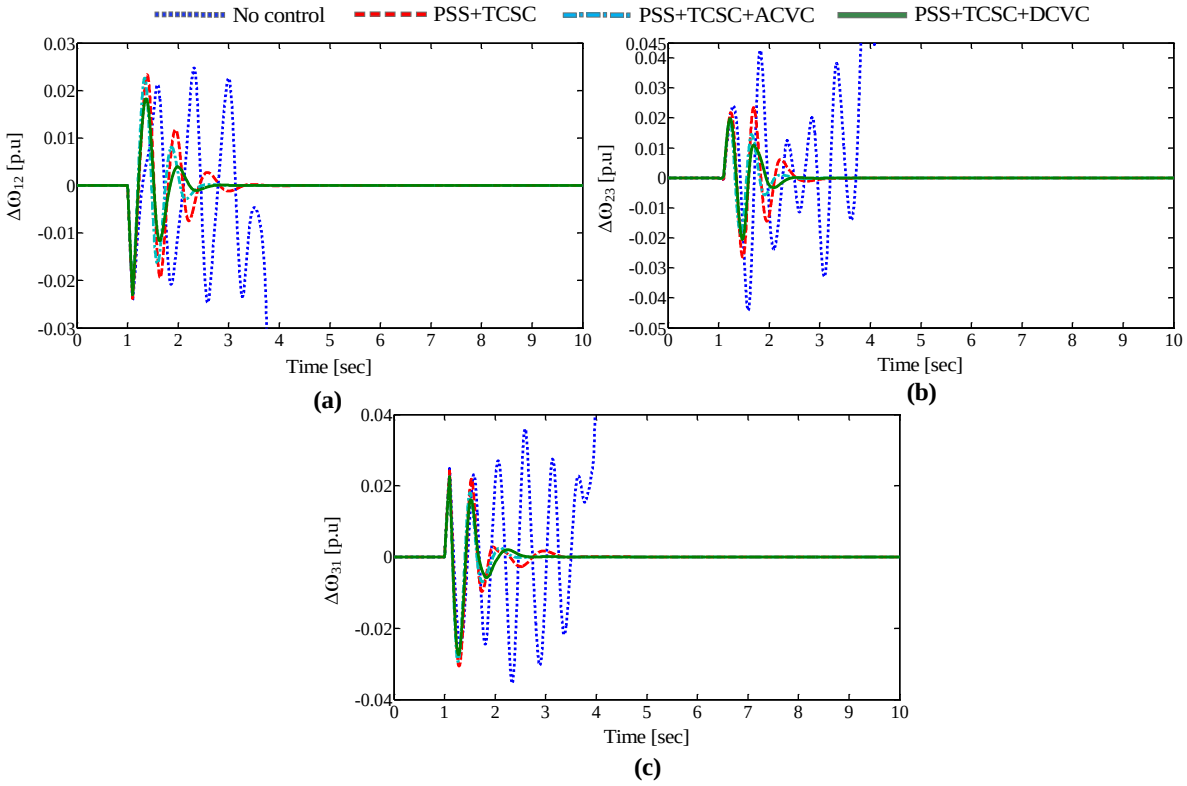

Figure 6.15: **Response of test system with AAPSO tuned coordinated designs for a six cycle fault under heavy load (a) Δω12 (b) Δω23 (c) Δω31**

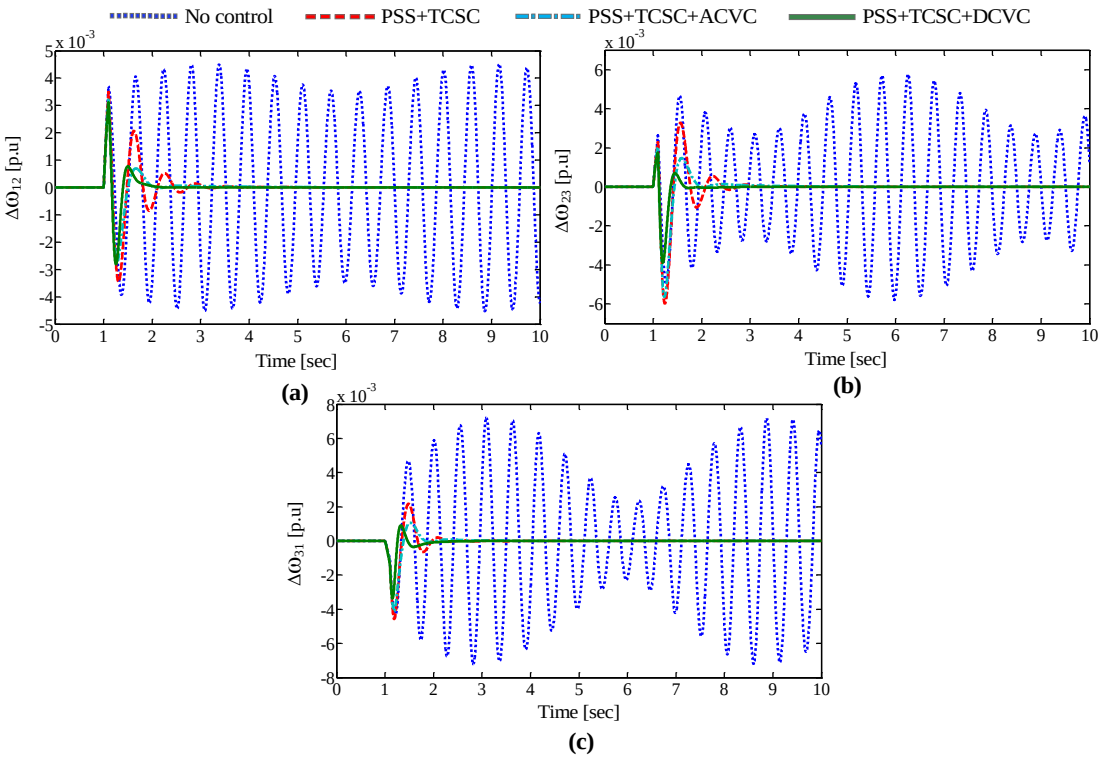

Figure 6.16: **Response of test system with AAPSO tuned coordinated designs for a six cycle fault under light load (a) Δω12 (b) Δω23 (c) Δω31**

To test the robustness of the proposed controllers the system operated under heavy and light load conditions and the corresponding response curves for different control schemes are shown in Figures 6.15 and 6.14. The system operated in heavy load condition loses its synchronism without controller. While with the proposed coordinated designs, the system remains stable after being subjected to a severe disturbance. In all operating points, the test system guarantees the overall stability with AAPSO based hybrid coordinated controller.

Test system response with IWO tuned coordinated controllers:

The system response with IWO tuned coordinated designs over a wide range of operating conditions are discussed here. The simulation results demonstrated the comparison of different control designs namely no control, IWO based coordinated design (PSS+TCSC), IWO based hybrid coordinated designs (PSS+TCSC+ACVC) and (PSS+TCSC+DCVC). The system response with different control designs for a six cycle fault disturbance under normal, heavy and light load conditions is plotted in Figures 6.17 – 6.20. The rotor angle responses and speed oscillations under normal load condition with different controllers are shown in Figures 6.17 and 6.18. Also, the inter area speed oscillations under heavy and light load conditions are given in Figures 6.19 and 6.20 respectively. From the simulations results, it is noticed that in all operating conditions, open loop system is highly oscillatory in nature and very poor damping characteristics. On the other hand, the IWO based coordinated designs greatly enhance the damping characteristics of test system independent of operating conditions. Furthermore among all coordinated designs, the proposed IWO based hybrid design (PSS+TCSC+DCVC) showed great damping effect.

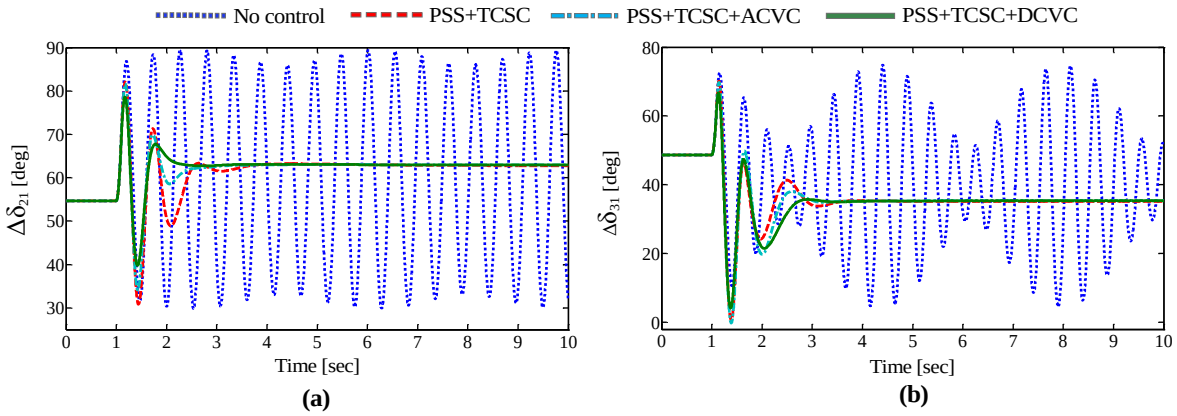

Figure 6.17: R**esponse of test system with IWO tuned coordinated designs for a six cycle fault under normal load (a) $\Delta\delta_{21}$ (b) $\Delta\delta_{31}$**

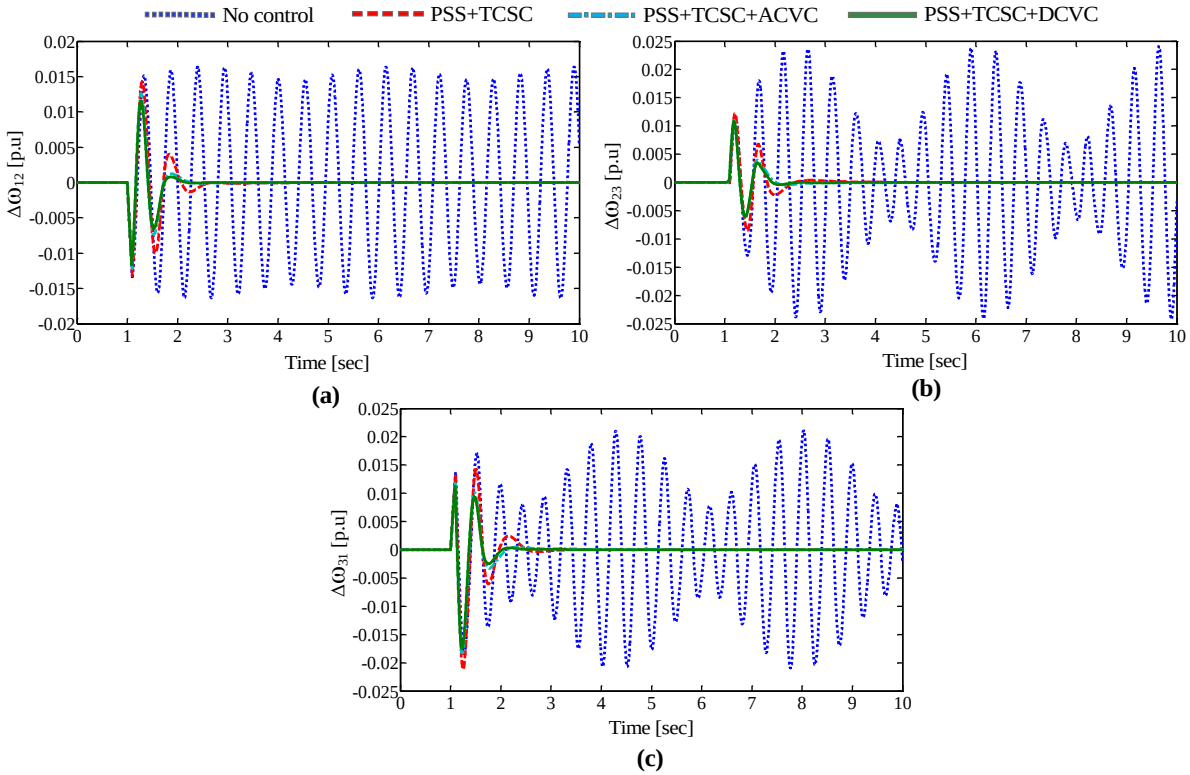

Figure 6.18: **Response of test system with IWO tuned coordinated designs for a six cycle fault under normal load (a) Δω12 (b) Δω23 (c) Δω31**

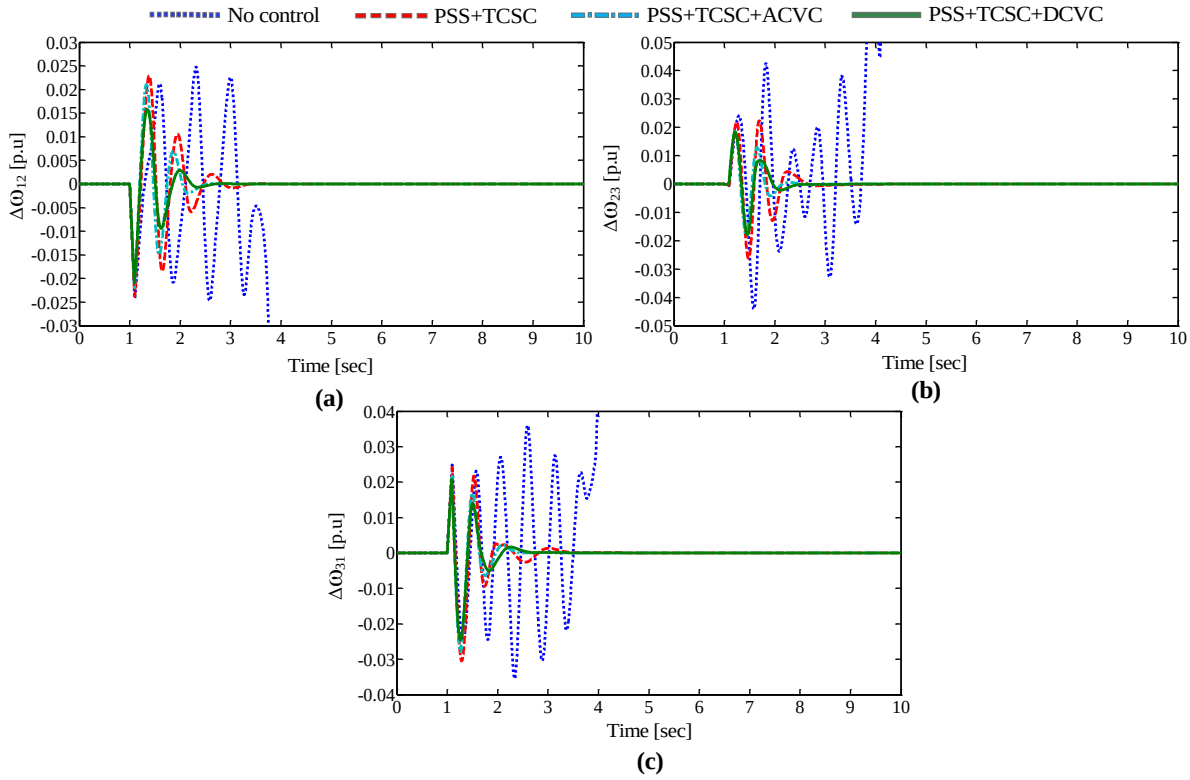

Figure 6.19: **Response of test system with IWO tuned coordinated designs for a six cycle fault under heavy load (a) Δω12 (b) Δω23 (c) Δω31**

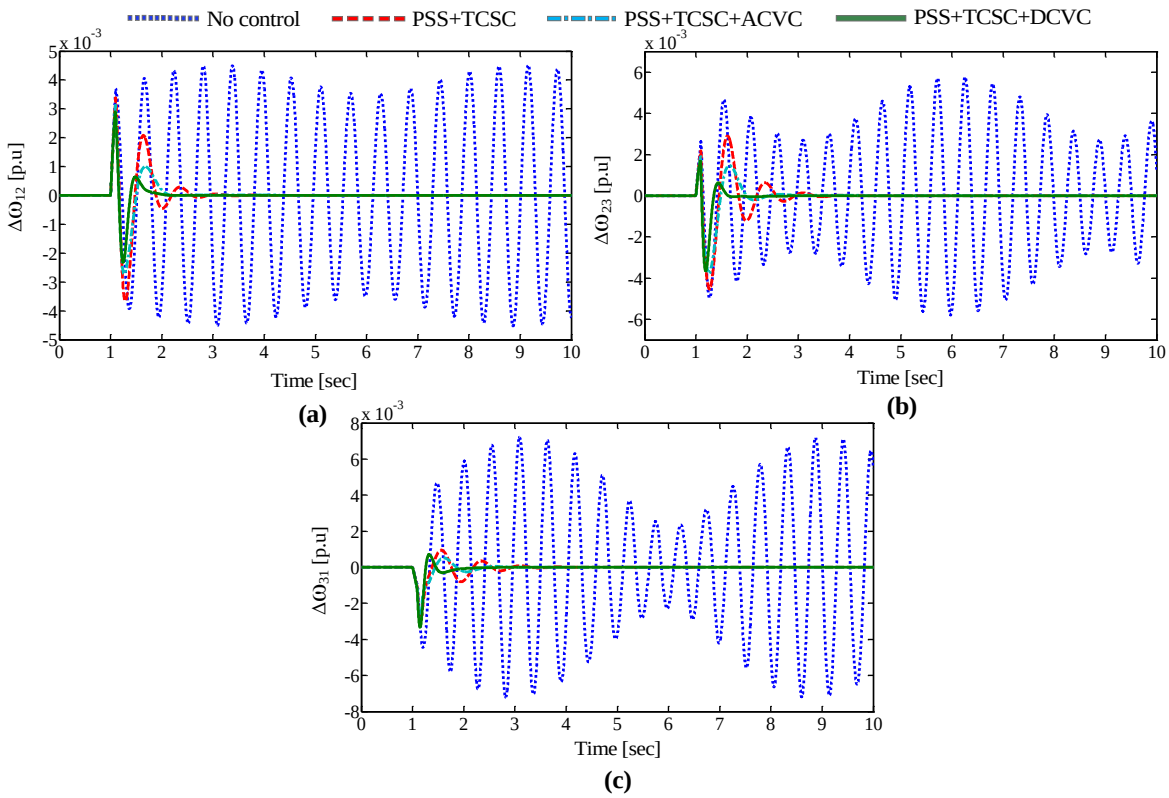

Figure 6.20: **Response of test system with IWO tuned coordinated designs for a six cycle fault under light load (a) Δω12 (b) Δω23 (c) Δω31**

Settling time comparison of different response cures:

To analyze the effectiveness of damping the system oscillations, comparisons are made among all the coordinated designs. The settling time comparisons of inter-area oscillations with AAPSO based coordinated controllers under normal, heavy and light load conditions are presented in Figure 6.21. Here, the hybrid design of (PSS+TCSC+DCVC) records good settling times as $T_s = 2.2, 2.3$ and 2.4s for normal load, $T_s = 2.6, 2.5$ and 2.6s for heavy load and $T_s = 2.3, 2.1$ and 2.1s for light load conditions respectively.

In the same way, the settling time comparison of speed oscillations with IWO based hybrid coordinated designs are graphed in Figure 6.22. In this case also, the hybrid design of (PSS+ TCSC+DCVC) attains best settling times over other controllers as $T_s = 2.3, 2.4$ and 2.3s for normal load, $T_s = 2.6, 2.5$ and 2.5s for heavy load and $T_s = 2.1, 1.8$ and 2.1s for light load conditions respectively. Therefore, the proposed hybrid coordinated designs assured effective damping along with grater settling times to power oscillations. By observing these

settling time comparison plots, it is concluded that the IWO based designs overtakes the effectiveness of AAPSO based coordinated designs.

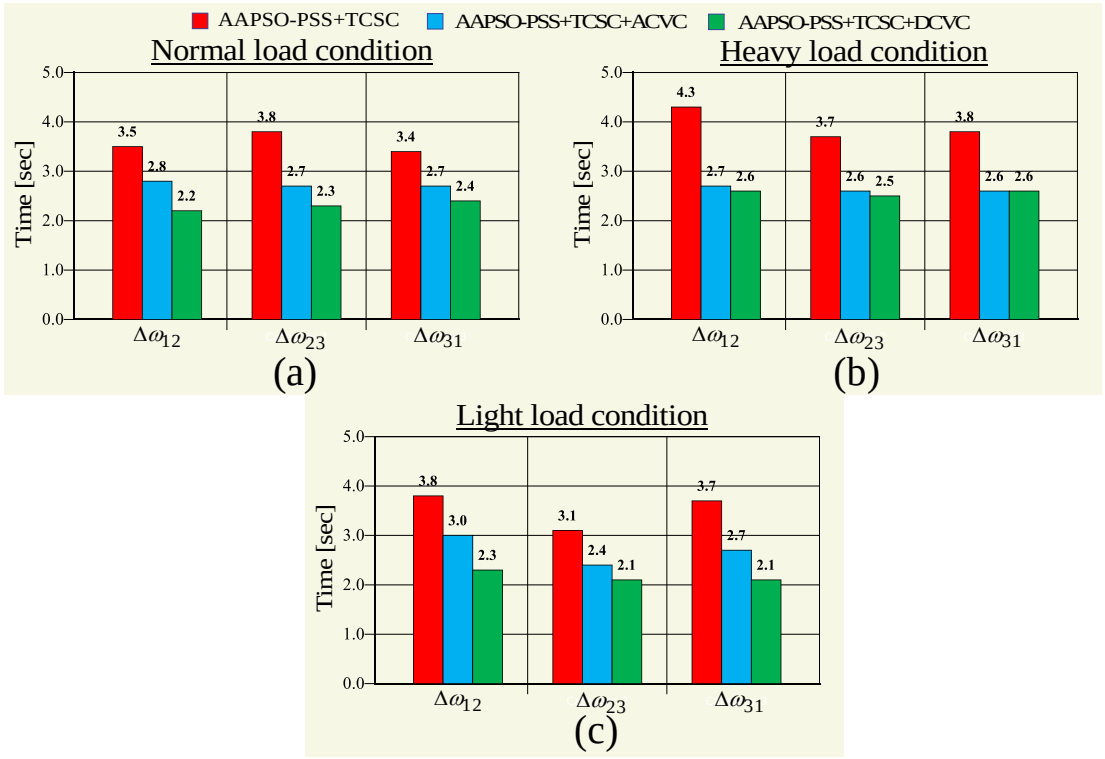

Figure 6.21: **Settling time comparison of speed oscillations with AAPSO based coordinated designs (a) Normal load (b) Heavy load (c) Light load**

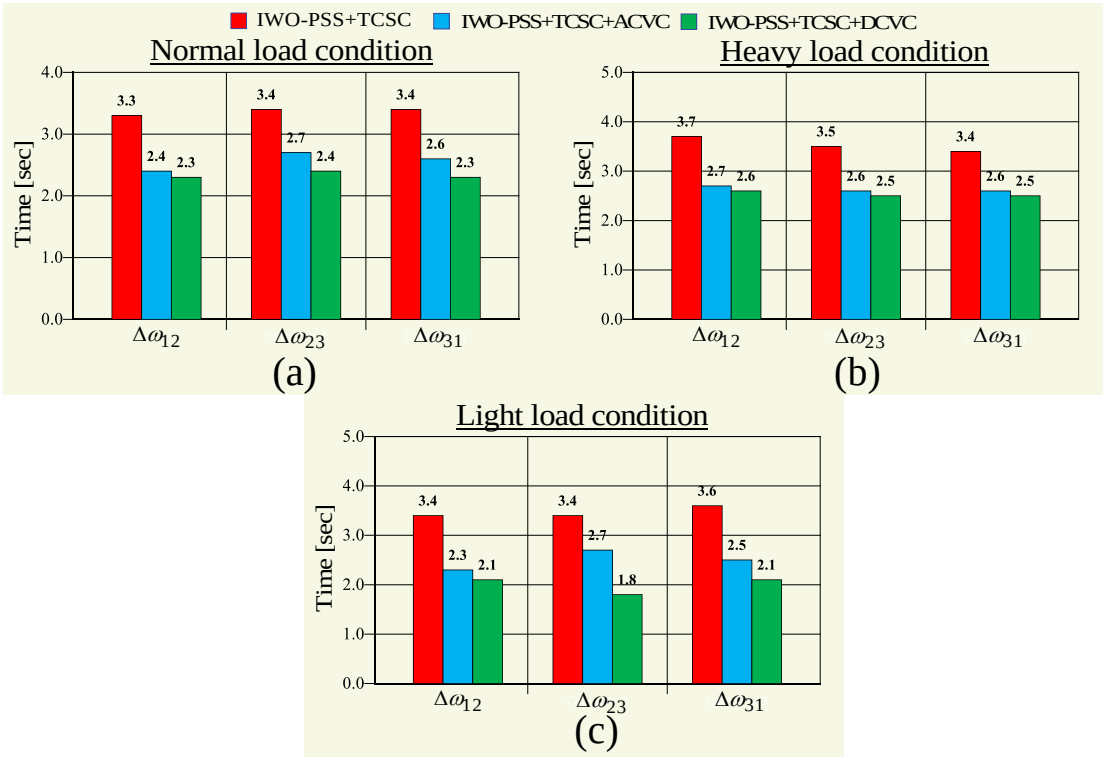

Figure 6.22: **Settling time comparison of speed oscillations with IWO based coordinated designs (a) Normal load (b) Heavy load (c) Light load**

6.3 4-Machine 11-Bus Power System

In this section, a 4-machine 11-bus power system known as "Kundur two area power system" (as shown in Figure 6.23) is considered for analysis. This two area test system has 4 generators, 2 loads and 11 buses. The details of the test system are given in [2]. Here, the generators are represented by G_1, G_2, G_3 and G_4, and the loads are represented as load A and load B. Moreover, the system has two areas namely, area 1 and area 2. In each area, two generators are installed like the generators G_1 and G_2 are belong to Area 1, G_3 and G_4 are in Area 2. Hence, analysis on this type of test power system will help to observe the behavior of proposed coordinated designs for local as well as inter-area oscillations. The same kind of analysis as mentioned in the previous section with different coordinated designs is done here.

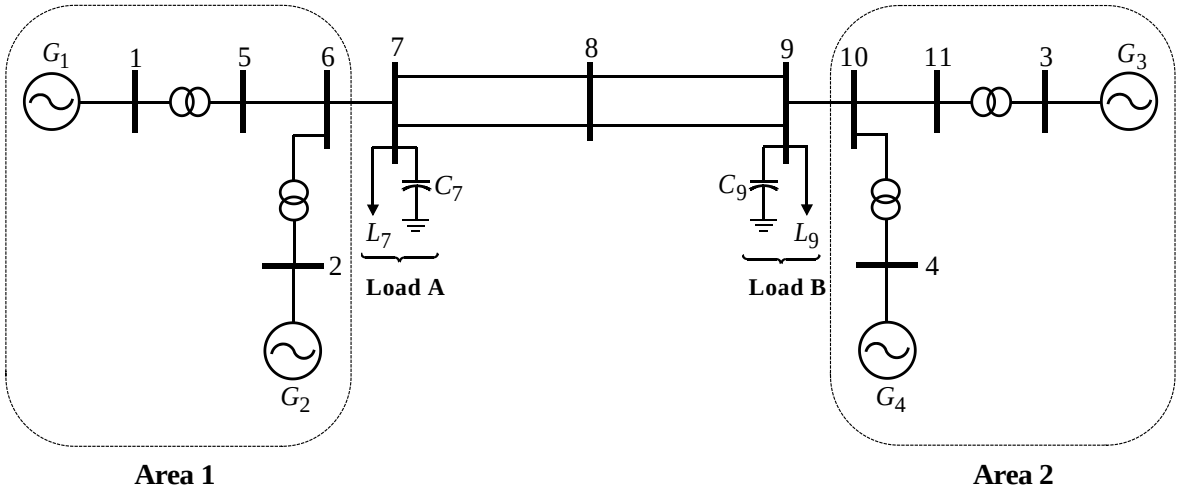

Figure 6.23: **4-machine 11-bus two-area power system**

6.3.1 Two Area System with PSS, TCSC and SVC Damping Controllers

From the Figure 6.23, it is observed that the two areas of the system are connected by the transmission lines between buses 7-8 and 8-9. To control the power transmission and maintain over all stability of the system in two areas, the buses 7, 8 and 9 are most preferable locations for installing external controllers like TCSC, SVC and STATCOM. Hence, in this work, the test power system is employed with four PSS as each PSS on each generator, a TCSC is installed in series with one of the transmission lines between buses 8-9, and a SVC installed at bus 8. The test power system is operated in three distinct load conditions as given in Table 6.10.

Table 6.10: **Operating conditions of test power system with TCSC and SVC (p.u)**

	Normal		Heavy		Light	
	P	**Q**	**P**	**Q**	**P**	**Q**
Generator						
G_1	6.6957	0.9351	7.2514	1.2580	5.7770	0.6107
G_2	7.0000	0.5246	8.4000	1.2397	5.6000	-0.0824
G_3	7.2000	1.0917	8.6400	1.7157	5.7600	0.6061
G_4	7.0000	0.7580	8.4000	1.7924	5.6000	-0.0905
Load						
A	9.50	1.00	11.40	1.20	7.60	0.80
B	17.50	2.50	21.00	3.00	14.00	2.00

A. EigenValue Analysis and Discussion

The hybrid coordinated design procedure is formulated as an optimization problem and an eigen value based objective function is minimized using AAPSO and IWO algorithms. The optimal control parameter values of proposed coordinated controllers are obtained at the end of these algorithms as mentioned in Tables 6.11 and 6.12. A comparison of objective function convergence rate using AAPSO and IWO algorithms is shown in Figure 6.24. From the results, it is found that the IWO algorithm gives the fast convergence rate compare to that of AAPSO algorithm. Here, the IWO reached its convergence value nearer to 55 iterations, whereas AAPSO reached about 69 iterations.

Poorly damped electromechanical mode eigen values and their damping ratios of the test system under different load conditions are provided in Table 6.13. The system without controller provides very poor damping factors and damping ratios under all three load conditions. The AAPSO based coordinated design helps in shifting the very poor damped eigen values to left of the D-shape in *S*-plane. The poor damping factors are shifted from $\sigma = -0.0076, 0.0075 \text{and} -0.0073$ to $\sigma = -1.0995, -0.9946 \text{and} -1.1506$ for normal, heavy and light load conditions respectively. Also, the system with IWO based coordinated design improved the damping factors for normal, heavy and light load conditions as $\sigma = -1.0895, -0.9829 \text{and} -1.1303$ respectively. While the damping ratios are also increases to large extent to keep the system more stable for the test system with AAPSO and IWO based proposed designs.

Table 6.11: **Optimal control parameter values obtained using AAPSO algorithm**

Control parameters	PSS1	PSS2	PSS3	PSS4	TCSC	SVC
K_S	26.3893	24.7408	25.2296	30.5312	1.0430	1.1574
T_1	0.4324	0.4712	0.3843	0.5143	0.2112	0.2864
T_3	0.4088	0.5316	0.5072	0.3676	0.3061	0.3293

Table 6.12: **Optimal control parameter values obtained using IWO algorithm**

Control parameters	PSS1	PSS2	PSS3	PSS4	TCSC	SVC
K_S	30.9824	26.5080	28.5008	27.8992	0.9627	1.1782
T_1	0.3356	0.4579	0.3914	0.4628	0.2681	0.2344
T_3	0.3826	0.4923	0.4877	0.3517	0.1954	0.2015

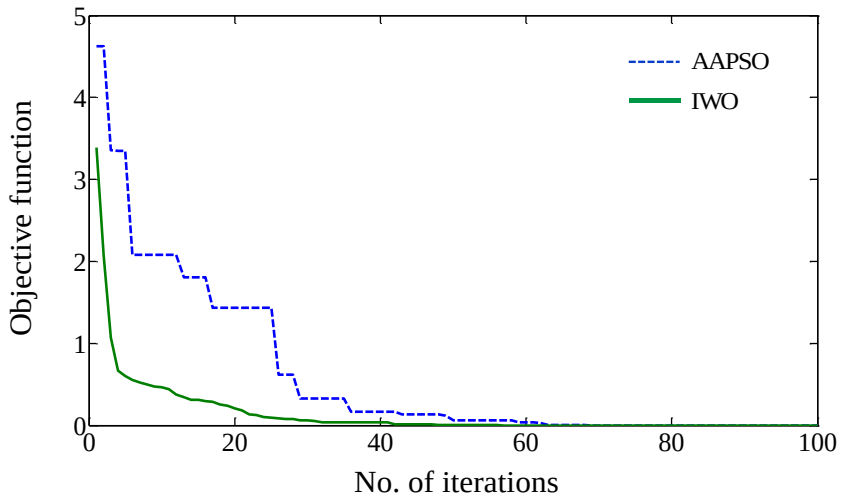

Figure 6.24: **Convergence of objective function**

B. Time Domain Simulations and Discussion

The time domain simulations of the test system are conducted for a 6 cycle three-phase fault. It is applied on one of the transmission lines between the buses 7-8, and this fault is cleared by tripping the line using circuit breakers permanently. This analysis is done on the test system with proposed control designs using two distinct optimization algorithms. In each case, all three operating conditions are applied on the system to test the robustness of proposed designs.

Test system response with AAPSO tuned coordinated controllers:

Figures 6.25 – 6.28 represents the test system dynamic response with AAPSO algorithm based different coordinated designs. The test system response under normal load condition is compared over different control schemes as shown in Figure 6.25 and 6.26. The local as well as inter area rotor angle oscillations of the test system are compared and shown in Figure 6.25. Here, the responses $\Delta\delta_{12}$ and $\Delta\delta_{34}$ represent local area rotor angle oscillations of area 1 and area 2 respectively. The responses $\Delta\delta_{13}$ and $\Delta\delta_{14}$ represent inter-area rotor angle oscillations of area 1 to area 2. In the similar way, the local-area speed oscillations ($\Delta\omega_{12}$ and $\Delta\omega_{34}$) along with inter-area speed oscillations ($\Delta\omega_{13}$ and $\Delta\omega_{14}$) of the test power system with different designs under normal load are presented in Figure 6.26. Also, the test system under heavy and light load condition responses $\Delta\omega_{12}$, $\Delta\omega_{13}$, $\Delta\omega_{14}$ and $\Delta\omega_{34}$ for AAPSO based different coordinated designs are compared in Figures 6.27 and 6.28 respectively. In all these responses, the different control schemes such as AAPSO based (PSS+TCSC), AAPSO based (PSS+SVC) and AAPSO based (PSS+TCSC+SVC) are compared. By analyzing all these responses, it is clear that the system with proposed hybrid design controllers has excellent damping characteristics compare to other designs.

Table 6.13: **Electromechanical modes and ζ under different load conditions**

No control	AAPSO-(PSS+TCSC+SVC)	IWO-(PSS+TCSC+SVC)
Normal load (λ_i, ζ_i)		
-0.0091±7.0550i, 0.0013	-3.3126±5.7101i, 0.5018	-3.3194±5.6022i, 0.5097
-0.0080±6.7455i, 0.0012	-2.8074±5.3487i, 0.4647	-2.8057±5.1966i, 0.4751
-0.0076±5.2742i, 0.0014	-1.0995±4.2987i, 0.2478	-1.0895±4.2329i, 0.2493
Heavy load (λ_i, ζ_i)		
-0.0093±7.2107i, 0.0013	-3.2373±5.8749i, 0.4826	-3.2375±5.7670i, 0.4895
0.0079±6.8993i, -0.0011	-2.7413±5.4990i, 0.4461	-2.7323±5.3497i, 0.4548
0.0077±5.2434i, -0.0015	-0.9946±4.4025i, 0.2204	-0.9829±4.3376i, 0.2210
Light load (λ_i, ζ_i)		
-0.0089±6.7892i, 0.0013	-3.2941±5.4262i, 0.5189	-3.2910±5.3335i, 0.5251
-0.0081±6.4788i, 0.0012	-2.7764±5.0752i, 0.4799	-2.7641±4.9406i, 0.4883
-0.0073±5.1913i, 0.0014	-1.1506±4.1160i, 0.2692	-1.1303±4.0589i, 0.2682

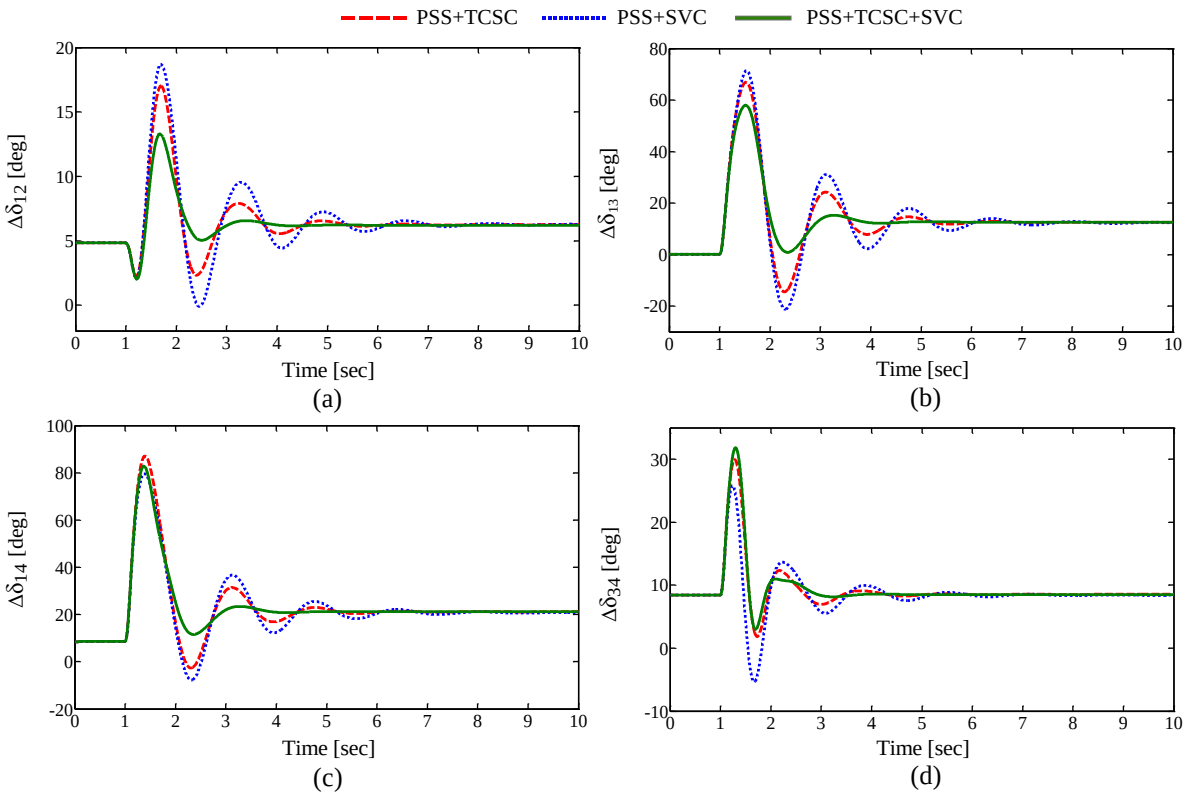

Figure 6.25: R**esponse of test system with AAPSO tuned coordinated designs for a six cycle fault under normal load (a) Δδ12 (b) Δδ13 (c) Δδ14 (d) Δδ34**

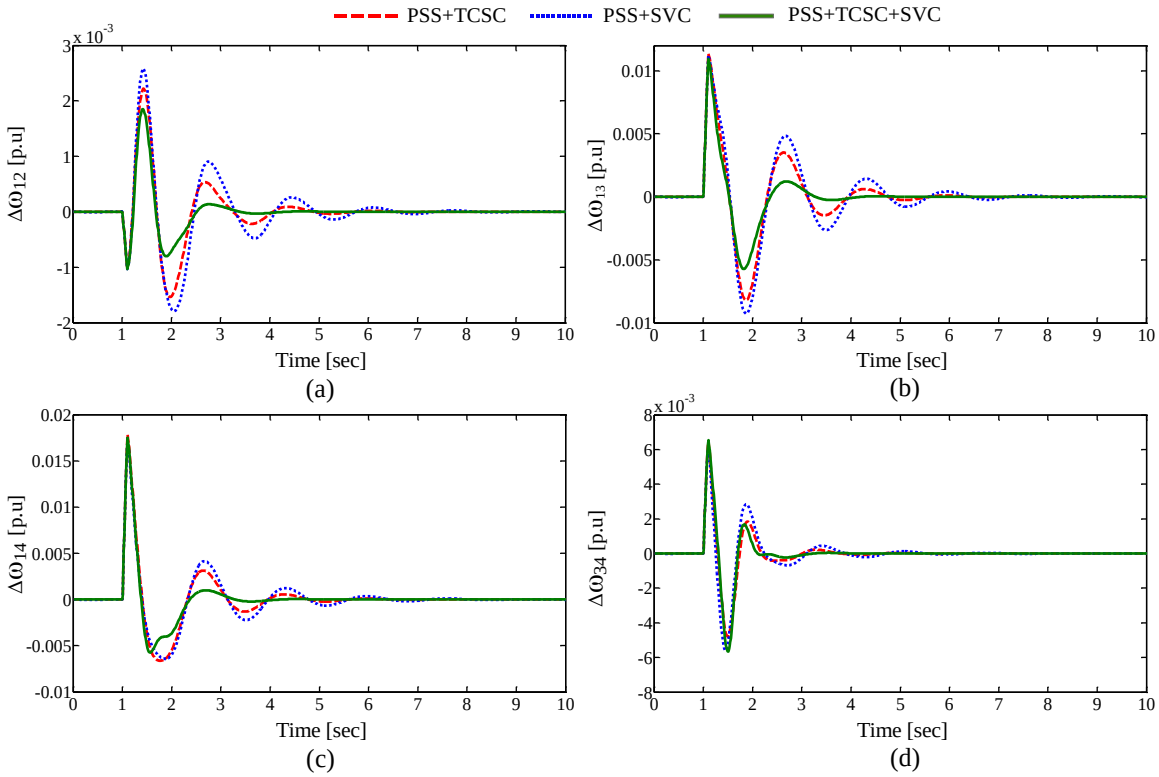

Figure 6.26: R**esponse of test system with AAPSO tuned coordinated designs for a six cycle fault under normal load (a) Δω12 (b) Δω13 (c) Δω14 (d) Δω34**

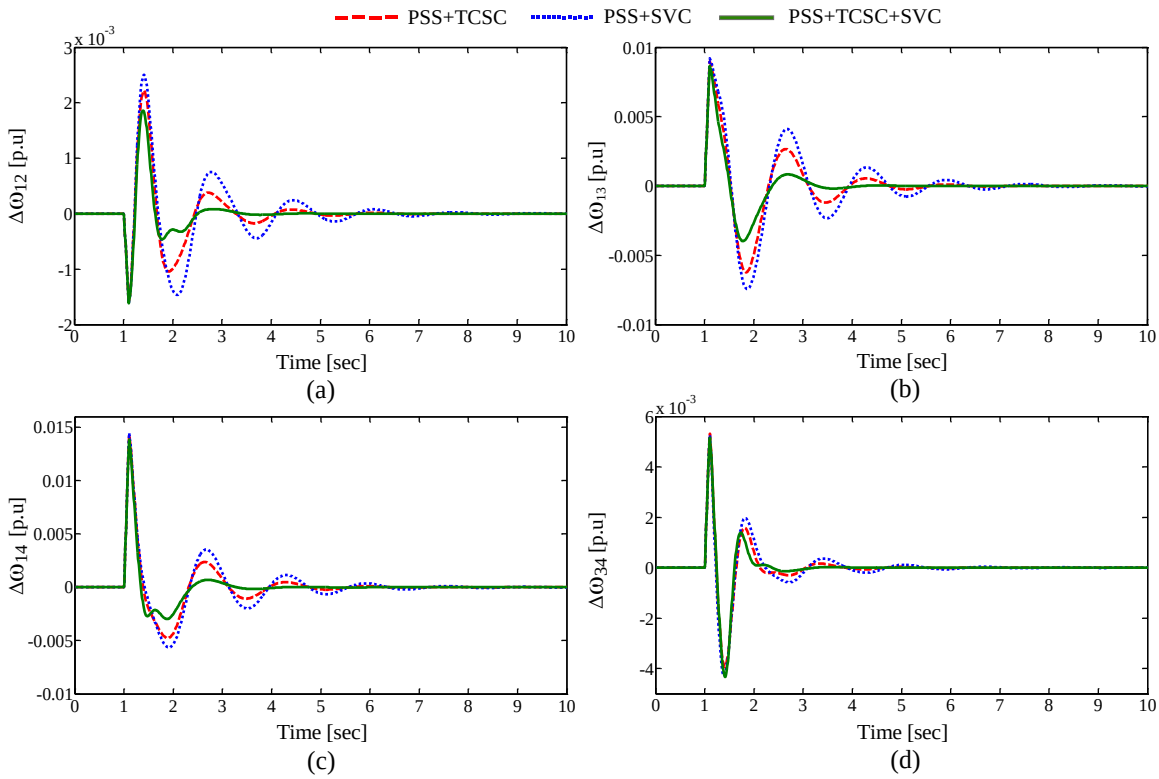

Figure 6.27: **Response of test system with AAPSO tuned coordinated designs for a six cycle fault under heavy load (a) Δω12 (b) Δω13 (c) Δω14 (d) Δω34**

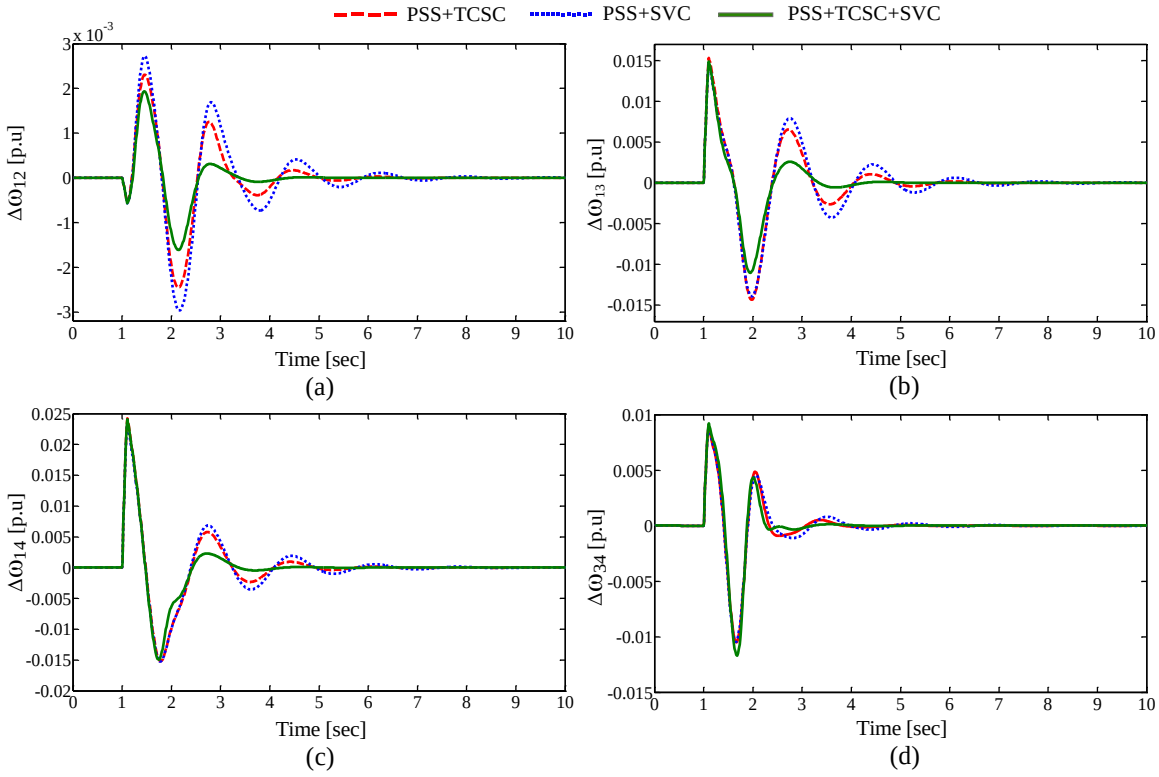

Figure 6.28: **Response of test system with AAPSO tuned coordinated designs for a six cycle fault under light load (a) Δω12 (b) Δω13 (c) Δω14 (d) Δω34**

Test system response with IWO tuned coordinated controllers:

Now, the system response with IWO tuned coordinated controller is analyzed for a severe disturbance under three distinct load conditions. The Figure 6.29 represents the rotor angle deviations between different generators of the test system with different control schemes under normal load. The local and inter-area oscillations of the test system under normal load are compared for IWO based different coordinated designs in Figure 6.30. Moreover under heavy and light load conditions, the system dynamic response is shown in Figures 6.31 and 6.32 respectively. In all these response curves over three different operating conditions, the proposed IWO based (PSS+TCSC+SVC) provides great damping behavior compared to other designs like, IWO based (PSS+TCSC), IWO based (PSS+SVC).

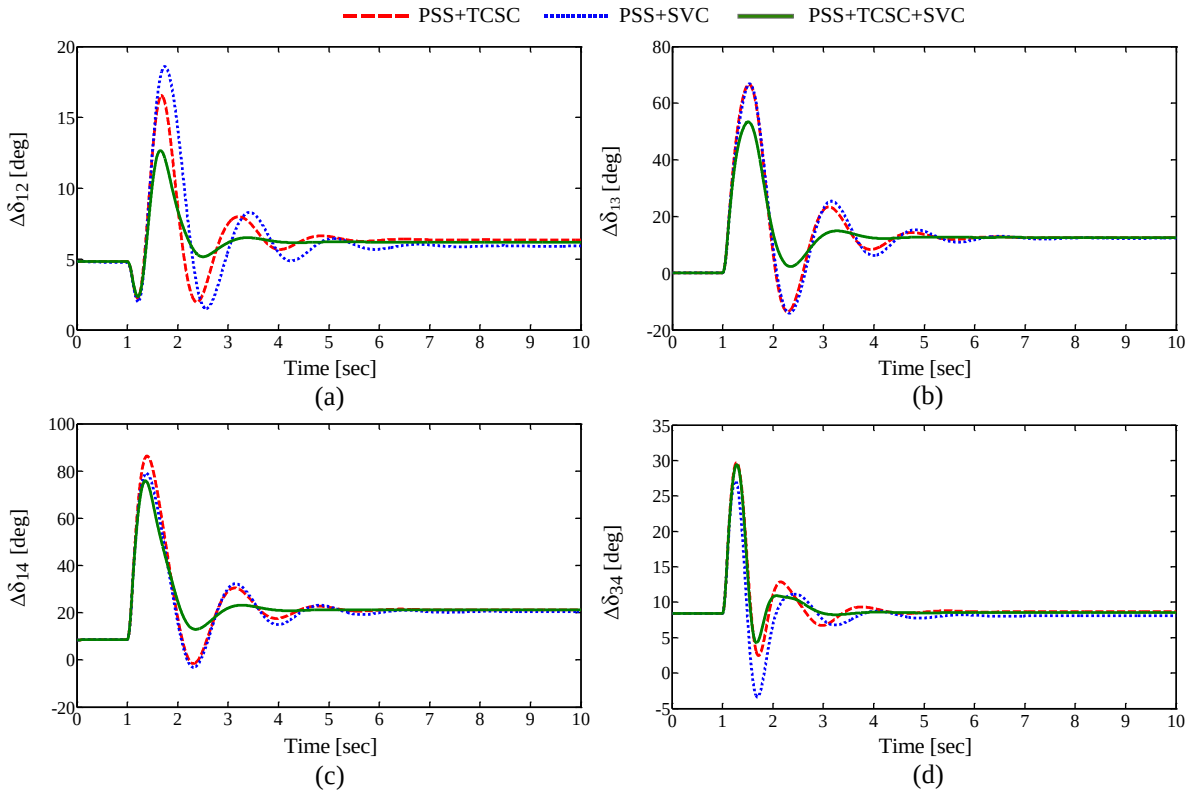

Figure 6.29: R**esponse of test system with IWO tuned coordinated designs for a six cycle fault under normal load (a) Δδ12 (b) Δδ13 (c) Δδ14 (d) Δδ34**

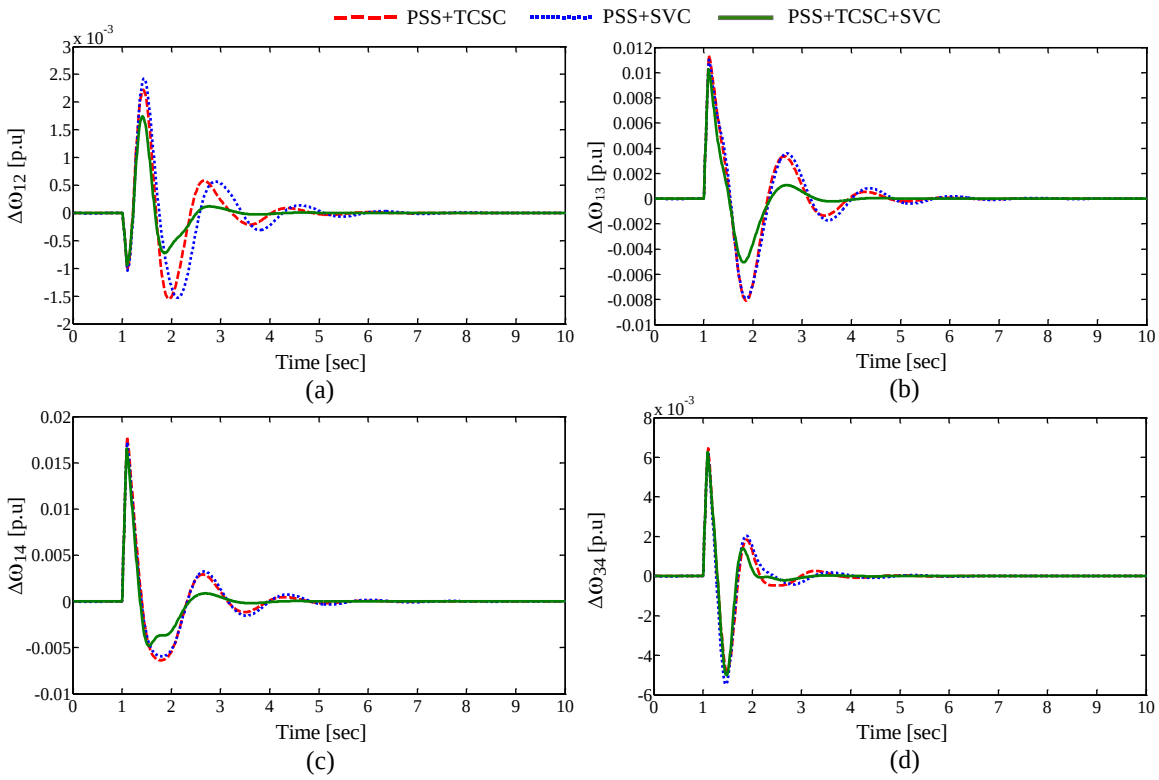

Figure 6.30: R**esponse of test system with IWO tuned coordinated designs for a six cycle fault under normal load (a) Δω12 (b) Δω13 (c) Δω14 (d) Δω34**

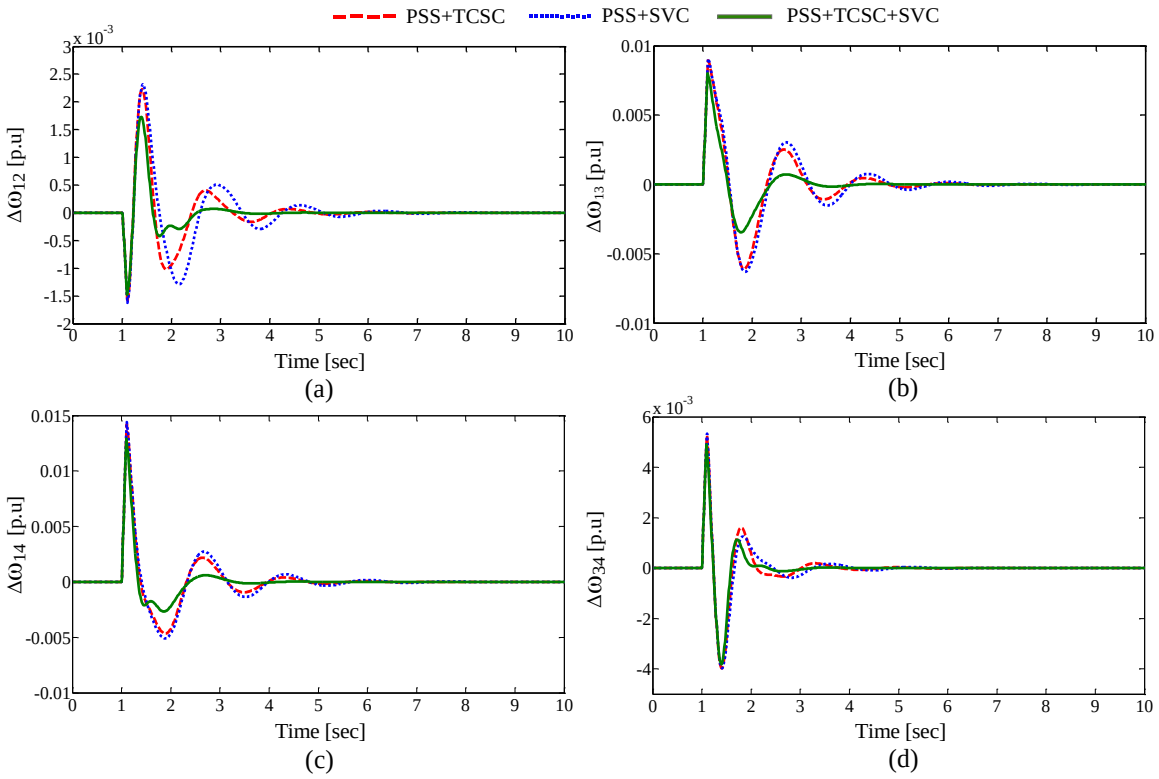

Figure 6.31: R**esponse of test system with IWO tuned coordinated designs for a six cycle fault under heavy load (a) Δω12 (b) Δω13 (c) Δω14 (d) Δω34**

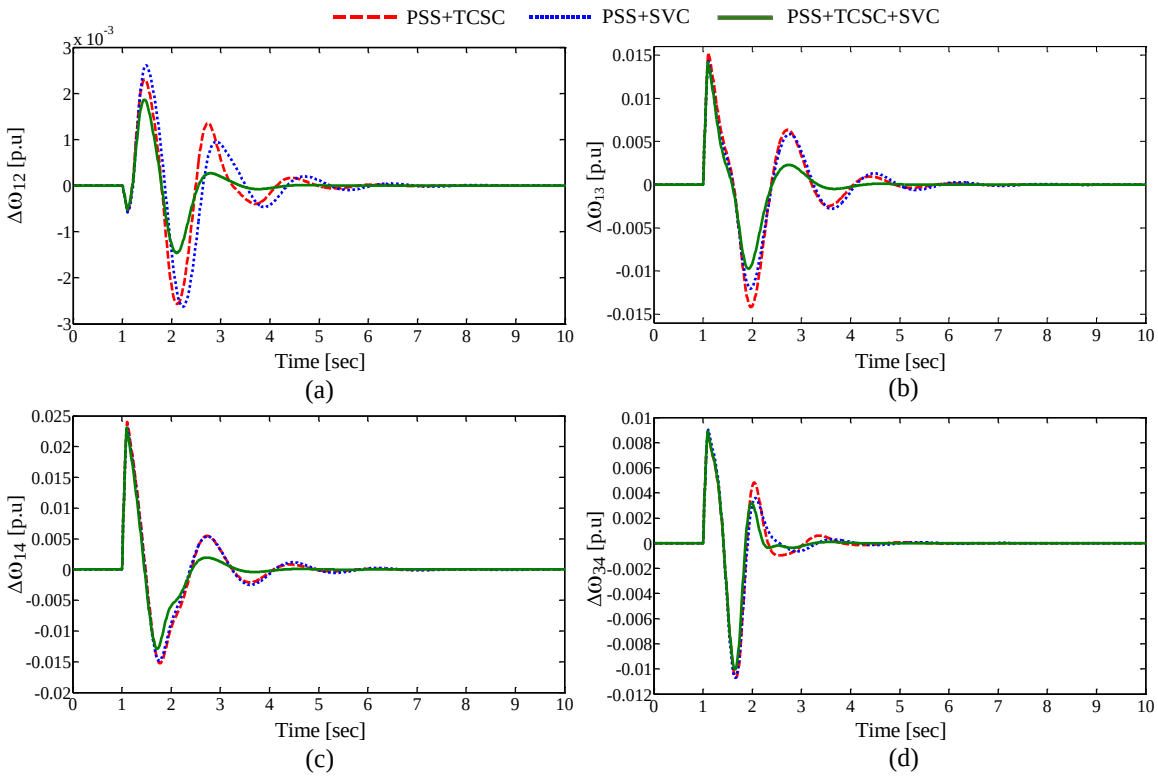

Figure 6.32: R**esponse of test system with IWO tuned coordinated designs for a six cycle fault under light load (a) Δω12 (b) Δω13 (c) Δω14 (d) Δω34**

Settling time comparison of different response cures:

In this section, the settling time for speed oscillations of test power system with different coordinated designs under all three operating conditions are compared and analyzed to verify the effectiveness of proposed hybrid design. The settling time comparisons of local and inter-area oscillations of test system with AAPSO based coordinated controllers under normal, heavy and light load conditions are presented in Figure 6.33. Here, the proposed hybrid design (PSS+TCSC+SVC) registers good settling times $T_s = 4.5, 4.6, 4.2 \text{ and } 3.6\text{s}$ for normal load, $T_s = 4.6, 4.4, 4.3 \text{ and } 3.4\text{s}$ for heavy load and $T_s = 4.4, 4.5, 4.5 \text{ and } 3.5\text{s}$ for light load conditions.

Also, the settling time comparison of speed oscillations Δω12, Δω13, Δω14 and Δω34 with IWO based hybrid coordinated designs is plotted in Figure 6.34. In this situation also, the hybrid design (PSS+TCSC+SVC) achieved top settling times than other controllers as $T_s = 4.4, 4.3, 4.1 \text{ and } 3.3\text{s}$ for normal load, $T_s = 3.8, 4.3, 4.3 \text{ and } 3.3\text{s}$ for heavy load and $T_s = 4.3, 4.4, 4.3 \text{ and } 3.5\text{s}$ for light load conditions. Thus, the proposed hybrid coordinated designs guaranteed effective damping along with lesser settling times. On verifying these

settling times comparison plots, it is concluded that the effectiveness of IWO based designs is better than that of AAPSO based coordinated designs.

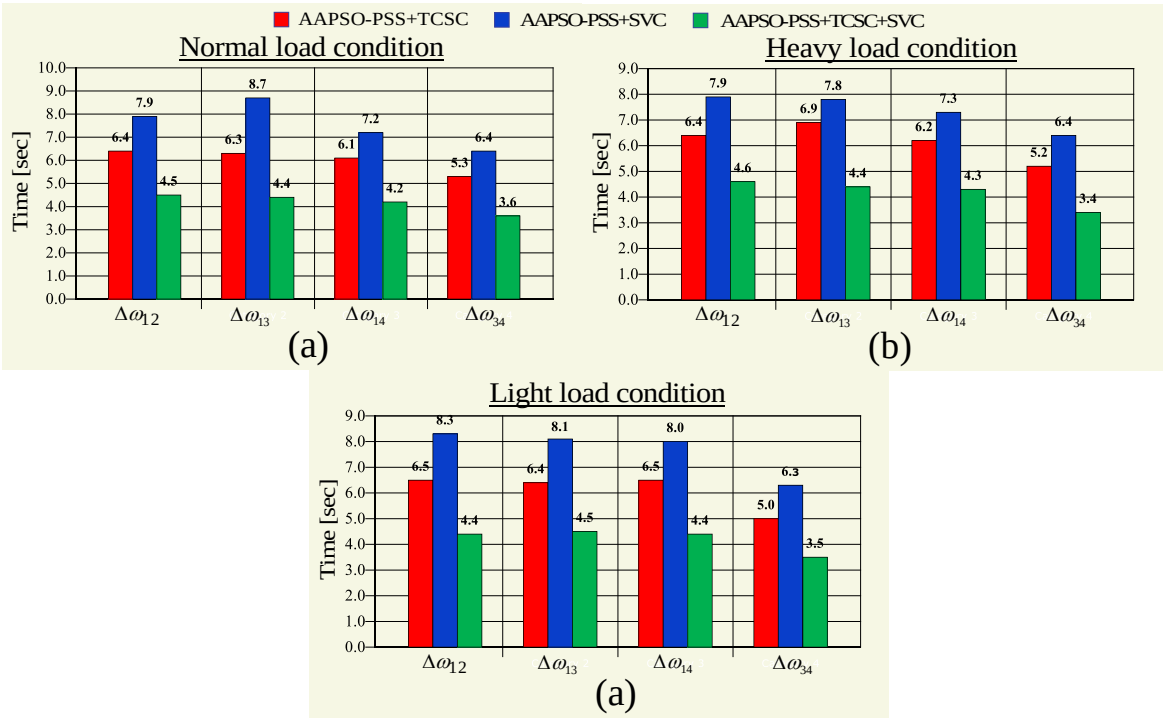

Figure 6.33: **Settling time comparison of speed oscillations with AAPSO based coordinated designs (a) Normal load (b) Heavy load (c) Light load**

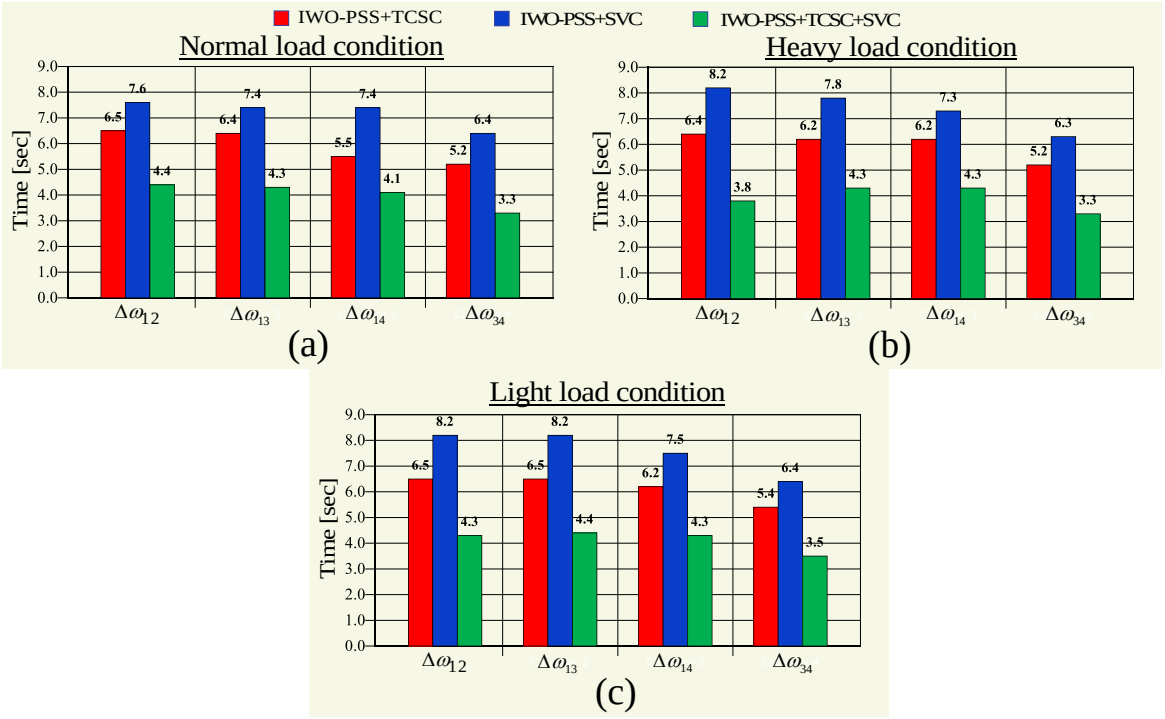

Figure 6.34: **Settling time comparison of speed oscillations with IWO based coordinated designs (a) Normal load (b) Heavy load (c) Light load**

6.3.2 Two Area System with PSS, TCSC and STATCOM Damping Controllers

This time, the test power system has engaged with 4 PSS such that each PSS mounted on each generator, a TCSC is connected in series with one of the parallel transmission lines 8-9, and a STATCOM is connected in shunt with bus 8. Here, the STATCOM has two internal damping controllers namely ACVC and DCVC which are discussed in Chapter 3. The three operating conditions normal, heavy, and light load values are listed in Table 6.14. In this section, the eigen value analysis and transient analysis of the system with AAPSO and IWO based designs are discussed.

Table 6.14: **Operating conditions of test system with TCSC and STATCOM (p.u)**

	Normal		**Heavy**		**Light**	
	P	**Q**	**P**	**Q**	**P**	**Q**
Generator						
G_1	6.8502	0.9947	7.4230	1.3272	5.9093	0.6584
G_2	7.0000	0.6339	8.4000	1.3583	5.6000	0.0156
G_3	7.2000	1.0251	8.6400	1.6510	5.7600	0.5373
G_4	7.0000	0.5591	8.4000	1.6014	5.6000	-0.2975
Load						
A	9.50	1.00	11.40	1.20	7.60	0.80
B	17.50	2.50	21.00	3.00	14.00	2.00

Table 6.15: **Optimal control parameter values obtained using AAPSO algorithm**

Control parameters	**PSS1**	**PSS2**	**PSS3**	**PSS4**	**TCSC**	**DCVC**
K_S	28.3256	30.3853	27.4825	31.1393	1.2609	0.9785
T_1	0.4015	0.4356	0.5387	0.3960	0.3173	0.2213
T_3	0.5126	0.3583	0.4544	0.4656	0.2601	0.3385

Table 6.16: **Optimal control parameter values obtained using IWO algorithm**

Control parameters	**PSS1**	**PSS2**	**PSS3**	**PSS4**	**TCSC**	**DCVC**
K_S	26.5647	29.6273	32.7598	24.1566	1.1960	1.0192
T_1	0.3845	0.3734	0.4632	0.3015	0.2618	0.2054
T_3	0.4569	0.3318	0.4251	0.5123	0.1957	0.2768

A. Eigen Value Analysis and Discussion

The design of proposed coordinated controller is modelled as an optimization problem and the eigen value based objective function is minimized via AAPSO and IWO algorithms. At the end of these optimization algorithms, the best control parameter values of coordinated designed controllers are obtained. The obtained control parameter values for AAPSO and IWO algorithms are given in Table 6.15 and 6.16 respectively. Then, the eigen value analysis is done and the eigen values of system with proposed designs are compared with the open loop system. The comparison of poorly damped eigen values of test system with proposed AAPSO and IWO based coordinated design of PSS, TCSC and STATCOM damping controllers is provided in Table 6.17. The test system with proposed design successfully shifted the poorly damped eigen values to left side of *S*-plane and the damping ratios of these eigen values are also greatly improved. The damping ratios are improved from $\sigma = 0.0001, 0.0001, \text{and } 0.00009$ to $\sigma = 0.5256, 0.5050, \text{and } 0.5419$ with effect of AAPSO based design and with IWO based coordinated design, the damping ratios are improved to $\sigma = 0.5469, 0.5262, \text{and } 0.5623$ for normal, heavy and light loads respectively.

Table 6.17: **Electromechanical modes and ζ under different load conditions**

No control	AAPSO-(PSS+TCSC+DCVC)	IWO-(PSS+TCSC+DCVC)
Normal load (λ_i, ζ_i)		
-0.0007±7.0618i, 0.0001	-3.4231±5.5411i, 0.5256	-3.5107±5.3741i, 0.5469
-0.0028±6.7551i, 0.0004	-2.9149±5.222i, 0.4874	-3.0045±5.0773i, 0.5093
-0.0064±5.2724i, 0.0012	-1.1364±4.2551i, 0.2580	-1.1732±4.2038i, 0.2688
Heavy load (λ_i, ζ_i)		
-0.0008±7.2147i, 0.0001	-3.338±5.7044i, 0.5050	-3.4174±5.523i, 0.0.5262
0.0027± 6.9079i, -0.0003	-2.8352±5.3660i, 0.4672	-2.9320±5.2268i, 0.4892
0.0067±5.2379i, -0.0013	-1.0233±4.3615i, 0.2284	-1.0605±4.3100i, 0.2389
Light load (λ_i, ζ_i)		
-0.0006±6.8024i, 0.00009	-3.4051±5.28i, 0.5419	-3.4952±5.1395i, 0.5623
-0.0034±6.4924i, 0.0005	-2.8782±4.9740i, 0.5008	-2.9583±4.8328i, 0.5221
-0.0069±5.1951i, 0.0013	-1.1831±4.077i, 0.2787	-1.2160±4.0293i, 0.2889

From these damping characteristics, the AAPSO and IWO based hybrid designs provided robustness to the system under all operating conditions. IWO based designs reached slightly better damping values than AAPSO based designs.

B. Time Domain Simulations and Discussion

The transient analysis of the test system is conducted for a 6 cycle three-phase fault. It is applied on one of the transmission lines between the buses 7-8 with starting time 1sec, and the fault was cleared by removing the line using circuit breakers permanently. In this analysis, the system with IWO and AAPSO based coordinated designs are tested under a wide range of operating points. At the end of this section, a comparison is made for the settling times of different oscillations with different designs.

Test system response with AAPSO tuned coordinated controllers:

Test system response with AAPSO tuned coordinated designs are compared for different loading conditions. Figures 6.35 and 6.36 represent the local along with inter-area rotor angle and speed oscillations of the test system under normal load condition. The local and inter-area oscillations of test power system under heavy and light load conditions are presented in Figures 6.37 and 6.38 respectively. In all these figures, the coordinated designs proved their effectiveness in suppressing the local area oscillations together with inter-area oscillations of test power system over a wide range of operating conditions. Moreover the proposed AAPSO based hybrid design (PSS+TCSC+DCVC) showed better damping performance compared to AAPSO based hybrid design (PSS+TCSC+ACVC) and AAPSO based coordinated design (PSS+TCSC). Hence the hybrid coordinated designs outshines the other coordinated designs in transient stability enhancement.

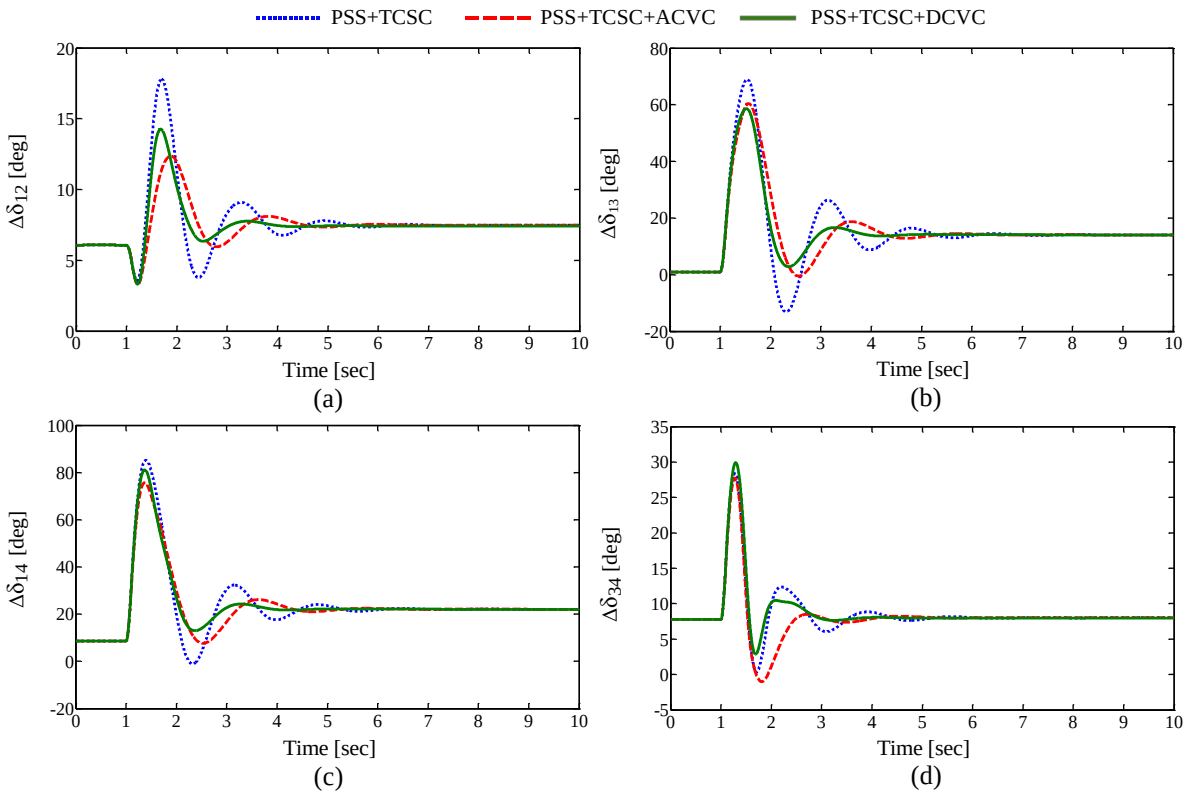

Figure 6.35: R**esponse of test system with AAPSO tuned coordinated designs for a six cycle fault under normal load (a) Δδ12 (b) Δδ13 (c) Δδ14 (d) Δδ34**

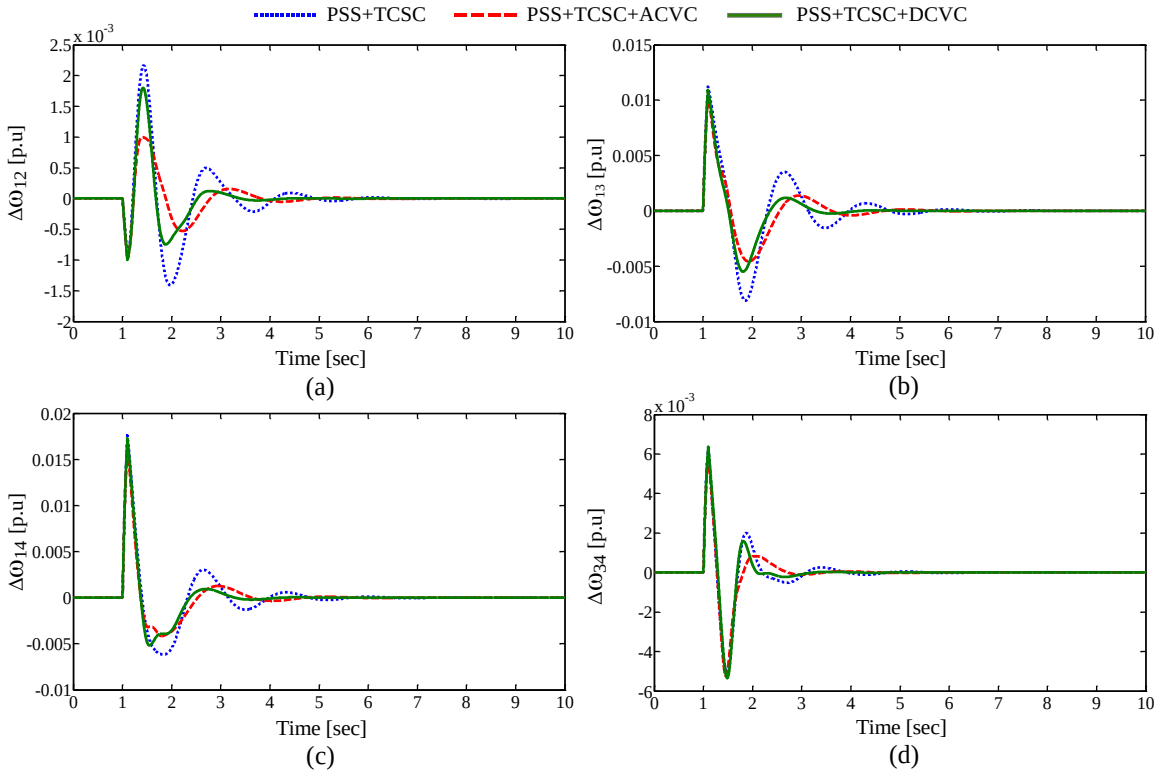

Figure 6.36: R**esponse of test system with AAPSO tuned coordinated designs for a six cycle fault under normal load (a) Δω12 (b) Δω13 (c) Δω14 (d) Δω34**

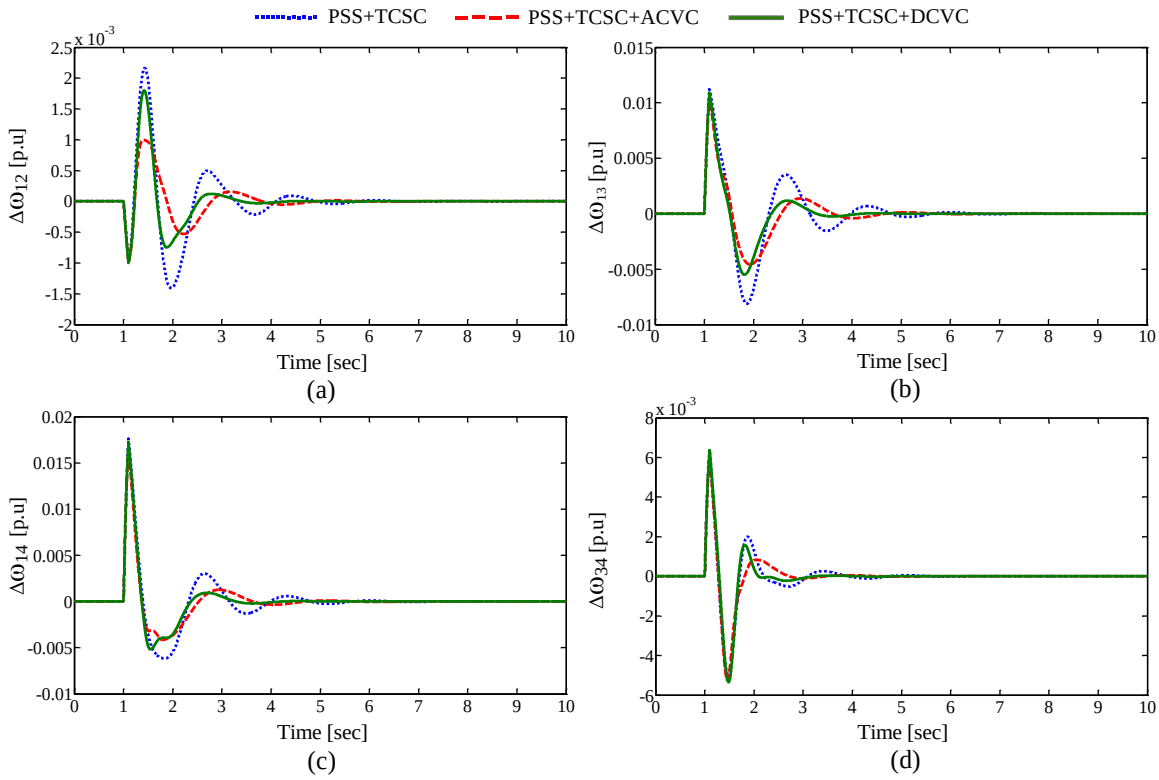

Figure 6.37: **Response of test system with AAPSO tuned coordinated designs for a six cycle fault under heavy load (a) $\Delta\omega_{12}$ (b) $\Delta\omega_{13}$ (c) $\Delta\omega_{14}$ (d) $\Delta\omega_{34}$**

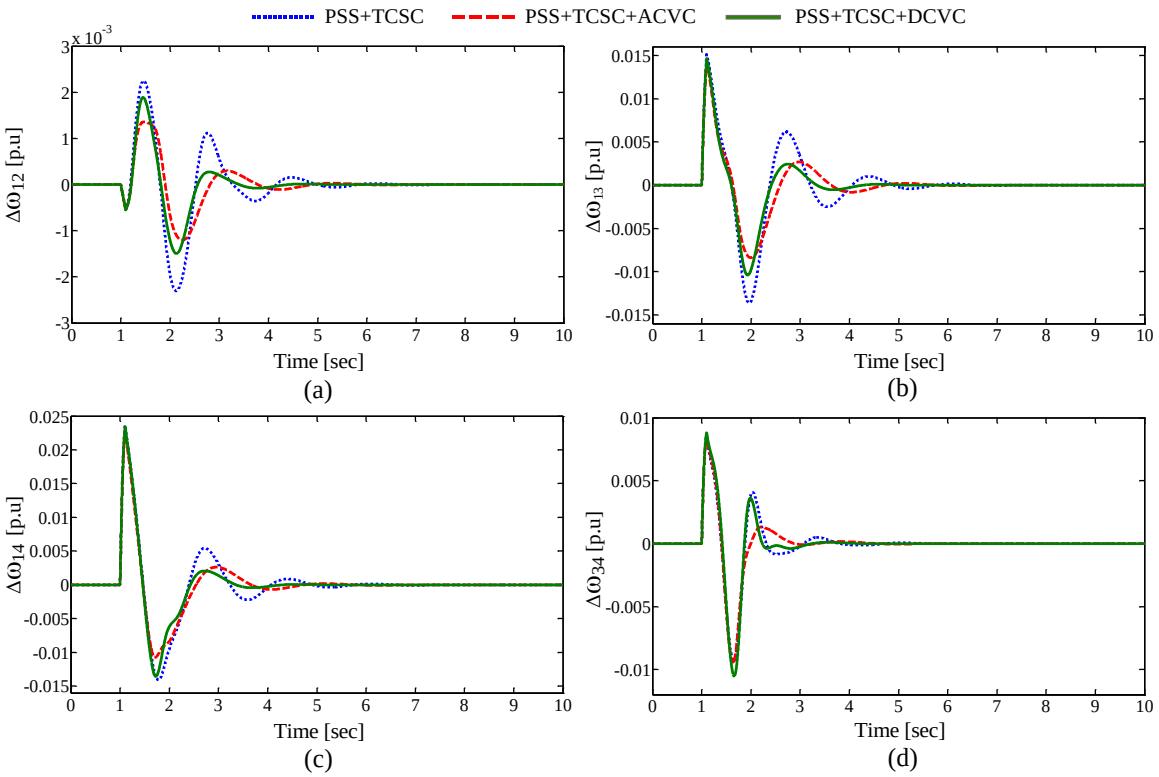

Figure 6.38: **Response of test system with AAPSO tuned coordinated designs for a six cycle fault under light load (a) $\Delta\omega_{12}$ (b) $\Delta\omega_{13}$ (c) $\Delta\omega_{14}$ (d) $\Delta\omega_{34}$**

Test system response with IWO tuned coordinated controllers:

The transient stability analysis is extended to the system with IWO tuned coordinated designed controllers under different loading conditions. The rotor angle deviations of different area generators under normal load condition are compared for IWO based different controller designs in Figure 6.39. The speed deviations of different areas are compared in Figure 3.40 under normal load condition. Similarly, the Figures 6.41 and 6.42 represent the oscillations $\Delta\omega_{12}$, $\Delta\omega_{13}$, $\Delta\omega_{14}$ and $\Delta\omega_{34}$ of the test system under both heavy and light load conditions. From the comparison of these response curves, it is concluded that the performance of IWO based hybrid design (PSS+TCSC+DCVC) outshines the performance of IWO based hybrid coordinated design of (PSS+TCSC+ACVC) and IWO based coordinated design (PSS+TCSC) in all operating points.

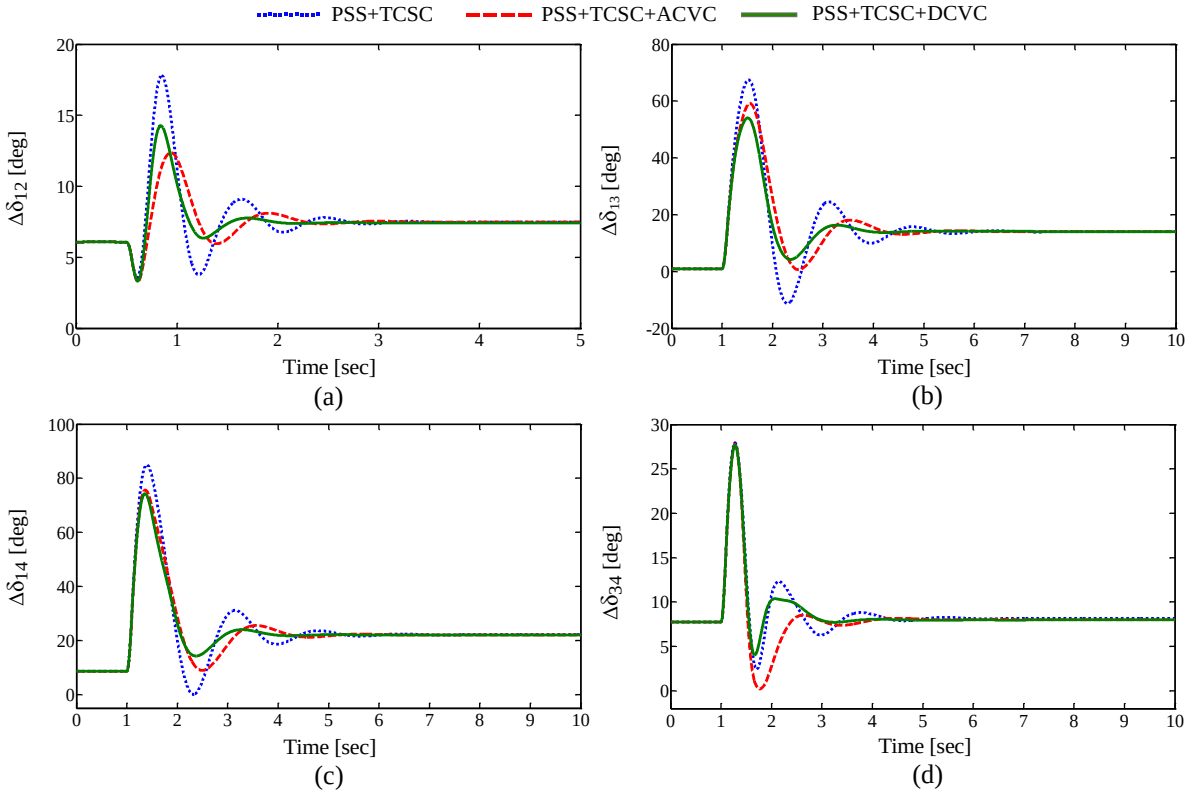

Figure 6.39: R**esponse of test system with IWO tuned coordinated designs for a six cycle fault under normal load (a) $\Delta\delta_{12}$ (b) $\Delta\delta_{13}$ (c) $\Delta\delta_{14}$ (d) $\Delta\delta_{34}$**

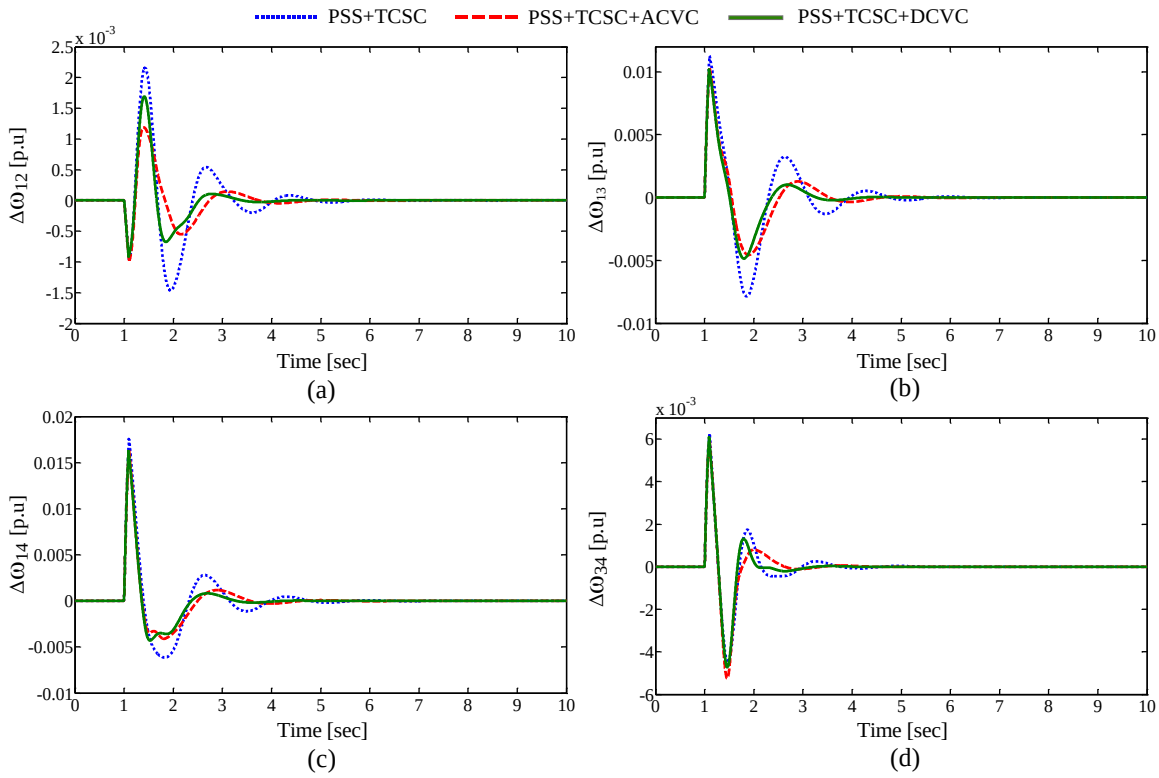

Figure 6.40: R**esponse of test system with IWO tuned coordinated designs for a six cycle fault under normal load (a) Δω12 (b) Δω13 (c) Δω14 (d) Δω34**

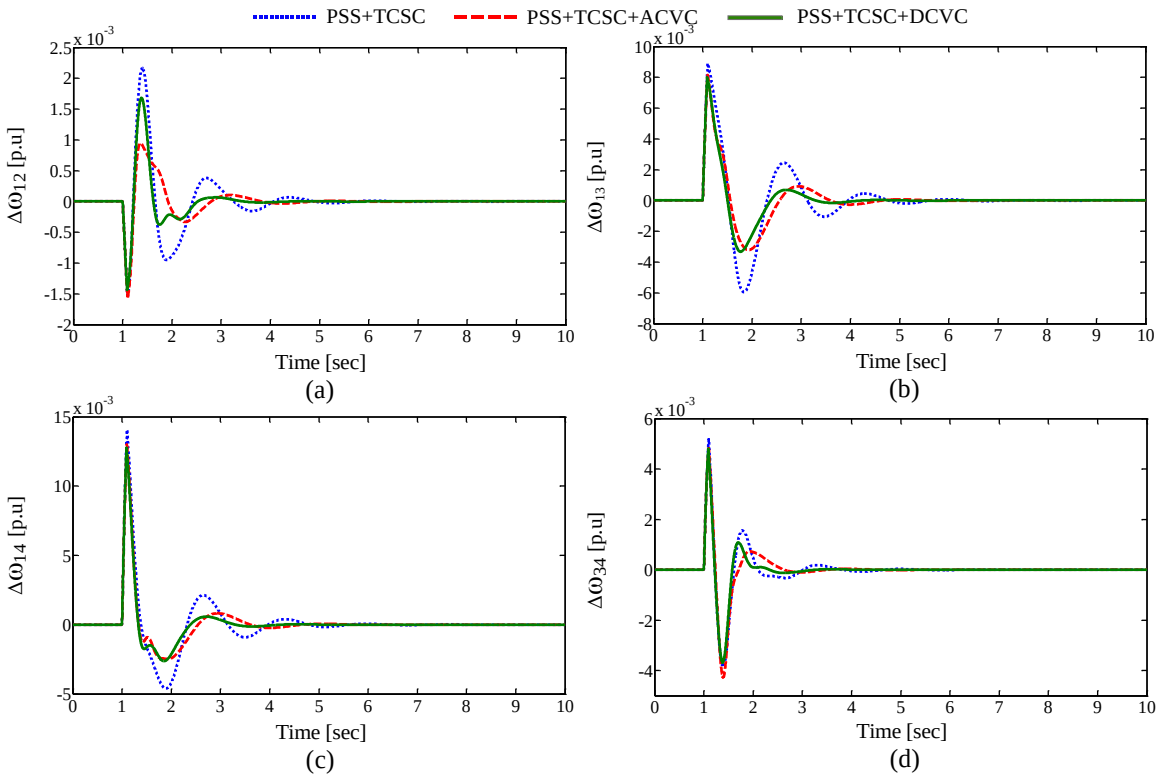

Figure 6.41: R**esponse of test system with IWO tuned coordinated designs for a six cycle fault under heavy load (a) Δω12 (b) Δω13 (c) Δω14 (d) Δω34**

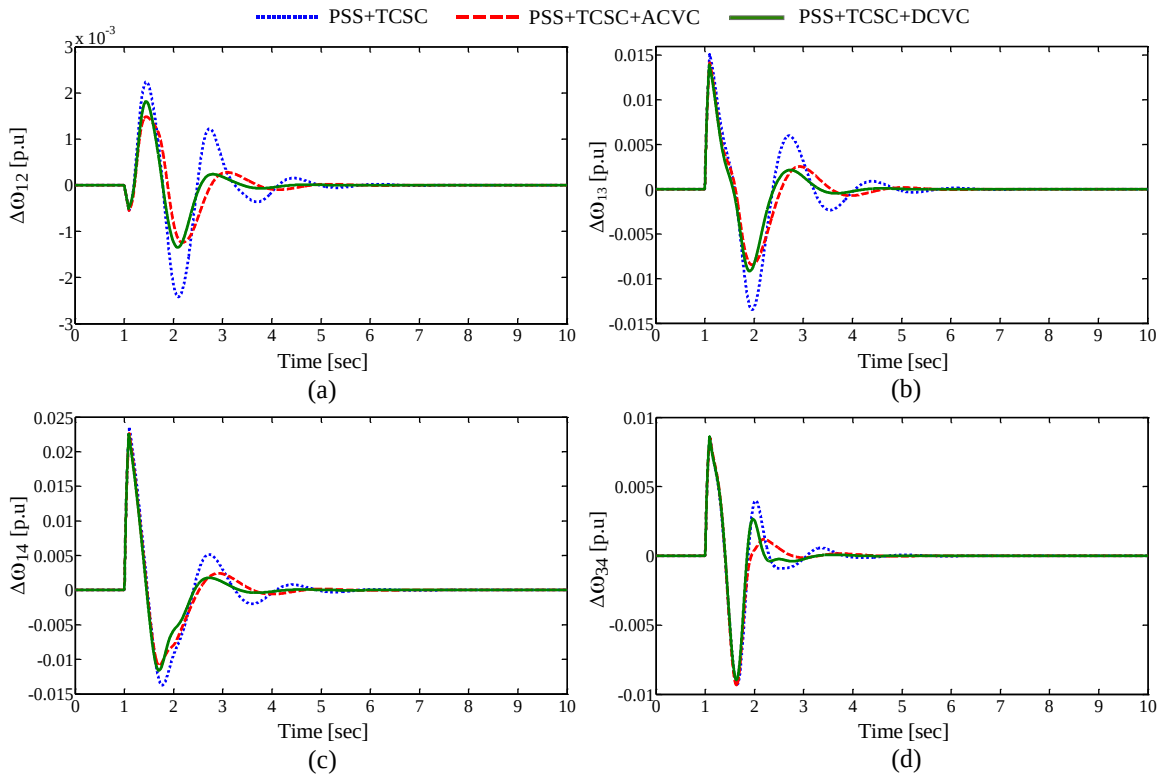

Figure 6.42: R**esponse of test system with IWO tuned coordinated designs for a six cycle fault under light load (a) Δω12 (b) Δω13 (c) Δω14 (d) Δω34**

Settling time comparison of different response cures:

The settling times of local and inter-area speed oscillations of test system with different coordinated designs are compared in this section. The settling time comparisons for oscillations $\Delta\omega_{12}$, $\Delta\omega_{13}$, $\Delta\omega_{14}$ and $\Delta\omega_{34}$ of test system with AAPSO based coordinated controllers under normal, heavy and light load conditions are presented in Figure 6.32. The proposed AAPSO based hybrid coordinated design (PSS+TCSC+DCVC) provided great settling times as $T_s = 4.4, 4.3, 4.4 \text{ and } 3.3\text{s}$ for normal load, $T_s = 4.4, 4.3, 4.4 \text{ and } 3.3\text{s}$ for heavy load and $T_s = 4.5, 4.4, 4.3 \text{ and } 3.4\text{s}$ for light load conditions.

Likewise, the test system with IWO based hybrid coordinated designs settling times comparison of speed oscillations $\Delta\omega_{12}$, $\Delta\omega_{13}$, $\Delta\omega_{14}$ and $\Delta\omega_{34}$ are plotted in Figure 6.33. In this figure, the hybrid design (PSS+TCSC+DCVC) attains great settling times than other coordinated designs as $T_s = 4.3, 4.3, 4.1 \text{ and } 3.3\text{s}$ for normal load, $T_s = 3.7, 4.4, 4.3 \text{ and } 3.3\text{s}$ for heavy load and $T_s = 4.4, 4.4, 4.4 \text{ and } 3.4\text{s}$ for light load conditions respectively. On close observation of these settling time values, the proposed hybrid coordinated designs evidences

grater settling times. With the help of these comparison graphs, it is concluded that the effectiveness of IWO based designs are superior to AAPSO based coordinated designs.

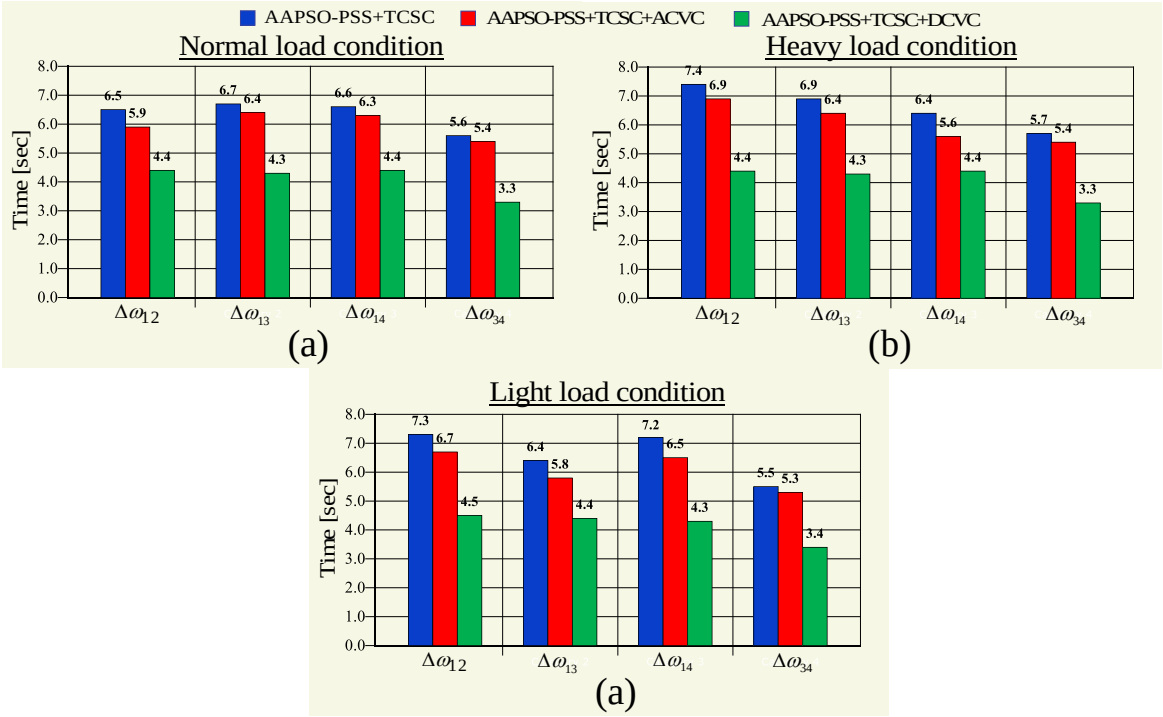

Figure 6.43: **Settling time comparison of speed oscillations with AAPSO based coordinated designs (a) Normal load (b) Heavy load (c) Light load**

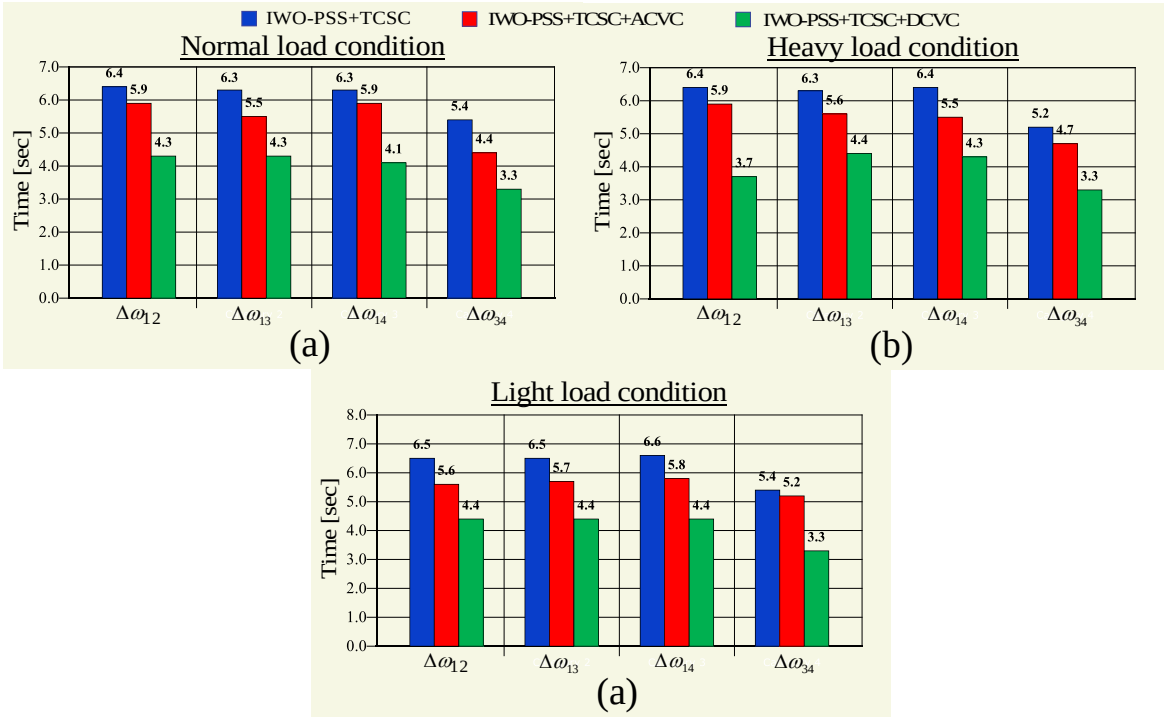

Figure 6.44: **Settling time comparison of speed oscillations with IWO based coordinated designs (a) Normal load (b) Heavy load (c) Light load**

Finally, by analyzing the eigenvalues and time-domain simulation results it is concluded that the proposed hybrid designs are robust and more effective than other coordinated designs for severe disturbances. However, to implement the proposed designs in real world they need to be tested first by the real-time hardware simulators. So that the proposed designs are implemented and validated in real-time using OPAL-RT hardware simulator laboratory setup and it is discussed in next chapter.

6.4 Summary

The performances of proposed hybrid coordinated designs are analyzed in multi-machine system environment in this chapter. In this work, two distinct multi-machine test power systems are considered and operated over a wide range of load conditions. The eigen value analysis and transient stability analysis are done for both the test systems with AAPSO and IWO based coordinated control designs. The proposed hybrid designs provided the integral damping of PSS, series and shunt FACTS controllers together to get best performance. The proposed designs successfully shifted the poorly damped electromechanical mode eigen values to the left of D-shape curve in *S*-plane. Moreover the damping characteristics of test system with proposed control designs are significantly enhanced in all operating conditions. Furthermore, the settling time comparison of different designs demonstrated that the proposed hybrid designs are far better than the other control designs. In summary, the proposed IWO based hybrid coordinated control designs slightly outperforms the proposed AAPSO based designs.

Chapter 7

Introduction to RT-LAB and Real-Time Implementation of Proposed Coordinated Designs in Multi-Machine Power System

Chapter 7

Introduction to RT-LAB and Real-Time Implementation of Proposed Coordinated Designs in Multi-Machine Power System

7.1 Introduction

Chapter 6 analyzed the performance of different hybrid designs in multi-machine power systems for a severe disturbance. Two multi-machine power systems are considered and those are operated under three different load conditions. In each case, the performance of proposed hybrid designs outperforms the other coordinated designs. But, it is necessary to validate the performance of proposed designs in real-time. In this chapter, a brief introduction about real-time simulators and their salient features are provided. The procedure to interface MATLAB models with real-time hardware simulator is discussed. Finally, the performance of proposed hybrid coordinated designs are validated and compared with other coordinated designs in real-time using OPAL-RT hardware simulator. In the last section, the real-time hardware results are provided and these results concluded that the performances of proposed designs are great enough to damp power system oscillations under severe disturbance.

7.2 Introduction to RT-LAB

Simulation tools have been widely used for the design and enhancement of electrical systems since the mid twentieth century. The evolution of simulation tools has progressed in step with the evolution of computing technologies. In recent years, computing technologies have upgraded dramatically in performance and become extensively available at a steadily decreasing cost. Consequently, simulation tools have also seen dramatic performance gains and there is a steady decrease in cost. Researchers and engineers now have access to affordable, high performance simulation tools that were previously too costly, except for the largest manufacturers and utilities. RT-LAB [113**,** 114], fully integrated with MATLAB/Simulink, is the open Real-Time Simulation software environment that has revolutionized the way Model-based Design is performed. RT-LAB's flexibility and

scalability allow it to be used in virtually any simulation or control system application, and to add computing-power to simulations, where and when it is needed.

This simulator was developed with the aim of meeting the transient simulation needs of electromechanical drives and electric systems while solving the limitations of traditional real-time simulators. It is based on a central principle, the use of extensively available, user-friendly and highly competitive commercial products (PC platform, Simulink). The real-time simulator consists of two main tools; a real-time distributed simulation package (RT-LAB) [115] for the execution of Simulink block diagrams on a PC-cluster, and algorithmic toolboxes designed for the fixed time-step simulation of stiff electric circuits and their controllers. Real-time simulation [116] and Hardware-In-the-Loop (HIL) applications [117-119] are progressively recognized as essential tools for engineering design and especially in power electronics and electrical systems [120].

7.2.1 Salient Features of Real-Time Simulation

a) Gaining time

- Allowing test engineers to gain time in the testing process.
- Find problems at an earlier stage in the design process.
- Proceeding to a device design while the actual system is not physically available.

b) Lowering cost

- Reduces enormous cost on testing a new device under real conditions.
- The real-time system could test many possible configurations without physical modification.
- Reduction of total cost over the entire project and system life cycle.

c) Increasing test functionalities

- Fake and test all possible scenarios that could happen in real life in a secure and simulated environment.
- High flexibility by being able to modify all parameters and signals of the test system at a glance.

7.2.2 Real-Time Simulation Definitions

Fixed-step solvers solve the model at regular time intervals from the beginning to the end of the simulation. The size of the interval is known as the step size (T_s). Generally, decreasing

T_s increases the accuracy of the results while increasing the time required for simulating the system [121].

Time Step:

In a real-time system [122], we define the time step as a predetermined amount of time (ex: T_s = 10 µs, 1 ms, or 5 ms). Inside this amount of time, the processor has to read input signals, such as sensors, to perform all necessary calculations, such as control algorithms, and to write all outputs, such as control actuators. Inputs or Outputs highest frequency sampling consideration, generally decreasing the time step increases the accuracy of the results while increasing the time required simulating the system. The rule of thumb is to have around 10 to 20 samples per period for an AC signal. For a 1kHz signal: $1/20 \times 1kHz = 50\mu s$.

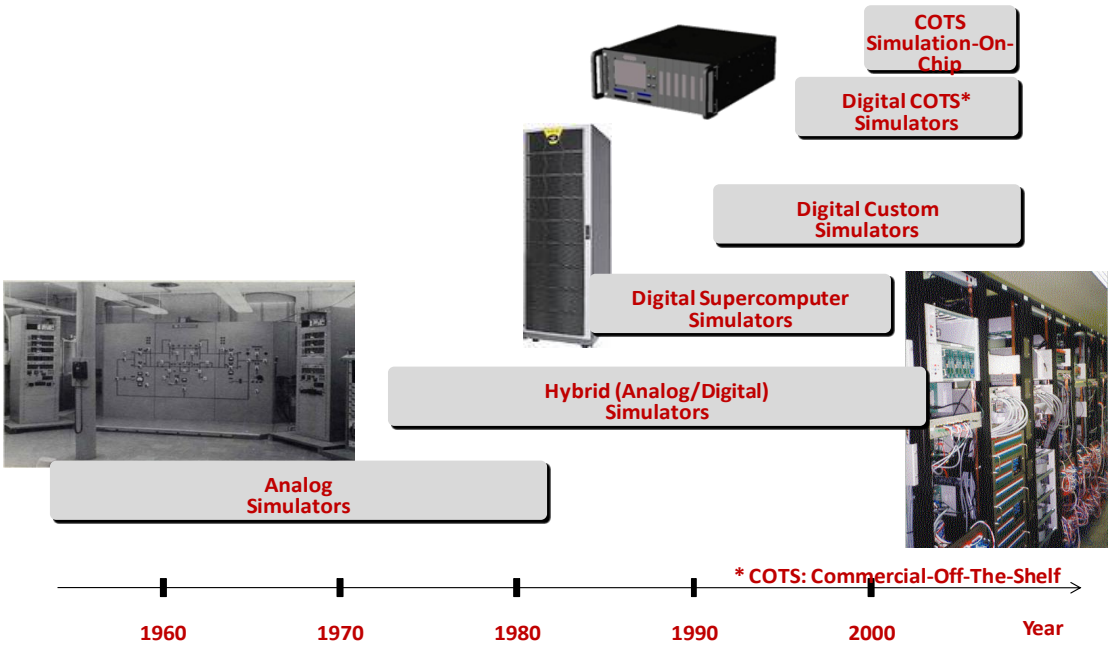

Figure 7.1: **Evolution of RT-LAB simulator**

7.3 Evolution of Real-Time Simulators

Simulator technology has evolved from physical/analogue simulators (high-voltage direct current (HVDC) simulators & transient network analysers (TNAs)) for electromagnetic transient (EMT) and protection & control studies, to hybrid TNA/Analogue/Digital simulators capable of studying EMT behaviour, to fully digital real-time simulators, as illustrated in Figure 7.1. Physical simulators served their purpose well. However, they were very large, expensive and required highly skilled technical teams to handle the tedious jobs

of setting up networks and maintaining extensive inventories of complex equipment [121]. With the development of microprocessor and floating-point DSP technologies, physical simulators have been gradually replaced with fully digital real-time simulators. Figure 7.2 gives the details of speed, cost and size of RT-LAB Simulators

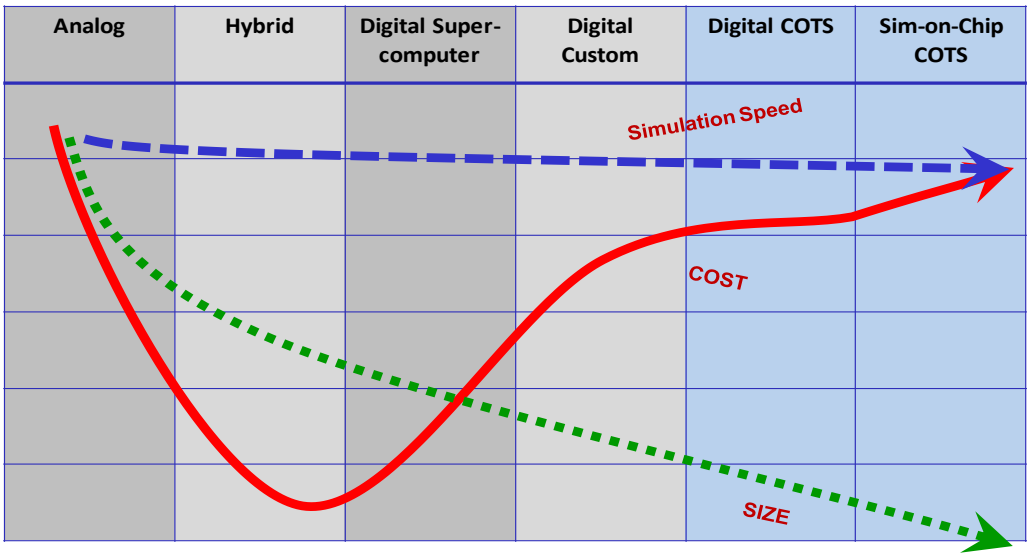

Figure 7.2: **Speed, cost and size of RT-LAB simulators**

COTS-based high-end real-time simulators equipped with multi-core processors have been used in aerospace, robotics, automotive and power electronic system design & testing for a number of years. Recent advancements in multi-core processor technology means that such simulators are now available for the simulation of EMT expected in large-scale power grids, micro grids, wind farms and power systems installed in all-electric ships and aircraft. These simulators, operating under Windows, LINUX and standard real-time operating systems (RTOS), have the potential to be compatible with a large number of commercially available power system analysis software tools, such as PSS/E (Power System Simulator for Engineering), EMTP-RV (Electro Magnetic Transients Program - Restructured Version) and PSCAD (Power Systems Computer Aided Design), as well as multi-domain software tools such as SIMULINK and DYMOLA. The integration of multi-domain simulation tools with electrical simulators enables the analysis of interactions between electrical, power electronic, mechanical and fluid dynamic systems.

The latest trend in real-time simulation consists of exporting simulation models to FPGA (Field-Programmable Gate Array). This approach has many advantages. First, computation time within each time step is almost independent of system size because of the parallel nature of FPGAs [123]. Second, overruns cannot occur once the model is running and timing

constrains are met. Last but most importantly, the simulation time-step can be very small, in the order of 250 nanoseconds. There are still limitations on model size since the number of gates is limited in FPGAs. However, this technique holds promise.

7.4 RT-LAB Simulator Architecture

7.4.1 Block Diagram and Schematic Interface

The present real-time electric simulator is based on RT-LAB real-time, distributed simulation platform; it is optimized to run Simulink in real-time, with efficient fixed-step solvers, on PC Cluster [124]. Based on COTS non-proprietary PC components, RT-LAB is a flexible real-time simulation platform, for the automatic implementation of system-level, block diagram models, on standard PCs. It uses the popular MATLAB/Simulink (Matrix Laboratory) as a front-end for editing and viewing graphic models in block-diagram format. The block diagram models become the source from which code can be automatically generated, manipulated and downloaded onto target processors (Pentium and Pentium-compatible) for real-time or distributed simulation.

7.4.2 Inputs and Outputs (I/O)

A requirement for real-time HIL applications is interfacing with real world hardware devices, controller or physical plant alike. In the RT-LAB real-time simulator, I/O interfaces are configured through custom blocks, supplied as a Simulink toolbox. The engineer merely needs to drag and drop the blocks to the graphic model and connect the inputs and outputs to these blocks, without worrying about low-level driver programming. RT-LAB manages the automatic generation of I/O drivers and models code so to direct the model's data flow onto the physical I/O cards.

7.4.3 Simulator Configuration

In a typical configuration (Figure 7.3), the RT-LAB simulator consists of

- One or more target PCs (computation nodes); one of the PCs (Master) manages the communication between the hosts and the targets and the communication between all other target PCs. The targets use the REDHAT real-time operating system.
- One or more host PCs allowing multiple users to access the targets; one of the hosts has the full control of the simulator, while other hosts, in read-only mode, can receive and display signals from the real-time simulator.

- I/Os of various Types (analog in and out, digital in and out, PWM in and out, timers, encoders, etc).

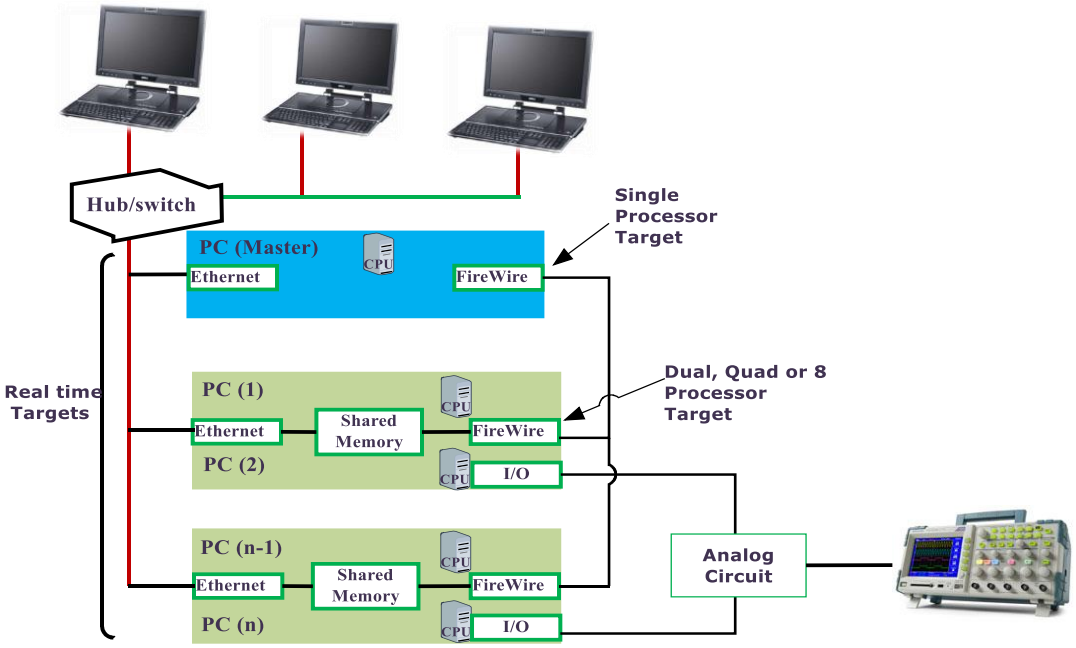

Figure 7.3: **RT-LAB simulator architecture**

The simulator uses the following communication links:

- Ethernet connection (100 Mb/s) between the hosts and target PCs.
- Ethernet connection between target nodes allowing parallel computation of models with low and medium step size (in 'msec' range), or for free-running, on real-time simulation.
- Fast shared-memory communication between processors on the same motherboard (dual, quad or 8 processors)
- Fast IEEE 1394 (FireWire) communication links (400 Mb/s) between target PCs for parallel simulation of models with small step sizes (down to 20 µs) and tight communication constraints (power systems, electric drive control, etc).

7.5 Working of RT-LAB

RT-LAB allows the user to readily convert MATLAB models, via Real-time workshop (RTW), and then to conduct Real-time simulation of those models executed on multiple target computers equipped with multi-core PC processors [11**8**]. This is used particularly for HIL and rapid control prototyping applications [12**5**]. RT-LAB transparently handles

synchronization, user interaction, real world interfacing using I/O boards and data exchanges for seamless distributed execution.

7.5.1 Single Target Configuration

In this configuration (Figure 7.4 and 7.5), typically used for rapid control prototyping, a single computer runs the plant simulation or control logic. One or more hosts may connect to the target via an Ethernet link. The target uses QNX or Linux as the RTOS *(*real-time operating system) [126] for fast simulation or for applications where real-time performance is required. RT-LAB [113, 114], used Red Hat ORT which is the standard Red Hat distribution package with an optimized set of parameters to reach real-time performance enabling to reach model time step as low as 10 micro sec on multi-core processors.

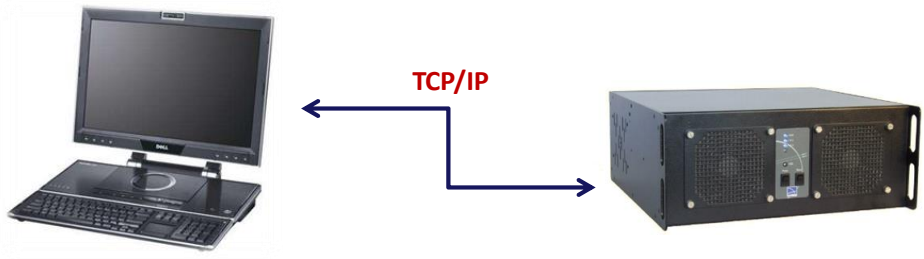

Figure 7.4: **RT-LAB simulator with single target system**

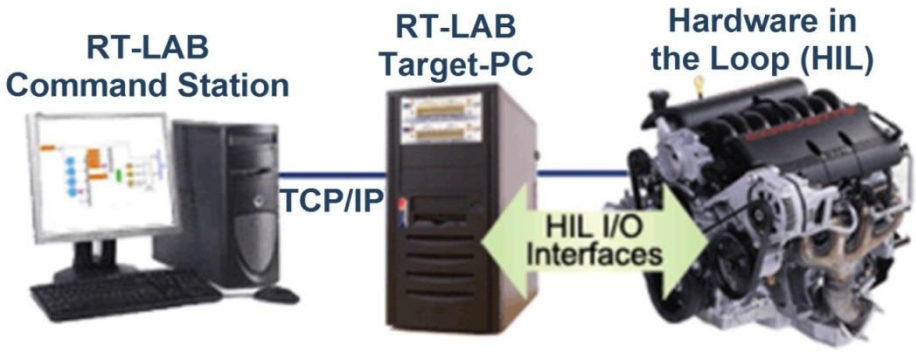

Figure 7.5: **RT-LAB simulator with single target system and HIL**

7.5.2 Distributed Target Configuration

The distributed configuration (Figure 7.6 and 7.7) allows for complex models to be distributed over a cluster of multi-core PCs [118] running in parallel. The target nodes in the cluster communicate between each other with low latency protocols such as FireWire, Signal wire or Infinite Band, fast enough to provide reliable communication for real-time applications.

The real-time cluster is linked to one or more host stations through a TCP/IP (Transmission Control Protocol / Internet Protocol) network. Here again, the cluster of PCs can be used for Real-Time applications (using QNX or Red Hawk Linux), or fast simulation of complex systems (using QNX, Red Hawk or Windows). RT-LAB PC-cluster targets are designed for flexible and reconfigurable mega-simulation. The user can build and expand the PC-cluster as needed, then redeploy the PCs for other applications when the simulation is done. RT-LAB can accommodate up to 64 nodes running in parallel.

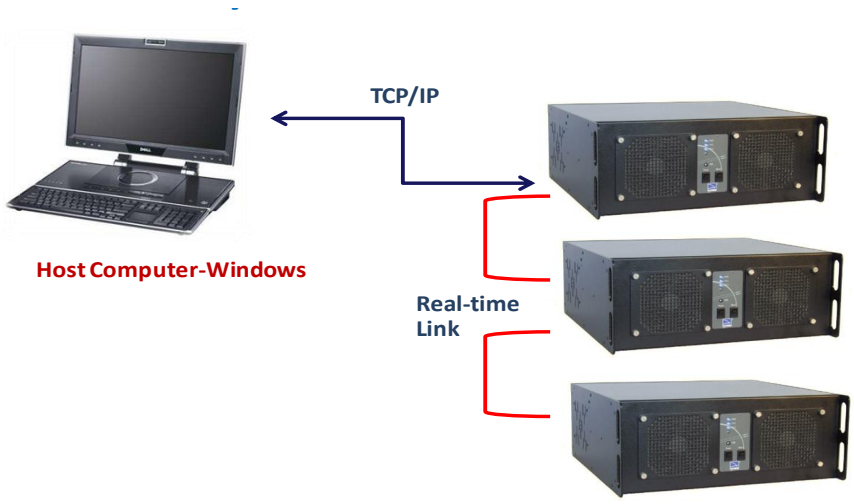

Figure 7.6: **RT-LAB simulator with distributed target system**

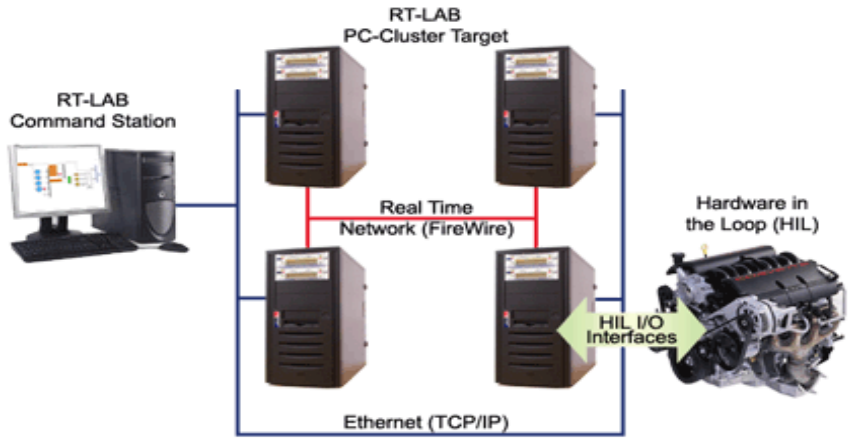

Figure 7.7: **RT-LAB simulator with distributed target system and HIL**

7.5.3 Simulator Solvers

The RT-LAB electrical simulator uses advanced fixed time-step solvers and computational techniques designed for the strict constraints of real-time simulation of stiff systems. They are implemented as a Simulink toolbox called ARTEMIS [115] (Advanced Real-Time

Electro-Mechanical Transient Simulator), which is used with the 'SimPowerSystems'. PSB (Power System Block set) is a Simulink toolbox that enables the simulation of electric circuits and drives within the Simulink environment. While PSB now supports a fixed-time-step solver based on the Tustin method, PSB alone is not suitable for real-time simulation due to many serious limitations, including iterative calculations to solve algebraic loops, dynamic computation of circuit matrices, un-damped switching oscillations, and the need for a very small step size which greatly slows down the simulation. The ARTEMIS solver uses a high-order fixed time-step integration algorithm that is not prone to numerical oscillations, and advanced computational techniques necessary for the real-time simulation of power electronic systems and drives such as:

- Exploitation of system topology to reduce matrices size and number by splitting the equations of separated systems.
- Support for parallel processing suitable for distributed simulation of large systems
- Implementation of advanced techniques for constant computation time.
- Strictly non-iterative integration.
- Real-time compensation of switching events occurring anywhere inside the time step, enabling the use of realistic simulation step sizes while ensuring a good precision of circuits with switches (GTO, IGBT, etc).

7.5.4 RT-LAB Simulation Development Procedure

Electric and power electronic systems are created on the host personal computer by interconnecting:

- Electrical components from component model libraries available in the Power System Block-set (PSB).
- Controller components and other components from Simulink and its toolboxes that are supported by Real-Time-Workshop (RTW).
- I/O blocks from the simulator I/O tool boxes. The easy to use drag and drop Simulink interface issued at all stages of the process.
- These systems are then simulated and tuned off-line in the MATLAB/Simulink environment [115]. ARTEMIS fixed step solvers are used for the electric part and Simulink native solvers for the controller and other block-diagram parts. Finally, the model is automatically compiled and loaded to the PC-Cluster with RT-LAB simulation interface [116].

The simulator software converts Simulink and 'SimPowerSystems' non-real-time models to real-time simulation by providing support for:

- *Model Distribution:* If a model is too complex to be computed within the time step, the simulator allows the model to be distributed over several processors, automatically handling the inter-processor communication through TCP/IP, FireWire or Shared Memory. Electric systems can be separated by using natural delay in the system (Analog-to-Digital conversion delays, filtering delays, transmission lines, etc).
- *Multi-rate Computation:* Not all the components in a system need to be executed at very small time steps. If the system can be separated into subsystems and executed at different update rates, cycles can be freed up for executing the subsystem(s) that need to be updated faster.
- *Specialized Solvers:* The simulator uses libraries of specialized solvers (ARTEMIS) and blocks that address many of the mathematical problems that arise when taking a model to real-time, such as new fixed step integrators that reduce the errors introduced when replacing a variable step integrator, and special tool box that compensate for errors introduced when events occur between time steps (RT-Events).
- *Software and Hardware Interfaces:* In addition to wide range of I/O Types and boards, the simulator includes a comprehensive application program interface (API) that allows signals in the model to be used in other on-line software for visualization and interaction.

7.6 PCI OP5142 Configuration

The OP5142, shown in Figure 7.8, is one of the key building blocks in the modular OP5000 I/O system from Opal- RT Technologies [115]. It allows the incorporation of FPGA technologies in RT-LAB simulation clusters for distributed execution of HDL (Hardware description language) functions and high-speed, high-density digital I/O in real-time models. Based on the highest density Xilinx Spartan-3 FPGAs, the OP5142 can be attached to the backplane of an I/O module of either a Wanda 3U- or Wanda 4U-based OPAL-RT simulation system. It communicates with the target PC via a PCI-Express (Peripheral Component Interconnect - Express) ultra-low-latency real-time bus interface.

The OP5142 includes connectivity to up to four 4U digital and/or analog I/O conditioning modules. This allows the incorporation of task-specific I/O hardware, such as high-speed analog signal capture and generation. Furthermore, FPGA [123] developers can incorporate their own functionality, using the System Generator for DSP toolbox or their favorite HDL development tool, through the PCI interface without the need for connecting to the JTAG (Joint Test Action Group) interface. Configuration files can be uploaded and stored on the built-in Flash memory for instant start up. The PCI-Express port on the OP5142 adapter board allows the user to connect the distributed processors together and operate at faster cycle times than ever before. This real-time link takes advantage of the FPGA [123] power to deliver up to 2.5 Gbits/s full-duplex transfer rates. The details and key features of OP5142 are given in [127].

Figure 7.8: **OP5142 layout**

7.7 Interfacing MATLAB/SIMULINK Models in Real-Time Environment

To interface any MATLAB/SIMULINK model with OPAL-RT hardware simulator, the following procedural steps are involved:

1. Open a project in RT-LAB, and then add the MATLAB/SIMULINK model to the real-time environment.
2. Then edit the model in RT-LAB, which is opened with MATLAB software. In this we have to form the entire model into two subsystems named as ‘sm_master’ and ‘sc_console’ so that it can be compatible with RT-LAB.

3. The development properties of the model have to set such that it can be implemented in real-time in target processors. In this work, the target platform is set in Red hat mode.
4. Build the model in RT-LAB, in this operation the model is converted into C code and that generated C code is transferred to target PC to compile the model in real time.
5. Now set the properties of subsystems and assign them to physical nodes. Here, the target pc is assigned to 'sm_master' subsystem which allows editing and running the model in the target PC.
6. Set the hardware in synchronized mode in order to run the model in real-time. At this point, OPAL-RT I/O board clock is synchronized with external hardware timer.
7. Load the model on the target. In this process of loading model, the RT-LAB opens console block to make ready for execution.
8. Execute the model in RT-LAB. During execution, the model runs in real-time hardware simulator and the output of model will be displayed in mixed signal oscilloscope (MSO). To stop the model there is a reset button in control window of RT-LAB, this will stop acquisition and closes the console.

However, reset and close the existing model then follow the steps (1) to (8) to run another new model in RT-LAB.

7.8 Performance analysis of 3-Machine 9-Bus Power System in Real-Time

In this case, the performance of 3-machine 9-bus power system with proposed hybrid designs are analyzed for a 6 cycle 3-phase fault disturbance. To examine the robustness under severe disturbance, the system with proposed designs is tested under three different loading conditions namely normal, heavy and light load conditions as mentioned in Table 6.1, which is provided in Chapter 6. In the test system, a three-phase fault is applied on line 9-6 with fault starting time at 1s and it continues for duration of 100ms (i.e. a six cycle fault).

The real-time performance of test system with different coordinated designs, which are tuned via AAPSO and IWO algorithms, is examined using OPAL-RT hardware simulator. The laboratory OPAL-RT hardware simulator setup is shown in Figure 7.9, which consists of a host PC that is connected to a target PC. Also, the setup consists of MSO to save and examine the real-time results.

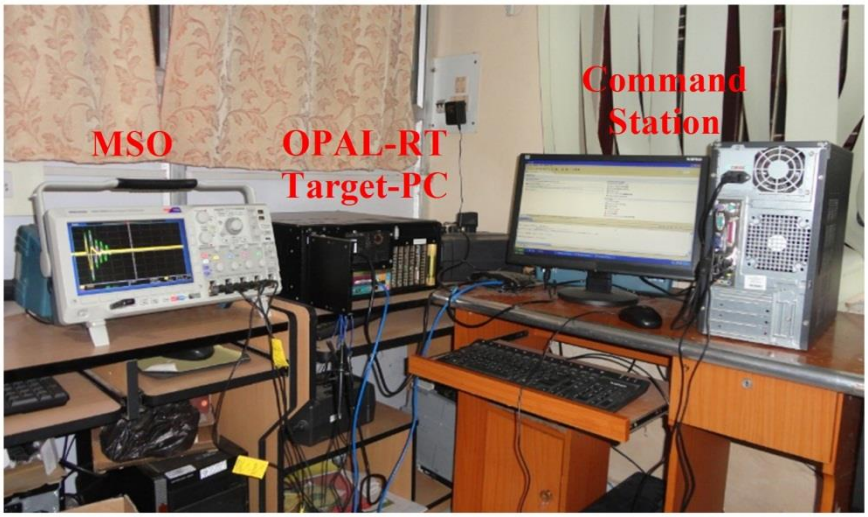

Figure 7.9: **Laboratory setup of OPAL-RT hardware simulator**

7.8.1 Real-Time Performance Analysis of Test System with PSS, TCSC and SVC Damping Controllers

The real-time performance of test system with PSS, TCSC and SVC damping controller is studied using OPAL-RT hardware simulator. The optimal parameter values of proposed hybrid coordinated design are obtained at the end of corresponding optimization algorithms. The obtained values are given in Chapter 6 (at section 6.2.1). Now with those optimal controller settings, real-time results are extracted using OPAL-RT hardware simulator.

A. Real-Time Response with AAPSO Tuned Coordinated Controllers:

The real-time responses of test system with AAPSO tuned coordinated controller are shown in Figure 7.10 and 7.11. The rotor angle oscillation responses $\Delta\delta_{21}$ and $\Delta\delta_{31}$ of the test system under normal load condition are shown in Figure 7.10. The inter-area oscillations $\Delta\omega_{12}, \Delta\omega_{23}$ and $\Delta\omega_{31}$ are shown in Figure 7.11 for different load conditions. The real-time responses of inter-area oscillations under normal load condition for different control designs are compared in the Figure 7.11(a)-7.11(c). Similarly, the real-time responses under heay and light load conditions are compared in Figures 7.11(d)-7.11(f), and 7.11(g)-7.11(i) respectively. By inspecting these real-time responses, it is observed that the proposed coordinated designs are very good enough in damping the rotor angle and also inter-area oscillations. Predominantly the hybrid coordinated design provides excessive damping characteristics than the other two designs.

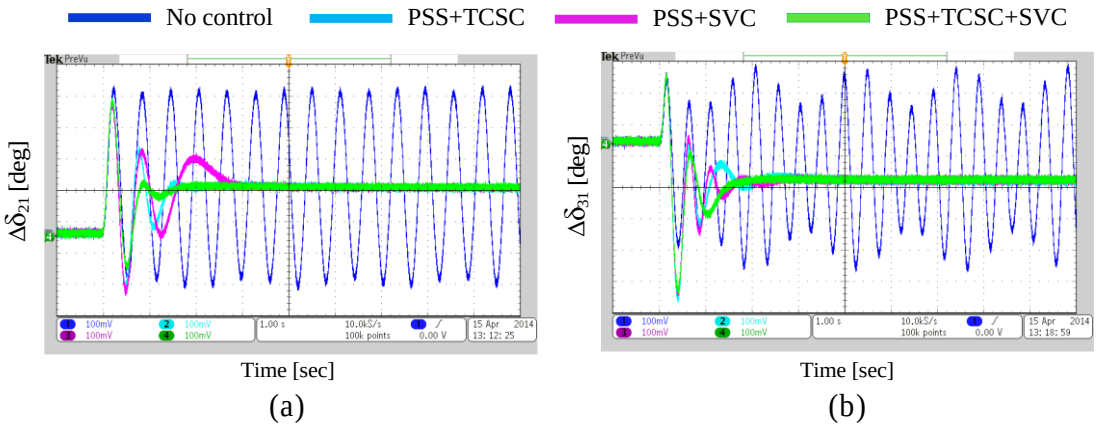

Figure 7.10: **Real-time response of test system with AAPSO tuned coordinated designs for a six cycle fault under normal load (a) $\Delta\delta_{21}$ (b) $\Delta\delta_{31}$**

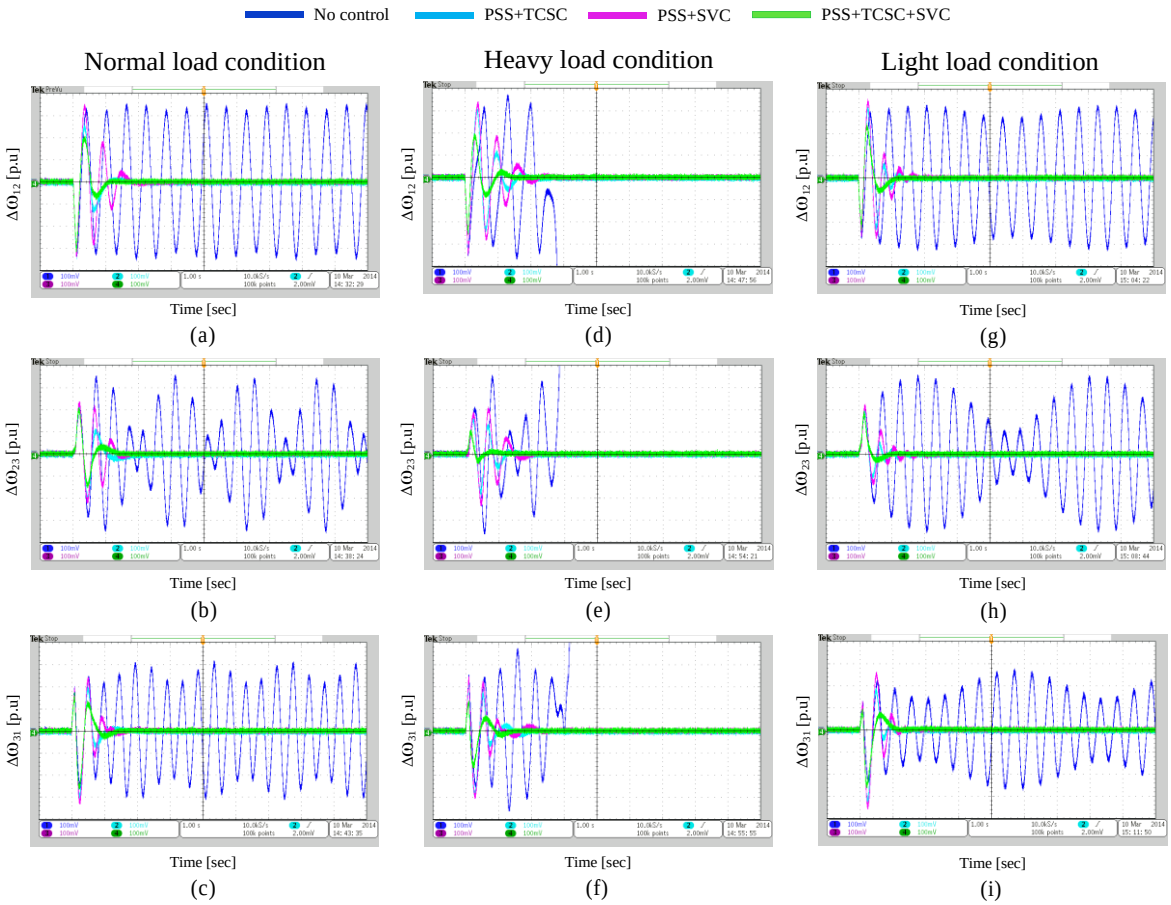

Figure 7.11: **Real-time response of test system with AAPSO tuned coordinated designs for a six cycle fault under normal, heavy and light load**

B. Real-Time Response with IWO Tuned Coordinated Controllers:

Figures 7.12 and 7.13 show the system real-time response curves with different IWO tuned coordinated controllers. Figure 7.12 represents the comparison of rotor angle variations and Figures 7.13(a)-7.13(b) represent the real-time responses of inter-area speed oscillations for

different control designs under normal load condition. The real-time responses of the system under heavy and light load conditions are shown in Figures 7.13(d)-7.13(f) and 7.13(g)-7.13(i) respectively.

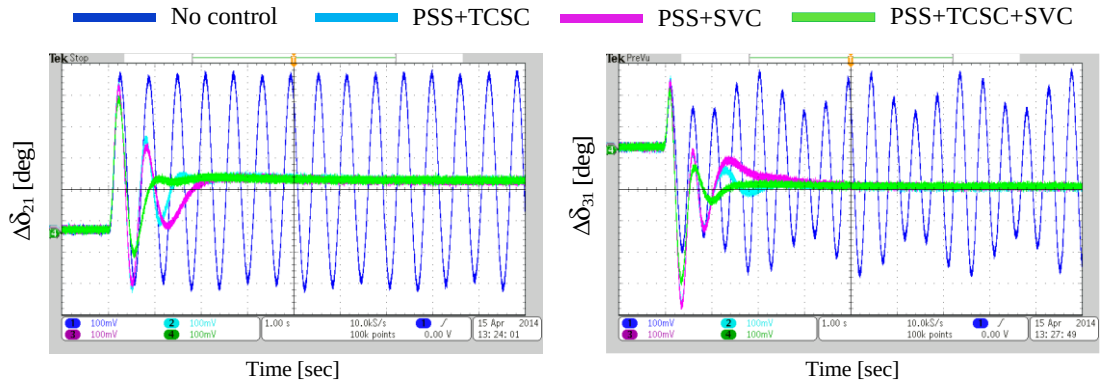

Figure 7.12: **Real-time response of test system with IWO tuned coordinated designs for a six cycle fault under normal load (a) $\Delta\delta_{21}$ (b) $\Delta\delta_{31}$**

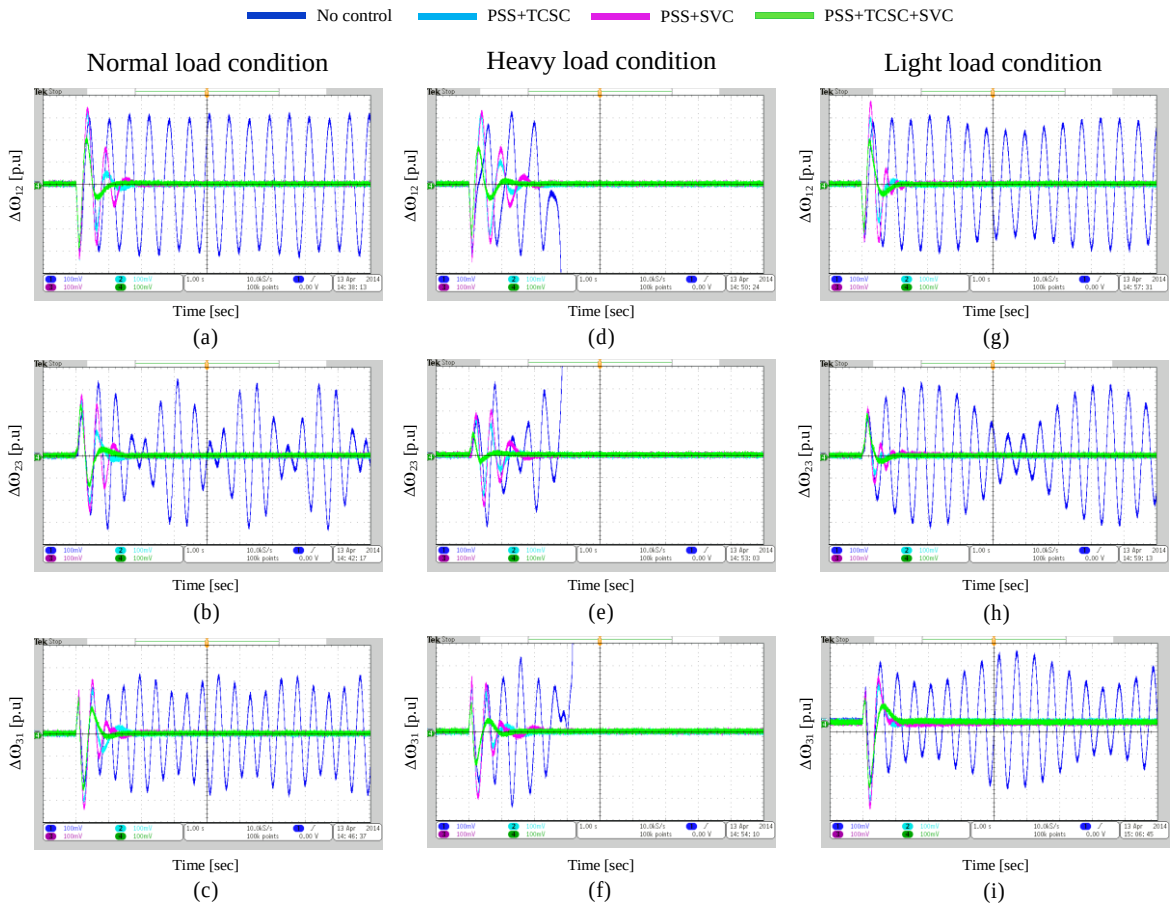

Figure 7.13: **Real-time response of test system with IWO tuned coordinated designs for a six cycle fault under normal, heavy and light load**

From all these real-time responses, it is observed that the open loop system (i.e. system has no control) is not capable to damp system oscillations. But the system with IWO based coordinated designs like (PSS+TCSC), (PSS+SVC) and hybrid coordinated design (PSS+TCSC+SVC) provides good damping stability to the system under all operating conditions. Moreover, the proposed coordinated design of all three controllers provided abundant damping effect for the rotor angle as well as inter-area speed oscillations.

7.8.2 Real-Time Performance Analysis of Test System with PSS, TCSC and STATCOM Damping Controllers

Now, the performance of test system with PSS, TCSC and STATCOM damping controllers is observed in real-time using OPAL-RT hardware simulator. The optimal parameter values of different controllers via AAPSO and IWO algorithms are given in Chapter 6 (at section 6.2.2). With these optimal controller settings the MATLAB model is interfaced with OPAL-RT hardware simulator and real-time results are obtained.

A. Real-Time Response with AAPSO Tuned Coordinated Controllers:

The real-time rotor angle variations of test system under normal load condition with different control schemes are compared in Figure 7.14. Real-time responses of $\Delta\omega_{12}$, $\Delta\omega_{23}$ and $\Delta\omega_{31}$ under normal, heavy, and light load conditions are compared in Figure 7.15. Here, four control schemes are compared namely, no control, coordinated design (PSS+TCSC), hybrid coordinated designs of PSS, TCSC and STATCOM damping controllers (ACVC and DCVC). By analysing the real-time responses, the proposed hybrid designs AAPSO-(PSS+TCSC+ACVC) and AAPSO-(PSS+TCSC+DCVC) provided good damping for rotor angle as well as inter-area speed oscillations.

B. Real-Time Response with IWO Tuned Coordinated Controllers:

The real-time system response with IWO tuned coordinated designs over a wide range of operating conditions are discussed here. The real-time rotor angle responses with different controllers are shown in Figure 7.16. Also, the inter area speed oscillations under normal, heavy and light load conditions are given in Figure 7.17. From the real-time analysis, it is noticed that in all operating conditions open loop system is highly oscillatory in nature and very poor damping characteristics. On the other hand, the IWO based coordination designs greatly enhances the damping characteristics of test system independent of operating

conditions. Additionally among all coordinated designs, the IWO based hybrid design (PSS+TCSC+DCVC) shows great damping characteristics.

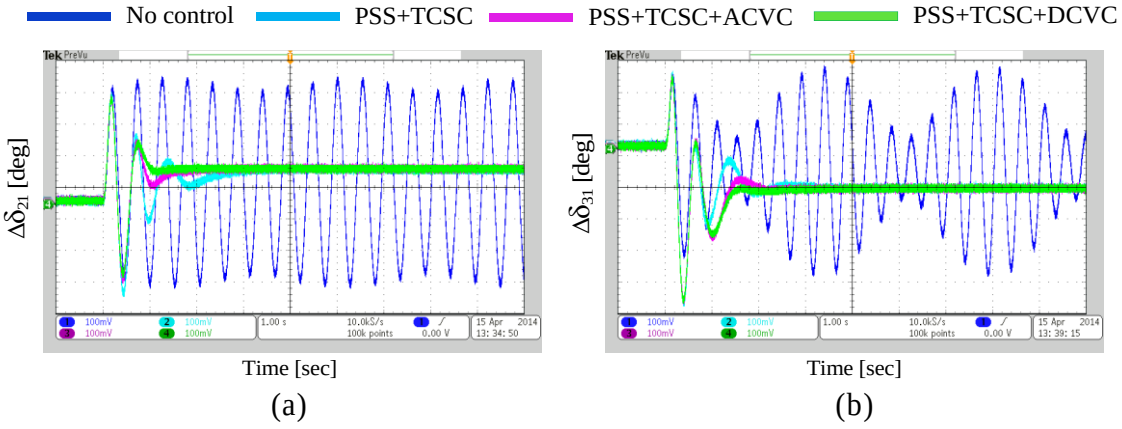

Figure 7.14: **Real-time response of test system with AAPSO tuned coordinated designs for a six cycle fault under normal load (a) $\Delta\delta_{21}$ (b) $\Delta\delta_{31}$**

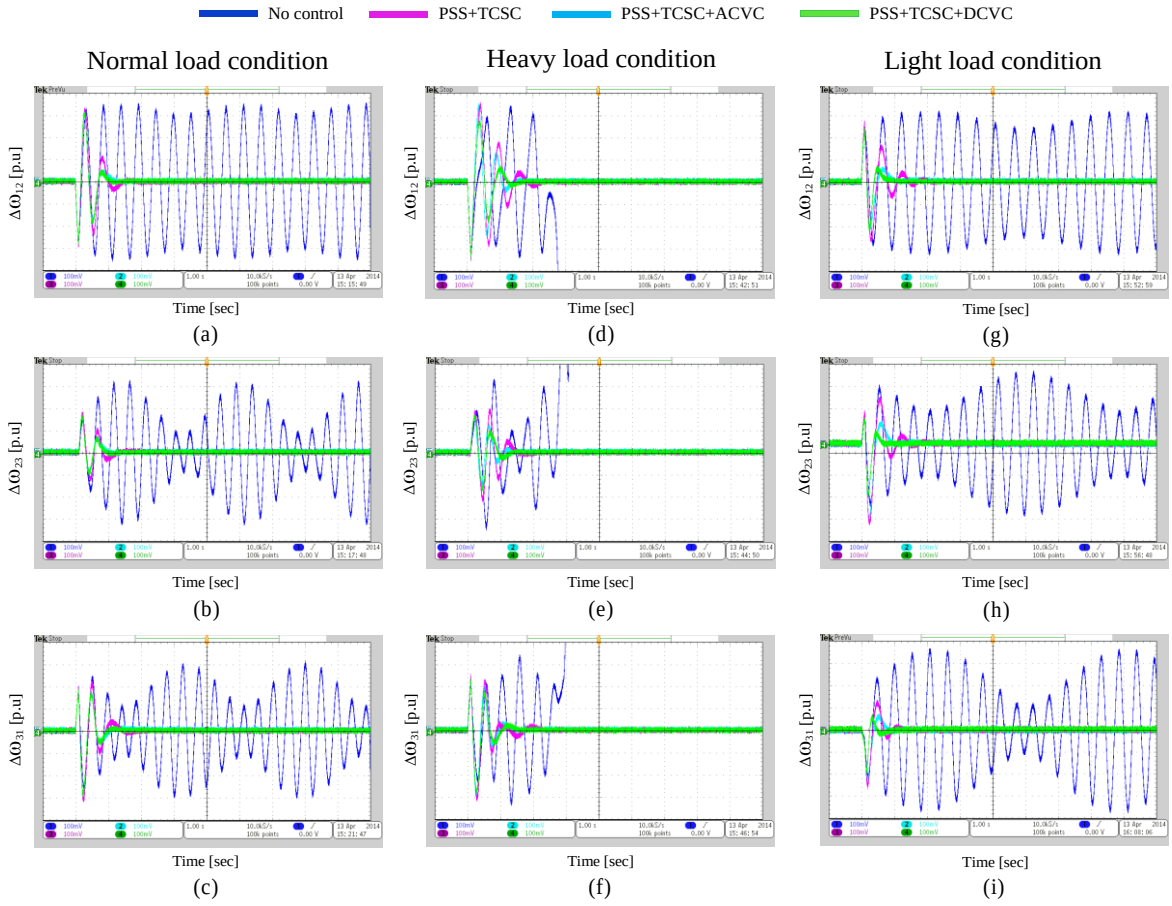

Figure 7.15: **Real-time response of test system with AAPSO tuned coordinated designs for a six cycle fault under normal, heavy and light load**

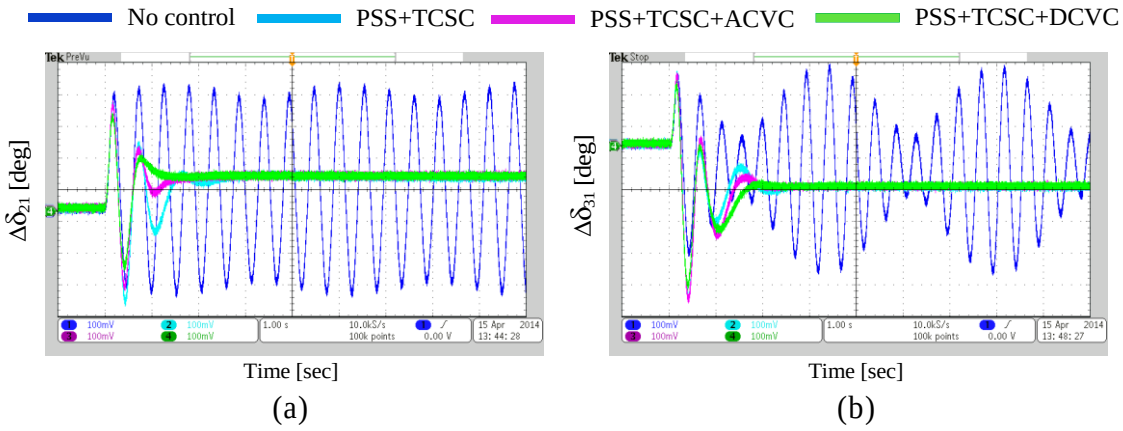

Figure 7.16: **Real-time response of test system with IWO tuned coordinated designs for a six cycle fault under normal load (a) $\Delta\delta_{21}$ (b) $\Delta\delta_{31}$**

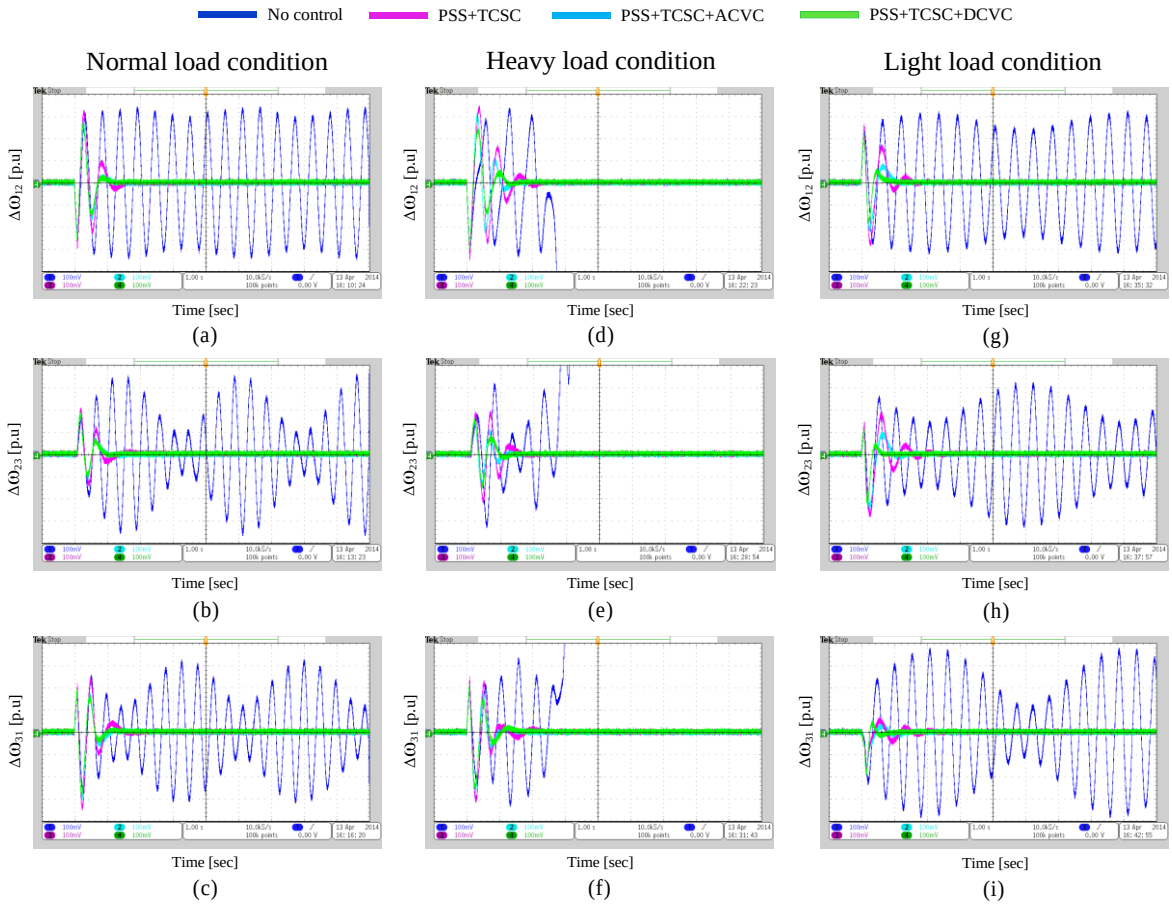

Figure 7.17: **Real-time response of test system with IWO tuned coordinated designs for a six cycle fault under normal, heavy and light load**

7.9 Performance of 4-Machine 11-Bus power system in Real-Time

To observe the behavior of proposed coordinated controllers for local as well as inter-area oscillations two area 4-machine 11-bus power system is considered for analysis.

7.9.1 Real-Time Performance Analysis of Two Area System with PSS, TCSC and SVC Damping Controllers

In this work, the test power system is operated in three distinct load conditions as mentioned in Table 6.10 of Chapter 6. The control parameters settings obtained for AAPSO and IWO algorithms are given in Chapter 6, section 6.3.1. Now the real-time simulations are done for a 6 cycle three-phase fault and the fault was cleared by tripping the line permanently using circuit breakers.

A. Real-Time Response with AAPSO Tuned Coordinated Controllers:

The real-time responses of local area rotor angle oscillations of area 1 and area 2 ($\Delta\delta_{12}$ and $\Delta\delta_{34}$) and inter-area rotor angle oscillations of area 1 to area 2 ($\Delta\delta_{13}$ and $\Delta\delta_{14}$) are compared for different control designs under normal load condition are shown in Figure 7.18. In the similar way, the local-area speed oscillations $\Delta\omega_{12}$ and $\Delta\omega_{34}$ along with inter-area speed oscillations $\Delta\omega_{13}$ and $\Delta\omega_{14}$ of the test power system with different designs under normal, heavy and light load are presented in Figure 7.19. Here the different control schemes such as AAPSO based (PSS+TCSC), AAPSO based (PSS+SVC) and AAPSO based hybrid design (PSS+TCSC+SVC) are compared. By analyzing all these responses, the system with proposed hybrid design controllers has excellent damping characteristics than other designs are noticed.

B. Real-Time Response with IWO Tuned Coordinated Controllers:

The Figure 7.20 represents the real-time responses of rotor angle deviations between different generators of the test system with different control schemes under normal load. The local and inter-area oscillations of the test system under normal, heavy and light load are compared for IWO based different coordinated designs in Figure 7.21. Real-time responses show that the proposed IWO based coordinated design (PSS+TCSC+SVC) provides great damping and good settling times of all responses compared to other designs like IWO based (PSS+TCSC), IWO based (PSS+SVC) under all operating conditions.

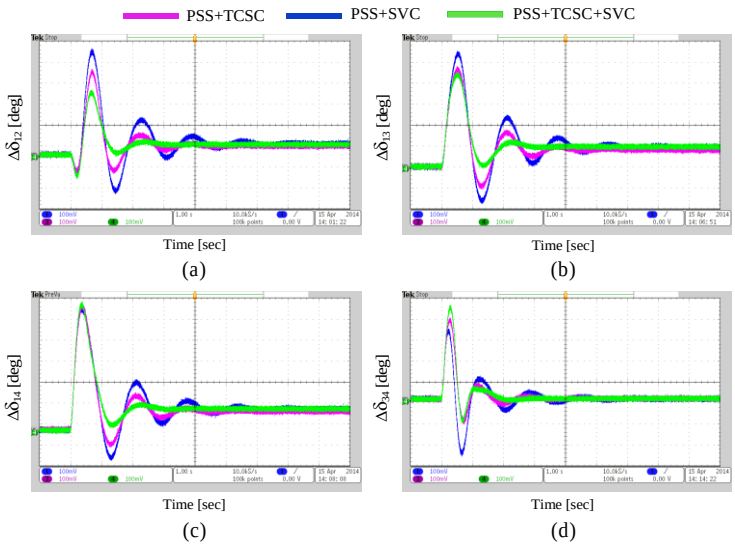

Figure 7.18: **Real-time response of test system with AAPSO tuned coordinated designs for a six cycle fault under normal load (a) Δδ12 (b) Δδ13 (c) Δδ14 (d) Δδ34**

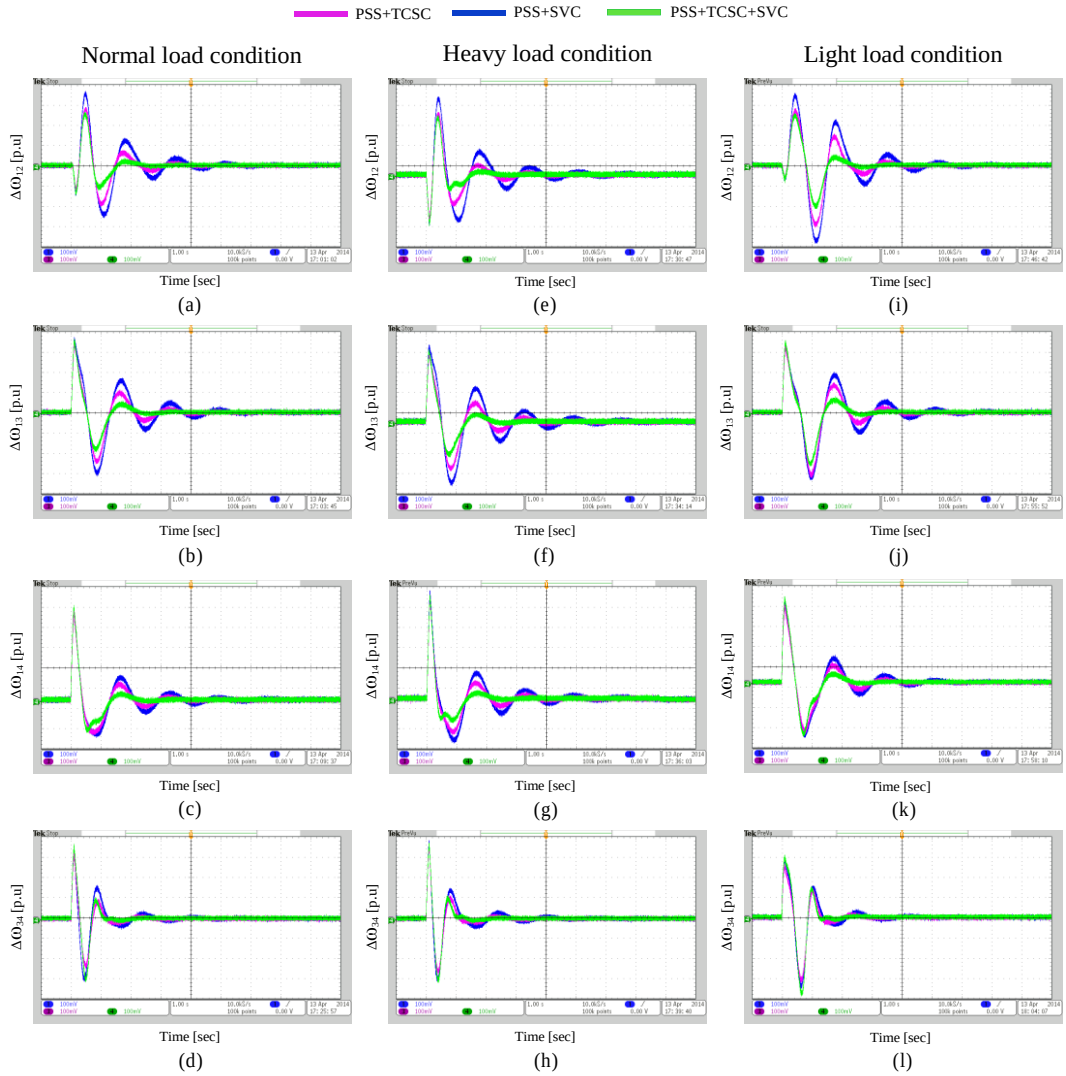

Figure 7.19: **Real-time response of test system with AAPSO tuned coordinated designs for a six cycle fault under normal, heavy and light load**

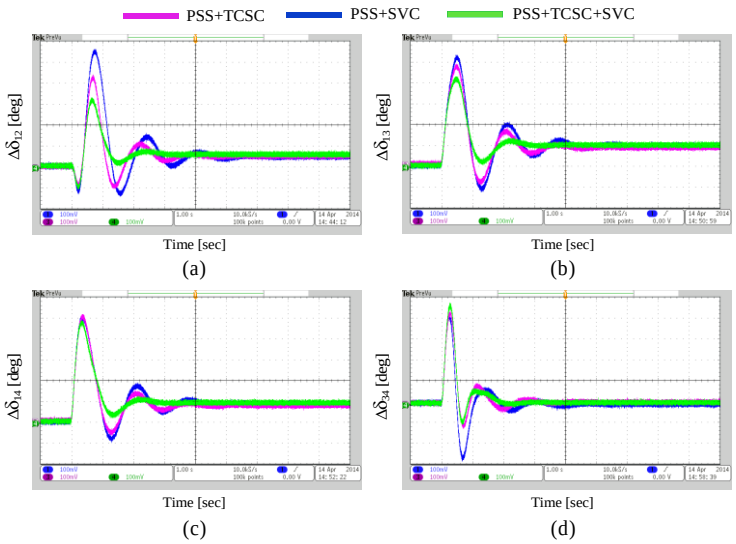

Figure 7.20: **Real-time response of test system with IWO tuned coordinated designs for a six cycle fault under normal load (a) $\Delta\delta_{12}$ (b) $\Delta\delta_{13}$ (c) $\Delta\delta_{14}$ (d) $\Delta\delta_{34}$**

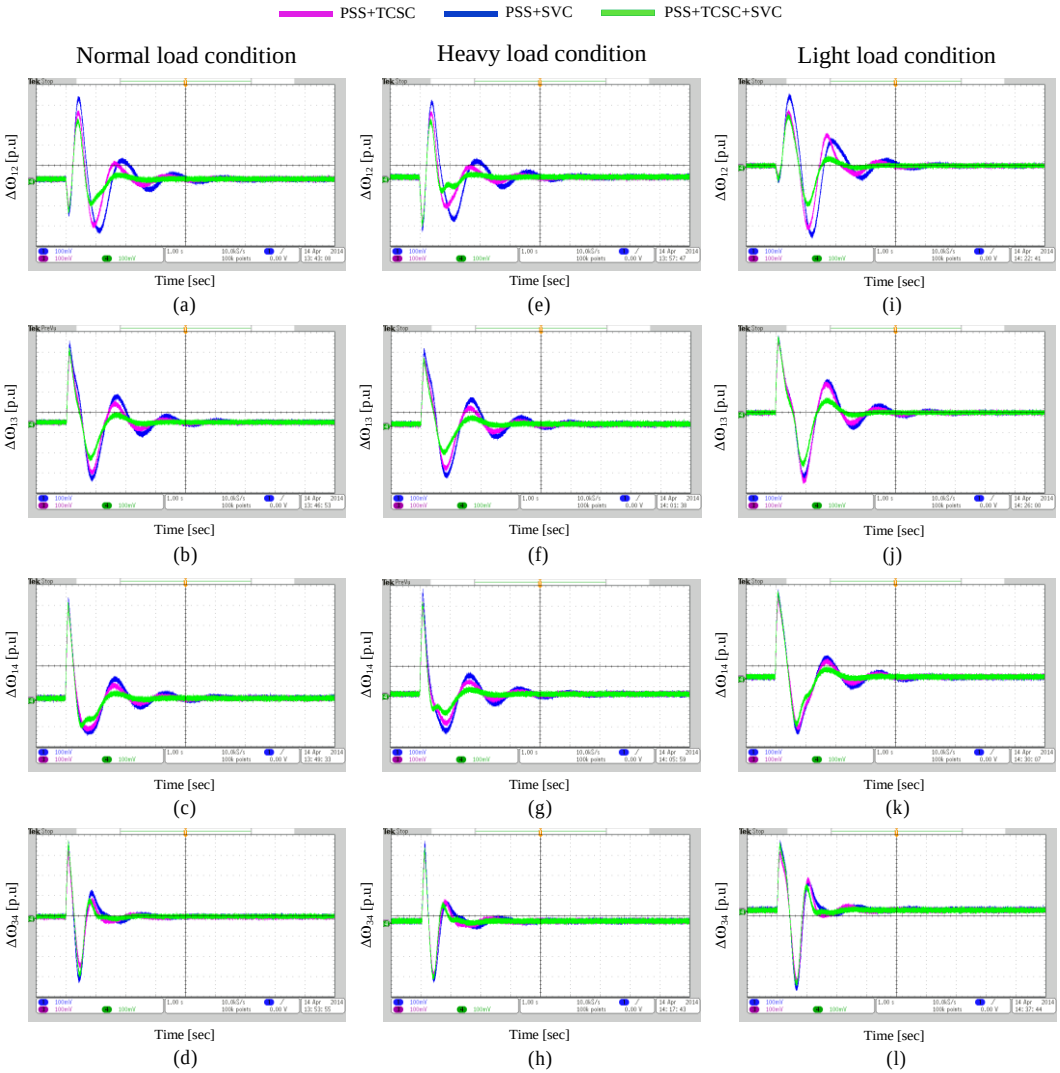

Figure 7.21: **Real-time response of test system with IWO tuned coordinated designs for a six cycle fault under normal, heavy and light load**

7.9.2 Real-Time Performance Analysis of Two Area System with PSS, TCSC and STATCOM Damping Controllers

The three operating conditions normal, heavy, and light load values are listed in Table 6.14 of Chapter 6. In this section, the transient analysis of the test system is conducted for a 6 cycle three-phase fault. In this analysis, the system with IWO and AAPSO based coordinated designs are tested under a wide range of operating points and the real-time results are provided.

A. Real-Time response with AAPSO Tuned Coordinated Controllers:

The real-time rotor angle responses of the test system with AAPSO tuned different controllers under normal load condition are compared in Figures 7.22. The local and inter-area speed oscillations of the test system with different control designs under normal, heavy and light load conditions are compared in real-time, which are shown in Figure 7.23. In all these real-time responses, the coordinated designs proved their effectiveness in suppressing the local-area oscillations along with inter-area oscillations of test power system over a wide range of operating conditions. Moreover the proposed AAPSO based hybrid design (PSS+TCSC+DCVC) shows better damping performance compared to AAPSO based hybrid design (PSS+TCSC+ACVC) and AAPSO based coordinated design (PSS+TCSC).

B. Real-Time Response with IWO Tuned Coordinated Controllers:

In Figure 7.24, the real-time responses of rotor angle oscillations under normal load condition are compared for different IWO based coordinated controllers. Also the speed deviations of different areas are compared in Figure 7.25 under normal, heavy and light load conditions. From the real-time results evaluation, it is concluded that the performance of IWO based hybrid design (PSS+TCSC+DCVC) outperforms the performance of IWO based hybrid coordinated design (PSS+TCSC+ACVC), IWO based coordinated design (PSS+TCSC) in all operating points.

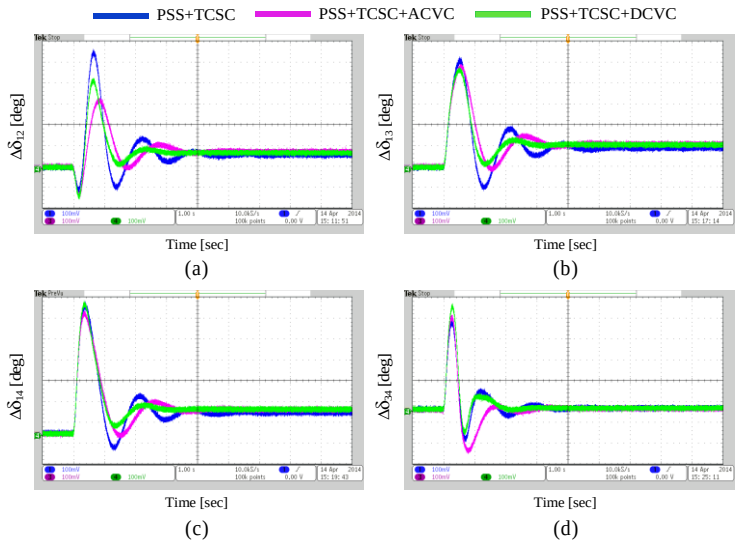

Figure 7.22: **Real-time Response of test system with AAPSO tuned coordinated designs for a six cycle fault under normal load (a) Δδ12 (b) Δδ13 (c) Δδ14 (d) Δδ34**

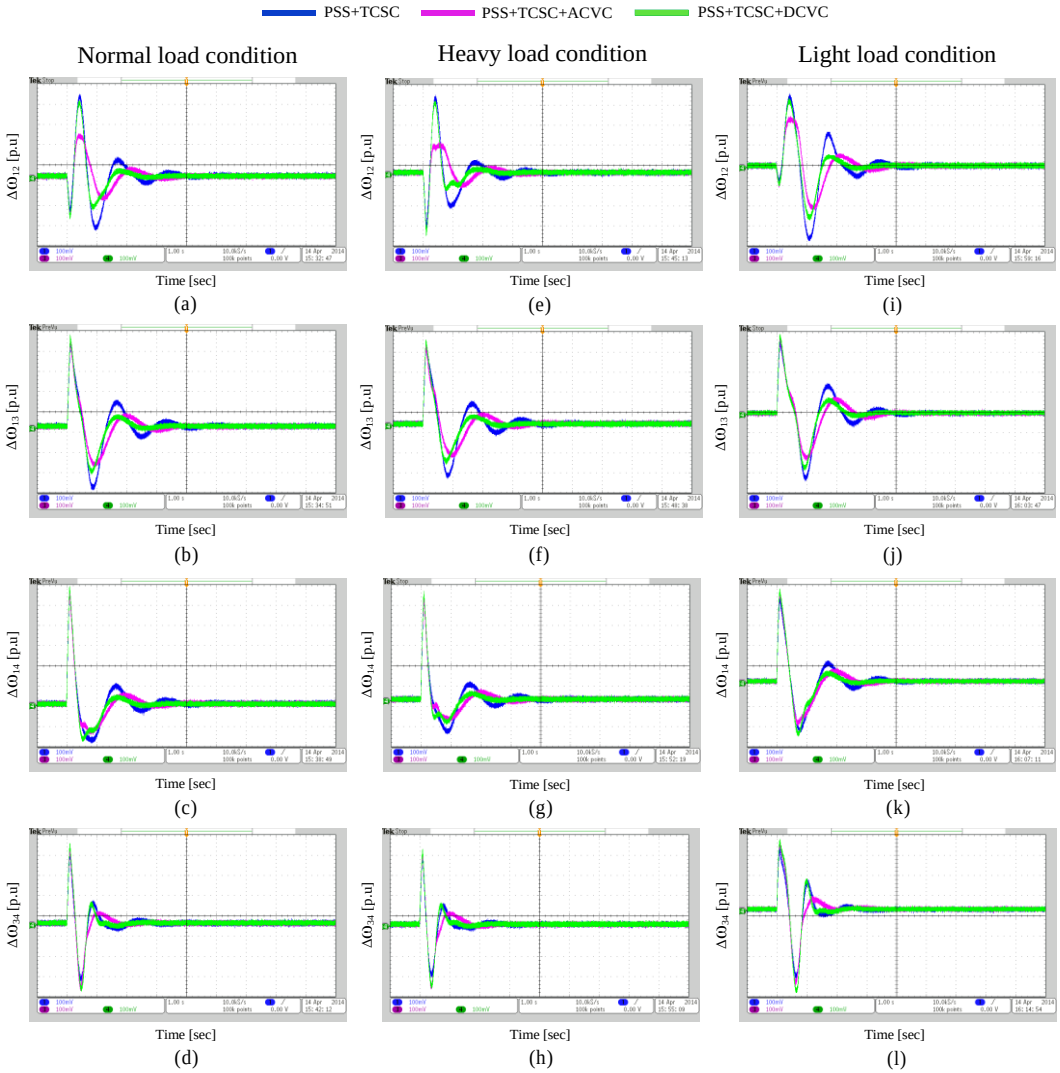

Figure 7.23: **Real-time response of test system with AAPSO tuned coordinated designs for a six cycle fault under normal, heavy and light load**

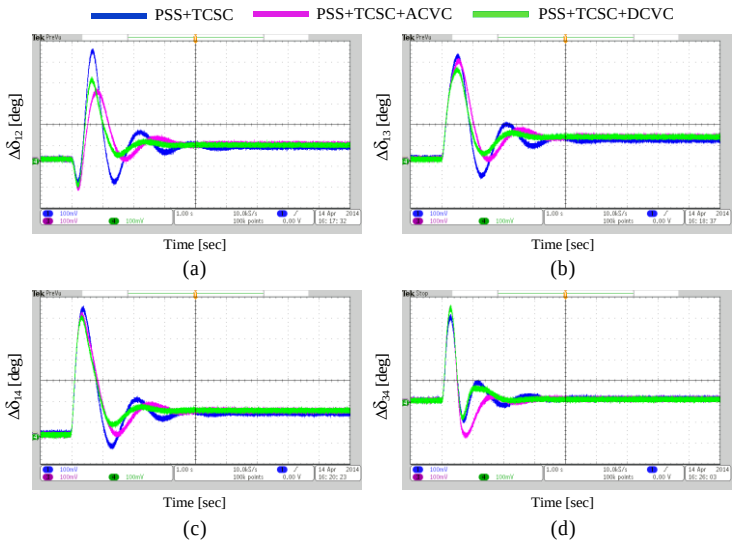

Figure 7.24: **Real-time response of test system with IWO tuned coordinated designs for a six cycle fault under normal load (a) $\Delta\delta_{12}$ (b) $\Delta\delta_{13}$ (c) $\Delta\delta_{14}$ (d) $\Delta\delta_{34}$**

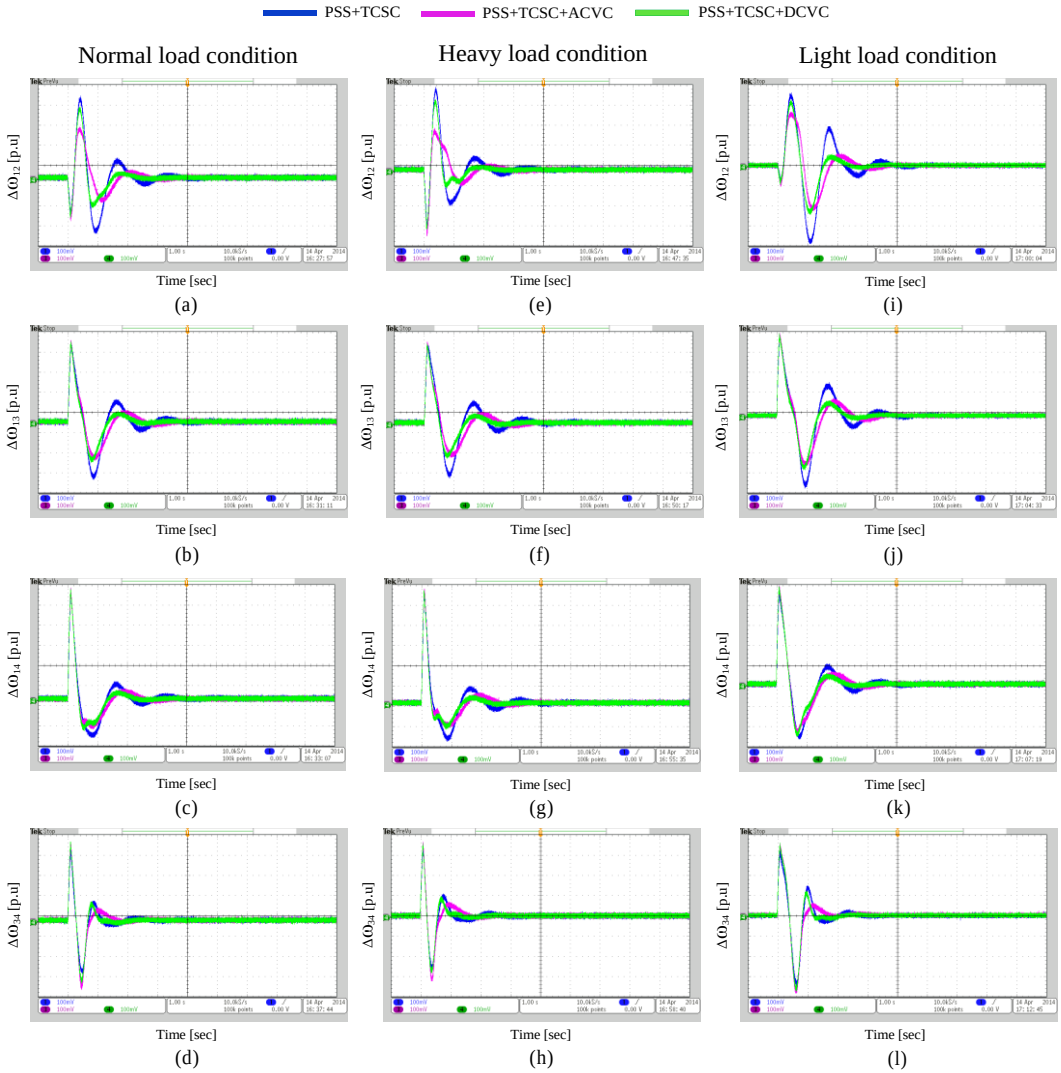

Figure 7.25: **Real-time response of test system with IWO tuned coordinated designs for a six cycle fault under normal, heavy and light load**

7.10 Summary

An introduction to RT-LAB and the salient features of real-time simulations are discussed in this chapter. Working of RT-LAB along in different configurations is demonstrated. The procedural steps to interface MATLAB models with real-time environment are explained in brief manner. The real-time validation of all proposed designs is done using OPAL-RT hardware simulator. Two test systems are considered for real-time hardware simulations and the results are provided. Finally the real-time responses of all the designs are exactly follows the time-domain simulations of the test systems presented in Chapter 6. These real-time responses also verify the effectiveness of proposed hybrid coordinated designs in damping and settling the power system oscillations.

Chapter 8

Conclusions and Future Scope

Chapter 8

Conclusions and Future Scope

8.1 Conclusions

In this research work, the main objective is to damp the power system oscillations and to enhance the system dynamic performance under severe disturbances. The research work started with introduction to power system and classification of stability. The modelling of different power system components, like generators, loads, transmission networks and excitation systems are presented. The performance of the system with conventional PSS under severe disturbance is analyzed. However, the PSS does not guarantee the system stability when the system conditions vary abruptly. Particularly, for the transmission lines loaded over a very long distance in a multi-machine system it is unable to damp the inter-area oscillations under severe disturbance. FACTS technology provides extensibility on AC transmission system over very long distances by controlling the active and reactive power flows. In this, we have considered three distinct FACTS controllers with power oscillation damping stabilizers. The PI based FACTS POD controllers are compared with lead-lag based FACTS POD controllers under different system operating conditions such as normal load, heavy load, light load and leading PF conditions. By observing the various response curves under different load conditions, the lead-lag based FACTS POD is quite competent in damping the power oscillations than PI based FACTS POD controllers.

To damp the local along with inter-area oscillations efficiently and improve the system dynamic performance further the coordinated design of PSS and FACTS damping controllers is much needed. The coordinated design problem of these controllers is formulated as an optimization problem. To solve this, an objective function is developed based on damping factors and damping ratios of the test system. The optimal parameter values of coordinated controllers are obtained by minimizing the objective function using modern optimization algorithms like AAPSO and IWO. Here, the coordinated designs (PSS+TCSC), (PSS+SVC) and (PSS+STATCOM) damping controllers via AAPSO algorithm are discussed in chapter 4. The hybrid coordinated designs (PSS+TCSC+SVC), and (PSS+TCSC+STATCOM) via IWO algorithm are proposed in chapter 5. The listed

design procedures are discussed and the performance analysis is carried out for a simple SMIB test system.

The damping characteristics of proposed hybrid designs are examined with multi-machine power systems in chapter 6. AAPSO and IWO algorithms are used to obtain the optimal control parameter values of different controllers in these proposed designs. The performance of different proposed designs is compared with the individual designed controllers using eigen value analysis and time-domain simulations.

On inspection of system eigen values, and damping ratios of electromechanical modes, the proposed coordinated controllers shifts significantly the electromechanical mode eigen values to the left half of the D shape in the *S*-plane. Moreover, it is observed that the damping factors of the test systems with the proposed designs are substantially enhanced. From the eigen value analysis, it is concluded that the proposed designs greatly enhanced the system stability and improved the damping characteristics of poorly damping electrometrical modes.

The dynamic performance of the test systems with different control schemes under different load conditions is compared for a six cycle 3-phase fault. Simulation results show that the proposed coordinated designs provided effective damping characteristics than that of individual designed controllers. Whereas the open loop system performance is highly oscillatory in all operating conditions. The settling times of different speed oscillations are greatly improved by proposed coordinated designs. The settling time comparison of different speed oscillations of the test system with AAPSO and IWO based proposed designs is done in Chapter 6. The comparison revealed that the settling times of IWO based designs are little quicker than AAPSO based designs. Hence, IWO based proposed designs are slightly superior to AAPSO based proposed designs in damping power oscillations.

Also, the proposed coordinated designs are validated in real-time using Opal-RT hardware simulator. The real-time results are compared for different coordinated designs with proposed designs for a 6-cycle 3-phase fault disturbance. The simulation results in chapter 6 are validated by implementing the test power system with proposed designs in real-time. Moreover, the OPAL-RT hardware results exactly follow the MATLAB simulation results. Hence, the proposed work is successfully implemented and validated in real-time.

On summary, all these results assure the effectiveness and robustness of the proposed designs in providing good damping characteristics to power system oscillations and improving power system dynamic performance over a wide range of operating conditions.

8.2 Future Scope

This research has explored some good ideas and suitable solutions. Based on the experience gained from this work, the following aspects require for further investigation.

- In this work, lead-lag based PSSs are used in proposed designs for damping of power oscillations. The modern PSSs designs (like PSS2B, PSS4B etc.) can be used for further improvement in damping of power oscillations.
- For the proposed hybrid designs TCSC damping controller is used as a series facts controller. Instead of this, incorporating VSC-based series FACTS controllers like SSSC can still improve power system dynamic performance.
- The robustness of proposed designs can be tested by implementing in large power systems (like, 10-machine 39-bus New England power system, 16-machine 68-bus NYPS-NETS test power system).
- Moreover, modern optimization techniques (seeker optimization, hybrid BFO-PSO algorithms etc.), adaptive methods (adaptive Neural Networks) and advanced control methods (Type -2 Fuzzy sets) can be used in future for optimal tuning of various controller in hybrid coordinated designs.
- Future prospects should be focus on the implementation of proposed designs in practical power system applications.

References

References

[1] IEEE/CIGIRE Joint Task Force on Stability Terms and Definitions, “Definitions and classification of power system stability,” IEEE Trans. on Power syst., vol. 19, no. 3, pp. 1387-1401, 2004.

[2] P. Kundur, “Power system stability and control,” New York: McGraw-Hill; 1994.

[3] C. P. Steinmetz, “Power control and stability of electric generating stations,” AIEE Trans., vol. XXXIX, no. 2, pp. 1215-1287, 1920.

[4] G. S. Vassell, “Northest blackout of 1965,” IEEE Power Engg., Review, pp. 4-8, 1991.

[5] N. G. Hingorani and L. Gyugyi, “Understanding FACTS: concepts and technology of flexible AC transmission systems,” New York: IEEE Press, 2000.

[6] K. R. Padiyar and R. K. Varma, “Concepts of static var system control for enhancing power transfer in long transmission lines,", Electric machines and Power Systems, vol.18, no. 4-5, pp.337-358, 1990.

[7] A. E. Hammad, “Analysis of power system stability enhancement by static var compensators", IEEE Trans., vol. PWRS-1, no. 4, pp. 222-227, 1986.

[8] K. R. Padiyar, “FACTS controllers in power transmission and distribution,” New Age Int. Publishers, 2007.

[9] L. Gyugyi, “A unified power flow controller concept for flexible AC transmission systems," IEE Proceedings-C, vol. 139, no. 4, pp. 323-331, 1992.

[10] C. Concordia, “Effect of prime-mover speed control characteristics on electric power system performance,” IEEE Transactions on Power Apparatus and Systems, vol. 88, no. 5, pp. 752-756, 1969.

[11] F. P. DeMello and C. Concordia, "Concepts of synchronous machine stability as affected by excitation control," IEEE Transactions on Power Apparatus and Systems, vol. 88, pp. 316-329, 1969.

[12] K. Fregene and D. Kennedy, “Stabilizing control of a high-order generator model by adaptive feedback linearization,” IEEE Transactions on Energy Conversion, vol.18, no.1, pp. 149- 156, 2003.

[13] Y. Yu and Q. Li, “Pole-placement power system stabilizers design of an unstable nine-machine system,” IEEE Trans. Pow. Sys., vol. 5, no. 2, pp. 352-358, 1990.

[14] M. K. El-Sherbiny, M. M. Hasan, G. El-Saady and Ali M. Yousef, “Optimal pole shifting for power system stabilization,” Electric Power Syst. Res., vol. 66, no. 3, pp.253–258, 2003.

[15] M. Nambu and Y. Ohsawa, “Development of an Advanced Power System Stabilizer Using a Strict Linearization Approach,” IEEE Trans. Pow. Sys., vol. 11, no. 2, pp. 813-818, 1996.

[16] C.T. Tse, K.W. Wang, C.Y. Chung and K.M. Tsang, "Robust PSS design by probabilistic eigenvalue sensitivity analysis," Electric Power Syst. Res., vol. 59, no. 1, pp.47–54, 2001.

[17] A. Soos and O. P. Malik, "An H2 optimal adaptive power system stabilizer," IEEE Trans. Energy Conv. vol. 17, no. 1, pp. 143-149, 2002.

[18] D.M. Lam and H. Yee, "A study of frequency responses of generator electrical torques for power system stabilizer design," IEEE Trans. Pow. Sys., vol. 13, no. 3, pp. 1136-1142, 1998.

[19] M. Ramirez-Gonzalez and O. P. Malik, "Self-tuned power system stabilizer based on a simple fuzzy logic controller," Electric Power Components and Systems, vol. 38, no. 4, 407-423, 2010.

[20] N. Hossein-zadeh and A. Kalam, "An indirect adaptive fuzzy-logic power system stabilizer," Int. J. Elect. Power and Energy Syst., vol. 24, no. 10, pp. 837-842, 2002.

[21] M. Soliman, A. L. Elshafei, F. Bendary and W. Mansour, "Design of a fuzzy multi-objective power system stabilizer," Euro. J. Cont. vol. 15, no. 6, pp. 649-664, 2009.

[22] Holland JH, "Adaptation in natural and artificial systems: An introductory analysis with applications to biology, control, and artificial intelligence," Oxford, England: U Michigan Press; 1975.

[23] S. Kirkpatrick, C. D. Gelatt and M. P. Vecchi, "Optimization by Simulated Annealing," Science, vol. 220, no. 4598, pp. 671-680, 1983.

[24] J. Kennedy and R. Eberhart, "Particle Swarm Optimization," Proceedings of the IEEE Int. Conf on Neural Networks, pp. 1942-1948, 1995.

[25] K. M. Passino, "Biomimicry of bacterial foraging for distributed optimization and control," IEEE Control Syst. Mag. vol. 22, no. 3, pp. 52–67, 2002.

[26] R. Storn and K. Price, "Differential Evolution - A simple and efficient adaptive scheme for global optimization over continuous spaces," Technical report Int. Comput Sci Instit Berkley; 1995.

[27] Y. L. Abdel-Magid and M. A. Abido, "Optimal multi objective design of robust power system stabilizers using genetic algorithms," IEEE Trans. Pow. Sys., vol. 18, no. 3, pp. 1125-1132, 2003.

[28] K. Sebaa and M. Boudour, "Optimal locations and tuning of robust power system stabilizer using genetic algorithms," Electric Power Syst. Res., vol. 79, no. 2, pp.406–416, 2009.

[29] M. A. Abido, "Robust Design of Multimachine Power System Stabilizers Using Simulated Annealing," IEEE Trans. Energy Conv. vol. 15, no. 3, pp. 297-304, 2000.

[30] M. A. Abido, "An efficient heuristic optimization technique for robust power system stabilizer design," Electric Power Syst. Res., vol. 58, no. 2, pp.53–62, 2001.

[31] M. A. Abido, "Optimal Design of Power–System Stabilizers using Particle Swarm Optimization," IEEE Trans. Energy Conv., vol. 17, no. 3, pp. 406-413, September 2002.

[32] H. Shayeghi, H.A. Shayanfar, A. Safari and R. Aghmasheh, "A robust PSSs design using PSO in a multi-machine environment," Energy Convers. Manage., vol. 51, pp. 696–702, 2010.

[33] H. E. Mostafaa, M. A. El-Sharkawyb, A. A. Emaryc and K. Yassind, "Design and allocation of power system stabilizers using the particle swarm optimization technique for an interconnected power system," Int. J. Elect. Power and Energy Syst., vol. 34, no. 1, pp. 57–65, 2012.

[34] S. Mishra, M. Tripathy and J. Nanda, "Multi-machine power system stabilizer design by rule based bacteria foraging," Electric Power Syst. Res., vol. 77, no. 12, pp.1593–1607, 2007.

[35] Z. Wang, C. Y. Chung, K. P. Wong and C. T. Tse, "Robust power system stabilizer design under multi-operating conditions using differential evolution," IET Pow. Trans. Distri., vol. 2, no. 5, pp. 690-700, 2008.

[36] A. H. M. A. Rahim and S. G. A. Nassimi, "Synchronous generator damping enhancement through coordinated control of exciter and SVC," IEE Proc. Genet. Transm. Distrib., vol. 143, no. 2, pp. 211–218, 1996.

[37] R. T. Byerly, D. T. Poznaniak and E. R. Taylor, "Static reactive compensation for power transmission system," IEEE Transactions on Power Apparatus and Systems, vol. 101, no. 10, pp. 3997–4005, 1982.

[38] A. E. Hammad, "Analysis of power system stability enhancement by static VAR compensators," IEEE Transactions on Power Systems, vol. 1, no. 4, pp. 222–227, 1986.

[39] K. R. Padiyar and R. K. Varma, "Damping torque analysis of static VAR system oscillations," IEEE Transactions on Power Systems, vol. 6, no. 2, pp. 458–465, 1991.

[40] H. F. Wang and F. J. Swift, "Application of the Phillips-Heffron model in the analysis of the damping torque contribution to power systems by SVC damping control," Int. J Elect. Power Energy Syst., vol.18, no. 5, pp. 307–313, 1996.

[41] H. F. Wang and F. J. Swift, "Capability of the static VAR compensator in damping power system oscillations," IEE Proc Gen. Trans. Distri., vol. 143, no. 4, pp. 353–358, 1996.

[42] P. Pourbeik and M. J. Gibbard, "Damping and synchronizing torques induced on generators by FACTS stabilizers in multi-machine power systems," IEEE Trans. Power Syst., vol. 11, no. 4, pp. 1920–1925, 1996.

[43] P. K. Dash, P. C. Panda, A. M. Sharaf, and E. F. Hill, "Adaptive controller for static reactive power compensators in power systems," IEE Pro Part-C, vol. 134, no. 3, pp. 256–264, 1987.

[44] Y. Y. Hsu and C H. Cheng "Design of a static VAR compensator using model reference adaptive control," Electric Power Syst. Res., vol. 13, pp. 129–138, 1987.

[45] M. Parniani and M. R. Iravani, "Optimal robust control design of static VAR compensators," IEE Proc Gen. Trans. Distr., vol. 145, no. 3, pp. 301–307, 1998.

[46] K.L. Lo and M.O. Sadegh, "Systematic method for the design of a full-scale fuzzy PID stability controller for SVC to control power system," IEE Proc.-Gen. Trans. Distrib., vol. 150, no. 3, pp. 297-304, 2003.

[47] Li-Ying Sun, Shaocheng Tong, and Yi Liu, "Adaptive backstepping sliding mode control of static var compensator," IEEE Transactions on Control Systems Technology, vol. 19, no. 5, pp. 1178-1185, 2011.

[48] S. M. Abd-Elazim and E. S. Ali, "Bacteria foraging optimization algorithm based SVC damping controller design for power system stability enhancement," Int. J Elect. Power Energy Syst., vol. 43, no. 1, pp. 933-940, 2012.

[49] Mohsen Farahani, "Intelligent control of SVC using wavelet neural network to enhance transient stability," Engineering applications of artificial intelligence, vol. 26, no. 1, pp. 272-280, 2013.

[50] Q. Zhao and J. Jiang, "A TCSC damping controller design using robust control theory," Int. J. Elect. Power and Energy Syst., vol. 20, no. 1, pp. 25-33, 1998.

[51] B. H. Li, Q. H. Wu, D. R. Turner, P. Y. Wang and X. X. Zhou, "Modelling of TCSC dynamics for control and analysis of power system stability," Int. J. Elect. Power and Energy Syst., vol. 22, no. 1, pp. 43-49, 2000.

[52] D. D. R. Alberto, A. C. Claudio and M. D. Victor, "A Study of TCSC Controller Design for Power System Stability Improvement," IEEE Trans. Pow. Syst., vol. 18, no. 4, pp. 1487-1496, 2003.

[53] P. C. Srivastava, Arindam Ghosh and S. V. Jayaram Kumar, "Model-based control design of a TCSC-compensated power system," Int. J. Elect. Power and Energy Syst., vol. 21, no. 4, pp. 299-307, 1999.

[54] D. Z. Fang, Y. Xiaodong, S. Wennan and H. F. Wang, "Oscillation transient energy function applied to the design of a TCSC fuzzy logic damping controller to suppress power system interarea mode oscillations," IEE Proc Gener Trans Distrib., vol. 150, no. 2, pp.233-238, 2003.

[55] Salman Hameed, Biswarup Das and Vinay Pant, "A self-tuning fuzzy PI controller for TCSC to improve power system stability," Electric Power Syst. Res., vol. 78, no. 10, pp. 1726-1735, 2008.

[56] Salman Hameed, Biswarup Das and Vinay Pant, "Reduced rule base self-tuning fuzzy PI controller for TCSC," Int. J. Elect. Power and Energy Syst., vol. 32, no. 9, pp. 1005-1013, 2010.

[57] X. R. Chen, N. C. Pahalawaththa, U. D. Annakkage and C. S. Kumble, "Design of decentralized output feedback TCSC damping controllers by using simulated annealing," IEE Proc Gener Trans Distrib., vol. 145, no. 5, pp. 553-558, 1998.

[58] H. Shayeghi, H. A. Shayanfar, S. Jalilzadeh and A. Safari, "TCSC robust damping controller design based on particle swarm optimization for a multi-machine power system," Energy Conv. Manage., vol. 51, no. 10, pp. 1873-1882, 2010.

[59] S. Panda and N. P. Padhy, "Comparison of particle swarm optimization and genetic algorithm for FACTS-based controller design," Applied soft comput., vol. 8, no. 4, 1418-1427, 2008.

[60] Sidhartha Panda, "Differential evolutionary algorithm for TCSC-based controller design," Simul. Model Pract. Theory, vol. 17, no. 10, pp. 1618-1634, 2009.

[61] E. S. Ali and S. M. Abd-Elazim, "TCSC damping controller design based on bacteria foraging optimization algorithm for a multimachine power system," Int. J Elect. Power Energy Syst., vol. 37, no. 1, pp. 23-30, 2012.

[62] D. J. Hanson, M. L. Woodhouse, C. Horwill, D. R. Monkhouse and M. M. Osborne, "STATCOM: a new era of reactive compensation," Power Engineering Journal, pp. 151–160, 2002.

[63] H. F. Wang, H. Li and H. Chen, "Application of cell immune response modeling to power system voltage control by STATCOM," IEE Proc.-Gen. Trans. Distrib., vol. 149, no. 1, pp. 102–107, 2002.

[64] M. A. Abido, "Analysis and assessment of STATCOM-based damping stabilizers for power system stability enhancement," Electric Power Syst. Res., vol. 73, no. 2, pp. 177–185, 2005.

[65] M. H. Haque, "Use of energy function to evaluate the additional damping provided by a STATCOM," Electric Power Syst. Res., vol. 72, no. 2, pp. 195–202, 2004.

[66] S. Panda and N. P. Padhy, "Optimal location and controller design of STATCOM for power system stability improvement using PSO," J of the Frank Insti.,vol. 345, no. 2, pp. 166–181, 2008.

[67] P. F. Puleston, S.A. Gonzalez and F. Valenciaga, "A STATCOM based variable structure control for power system oscillations damping," Int. J Elect. Power Energy Syst., vol. 29, no. 3, pp. 241-250, 2007.

[68] H. F. Wang, "Interactions and multivariable design of STATCOM AC and DC voltage control," Int. J Elect. Power Energy Syst., vol. 25, no. 5, pp. 387-394, 2003.

[69] M. A. Abido, "Power system stability enhancement using facts controllers: a review," The Arabian J Sci. Engg., vol. 34, no. 1B, pp. 153-172, 2009.

[70] I. A. Erinmez and A. M. Foss, "Static Synchronous Compensator (STATCOM)," Working Group 14.19, CIGRE Study Committee 14, Document No. 144, 1999.

[71] H. F. Wang and F. J. Swift, "Multiple stabilizer setting in multi-machine power systems by the phase compensation method." Int. J Elect. Power Energy Syst., vol. 20, no. 4, pp. 241-246, 1998.

[72] A. S. Bazanella and A. S. Silva, "Coordinated design of damping controllers for robustness of power systems stability," Int. J Elect. Power Energy Syst., vol. 23, no. 1, vol. 69-79, 2001.

[73] M. A. Furini, A. L. S. Pereira and P. B. Araujo, "Pole placement by coordinated tuning of power system stabilizers and FACTS-POD stabilizers," Int. J Elect. Power Energy Syst., vol. 33, no. 3, pp. 615-22, 2011.

[74] X. Y. Bian, C. T. Tse, J. F. Zhang and K. W. Wang, "Coordinated design of probabilistic PSS and SVC damping controllers," Int. J Elect. Power Energy Syst., vol. 33, no. 3, pp. 445-452.

[75] Amin Khodabakhshian, Mohammad Javad Morshed and Moein Parastegari, "Coordinated design of STATCOM and excitation system controllers for multi-machine power systems using zero dynamics method," Int. J Elect. Power Energy Syst., vol. 49, no. 1, pp. 269-279.

[76] M. A. Abido and Y. L. Abdel-Magid, "Coordinated design of a PSS and an SVC-based controller to enhance power system stability," Int. J Elect. Power Energy Syst., vol. 25, no. 9, pp. 695-704, 2003.

[77] S. M. Abd-Elazim and E. S. Ali, "Coordinated design of PSSs and SVC via bacteria foraging optimization algorithm in a multi-machine power system," Int. J Elect. Power Energy Syst., vol. 41, no. 1, pp. 44-53, 2012.

[78] D. Z. Fang, S. Q. Yuan, Y. J. Wang and T. S. Chung, "Coordinated parameter design of STATCOM stabilizer and PSS using MSSA algorithm," IET Gener. Transm. Distrib., vol. 1, no. 4, pp. 670-678, 2007.

[79] Sidhartha Panda, "Robust coordinated design of multiple and multi-type damping controller using differential evolution algorithm," Int. J Elect. Power Energy Syst., vol. 33, no. 4, pp. 1018-1130, 2011.

[80] M. A. Abido, "Pole placement technique for PSS and TCSC-based stabilizer design using simulated annealing," Int. J Elect. Power Energy Syst., vol. 22, no. 8, pp. 543-554, 2000.

[81] Y. L. Abdel-Magid and M. A. Abido, "Robust coordinated design of excitation and TCSC-based stabilizers using genetic algorithms," Electr. Power Syst. Res., vol. 69, no. 2-3, pp. 129-141, 2004.

[82] S. Panda and N. P. Padhy "Power System with PSS and FACTS Controller: Modelling, Simulation and Simultaneous Tuning Employing Genetic Algorithm," Int. J Electric Electronic Eng., vol. 1, no. 1, pp. 9-18, 2007.

[83] H. Shayeghi, A. Safari and H. A. Shayanfar, "PSS and TCSC damping controller coordinated design using PSO in multi-machine power system," Energy Conv. Manage., vol. 51, no. 12, pp. 2930-2937, 2010.

[84] S. Panda and N. P. Padhy, "Coordinated Design of TCSC Controller and PSS Employing Particle Swarm Optimization Technique," Int. J Comput. Inform Sci. Eng., vol. 1, no. 5, pp. 269-277, 2007.

[85] P. R. Dian, M. S. Siti and S. Y. Siti, "Particle Swarm Optimization: Technique, System and Challenges," Int. J Comput. Appli., vol. 14, no.1, pp. 19-27, 2011.

[86] E. S. Ali and S. M. Abd-Elazim, "Coordinated design of PSSs and TCSC via bacterial swarm optimization algorithm in a multi-machine power system," Int. J Elect. Power Energy Syst., vol. 36, no. 1, pp. 84-92, 2012.

[87] S. K. Tso, J. Liang, Q. Y. Zeng, K. L. Lo and X. X. Zhou, "Coordination of TCSC and SVC for stability improvement of power systems," Pro. 4th Int. Conf. Advances in Power System Control, Operation and Management, Hong Kong, November 1997.

[88] S. K. Tso, J. Liang and X. X. Zhou, "Coordination of TCSC and SVC for improvement of power system performance with NN-based parameter adaptation," Int. J. Elect. Power and Energy Syst., vol. 21, no. 4, pp. 235–244, 1999.

[89] Xianzhang Lei, Edwin N. Lerch and Dusan Povh, "Optimization and Coordination of Damping Controls for Improving System Dynamic Performance," IEEE Trans. Power Systems, vol. 16, no. 3, pp. 473 – 480, 2001.

[90] IEEE task force, "Current usage & suggested practicesin power system stability simulations for synchronous machines," IEEE Trans. Energy Conver., vol. 1, no. 1, pp. 77-93, 1986.

[91] P. L. Dandeno, R. L. Hauth and R. P. Schultz, "Effects of synchronous machine modeling in large scale system studies," IEEE Trans. Pow. Appat. Syst., vol. 92, no. 2, pp. 574-582, 1973.

[92] K. Prabhashankar and J. W. Janishewsy, "Digital simulation of multimachine power systems for stability studies," IEEE Trans. Pow. Appat. Syst., vol. 87, no. 1, pp. 73-80, 1968.

[93] H. Amhriz-PBrez, E. Acha, and C. R. Fuerte-Esquivel, "Advanced SVC models for Newton-Raphson load flow and Newton optimal power flow studies," IEEE Trans. Pow. Syst., vol. 15, no. 1, pp. 129-136, 2000.

[94] M. A. Pai, D. P. Sengupta and K. R. Padayar, "Small signal analysis of power systems," Alpha science international ltd.; 2004.

[95] R. M. Mathur and R. K. Varma, "Thyristor-Based FACTS Controllers for Electrical Transmission Systems," IEEE press: piscataway; 2002.

[96] H. F. Wang, "Phillips-Heffron model of power systems installed with STATCOM and applications," IEE Proc. Gener. Trans. Distrib., vol. 146, no. 5, pp. 521-527, 1999.

[97] S. Panda, B. K. Sahu and P. K. Mohanty, "Design and performance analysis of PID controller for an automatic voltage regulator system using simplified particle swarm optimization," J. of the Franklin Institute, vol. 349, no. 8, pp. 2609-2625, 2012.

[98] P. Cominos and N. Munro, "PID controllers: recent tuning methods and design to specification," IEE Proc. Control Theory Appl., vol. 149, no. I, pp. 46-53, 2002.

[99] R. C. Eberhart and J. Kennedy, "A new optimizer using particle swarm theory," in proceedings of the sixth Int. Sym. on Micro Machine and Human Science, pp. 39-43, 1995.

[100] Y. Shi and R. C. Eberhart, "Empirical study of particle swarm optimization," in Proc. IEEE Int. Conf. Evolutionary Computation vol. 3, pp. 101-106, 1999.

[101] C. M. Lim and S. Elangovan,"Design of stabilisers in multi-machine power systems," IEE Proc. Gen. Trans. Dist., vol. 132, no. 3, pp. 146-153, 1985.

[102] P. M. Anderson and A. A. Fouad, "Power system control and stability," New York: IEEE Press; 1994.

[103] M. Clerc and J. Kennedy, "The particle swarm – explosion, stability, and convergence in a multidimensional complex space," IEEE Trans. Evol. Comput., vol. 6, no. 1, pp. 58-73, 2002.

[104] A. Ratnaweera, S. K. Halgamuge and H. C. Watson, "Self-organizing hierarchical particle swarm optimizer with time-varying acceleration coefficients," IEEE Trans. Evol. Comput., vol. 8, no. 3, pp. 240-255, 2004.

[105] A. R. Mehrabian and C. Lucas, "A novel numerical optimization algorithm inspired from weed colonization," Ecolog. Inform., vol. 1, no. 4, pp. 355-366, 2006.

[106] E. Pourjafari and H. Mojallali, "Solving nonlinear equations systems with a new approach based on invasive weed optimization algorithm and clustering," Swarm Evolut. Comput., vol. 4, no. 1, pp. 33-43, 2012.

[107] S. Karimkashi and A. A. Kishk, "Invasive Weed Optimization and its Features in Electromagnetics," IEEE Trans. Anten. Propag., vol. 58, no. 4, pp. 1269-1278, 2010.

[108] S. H. Sedighy, A. R. Mallahzadeh, M. Soleimani and J. Rashed-Mohassel, "Optimization of Printed Yagi Antenna Using Invasive Weed Optimization (IWO)" IEEE Anten. Wirele. Propag. Lett., vol. 9, pp. 1275-1278, 2010.

[109] G. G. Roy, S. Das, P. Chakraborty and P. N. Suganthan, "Design of Non-Uniform Circular Antenna Arrays Using a Modified Invasive Weed Optimization Algorithm," IEEE Trans. Anten. Propag., vol. 59, no. 1, pp. 110-118, 2011.

[110] F. M. Monavar, N. Komjani and P. Mousavi, "Application of Invasive Weed Optimization to Design a Broadband Patch Antenna with Symmetric Radiation Pattern," IEEE Anten. Wirele. Propag. Lett., vol. 10, pp. 1369-1372, 2011.

[111] K. P. Bagadi and S. Das, "Minimum symbol error rate multiuser detection using an effective invasive weed optimization for MIMO/SDMA–OFDM system," Int. J. Commun. Syst., DOI: 10.1002/dac.2579, 2013.

[112] A. H. Nikoofard, H. Hajimirsadeghi, A. Rahimi-Kian and C. Lucas, "Multi objective invasive weed optimization: Application to analysis of Pareto improvement models in electricity markets," Appli. Soft Comput., vol. 12, no. 1, pp. 100-112, 2012.

[113] A. K. Panda and Suresh Mikkili, "FLC based shunt active filter control strategies for mitigation of harmonics with different fuzzy MFs using MATLAB and real-time digital simulator," Int. J. Elect. Power and Energy Syst., vol. 47, pp. 313-336, 2013.

[114] R. Narne and P. C. Panda, "PSS with SVC damping controllers coordinated design and real-time implementation in multi-machine power system using advanced adaptive PSO" International Journal of Emerging Electric Power Systems vol. 14, no. 5, pp. 487-498, 2013.

[115] RT-LAB Professional [online], available: http://www.opal-rt.com/product/rt-lab-professional

[116] Real time simulation [online], available : en.wikipedia.org/wiki/Real-time_Simulation

[117] M. Papini and P. Baracos, “Real-time simulation, control and HIL with COTS computing clusters,” AIAA Modeling and Simulation Technologies Conference, Denver, CO, August 2001.

[118] C. Dufour, G. Dumur, J. N. Paquin, and J. Belanger, “A multicore pc-based simulator for the hardware-in-the-loop testing of modern train and ship traction systems,” 13th Power Electronics and Motion Control Conference, Poland, pp.1475–1480, 2008.

[119] D. Auger, “Programmable hardware systems using model-based design,” IET and Electronics Weekly Conference on Programmable Hardware Systems, London, pp. 1-12, 2008.

[120] V. Q. Do, J. C. Soumagne, G. Sybille, G. Turmel, P. Giroux, G. Cloutier and S. Poulin, “Hypersim, an Integrated Real-Time Simulator for Power Networks and Control Systems,” ICDS’99, Vasteras, Sweden, pp 1-6, may 1999.

[121] J Belanger, P Venne and JN Paquin, “The What, Where and Why of Real-Time Simulation,” pp. 37-49, 2010.

[122] Simon Abourida, Christian Dufour, Jean Bélanger and Vincent Lapointe, “Real-Time, PC-Based Simulator of Electric Systems and Drives,” International Conference on Power Systems Transients – IPST, New Orleans, USA, 2003.

[123] M. Matar and R. Iravani, “FPGA Implementation of the Power Electronic Converter Model for Real-Time Simulation of Electromagnetic Transients,” IEEE Transactions on Power Delivery, vol. 25, no. 2, pp. 852-860, 2010.

[124] J. A. Hollman and J. R. Marti, “Real Time Network Simulation with PC-Cluster,” IEEE Trans. Power Systems, vol. 18, no. 2, pp. 563-569, 2008.

[125] J. F. Cecile, L. Schoen, V. Lapointe, A. Abreu, and J. Belanger, (2006) www.opal-rt.com. [Online] available : http://www.opalrt.com/technical-document/distributed-real-time frame work dynamic management heterogeneous co-simulations

[126] J. Belanger, V. Lapointe, C. Dufour, and L. Schoen, “eMEGAsim: An Open High-Performance Distributed Real- Time Power Grid Simulator. Architecture and Specification,” International Conference on Power Systems (ICPS’07), Bangalore, India, pp. 12-14, 2007.

[127] Suresh Mikkili and A. K. Panda, “Simulation and real-time implementation of shunt active filter id–iq control strategy for mitigation of harmonics with different fuzzy membership functions,” IET Power Electronics, Vol. 5, No. 9, pp.1856 – 1872, 2012.

Appendix

Appendix A.

Computational parameters in Chapter 4:

A.1 For linearization of power system with PSS and SVC controller

$X_{dT} = X_d^1 + X_T;$	$X_{qT} = X_q + X_T;$	$X_{dTB} = X_d^1 + X_T + 1/B_{SVC};$
$X_{qTB} = X_q + X_T + 1/B_{SVC};$	$X_{dTL} = X_d^1 + X_T + X_L;$	$X_{qTL} = X_q + X_T + X_L;$
$X_{DBL} = [X_{dT} X_L B_{SVC} + X_{dTL}];$	$X_{DT} = [X_{dT} X_L + (X_{dTL}/B_{SVC})];$	
$X_{QT} = [X_{qT} X_L + (X_{qTL}/B_{SVC})];$		
$a_1 = \frac{X_{dTB}}{X_{DT}} V_b \sin\delta;\ \ a_3 = \frac{1}{X_{DBL}};$	$a_5 = \frac{X_{DT} - X_{dTB}X_{dTL}}{X_{DT}^2 B_{SVC}^2} V_b \cos\delta - \frac{X_{dT}X_L}{X_{DBL}^2} E_q^{'};$	
$b_1 = \frac{X_{qTB}}{X_{QT}} V_b \cos\delta;$	$b_5 = \frac{X_{qTB}X_{qTL} - X_{QT}}{X_{QT}^2 B_{SVC}^2} V_b \sin\delta;$	
$c_1 = -\frac{X_{dT}}{X_{DT}} V_b \sin\delta;\ \ c_3 = \frac{X_L}{X_{DT}};$	$c_5 = \frac{X_L X_{dTL}}{X_{DT}^2 B_{SVC}^2} E_q^{'} + \frac{X_{DT}X_{dTL}}{X_{DT}^2 B_{SVC}^2} V_b \cos\delta;$	
$d_1 = -\frac{X_{qT}}{X_{QT}} V_b \cos\delta;$	$d_5 = -\frac{X_{qT}X_{qTL}}{X_{QT}^2 B_{SVC}^2} V_b \sin\delta;$	
$e_i = a_i + c_i \quad for\ i = 1,3,5;$	$f_i = b_i + d_i \quad for\ i = 1,5;$	$g_i = X_q f_i \quad for\ i = 1,5;$
$h_i = -X_d^{'} e_i \quad for\ i = 1,5;$	$h_3 = 1 - X_d^{'} e_3;$	
$i_i = [V_{td}\ g_i + V_{tq}\ h_i]/V_t \quad for\ i = 1,5;$	$i_3 = [V_{tq}\ h_3]/V_t;$	
$j_i = V_{td}\ e_i + I_d\ g_i + V_{tq}\ f_i + I_q\ h_i \quad for\ i = 1,5;$	$j_3 = V_{td}\ e_3 + I_q\ h_3;$	

A.2 For linearization of power system with PSS and TCSC controller

$X_{TCL} = X_T - X_{TCSC} + X_L;$	$X_{DT} = X_d^{'} + X_{TCL};$	$X_{QT} = X_q + X_{TCL};$
$a_1 = \frac{1}{X_{DT}} V_b \sin\delta;\ \ a_3 = \frac{1}{X_{DT}};$	$a_5 = -\frac{V_b \cos\delta - E_q^{'}}{X_{DT}^2};$	
$b_1 = \frac{1}{X_{QT}} V_b \cos\delta;$	$b_5 = \frac{1}{X_{QT}^2} V_b \sin\delta;$	
$c_i = X_q\ b_i \quad for\ i = 1,5;$	$d_i = -X_d^{'}\ a_i \quad for\ i = 1,5;$	$d_3 = 1 - X_d^{'}\ a_3;$

$e_i = [V_{td}\ c_i + V_{tq}\ d_i]/V_t \quad for\ \ i = 1{,}5\,;$	$e_3 = [V_{tq}\ d_3]/V_t\,;$
$f_i = V_{td}\ a_i + I_d\ c_i + V_{tq}\ b_i + I_q\ d_i \quad for\ \ i = 1{,}5\,;$	$f_3 = V_{td}\ a_3 + I_q\ d_3;$

A.3 For linearization of power system with PSS and STATCOM controllers

$X_{dT} = X_d^1 + X_T\,;$	$X_{qT} = X_q + X_T\,;$	$X_{dTS} = X_d^1 + X_T + X_S\,;$
$X_{qTS} = X_q + X_T + X_S\,;$	$X_{dTL} = X_d^1 + X_T + X_L\,;$	$X_{qTL} = X_q + X_T + X_L\,;$
$X_{DT} = [X_{dT}X_S + X_L X_{dTS}]\,;$	$X_{QT} = [X_{qT}X_S + X_L X_{qTS}]\,;$	
$a_1 = \frac{m_S}{C_{DC}}\cos\alpha_S\,; \quad a_2 = \frac{m_S}{C_{DC}}\sin\alpha_S\,;$	$a_3 = \frac{1}{C_{DC}}[I_{Sd}\cos\alpha_S + I_{Sq}\sin\alpha_S]\,;$	
$a_4 = \frac{m_S}{C_{DC}}[I_{Sq}\cos\alpha_S - I_{Sd}\sin\alpha_S]\,;$		
$b_1 = \frac{X_{dTS}}{X_{DT}}V_b\sin\delta\,;$	$b_3 = \frac{X_S}{X_{DT}}\,;$	$b_5 = \frac{X_{dT}}{X_{DT}}\frac{m_S}{2}\sin\alpha_S\,;$
$b_6 = \frac{X_{dT}}{X_{DT}}\frac{V_{DC}}{2}\sin\alpha_S\,;$	$b_7 = \frac{X_{dT}}{X_{DT}}\frac{m_S V_{DC}}{2}\cos\alpha_S\,;$	$c_1 = \frac{X_{qTS}}{X_{QT}}V_b\cos\delta\,;$
$c_5 = -\frac{X_{qT}}{X_{QT}}\frac{m_S}{2}\cos\alpha_S\,;$	$c_6 = -\frac{X_{qT}}{X_{QT}}\frac{V_{DC}}{2}\cos\alpha_S\,;$	$c_7 = \frac{X_{qT}}{X_{QT}}\frac{m_S V_{DC}}{2}\sin\alpha_S\,;$
$d_1 = -\frac{X_{dT}}{X_{DT}}V_b\sin\delta\,;$	$d_3 = \frac{X_L}{X_{DT}}\,;$	$d_5 = -\frac{X_{dTL}}{X_{DT}}\frac{m_S}{2}\sin\alpha_S\,;$
$d_6 = -\frac{X_{dTL}}{X_{DT}}\frac{V_{DC}}{2}\sin\alpha_S\,;$	$d_7 = -\frac{X_{dTL}}{X_{DT}}\frac{m_S V_{DC}}{2}\cos\alpha_S\,;$	$e_1 = -\frac{X_{qT}}{X_{QT}}V_b\cos\delta\,;$
$e_5 = \frac{X_{qTL}}{X_{QT}}\frac{m_S}{2}\cos\alpha_S\,;$	$e_6 = -\frac{X_{qTL}}{X_{QT}}\frac{V_{DC}}{2}\cos\alpha_S\,;$	$e_7 = -\frac{X_{qTL}}{X_{QT}}\frac{m_S V_{DC}}{2}\sin\alpha_S$
$f_i = b_i + d_i \quad for\ \ i = 1{,}3{,}5{,}6{,}7\,;$	$g_i = c_i + e_i \quad for\ \ i = 1{,}5{,}6{,}7\,;$	$h_i = X_q g_i \quad for\ \ i = 1{,}5{,}6{,}7$
$i_i = -X_d^{'}\ f_i \quad for\ \ i = 1{,}5{,}6{,}7\,;$	$i_3 = 1 - X_d^{'}\ f_3;$	

$j_i = [V_{td}\ h_i + V_{tq}\ i_i]/V_t \quad for\ \ i = 1{,}5{,}6{,}7\,;$	$j_3 = [V_{tq}\ i_3]/V_t\,;$
$k_i = V_{td}\ f_i + I_d\ h_i + V_{tq}\ g_i + I_q\ i_i \quad for\ \ i = 1{,}5{,}6{,}7\,;$	$k_3 = V_{td}\ f_3 + I_q\ i_3;$
$l_i = a_1\ d_i + a_2\ e_i \quad for\ \ i = 1{,}5;$	$l_3 = a_1\ d_3\ ;$

$l_6 = a_1 d_6 + a_2 e_6 + a_3;$	$l_7 = a_1 d_7 + a_2 e_7 + a_4;$

Appendix B.

Computational parameters in Chapter 5:

B.1 For linearization of power system with PSS, TCSC and SVC controllers

$X_{dT} = X_d^1 + X_T;$	$X_{qT} = X_q + X_T;$	$X_{LTC} = X_L - X_{TCSC};$
$X_{dTLTC} = X_{dT} + X_{LTC};$	$X_{qTLTC} = X_{qT} + X_{LTC};$	$X_{dTB} = X_{dT} + 1/B_{SVC};$
$X_{qTB} = X_{qT} + 1/B_{SVC};$	$X_{DB} = X_{dT} + X_{LTC}(1 + X_{dT} B_{SVC});$	
$X_{DT} = [X_{dT}/B_{SVC} + X_{LTC} X_{dTB}];$	$X_{QT} = [X_{qT}/B_{SVC} + X_{LTC} X_{qTB}];$	
$a_1 = \frac{X_{dTB}}{X_{DT}} V_b \sin\delta;\quad a_3 = \frac{1}{X_{DB}};$	$a_5 = \frac{1 + X_{dT} B_{SVC}}{X_{DB}^2} E_q^{'} - \frac{X_{dTB}^2}{X_{DT}^2} V_b \cos\delta;$	
$a_6 = \frac{X_{dTB}(X_{dT} + X_{LTC}) - X_{DT}}{X_{DT}^2 B_{SVC}^2} V_b \cos\delta - \frac{X_{LTC} X_{dT} B_{SVC}}{X_{DB}^2} E_q^{'}$		
$b_1 = \frac{X_{qTB}}{X_{QT}} V_b \cos\delta;$	$b_5 = \frac{X_{qTB}^2}{X_{QT}^2} V_b \sin\delta;$	
$b_6 = \frac{X_{qTB}(X_{qT} + X_{LTC}) - X_{QT}}{X_{DT}^2 B_{SVC}^2} V_b \sin\delta$	$c_1 = -\frac{X_{dT}}{X_{DT}} V_b \sin\delta;\quad c_3 = \frac{X_{LTC}}{X_{DT}};$	
$c_5 = \frac{X_{LTC} X_{dTB} - X_{DT}}{X_{DT}^2} E_q^{'} + \frac{X_{dT} X_{dTB}}{X_{DT}^2} V_b \cos\delta;$		
$c_6 = \frac{X_{dT} X_{LTC} + X_{LTC}^2}{X_{DT}^2 B_{SVC}^2} E_q^{'} + \frac{X_{dT}^2 + X_{dT} X_{LTC}}{X_{DT}^2 B_{SVC}^2} V_b \cos\delta;$		
$d_1 = -\frac{X_{qT}}{X_{QT}} V_b \cos\delta;$ $d_5 = -\frac{X_{qT} X_{qTB}}{X_{QT}^2} V_b \sin\delta;$	$d_6 = -\frac{X_{qT} + X_{qT} X_{LTC}}{X_{QT}^2 B_{SVC}^2} V_b \sin\delta;$	
$e_i = a_i + c_i \quad for\ i = 1,3,5,6;$	$f_i = b_i + d_i \quad for\ i = 1,5,6;$	$g_i = X_q f_i \quad for\ i = 1,5,6;$
$h_i = -X_d^{'} e_i \quad for\ i = 1,5,6;$	$h_3 = 1 - X_d^{'} e_3;$	

$i_i = [V_{td}\ g_i + V_{tq}\ h_i]/V_t \quad for\ \ i = 1,5,6;$	$i_3 = [V_{tq}\ h_3]/V_t;$
$j_i = V_{td}\ e_i + I_d\ g_i + V_{tq}\ f_i + I_q\ h_i \quad for\ \ i = 1,5,6;$	$j_3 = V_{td}\ e_3 + I_q\ h_3;$

B.2 For linearization of power system with PSS, TCSC and STATCOM controllers

$X_{dT} = X_d^1 + X_T;$	$X_{qT} = X_q + X_T;$	$X_{dTS} = X_d^1 + X_T + X_S;$
$X_{qTS} = X_q + X_T + X_S;$	$X_{LTC} = X_L - X_{TCSC};$	$X_{dTLTC} = X_d^1 + X_T + X_{LTC};$
$X_{qTLTC} = X_q + X_T + X_{LTC};$	$X_{DT} = [X_{dT}X_S + X_{LTC}X_{dTS}];$	$X_{QT} = [X_{qT}X_S + X_{LTC}X_{qTS}];$
$a_1 = \frac{m_S}{C_{DC}}\cos\alpha_S;\quad a_2 = \frac{m_S}{C_{DC}}\sin\alpha_S;$	$a_3 = \frac{1}{C_{DC}}[I_{Sd}\cos\alpha_S + I_{Sq}\sin\alpha_S];$	
$a_4 = \frac{m_S}{C_{DC}}[I_{Sq}\cos\alpha_S - I_{Sd}\sin\alpha_S]$		
$b_1 = \frac{X_{dTS}}{X_{DT}}V_b\sin\delta;$	$b_3 = \frac{X_S}{X_{DT}};$	$b_5 = \frac{X_{dT}}{X_{DT}}\frac{m_S}{2}\sin\alpha_S;$
$b_6 = \frac{X_S X_{dTS}}{X_{DT}^2}E_q^{'} + \frac{X_{dT}X_{dTS}}{X_{DT}^2}\frac{m_S V_{DC}}{2}\sin\alpha_S - \frac{X_{dTS}^2}{X_{DT}^2}V_b\cos\delta;$		
$b_7 = \frac{X_{dT}}{X_{DT}}\frac{V_{DC}}{2}\sin\alpha_S;$	$b_8 = \frac{X_{dT}}{X_{DT}}\frac{m_S V_{DC}}{2}\cos\alpha_S;$	$c_1 = \frac{X_{qTS}}{X_{QT}}V_b\cos\delta;$
$c_5 = -\frac{X_{qT}}{X_{QT}}\frac{m_S}{2}\cos\alpha_S;$	$c_6 = \frac{X_{qTS}^2}{X_{QT}^2}V_b\sin\delta - \frac{X_{qT}X_{qTS}}{X_{QT}^2}\frac{m_S V_{DC}}{2}\cos\alpha_S;$	
$c_7 = -\frac{X_{qT}}{X_{QT}}\frac{V_{DC}}{2}\cos\alpha_S;$	$c_8 = \frac{X_{qT}}{X_{QT}}\frac{m_S V_{DC}}{2}\sin\alpha_S;$	$d_1 = -\frac{X_{dT}}{X_{DT}}V_b\sin\delta;$
$d_3 = \frac{X_L}{X_{DT}};$	$d_5 = -\frac{X_{dTL}}{X_{DT}}\frac{m_S}{2}\sin\alpha_S;$	
$d_6 = \frac{X_{LTC}X_{dTS} - X_{DT}}{X_{DT}^2}E_q^{'} + \frac{X_{dT}X_{dTS}}{X_{DT}^2}V_b\cos\delta + \frac{X_{DT} - X_{dTLTC}X_{dTS}}{X_{DT}^2}\frac{m_S V_{DC}}{2}\sin\alpha_S;$		
$d_7 = -\frac{X_{dTLTC}}{X_{DT}}\frac{V_{DC}}{2}\sin\alpha_S;$	$d_8 = -\frac{X_{dTLTC}}{X_{DT}}\frac{m_S V_{DC}}{2}\cos\alpha_S;$	$e_1 = -\frac{X_{qT}}{X_{QT}}V_b\cos\delta;$
$e_5 = \frac{X_{qTLTC}}{X_{QT}}\frac{m_S}{2}\cos\alpha_S;$	$e_6 = -\frac{X_{qT}X_{qTS}}{X_{QT}^2}V_b\sin\delta + \frac{X_{qTLTC}X_{qTS} - X_{QT}}{X_{QT}^2}\frac{m_S V_{DC}}{2}\cos\alpha_S$	

$e_7 = -\frac{X_{qTLTC}}{X_{QT}} \frac{V_{DC}}{2} \cos \alpha_S ;$	$e_8 = -\frac{X_{qTLTC}}{X_{QT}} \frac{m_S V_{DC}}{2} \sin \alpha_S ;$	
$f_i = b_i + d_i \quad for\ i = 1,3,5,6,7,8$;	$g_i = c_i + e_i \quad for\ i = 1,5,6,7,8;$	$h_i = X_q g_i \quad for\ i = 1,5,6,7,8;$
$i_i = -X_d^{'}\ f_i \quad for\ i = 1,5,6,7,8;$	$i_3 = 1 - X_d^{'}\ f_3;$	
$j_i = [V_{td}\ h_i + V_{tq}\ i_i] / V_t \quad for\ i = 1,5,6,7,8;$	$j_3 = [V_{tq}\ i_3] / V_t ;$	
$k_i = V_{td}\ f_i + I_d\ h_i + V_{tq}\ g_i + I_q\ i_i \quad for\ i = 1,5,6,7,8;$	$k_3 = V_{td}\ f_3 + I_q\ i_3;$	
$l_i = a_1\ d_i + a_2\ e_i \quad for\ i = 1,5,6;$	$l_3 = a_1\ d_3$;	
$l_7 = a_1\ d_7 + a_2\ e_7 + a_3;$	$l_8 = a_1\ d_8 + a_2\ e_8 + a_4;$	

Dissemination of the Work

Dissemination of the Work

INTERNATIONAL JOURNALS: - 5

1) **Rajendraprasad Narne** and P.C. Panda, "Co-ordinated Design of PSS with Multiple FACTS Controllers in Multi-machine Power System using Advanced Adaptive PSO," International Review of Electrical Engineering (IREE), vol. 8, no. 2, pp. 858-866, 2013.
2) **Rajendraprasad Narne** and P.C. Panda, "PSS with SVC Damping Controllers Coordinated Design and Real-time Implementation in Multi-machine Power System using Advanced Adaptive PSO," International Journal of Emerging Electric Power Systems, vol. 14, no. 5, pp. 487-498, 2013.
3) **Rajendraprasad Narne** and P.C. Panda, "Coordinated Design of PSS with Multiple FACTS Controllers using Advanced Adaptive PSO," International Journal on Electrical Engineering and Informatics, vol. 5, no. 3, pp. 361-376, 2013.
4) **Rajendraprasad Narne** and P.C. Panda, "PSS with Multiple FACTS Controllers Coordinated Design and Real-Time Implementation Using Advanced Adaptive PSO," International Journal of Electrical, Electronic Science and Engineering, vol. 8, no. 1, pp. 144-154, 2014.
5) **Rajendraprasad Narne** and P.C. Panda, "Advanced Adaptive PSO based Hybrid Coordinated Design of PSS with Series and Shunt FACTS Controllers in multi-machine power system and Real-time Implementation," Iranian Journal of Electrical & Electronic Engineering (Accepted).

INTERNATIONAL JOURNALS (Under Review): - 3

6) **Rajendraprasad Narne** and P.C. Panda, "Invasive Weed Optimization based Optimal coordinated design and Real-time implementation of PSSs with TCSC damping controller," International Journal of Electrical Power and Energy Systems (Under review).
7) **Rajendraprasad Narne** and P.C. Panda, "Optimal TCSC controller design, Simulation and Real-time Implementation in multi-machine power system using Invasive Weed Optimization," International Journal on Electrical Engineering and Informatics (Under review).
8) **Rajendraprasad Narne** and P.C. Panda, "PSS and TCSC Damping Controller Coordinated Design with Real-Time Implementation in a Multi-Machine Power System," International Journal of Emerging Electric Power Systems (Under review).

INTERNATIONAL CONFERENCES:- 8

1) **Rajendraprasad Narne**, P. C. Panda and Jose P Therattil, "Transient Stability Enhancement using Coordinated Control between PSS and TCSC-Based Controllers," IEEE Joint International Conference on Power Electronics, Drives and Systems (PEDS), Singapore, 2011.
2) **Rajendraprasad Narne**, Jose P. Therattil, Laxmidhar Shau and P. C. Panda, "Dynamic Stability Enhancement Using Self-Tuning Static Synchronous Compensator," IEEE conference on Process automation control and computing, Coimbatore, pp 1-5, 2011.
3) **Rajendraprasad Narne**, P.C. Panda and Jose P Therattil, "Improving Power System Transient Stability by PSS and Hybrid Fuzzy-PI based TCSC Controllers," IEEE student conference on engineering and systems, NIT Allahabad, 2012.
4) **Rajendraprasad Narne**, P.C. Panda and Jose P. Therattil, "Genetic Algorithm based Simultaneous Coordination of PSS and FACTS Controllers for Power Oscillations Damping," IEEE International Conference on Sustainable Energy Technologies (ICSET'12), Kathmandu, Nepal, Sept.2012,
5) **Rajendraprasad Narne**, P.C. Panda and Jose P. Therattil, "Damping of Inter-area Oscillations in Power System using Genetic Optimization Based Coordinated PSS with FACTS Stabilizers," Annual IEEE India Conference (INDICON), Dec. 2012.
6) **Rajendraprasad Narne** and P. C. Panda, "Optimal Coordinate Control of PSS with Series and Shunt FACTS Stabilizers for Damping Power Oscillations," IEEE International Conference on Power Electronics, Drives and Energy Systems, IISC Bangalore, Dec.2012.
7) **Rajendraprasad Narne** and P. C. Panda, "Advanced Adaptive PSO Based Co-ordinated design of PSS with Multiple FACTS Controllers in Multimachine Power System," 5th International Conference on Computer Applications in Electrical Engineering-Recent Advances, IIT Roorkee, 2013.
8) Sunil Kumar Sunkara, **Rajendraprasad Narne** and P. C. Panda, "Co-ordinated Tuning of PSS with TCSC Damping Controller through Advanced Adaptive PSO for a Multi-machine Power System," IEEE International Conference on Energy Efficient Technologies for Sustainability, Apr. 2013.